Elucidating the Role of BMI1 in Lung and Colon Tumor Maintenance and Progression

by

Elaine Yih-Shuen Kuo

B.S. Biology
Stanford University, 2015

Submitted to the Department of Biology
in Partial Fulfilment of the Requirements for the Degree of

Doctor of Philosophy in Biology
at the Massachusetts Institute of Technology

February 2022

Signature of Author: _____
Department of Biology

Certified by: _____
Jacqueline A. Lees
Virginia and D.K. Ludwig Professor for Cancer Research
Associate Department Head, Biology
Thesis Supervisor

Accepted by: _____
Amy Keating
Professor of Biology and Biological Engineering
Co-Director, Biology Graduate Committee

`

Elucidating the Role of BMI1 in Lung and Colon Tumor Maintenance and Progression

by

Elaine Yih-Shuen Kuo

Submitted to the Department of Biology on December 20, 2021 in Partial Fulfillment of the Requirements for the Degree of Doctor of Philosophy in Biology

ABSTRACT

Cancer is a highly dynamic disease characterized by dedifferentiation, heterogeneity, and plasticity. It is postulated that within heterogeneous tumor tissues, there exists a subpopulation of cells, termed cancer stem cells (CSCs), with the ability to initiate and support tumor growth, promote metastatic spreading, and drive relapse following chemoradiotherapy. Given the high tumorigenic potential of these cells, there is strong interest in identifying methods to specifically target and eradicate CSCs. B lymphoma Mo-MLV insertion region 1 homolog (BMI1) is an epigenetic regulator important for stem cell self-renewal and differentiation, and it is also a proto-oncogene that is overexpressed in a wide variety of cancer types. Given its role in normal stem cell biology and its overexpression in cancer, there is strong interest in inhibiting BMI1 as a method of targeting CSCs. In this thesis, I will examine the role of BMI1 in tumor initiation, maintenance, and progression in lung and colon cancer, two cancer types in which BMI1 is overexpressed. Using genetically engineered mouse models, we determine that in oncogenic KRAS-driven lung adenocarcinomas, with or without *Trp53* deletion, genetic ablation of *Bmi1* at tumor initiation induces a pronounced proliferation defect and consequently significant suppression of tumor development and thus extension of lifespan. In stark contrast, *Bmi1* deletion in established lung adenocarcinomas does not impair tumor progression, CSC numbers or capacity, or metastatic potential, and instead, upregulates transcriptional programs associated with lung adenocarcinoma dedifferentiation and progression. Similarly, *Bmi1* deletion in established colon tumors does not impair colon cancer progression. Our work demonstrates that the effects of BMI1 loss are highly dependent on the context and timing of deletion relative to tumor development, and our findings raise concern over the use of BMI1 inhibitors as cancer treatments.

Thesis Supervisor: Jacqueline A. Lees
Title: Professor of Biology

`

ACKNOWLEDGEMENTS

I am in the fortunate position to have received endless support from many individuals during my time in graduate school, and I would like to thank them here.

First, I would like to thank my advisor and mentor Prof. Jacqueline A. Lees for her unwavering support throughout my graduate career. Jackie has constantly provided encouragement, advice, and understanding, and I am grateful to her for pushing me to develop confidence in myself and independence. Her kindness and dedication to mentoring is truly inspirational. I would also like to thank Prof. Tyler Jacks and Prof. Matthew Vander Heiden, both of whom have provided valuable insight and support throughout completion of these studies.

I would like to thank “Team BMI1” members, all of whom have generously provided valuable insight and stimulating discussions throughout my time on these projects. I want to thank Rachit Neupane for his mentorship, guidance, and limitless patience while I navigated through graduate school, and I truly treasure our friendship. I am grateful to Paul Danielian for not only being an outstanding lab manager but also for patiently assisting and advising me on many aspects of these studies. I would like to thank Pedro Pozo for his endless enthusiasm and camaraderie through long experiments. I want to thank Molly Wilson for her advice, friendship, and constant encouragement throughout graduate school. It was an immense pleasure working with you all.

I am grateful to the entire Lees Lab for providing such an engaging and nurturing environment to work and learn in. From lab meetings to social outings to late night discussions in lab, it has been an absolute joy to spend time with and learn from all of you. I want to personally thank Grace Phelps for her endless support, friendship, and positivity throughout my time in the Lees Lab.

I want to thank Theresa Hwang and Juhee Park Morehouse for being the most caring and loving friends anyone could ask for. Thank you for celebrating the highs with me, taking care of me and encouraging me through the lows, and for constantly providing me with laughter and happiness.

Lastly, I would like to thank my family, who have provided unconditional love and encouragement throughout graduate school. It has been a long journey, and I am grateful for your unwavering support through it all.

`

TABLE OF CONTENTS

`

`

CHAPTER 1: Introduction

`

Cancer is the second leading cause of deaths worldwide. There were 19.3 million new cancer cases and nearly 10 million cancer deaths estimated in 2020, and cancer incidence and mortality rates are projected to grow rapidly (Sung et al., 2021). Despite continued advancements in screening, diagnostics, and therapeutics, the treatment of cancer, particularly advanced disease, remains an unmet clinical need. Cancer therapy is greatly challenged by the nature of the disease. Under its simplest description, tumorigenesis is initiated by a key mutation in an oncogene or tumor suppressor. This mutation stimulates unrestrained proliferation, and the accumulation of additional mutations drives the transition of normal, healthy cells into malignant cells that can invade local tissue, disseminate to other parts of the body, disrupt normal tissue function, and cause death (Hanahan and Weinberg, 2011). However, it has become increasingly apparent that cancer is a highly dynamic disease characterized by intratumoral heterogeneity and plasticity. Subpopulations of phenotypically distinct cancer cells can exist within a single tumor, and cancer cells can switch between different states, including states characterized by stem-like properties. Moreover, epigenetic aberrations clearly play a critical role in enabling tumor cell plasticity and tumorigenesis. In the following sections of the Introduction, I will provide an overview of cancer stem cells (CSCs) and their roles in generating intratumoral heterogeneity and cancer cell plasticity. Then, I will discuss epigenetic regulation in cancer and focus on a specific epigenetic regulator, BMI1, as a target for CSCs. Finally, I will discuss our two cancer types of interest, lung and colon adenocarcinoma, and the potential of targeting BMI1 in both cancer contexts.

`

I. OVERVIEW OF CANCER STEM CELLS

Intratumoral heterogeneity and the cancer stem cell (CSC) model

Intratumoral heterogeneity, or co-existence of molecularly and phenotypically distinct subpopulations of cancer cells within a single tumor, has been a long-observed phenomenon[1]. Morphological heterogeneity within tumors was first observed in the 1830s when physiologists Johannes Muller and Rudolph Virchow examined human tumor samples under the microscope and noted histologically distinct subpopulations of cells within the same tumor (David, 1988; Titford, 2010). Since these formative observations, molecular biology techniques have confirmed that tumor subpopulations are not only morphologically distinct, but also exhibit molecular and phenotypic differences. Multi-region exome sequencing of individual tumors, as well as pan-cancer analyses, have revealed that patient tumors are genetically and spatially heterogeneous with multiple subclones existing within the same tumor (Andor et al., 2016; Gerlinger et al., 2012). Moreover, variation in the prevalence of oncogenic mutations within a tumor can affect treatment response and relapse (Bedard et al., 2013; Piotrowska et al., 2015). Although intratumoral heterogeneity is a well-documented feature of cancer, the molecular mechanisms propelling tumor heterogeneity, and the design of treatments to successfully eradicate multiple subpopulations within a tumor, remain under active investigation and debate.

Two historically predominant theories for the origins of intratumoral heterogeneity are the clonal evolution model and the cancer stem cell (CSC) model. In the clonal evolution model, proposed by Peter Nowell in 1976, a nonmalignant cell acquires a mutation that confers a growth advantage, leading to neoplastic proliferation of a malignant clone (Nowell, 1976). Genomic instability generates genetic diversity, and iterative rounds of diversification and

[1] Cancerous tissues are complex ecosystems consisting of transformed cells, immune cells, stromal cells, and other cell types in the tissue microenvironment. In this thesis, I will refer to intratumoral heterogeneity as the heterogeneity between transformed cells.

`

natural selection lead to the outgrowth of multiple molecularly and phenotypically distinct subclones within a tumor.

On the other hand, the CSC model posits that the heterogeneous population of cancer cells are organized hierarchically, with a subset of cells, termed cancer stem cells (CSCs), at the apex (Medema, 2013; Visvader and Lindeman, 2012). Reminiscent of normal, tissue-specific stem cells, which maintain tissue homeostasis through self-renewal and differentiation into various specialized cell types, CSCs self-renew and divide to generate phenotypically diverse progeny that make up the bulk of the tumor. Notably, only CSCs are endowed with the ability to initiate and propagate tumors, while the majority of the tumor cells are non-CSCs that do not possess this ability (Figure 1, left panel). Early support for the CSC model originated from seminal investigations of embryonal carcinomas and teratomas in the 1960s. Kleinsmith and Pierce demonstrated that injection of a single embryonal carcinoma cell into mice could give rise to teratomas with multilineage differentiation (Kleinsmith and Pierce, 1964). These findings both demonstrated the pluripotency of embryonal carcinoma cells and provided support for the existence of CSCs within tumor tissues (Kleinsmith and Pierce, 1964).

Research and interest into targeting CSCs have been greatly driven by the identification of CSCs in a number of tissue types. CSC existence and activity are generally assessed through transplantation assays in which subsets of cancer cells are isolated based on a distinct repertoire of cell surface markers (Rycaj and Tang, 2015). Upon secondary transplantation into recipient mice, CSCs have the ability to initiate tumors that recapitulate the phenotypic heterogeneity of the parent tumor. One of the earliest demonstrations for the existence of CSCs was in acute myeloid leukemia where a rare subset of cells, distinguished by the expression of the cell surface proteins $CD34^{+}CD38^{-}$, had the capacity to initiate acute myeloid leukemia upon transplantation into immunocompromised mice (Lapidot et al., 1994). Subsequent studies have led to identification of CSCs in solid tumors, including breast cancer, colon cancer, prostate cancer, lung cancer, and glioma (Al-Hajj et al., 2003; Curtis et al., 2010; Hurt et al., 2008; Lathia

`

et al., 2015; O'Brien et al., 2007a; Ricci-Vitiani et al., 2007a; Zheng et al., 2013). Lineage tracing assays, in which a single cell (or a group of cells) and its progeny are marked and tracked, have also confirmed the existence of CSCs. For example, lineage tracing in mouse intestinal cancer models revealed that single Lgr5^{+} adenoma cells can expand and generate heterogeneous adenomas (Schepers et al., 2012).

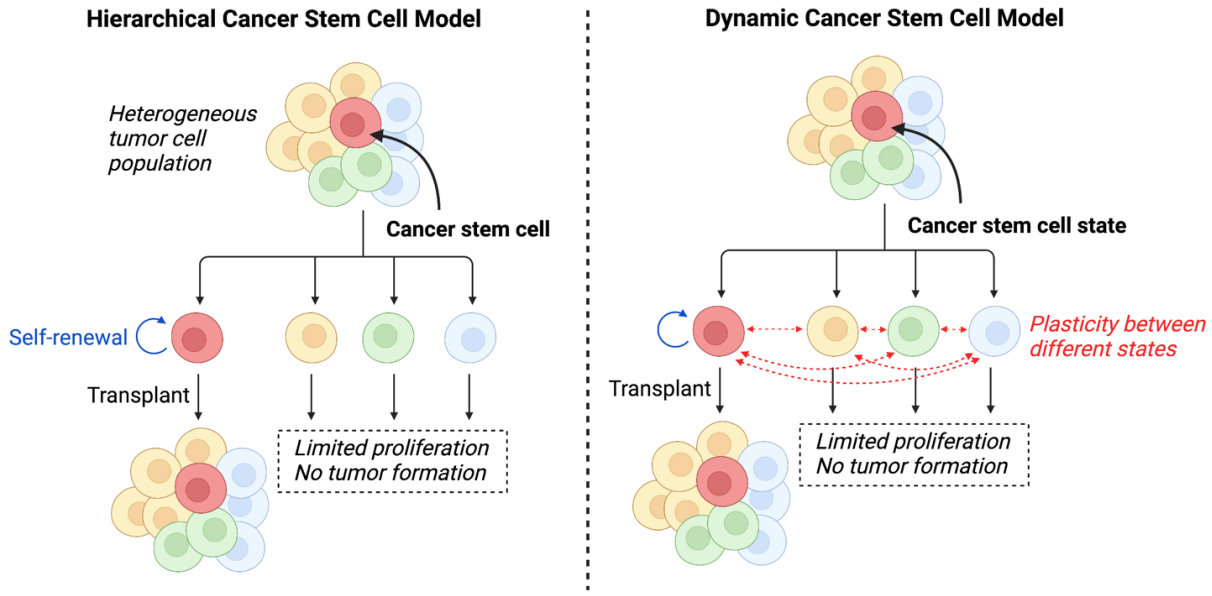

Figure 1. Schematic of the hierarchical CSC model (left panel) and dynamic CSC model (right panel). In the hierarchical CSC model, rare CSCs (indicated in red) self-renew and propagate tumors that phenocopy the parental tumor upon transplant, while non-CSCs have limited proliferative ability and are incapable of tumor propagation. In contrast, the dynamic CSC model posits that cancer cells can dynamically transition between CSC and non-CSC states. Created with BioRender.com.

Characteristics and plasticity of CSCs

CSCs have been portrayed to possess a number of properties. First, as described above, a functional characteristic of CSCs is the ability to initiate and propagate tumors that phenotypically copy the parent tumor upon serial transplantation. Second, CSCs have been tightly linked to metastatic dissemination. For example, single-cell analyses of metastatic breast cancer cells, isolated from xenografts of patient-derived human breast tumors, revealed that certain populations of metastatic cells are enriched for programs associated with cancer stemness, including expression of the pluripotency factors OCT4 and SOX2 (Lawson et al.,

`

2015). Breast CSCs also exhibit the ability to undergo epithelial-to-mesenchymal transitions, which is a critical step in the metastatic cascade and tumor dissemination (Liu et al., 2014).

Third, CSCs are described to be therapy-resistant, and persistence of CSCs following treatment can drive relapse. In fact, studies have demonstrated that chemotherapy treatment promotes enrichment for cancer cells expressing known CSC markers or stemness programs (Martins-Neves et al., 2016; Thakur and Ray, 2017). A number of mechanisms have been proposed to mediate CSC therapy resistance. The slow-cycling and quiescent nature of CSCs renders them resistant to chemotherapies and radiation therapies that typically target highly proliferative cells. For example, a study demonstrated that $CD13^+$ liver CSCs are predominantly in the G0 phase of the cell cycle, and these CSCs persist after treatment with the chemotherapeutic drug doxorubicin, which targets actively cycling cells (Haraguchi et al., 2010). In addition, CSCs have been shown to upregulate members of the ATP binding cassette (ABC) family, which are known to export chemotherapeutics out of cells (Begicevic and Falasca, 2017). Furthermore, CSCs can exhibit enhanced DNA repair activity, rendering them resistant to radiation therapy (Desai et al., 2014).

It is critical to note that the CSC model is evolving. Rather than a strict, static organization of CSCs, there is increasing evidence that cancer cells display plasticity and can dynamically switch between different cellular states, including CSC and non-CSC states (Figure 1, right panel). For example, studies using human breast cancer cells demonstrated that non-CSCs can convert to a CSC state, and such plasticity is influenced by epithelial-to-mesenchymal transition programs and signals from the microenvironment (Chaffer et al., 2011, 2013). In intestinal cancer, ablation of $Lgr5^+$ colorectal cells (the putative population of CSCs) is followed by replenishment of the CSC pool from reversion of more differentiated, $Lgr5^-$ cells into $Lgr5^+$ CSCs (Shimokawa et al., 2017). In addition, elevated levels of the inflammatory signal protein NF-κB can induce dedifferentiation of intestinal non-CSCs to tumor-initiating CSCs, suggesting that environmental cues can modulate CSC plasticity (Schwitalla et al., 2013). In

`

light of these and similar findings, there is an emerging model in which tumor cells are not arranged strictly in a hierarchy, but rather, CSC is a state in which cells, including non-CSCs, can dynamically switch into and out of (Chaffer and Weinberg, 2015). This model, called the dynamic cancer stem cell model, provokes important questions and concerns regarding the efficacy of treatments targeting CSCs, as plasticity may endow CSCs to transition between therapy-resistant and -sensitive states.

It should also be noted that the conceptual framework, existence, and terminology of CSCs remain under active investigation and discussion. As described above, the CSC model makes the important assumption that tumor cells exist in a hierarchy with only a rare subset of cells capable of tumor initiation or propagation. However, it has been demonstrated that the frequency of CSCs may not be as rare as initially believed. For example, tumor-initiating cell frequency was up to 27% in melanoma, and tumor-propagating ability may be highly dependent on the method of tumor cell isolation and transplant (Quintana et al., 2008; Vessoni et al., 2020). These findings, as well as the observations of CSC plasticity, have led to the increasing popularity for the term, tumor-propagating cell (TPC), that encompasses cancer cells with the functional property of propagating tumors upon serial transplantation, without the assumption of a hierarchical organization as in the CSC model.

Targeting CSCs as cancer therapies

Despite our evolving knowledge of CSCs and cancer cell plasticity, there is continued interest in developing treatments that selectively target and eliminate CSCs due to their high tumorigenic potential and ability to evade chemoradiotherapy. A number of strategies are being investigated based upon the biological properties of CSCs. These include targeting drug efflux pumps to combat drug resistance and inhibiting DNA repair pathways to increase susceptibility of CSCs to chemoradiotherapies (Turdo et al., 2019).

`

Another method to selectively eliminate CSCs is to inhibit proteins integral for normal stem cell function. It has been observed that CSCs exploit various signaling pathways important for normal stem cell self-renewal. For example, colon CSCs have been characterized by high Wnt activity, which is a key regulator of intestinal stem cell self-renewal capacity (Vermeulen et al., 2010a). Hedgehog and Notch signaling are self-renewal pathways utilized in both tissue stem cells and CSCs (Borah et al., 2015). Furthermore, pan-cancer analyses have revealed that gene signatures derived from adult epithelial stem cells are shared with aggressive cancers, suggesting that stemness is linked with tumor progression (Smith et al., 2018). These findings have led to an interest in eliminating CSCs through inhibiting proteins or pathways important for regulating stem cell self-renewal.

A key stem cell regulator that has received significant attention in targeting CSCs is B lymphoma Mo-MLV insertion region 1 homolog (BMI1). BMI1 is an epigenetic regulator and proto-oncogene important for normal tissue stem cell renewal and function. In the following sections, I will provide an overview of epigenetic regulation in cancer. I will then elaborate on BMI1's epigenetic roles in normal development as well as efforts to target BMI1 in cancer.

II. ROLE OF EPIGENETIC REGULATOR BMI1 IN STEM CELL BIOLOGY AND CANCER

Overview of epigenetic regulation in cancer

Epigenetic modifications refer to heritable alterations in gene expression that are not attributed to changes in the underlying DNA sequence. A number of epigenetic modifications, including DNA methylation, histone modifications, chromatin remodeling, and activity of non-coding RNAs, can affect the activity and expression of a particular gene. As an example, methylation of CpG islands in promoter regions, mediated by DNA methyltransferases, is associated with gene silencing (Moore et al., 2013). Histones, which package DNA in the nucleus, are commonly post-translationally modified, and various modifications are associated

`

with transcriptional activation or inactivation (Bannister and Kouzarides, 2011). ATP-dependent chromatin remodelers modulate positioning of nucleosomes and chromatin accessibility, influencing the ability of transcription factors to bind to DNA and activate or repress gene expression (Längst and Manelyte, 2015). Activity of non-coding RNAs provide additional layers of gene expression regulation (Mercer and Mattick, 2013; Yao et al., 2019).

Epigenetic regulation is essential for governing gene expression throughout normal development. For example, during differentiation of embryonic stem cells, the promoters of pluripotency-associated genes, such as *Oct4* and *Nanog*, become hypermethylated, leading to gene silencing accompanied by loss of self-renewal (Smith and Meissner, 2013). As stem cells differentiate into more specialized cell types, the epigenetic landscape reinforces expression or repression of genes integral for cell fate decision, an idea that C. H. Waddington famously conceptualized as marbles rolling down hills into specific grooves (Goldberg et al., 2007). In addition to lineage specification, epigenetic regulation is also critical for genomic imprinting, X-inactivation, body patterning, and other biological processes (Felsenfeld, 2014).

It is becoming increasingly evident that dysregulation of epigenetic pathways has profound effects on cancer development. Promoter hypermethylation of the tumor suppressor Retinoblastoma (*RB*) was first reported in 1989 (Greger et al., 1989). Since this initial observation, hypermethylation at the promoters of a number of tumor suppressor genes has been observed, including genes encoding cell cycle regulators, DNA repair proteins, and proteins involved in apoptotic pathways. For example, the promoters of the cell cycle regulator *CDKN2A* and apoptotic regulator *DAPK1* are frequently hypermethylated in human tumors across many cancer types (Esteller et al., 2001). In addition to altered methylation status at promoters, aberrant expression of histone modifiers and chromatin remodelers has been observed in cancerous tissues. As examples, EZH2, a component of the histone modifier Polycomb Repressive Complex 2 (PRC2), is commonly overexpressed in cancer, while components of the chromatin remodeling complex SWI/SNF are frequently inactivated (Jones et

`

al., 2018; Kleer et al., 2003; Masliah-Planchon et al., 2015; Melling et al., 2015). As I will elaborate in the context of lung and colon cancer in Sections III and IV of the Introduction, dysregulation or perturbation of epigenetic regulator activity can have significant effects on cancer cells, from affecting expression of individual genes to inducing global changes in the chromatin landscape (Chatterjee et al., 2018). Furthermore, epigenetic changes can modulate tumorigenicity, including acquisition of intratumoral heterogeneity and cancer cell plasticity (Flavahan et al., 2017). As epigenetic regulation and cancer progression are inextricably linked, elucidating the role of epigenetic regulators, and how they contribute to tumorigenesis, is essential for understanding tumor biology and designing effective therapies.

BMI1 is a component of the Polycomb Repressive Complex 1 (PRC1)

BMI1 is an epigenetic regulator important for transcriptional silencing during development. BMI1 was first identified in a screen for genes that cooperate with oncogenic *c-myc* during B-cell lymphomagenesis (van Lohuizen et al., 1991a). Shortly after, BMI1 was identified as a mammalian homologue to the *Drosophila melanogaster Polycomb sex comb (Psc)* gene, a Polycomb-group gene important for fly body segmentation through repression of Hox genes (van Lohuizen et al., 1991b). BMI1 was subsequently characterized as a member of the mammalian Polycomb group RING factor (PCGF) family, and while BMI1 itself does not have known enzymatic activity, it serves as a key regulatory element of the mammalian Polycomb Repressive Complex 1 (Cao et al., 2005).

Mammalian PRC1 complexes are highly diverse and essential for controlling gene expression during development. PRC1 complexes are generally classified into canonical and non-canonical PRC1 complexes. Canonical PRC1 complexes are composed of four core subunits, RING E3 ubiquitin ligase (RING1A/B), a PCGF family member (such as BMI1), CBX, and HPH, which collectively catalyze monoubiquitination of histone H2A on lysine 119 (Gil and O'Loghlen, 2014). Canonical PRC1 complexes are directed to silence target genes through

`

binding of the CBX subunit to H3K27 trimethylation (H3K27me^3) marks, which are placed on chromatin by Polycomb Repressive Complex 2 (PRC2; Figure 2). Upon recruitment to target genes, PRC1 monoubiquitinates H2AK119, leading to transcriptional repression (Cao et al., 2005; di Croce and Helin, 2013; Wang et al., 2004). In contrast, non-canonical PRC1 complexes can monoubiquitinate H2AK119 and repress target genes in the absence of PRC2 activity (Tavares et al., 2012). It remains unclear how PRC1 mediates transcriptional repression, whether through H2AK119ub-dependent or independent chromatin compaction, restraint of RNA polymerase II at promoters, or another mechanism (Pengelly et al., 2015; Zhou et al., 2008). To add further complexity, a recent study has also indicated that PRC1 may mediate transcriptional activation through formation of 3D enhancer-promoter loops (Loubiere et al., 2020). Characterization of PRC1 complexes, as well as the mechanism by which PRC1 modulates gene expression, remains an active area of research.

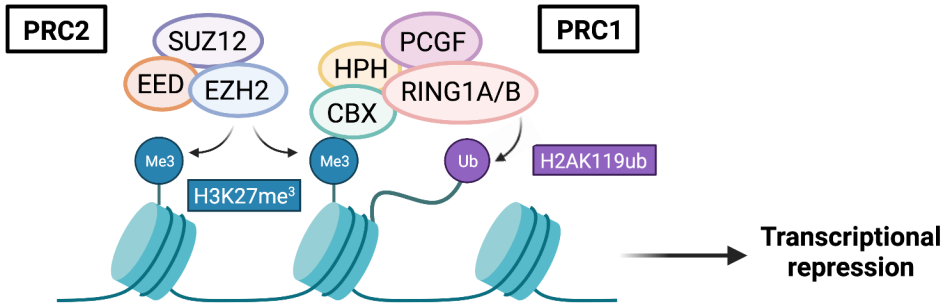

Figure 2. Schematic illustrating recruitment and activity of canonical PRC1. PRC2 deposits trimethylation marks on histone H3 lysine 27 (H3K27me^3). PRC1 is recruited through binding of the CBX subunit to H3K27me^3, and RING1A/B catalyze the addition of ubiquitin to histone H2A lysine 119 (H2AK119ub), leading to transcriptional repression. Created with BioRender.com.

Role of BMI1 in stem cell self-renewal and lineage specification

BMI1's role in normal development was initially uncovered through studies of germline *Bmi1* mutant (*Bmi1*$^{-/-}$) mice, in which *Bmi1* is deleted since fertilization (van der Lugt et al., 1994). Although viable, these mice exhibit a number of defects, including shortened lifespans, compromised immune systems, neurological abnormalities, and skeletal transformations (van

`

der Lugt et al., 1994). The hematopoietic and neurological defects were subsequently attributed to BMI1's role in tissue stem cell function, including regulation of self-renewal and differentiation. In post-natal germline *Bmi1*$^{-/-}$ mice, the numbers of hematopoietic stem and progenitor cells were determined to be markedly reduced (Iwama et al., 2004; Lessard and Sauvageau, 2003; Park et al., 2003). Upon secondary transplantation into immunocompromised mice, *Bmi1*$^{-/-}$ hematopoietic stem cells were unable to reconstitute hematopoietic lineages, indicating the requirement for BMI1 in the maintenance of hematopoietic stem cells (Park et al., 2003). Similarly, BMI1 loss leads to depletion and impaired self-renewal capacity of neural stem cells (Molofsky et al., 2003, 2005; Zencak et al., 2005).

The tissue stem cell defects observed upon BMI1 loss were in large part attributed to derepression of *Cdkn2a* and subsequent induction of apoptosis, cell cycle arrest, and/or cellular senescence. The *Cdkn2a* locus encodes two critical inhibitors of proliferation: p16^{INK4A} and p19^{ARF}. p16^{INK4A} inhibits cyclin-dependent kinases, thereby promoting pRB activation and cell cycle arrest, while p19^{ARF} inhibits MDM2, thus promoting p53 activation, cell cycle arrest, and apoptosis (Figure 3). Studies using *Bmi1*-deficient mouse embryonic fibroblasts (MEFs) showed that expression of p16^{INK4A} and p19^{ARF} becomes significantly upregulated in conjunction with poor proliferation and premature senescence entry, while overexpression of BMI1 leads to decreases in p16^{INK4A} and p19^{ARF} levels (Jacobs et al., 1999a). Germline knockout of both *Bmi1* and *Cdkn2a* substantially rescues hematopoietic and neural stem cell self-renewal (Molofsky et al., 2003; Oguro et al., 2006). However, survival and neural development of *Bmi1*$^{-/-}$ mice are not completely rescued with p16^{INK4A} and p19^{ARF} loss, hinting at BMI1's multifaceted roles (Bruggeman et al., 2005, 2007; Molofsky et al., 2005).

`

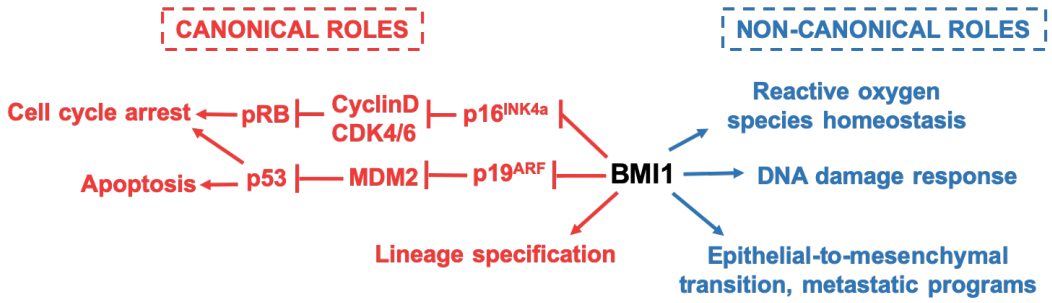

Figure 3. Diagram of BMI1's diverse biological roles. BMI1's canonical roles in repression of the *Cdkn2a* locus (which encodes $p16^{Ink4a}$ and $p19^{Arf}$) and lineage-specific transcription factors are crucial for tissue stem cell function. BMI1 is also implicated in reactive oxygen species homeostasis, DNA damage response, and regulation of metastatic programs, including epithelial-to-mesenchymal transition.

Indeed, aside from maintenance of tissue stem cell self-renewal through repression of $p16^{INK4A}$ and $p19^{ARF}$, one of BMI1's major function is regulation of developmental genes, including those involved with embryonal patterning, differentiation, and lineage specification. The skeletal transformation phenotype originally identified in the germline *Bmi1*$^{-/-}$ mutant mice was attributed to deregulation of several *Hox* genes in early embryos, leading to mispatterning and altered vertebral identity (van der Lugt et al., 1996). Chromatin immunoprecipitation assays confirmed binding of BMI1 to the promoters of *Hox* genes, including *HoxC13* and *HoxC5* (Cao et al., 2005; Wei et al., 2006). A study on hematopoietic stem cells indicated that loss of BMI1 leads to premature derepression of genes specific to the B lymphoid lineage, accompanied with enhanced B lymphopoiesis at the expense of T lymphopoiesis (Oguro et al., 2010). Characterization of genes regulating B lymphopoiesis revealed the binding of BMI1 to the promoters of B cell lineage developmental regulator genes, *Ebf1* and *Pax5*, indicating BMI1's role in controlling differentiation (Oguro et al., 2010). In addition, a study on cardiomyocyte reprogramming determined that BMI1 suppresses expression of cardiac-specific genes in fibroblasts, demonstrating BMI1's role in suppressing alternative lineage programs and maintaining cellular identity (Zhou et al., 2016).

Although initial studies of BMI1 focused on hematopoietic and neuronal stem cells, a multitude of studies have confirmed that BMI1 is highly expressed in a number of tissue stem

`

cell compartments, and germline loss of BMI1 activity compromises stem cell function. For example, bronchioalveolar stem cells (BASCs) isolated from *Bmi1*$^{-/-}$ mice exhibit defects in proliferation and self-renewal, concomitant with upregulation of $p16^{INK4A}$ and $p19^{ARF}$ (Dovey et al., 2008). In a separate study, BMI1 loss in BASCs was found to derepress a number of imprinted genes, such as p57, leading to impairment in stem cell self-renewal (Zacharek et al., 2011). In bone marrow cells, BMI1 is highly expressed in the stem cell compartment and its expression decreases in differentiated cells (Lessard et al., 1998). Furthermore, BMI1 is critical for regulating adipogenesis and osteogenesis in bone marrow stromal cells, and loss of BMI1 promotes adipocyte differentiation (Hu et al., 2019). BMI1 is highly expressed in the mouse mammary gland luminal compartment, and loss of BMI1 causes mammary growth defects and altered differentiation (Pietersen et al., 2008). Together, these findings have supported a model in which BMI1 is highly expressed in a multitude of tissue stem cells to support stem cell function, such as regulating self-renewal (through repression of *Cdkn2a*) and differentiation.

Non-canonical roles of BMI1

Over the past two decades, there has been accumulating evidence for the diversity of BMI1 targets and functions. Using mouse and human neuronal cells, Abdouh and colleagues determined that BMI1 accumulates at repetitive DNA sequences, and loss of BMI1 results in deficiency in constitutive heterochromatin formation (Abdouh et al., 2016). Furthermore, BMI1 localizes to sites of DNA damage and co-localizes with DNA damage repair proteins, such as ATM (Ginjala et al., 2011). Ablation of BMI1 impairs recruitment of DNA damage response machinery to chromatin, delaying DNA damage recognition and repair (Facchino et al., 2010). Additionally, aged *Bmi1*-heterozygous mice exhibit neurodegenerative symptoms resembling Alzheimer's disease, along with abnormalities in heterochromatin compaction and DNA damage response machinery at sites of repetitive DNA sequences in neural tissues (el Hajjar et al.,

`

2019). Thus, BMI1's role in heterochromatin formation and DNA damage repair can have important disease implications.

BMI1 is also associated with the regulation of reactive oxygen species (ROS) and mitochondrial function. Thymocytes isolated from *Bmi1*$^{-/-}$ mice exhibit elevated levels of ROS and mitochondrial defects, including diminished mitochondrial oxygen consumption (Liu et al., 2009). Treatment of *Bmi1*$^{-/-}$ mice with the ROS scavenger N-acetylcysteine partially rescues some defects, including thymocyte numbers and ROS levels, indicating BMI1's role in ROS homeostasis (Liu et al., 2009). A separate study also observed elevated ROS levels in *Bmi1*$^{-/-}$ neurons, and such ROS accumulation in these cells is dependent on increased p53 activity (Chatoo et al., 2009). Although the exact mechanisms by which BMI1 mediates ROS detoxification remain to be elucidated, these studies indicate BMI1's role in regulating cellular metabolism.

Targeting BMI1 in cancer

BMI1 is consistently overexpressed in multiple cancer types, and its expression is correlated with poor patient prognosis. In non-small cell lung cancer (NSCLC) patient tumor samples, BMI1 expression is associated with disease progression, and levels of $p16^{INK4A}$ and $p14^{ARF}$ are observed to be inversely correlated with BMI1 expression (Vonlanthen et al., 2001; Vrzalikova et al., 2008). Similarly, in patients with colorectal cancer (CRC), BMI1 is overexpressed in colon carcinoma cells relative to normal tissue, and higher BMI1 expression is associated with decreased overall survival and reduced disease-free survival (Alajez, 2016; Du et al., 2010; Kim et al., 2004). Furthermore, BMI1 protein expression is inversely correlated with levels of $p16^{INK4A}$ and $p14^{ARF}$ in patient CRC samples (Kim et al., 2004). Cancers arising from other tissue types, such as the cervix, breast, and ovary, also exhibit elevated BMI1 expression (Guo et al., 2011; Zhang et al., 2008).

`

Studies from our lab, along with many others, have demonstrated that BMI1 loss is detrimental to tumor initiation and progression, commonly through derepression through the *Cdkn2a* locus. One of the earliest descriptions of this effect came from a study of *c-Myc*-driven lymphomagenesis, where loss of one copy of *Bmi1* impaired lymphomagenesis through enhanced apoptosis (Jacobs et al., 1999b). The authors then demonstrated that the enhancement of proliferation and transformation of MEFs by BMI1 and MYC were in large part mediated through repression $p16^{INK4A}$ and $p19^{ARF}$ (Jacobs et al., 1999b). Other studies of hematopoietic cancers have demonstrated a similar role for BMI1 in supporting tumor progression through promoting proliferation and preventing cell cycle arrest. In a study of myeloid leukemia, fetal liver cells derived from germline $Bmi1^{-/-}$ mice were transformed by expression of *HoxA9* and *Meis1* (Lessard and Sauvageau, 2003). Although these leukemic cells did not initially demonstrate proliferative defects, the $Bmi1^{-/-}$ leukemic cells failed to form tumors upon secondary transplantation and exhibited proliferation arrest and apoptosis *in vitro*, providing evidence for BMI1's role in maintenance of tumor cells (Lessard and Sauvageau, 2003). Subsequent studies using murine models where BMI1 was lost early in embryogenesis have confirmed that BMI1 loss, and ensuing upregulation of $p16^{INK4A}$ and $p19^{ARF}$, is detrimental to tumor initiation or progression, including in lung and colon cancer (Dovey et al., 2008; Maynard et al., 2014). Given our strong interest in understanding BMI1's contribution to lung and colon tumorigenesis, I will elaborate on these findings in Sections III and IV of the Introduction.

Although the initial focus of BMI1-mediated tumor suppression was on derepression of $p16^{INK4A}$ and $p19^{ARF}$, recent studies have detailed BMI1's influence on tumorigenesis beyond suppression of the *Ink4a/Arf* locus. For example, genetic *Bmi1* ablation in a mouse model of *Kras*-driven pancreatic cancer impairs tumor initiation. The authors demonstrated that this tumor suppressive effect is not dependent on *Cdkn2a*, as crossing these mice into an $Ink4a^{-/-}$ background does not rescue the suppression of tumorigenesis. Rather, the tumor suppressive

`

effects were attributed to upregulation of ROS levels, indicating BMI1's role in regulating ROS homeostasis in cancer cells (Bednar et al., 2015). Such results mirror findings in normal, non-transformed thymocytes and neurons, where BMI1 contributes to ROS detoxification (Chatoo et al., 2009; Liu et al., 2009). In addition to regulating ROS homeostasis, multiple studies have also elucidated BMI1's role in cell migration, invasion, and metastasis. Research from our lab has demonstrated that BMI1 promotes migration and metastasis of melanoma (Ferretti et al., 2016). In addition, studies of head and neck squamous cell carcinoma and nasopharyngeal cells demonstrated that BMI1 promotes epithelial-mesenchymal transition, a process closely associated with invasion and metastatic spreading (Chen et al., 2017; Song et al., 2009; Yang et al., 2010). Furthermore, a study of Ewing sarcoma found that BMI1 promotes anchorage-independent growth through repressing genes involved in cell-cell and cell-matrix adhesion (Douglas et al., 2008). Such findings highlight BMI1's diverse roles in tumorigenesis.

Considering BMI1's function as a stem cell regulator, as well as its overexpression in cancer, there has been substantial interest in inhibiting BMI1 as a method of eliminating cancer stem cells (CSCs). As discussed in Section I of the Introduction, targeting CSCs is an attractive strategy in cancer therapy, due to their ability to resist therapeutic treatment, drive metastatic spreading, and propagate tumors. These properties of CSC, as well as BMI1's function in regulating stem cell activity, have fueled considerable interest in designing BMI1 inhibitors to eliminate CSCs. The first chemical BMI1 inhibitor described was PTC-209, which was identified using a reporter under transcriptional control of the 5' and 3' untranslated regions of the human *Bmi1* gene (Kreso et al., 2014). Multiple studies have demonstrated the deleterious effects of PTC-209 to tumorigenesis in a number of cancer types, including reducing colon cancer tumor-initiating cell frequency (Alzrigat et al., 2017; Bolomsky et al., 2016; Kreso et al., 2014; Sulaiman et al., 2019). However, PTC-209 exhibits poor pharmacokinetic properties, and in our hands, this compound is equally toxic to $Bmi1^{+/+}$ and $Bmi1^{-/-}$ cancer cells, indicating that its mechanism of cell death is not through inhibition of BMI1 (data not shown). More recently, two additional

`

chemical inhibitors, PTC-596 and PTC-028, have been described as BMI1 inhibitors (Dey et al., 2018). However, both compounds have been demonstrated to exert cytotoxic effects through mechanisms independent of BMI1 (Bolomsky et al., 2020; Flamier et al., 2020).

To investigate the effects of BMI1 loss, we have developed mouse models of lung and colon adenocarcinoma in which we can induce *Bmi1* deletion specifically in adult tumors. We believe that this strategy of genetic ablation (rather than use of the BMI1 inhibitors described above) enables us to effectively assess whether and how loss of BMI1 activity alters tumorigenesis. Furthermore, our mouse models permit temporal control over tumor initiation and *Bmi1* deletion, allowing for interrogation of the effects of BMI1 loss at multiple steps of lung and colon carcinogenesis. In the next sections, I will discuss the molecular drivers and characteristics of lung and colon adenocarcinoma development. In addition, I will elaborate on known roles for BMI1 and other epigenetic regulators in the initiation and progression of these diseases.

III. MOLECULAR DRIVERS AND PROGRESSION OF LUNG ADENOCARCINOMA

Lung cancer is the second most commonly diagnosed cancer and the leading cause of cancer deaths worldwide, claiming an estimated 1.8 million lives in 2020 (Sung et al., 2021). Despite substantial progress in lung cancer screening, tobacco control initiatives, and targeted therapies, the prognosis for lung cancer remains bleak. The 5-year survival rate of lung cancer patients is only 10% to 20% after diagnosis, as patients commonly present with advanced, metastatic disease at the time of diagnosis, and tumors frequently develop therapy resistance (Lim and Ma, 2019; Sung et al., 2021). The two major histologic types of lung cancer are small-cell lung cancer (SCLC) and non-small-cell lung cancer (NSCLC). Of the NSCLC subtypes, lung adenocarcinoma (LUAD) is the most frequent, representing about 40% of all lung cancers (Duma et al., 2019). Treatment of LUAD is greatly challenged by tumor evolution and

`

intratumoral heterogeneity, and there remains a critical need for development of effective treatment strategies.

Mutational landscape and treatments for lung adenocarcinoma (LUAD)

LUAD is characterized by a high mutational burden compared to many other tumor types (Kandoth et al., 2013). Exome sequencing of patient LUAD tumors revealed that *TP53* is the most commonly mutated gene, with 46% of the tumors exhibiting a *TP53* mutation (Collisson et al., 2014). Furthermore, oncogenic mutations in *KRAS* (35%) or *EGFR* (14%) are common, indicating a strong selective pressure to activate the EGFR-MAPK and/or PI3K-AKT signaling pathways. Mutations are also observed in the *KEAP1/NRF2* and *LKB1/AMPK* pathways, and the frequency of mutations varies by smoker status and gender of the patient (Collisson et al., 2014; Wang et al., 2021).

Over the past two decades, the advent of targeted therapies towards particular oncogenic alterations, as well as the development of immunotherapies, have propelled evolution of the LUAD treatment paradigm. LUAD patients are conventionally treated with cytotoxic chemotherapies, including cisplatin and other platinum-based chemotherapies, and for patients with advanced disease, chemotherapy remains the predominant treatment option (Lemjabbar-Alaoui et al., 2015). However, for patients (especially non-smokers) with particular mutations in EGFR, treatment with EGFR tyrosine kinase inhibitors (i.e. gefinitib and erlotinib) has demonstrated significant improvements in response rate and progression-free survival compared to treatment with first-line cytotoxic chemotherapies (Lee et al., 2015). For NSCLC patients presenting ALK translocations, treatment with ALK tyrosine kinase inhibitors has prolonged survival (Sullivan and Planchard, 2016). Furthermore, treatment with PD-1/PD-L1 immune checkpoint inhibitors for patients with advanced NSCLC has attracted considerable attention, with atezolizumab, an anti-PD-L1 monoclonal antibody, receiving FDA approval as a

`

first-line and adjuvant therapy in 2020 and 2021, respectively (Felip et al., 2021; Herbst et al., 2020).

Despite impressive clinical efficacy of targeted therapies towards specific oncogenic proteins in LUAD, the disease progresses in most patients in 9 to 12 months. This acquired therapy resistance has been attributed to various escape mechanisms, including pre-existence or adaptive evolution of a drug-resistant subclone that drives tumor re-emergence (Lim and Ma, 2019). Therefore, understanding LUAD tumor evolution and the origins of intratumoral heterogeneity remains vital for the development of effective treatment strategies.

Genetically engineered mouse models (GEMMs) of LUAD

Much of our understanding of LUAD development has been founded on investigations using genetically engineered mouse models (GEMMs) of LUAD. One of the most commonly used strategies to model LUAD in mice is expression of oncogenic *KRAS*, which is the most frequently mutated gene in patient LUAD tumors after *TP53*. In 2001, Johnson et al. constructed a mouse model of sporadic lung cancer, called the LA2 model, in which latent, oncogenic alleles of *Kras* are activated spontaneously *in vivo* through genetic recombination (Johnson et al., 2001). These mice exhibit lung lesions at an early age, which develop into poorly differentiated lung adenocarcinomas that histopathologically resembled human NSCLC (Johnson et al., 2001). Shortly after, an autochthonous GEMM with an inducible allele of oncogenic *Kras* was developed (Jackson et al., 2001). This GEMM harbors a conditional allele of oncogenic *Kras* (*Lox-STOP-Lox-Kras*^{G12D}) and upon, intranasal delivery of lentivirus carrying Cre recombinase, these mice develop *Kras*^{G12D}-driven lung tumors (Jackson et al., 2001). Progression of oncogenic *Kras*^{G12D}-driven lung tumors is accelerated upon combination with *Trp53* deletion, resulting in lung adenocarcinomas that recapitulate advanced human disease including invasion and metastasis (Jackson et al., 2005). Further studies have demonstrated that one of the putative cells-of-origin in these oncogenic *Kras*-driven tumors are alveolar type II (ATII) cells

`

(Sutherland et al., 2014; Xu et al., 2012). Since initial generation of these *Kras*^{G12D} and *Kras*^{G12D};*Trp53*$^{-/-}$ mice, additional conditional alleles for genes of interest as well as strategies enabling cell type-specific Cre expression have been added to these LUAD mouse models (Kwon and Berns, 2013). Furthermore, CRISPR/Cas9 systems can be integrated into the tumor induction process, enabling interrogation of the role of specific proteins in LUAD tumor maintenance and progression (Sanchez-Rivera et al., 2014).

It should be noted that these autochthonously generated *Kras*$^{G12D/+}$;*Trp53*$^{-/-}$ lung tumors exhibit markedly lower mutational burden than human (either smoker or non-smoker-associated) LUAD tumors (McFadden et al., 2016; Westcott et al., 2015). Although the high mutational burden, particularly observed in tumors of smokers, is not represented in these mouse models, usage of these reductionist GEMMs enables greater experimental control over few genetic alterations and permits unravelling of the critical mutational events that drive cancer progression versus passenger mutations.

Alterations of differentiation states and cancer cell plasticity during LUAD progression

Changes in differentiation state, such as dedifferentiation into a more stem-like or embryonic state or loss of lineage specificity, as well as acquisition of cell plasticity are hallmarks of tumor progression. These processes are especially evident in LUAD. A study of *Kras*$^{G12D/+}$;*Trp53*$^{-/-}$ GEMMs of LUAD determined that the pulmonary transcription factor NKX2.1 is consistently downregulated in metastatic primary tumors and metastases (Winslow et al., 2011). Further analyses revealed that NKX2.1 loss marks poorly differentiated lung tissues, which also upregulate HMGA2 (a transcription factor whose expression is normally restricted to embryonal tissues), hinting at NKX2.1's role in restraining tumor progression through maintenance of lung lineage specification (Winslow et al., 2011).

A subsequent study by Snyder and colleagues confirmed a critical role for NKX2.1 in regulating differentiation states during LUAD development (Snyder et al., 2013). The authors

`

determined that genetic ablation of *Nkx2.1* after establishment of *Kras*$^{G12D/+}$ or *Kras*$^{G12D/+}$;*Trp53*$^{-/-}$ lung tumors results in increased tumor burden concurrent with altered differentiation states, including emergence of mucinous tumor cells. Transcriptomic sequencing of *Nkx2.1*-deficient lung tumors revealed that NKX2.1 loss induces expression of gastric-associated genes including *Hnf4*α, a transcription factor that regulates gastrointestinal differentiation. As pulmonary and gastrointestinal tissues both originate from the embryonic foregut during normal development (Morrisey and Hogan, 2010), these findings indicate that NKX2.1 is a key regulator of pulmonary lineage and loss of NKX2.1 activates a latent gastric program (Snyder et al., 2013). The authors demonstrated that loss of both NKX2.1 and HNF4α is sufficient to induce upregulation of the embryonal protein HMGA2, and that the transcription factors FOXA1 and FOXA2 are critical for the activation of gastric differentiation programs in NKX2.1-deficient lung tumors (Camolotto et al., 2018; Snyder et al., 2013). Overall, these findings identify NKX2.1 as a key molecular player in the dedifferentiation process during lung tumor progression.

A recent study on LUAD evolution has provided valuable insight into plasticity and the origins of intratumoral heterogeneity in this disease. Marjanovic and colleagues induced expression of oncogenic *Kras*^{G12D} or oncogenic *Kras*^{G12D} with *Trp53* deletion in ATII cells and collected cells for single cell RNA sequencing at distinct stages of LUAD evolution (Marjanovic et al., 2020). Using the gene expression profiles of ATII cells and progressively advanced tumor cells, the authors determined that cell state heterogeneity increases during tumor progression. Furthermore, LUAD progression is associated with loss of ATII cell identity and emergence of expression patterns related to intestinal, gastric, and embryonic endodermal tissues, consistent with findings from Snyder et al. and Winslow et al. in that lung cancer progression is linked to loss of lung lineage specification and increased expression of latent gut and embryonic lineage programs (Marjanovic et al., 2020; Snyder et al., 2013; Winslow et al., 2011). Importantly, the authors identified a subpopulation of cells of highly mixed cellular identity, present from early

`

adenomas to advanced tumors, from which they derived a high-plasticity cell state signature (Marjanovic et al., 2020). Cells in this highly plastic state are able to generate heterogeneous tumor populations, demonstrate robust proliferative potential, and exhibit chemotherapy resistance (Marjanovic et al., 2020). These findings suggest that LUAD heterogeneity and tumor progression may be driven by a highly plastic cell state, rather than a static population of CSCs. Such intriguing analyses not only highlight the power of single cell sequencing in understanding intratumoral heterogeneity, but also underscore the ongoing evolution in our understanding of lung tumor cell plasticity and disease progression.

Epigenetic regulation in LUAD development

It is becoming increasingly evident that epigenetic pathways greatly influence or underlie many aspects of LUAD biology, including disease progression, intratumoral heterogeneity, adoption of altered differentiation states or cell identities, and acquisition of cell plasticity. Many studies have demonstrated that lung cancer development is accompanied by a number of epigenetic abnormalities. One of the first epigenetic aberrations documented was hypermethylation at the *Cdkn2a* locus, which is observed in early neoplastic lesions and persists throughout LUAD progression (Belinsky et al., 1998; Merlo et al., 1995; Nuovo et al., 1999; Selamat et al., 2011). In addition, mutations or altered expression of chromatin-associated complexes, including histone modifiers and chromatin remodelers, are commonly observed. For example, EZH2, a key component of PRC2 which catalyzes methylation of H3K27, is overexpressed in patient NSCLC tumors, and higher EZH2 expression is correlated with worse patient outcome (Wan et al., 2013; Wang et al., 2016). Inactivation of SMARCA4 (BRG1), a catalytic subunit of the chromatin remodeler SWI/SNF complex, are also present in approximately 10% of LUAD patients, and occurrence of these mutations can affect treatment efficacy (Schoenfeld et al., 2020).

`

Dysregulation of epigenetic modulator activity can significantly affect LUAD initiation and progression, and such effects can be highly dependent on the context in which the perturbation occurs. For example, a study demonstrated that overexpression of EZH2 in lung epithelial cells is sufficient to induce LUAD, and aberrant EZH2 upregulation alters the expression of regulators of cellular differentiation and growth signaling pathways (Zhang et al., 2016). Based on observations of EZH2's pro-oncogenic roles and its overexpression in LUAD, there has been strong interest in utilizing EZH2 inhibitors as cancer therapies (Kim and Roberts, 2016). Another example is G9a, a histone methyltransferase that catalyzes methylation of H3K9. Loss of G9a in $Kras^{G12D};Trp53^{-/-}$ GEMMs of LUAD promotes tumor progression, including increased frequency of mice with metastases, as well as elevated tumor-propagating cell frequency (Rowbotham et al., 2018). The study also determined that G9a regulates expression of genes associated with KRAS signaling and extracellular matrix remodeling, such as MMP10, and G9a loss promotes invasiveness of LUAD cells (Rowbotham et al., 2018). Furthermore, depletion of the histone demethylase KMD3a results largely in the opposite effects of G9a loss (i.e. tumor suppression), emphasizing the significance of histone methylation status in governing tumorigenic processes (Rowbotham et al., 2018). Given that G9a has been commonly described as an oncogene (Chen et al., 2010), this study underscores the importance of understanding the context-dependent effects of epigenetic regulator activity during tumor progression (Rowbotham et al., 2018).

SMARCA4/BRG1, of the chromatin remodeling complex SWI/SNF, serves as another example of an epigenetic regulator governing multiple biological processes in LUAD development. A recent study demonstrated that in LUAD cells, SMARCA4 interacts with the DNA replication machinery, including RPA complexes and ORC1 (Gupta et al., 2020). Loss of SMARCA4 in LUAD cells causes DNA replication stress, including induction of replication fork defects, increased levels of DNA damage, and upregulation of the DNA damage sensor ATR and ATR-mediated pathways (Gupta et al., 2020). The investigators also determined that

`

SMARCA4-deficient LUAD cells are particularly vulnerable to ATR inhibitors, likely due to the increased DNA damage response (Gupta et al., 2020). SMARCA4 also plays a role in lung lineage specification and dedifferentiation. Deletion of *Smarca4*, concurrent with oncogenic activation of $Kras^{G12D}$ and *Trp53* deletion, leads to LUAD tumors characterized by loss of pulmonary lineage identity and increased expression of metastatic programs (Concepcion et al., 2021). Intriguingly, the extent to which SMARCA4 loss promotes tumor progression is dependent on the lung cell type of origin (i.e. $Sftpc^{+}$ versus $CCSP^{+}$ cells), again demonstrating the context-dependent effects of epigenetic regulator activity (Concepcion et al., 2021).

The findings described above highlight the multifaceted roles of epigenetic regulators in lung tumorigenesis and underscore the importance of context when evaluating the effects of epigenetic regulator activity. In addition, single cell epigenetic profiling has revealed that LUAD cells exhibit a continuum of epigenetic states, from states resembling normal alveolar cells to metastatic or metastatic-like states (LaFave et al., 2020). These detailed epigenetic profiling studies emphasize that changes in the epigenetic landscape are fundamental to LUAD progression, and continued investigation into epigenetic regulation in LUAD will be critical for understanding the biology and progression of this disease.

Targeting BMI1 in LUAD

Given BMI1's overexpression in LUAD and correlation with poor prognosis, there has been interest in elucidating the molecular mechanisms by which BMI1 affects LUAD biology (Vonlanthen et al., 2001; Vrzalikova et al., 2008). Our lab and others have demonstrated an oncogenic role for BMI1 in LUAD development. When oncogenic KRAS-driven LUAD is induced in germline *Bmi1* wildtype and mutant mice, BMI1 loss leads to a $p19^{ARF}$-dependent reduction in tumor numbers, as well as a block on tumor progression at the hyperplastic stage (Dovey et al., 2008). In a BRAF-driven LUAD mouse model, germline BMI1 loss did not reduce the number of tumors initiated, but of tumors that did arise, BMI1 loss reduced tumor volumes as a

`

consequence of increased apoptosis and reduced proliferation (Becker et al., 2009). These data align with findings in the normal lung epithelial context, where BMI1 loss leads to impairment of the expansion of BASCs in response to injury, the effects of which were partially rescued by $p19^{ARF}$ loss, and derepression of imprinted genes, including p57, leading to impairment in stem cell self-renewal (Dovey et al., 2008; Zacharek et al., 2011). Together, these data argue for a pro-tumorigenic role of BMI1 in LUAD through suppression of *Cdkn2a*.

Such findings stimulate several potential areas of investigation. First, the LUAD studies described above utilize germline *Bmi1* mutant mice in which BMI1 protein has been lost since fertilization. However, germline *Bmi1* deletion is not reflective of treatment settings, where patients already present with tumors, and critically, the effects of post-embryonic BMI1 loss in LUAD tumors remain undetermined. Second, incomplete rescue of LUAD tumorigenesis and BASC function following $p19^{ARF}$ loss suggests that other downstream targets of BMI1 may be involved in LUAD tumorigenesis. Indeed, BMI1 has been documented to exert *Cdkn2a*-independent effects on tumorigenesis in other tumor types, including roles in ROS homeostasis, cell adhesion, and cell invasion and migration (Bednar et al., 2015; Douglas et al., 2008; Ferretti et al., 2016). Whether these or other BMI1 functions are contributing to tumor progression in the LUAD context is unclear. In Chapter 2 of this thesis, I will discuss our findings in depleting BMI1 at LUAD tumor initiation and after LUAD establishment and elucidate the role of BMI1 in these contexts.

IV. MOLECULAR DRIVERS AND PROGRESSION OF COLON CANCER

The second context in which this thesis addresses the consequences of BMI1 loss is colorectal cancer (CRC). CRC is the third most commonly diagnosed cancer and the second leading cause of cancer deaths worldwide, with over 900,000 deaths estimated worldwide in 2020 (Sung et al., 2021). Approximately 35-40% of CRC cases are associated with inherited

`

CRC susceptibility, such as a family history of the disease or inherited genetic mutations, including germline inactivation of the Wnt signaling negative regulator, *Apc,* or DNA repair genes such as *hMLH1* or *hMSH2* (Keum and Giovannucci, 2019). In contrast, the majority (60-65%) of CRC cases occur sporadically through acquisition of somatic mutations (Keum and Giovannucci, 2019). As elaborated upon in the following sections, sporadic CRC commonly develops through progressive accumulation of genetic mutations, beginning with aberrant activation of Wnt signaling (Fearon, 2011). It is also increasingly evident that non-genetic factors, such as physical inactivity, obesity, smoking, and poor diet, can greatly influence CRC initiation and development (Marley and Nan, 2016). Despite widespread adoption of early screening procedures and increased awareness of CRC risk factors, the high death rate of CRC patients underscores the need to understand CRC biology and develop therapeutic interventions, particularly to treat advanced disease.

Colon cancer development and treatment strategies

Colon cancer progression has been famously characterized by Fearon and Vogelstein as a multistep accumulation of genetic alterations (Fearon and Vogelstein, 1990). Drawing from mutational analyses of colon tumors, Fearon and Vogelstein proposed a model in which aberrant activation of Wnt/β-catenin signaling (through loss of *APC*) is the tumor-initiating event for colon cancer and drives hyperproliferation and formation of a benign hyperplasia (Fearon and Vogelstein, 1990). As the hyperplasia progresses into adenomas and eventually invasive and metastatic carcinomas, the tumor accrues specific genetic alterations, including oncogenic activation of *KRAS*, mutation in *TP53*, and loss of regions of chromosome 18q. Rather than the order of mutations, Fearon and Vogelstein emphasize that the accumulation of oncogenic mutations is the key driver of malignancy. Fearon and Vogelstein further proposed that four to five mutations are required for formation of a malignant tumor, and that this multistep

`

carcinogenesis model could be generalized to other epithelial tumor types (Fearon and Vogelstein, 1990).

Since initial description of the model, detailed molecular characterization and sequencing studies have illuminated a number of important biological processes that are dysregulated in colon cancer. In addition to inappropriate activation of Wnt/β-catenin signaling, with 80% of colon cancer patients exhibiting inactivating mutations in the Wnt antagonist *APC,* mutations in *TP53*, *KRAS*, *SMAD4*, *PIK3CA*, and DNA repair genes are frequently observed (The Cancer Genome Atlas Network, 2012). Colon cancers are further characterized by genomic instability, including chromosomal instability, such as abnormalities in chromosome number, and microsatellite instability, driven by loss of DNA repair activity (Rao and Yamada, 2013). Moreover, epigenetic alterations, such as CpG island methylator phenotype and hypermethylation at tumor suppressor genes, can further influence colon cancer progression (reviewed in Issa, 2004).

Treatments for colon cancer are dependent on the stage of tumor progression. For early stage colon cancers, the main treatments are surgical resection, followed by chemotherapy (e.g. treatment with 5-fluorouracil or oxaliplatin) if local invasion into nearby tissues is observed. For advanced colon cancers, particularly for metastatic diseases, the standard treatment is radiotherapy and chemotherapy. Targeted therapies, such as use of antibodies targeting EGFR and VEGF, have prolonged survival for some colon cancer patients, but efficacy is highly dependent on the mutations present in the tumor, and acquisition of resistance against targeted therapies is common (Maughan et al., 2011; Xie et al., 2020). Immune checkpoint inhibitors have demonstrated efficacy against colon tumors characterized by high microsatellite instability due to deficiencies in the DNA mismatch repair pathway (Le et al., 2017). However, for colon tumors with low mutational burden, which constitute the majority of colon cancer patients, immune checkpoint inhibitors exhibit very limited clinical efficacy (Ganesh et al., 2019). As the prognosis for metastatic colon cancer remains very poor with a 5-year survival rate of 12.5%,

`

there is an urgent need to understand the molecular mechanisms driving malignancy in this disease and develop methods to compromise tumor development.

In vitro *and* in vivo *models to study intestinal cancer*

Experimental model systems that recapitulate major features of colon cancer are valuable tools for elucidating the mechanisms underlying colon tumor initiation and progression. The advent of 3-dimensional (3D) organoid technology has revolutionized our ability to investigate intestinal biology and colon cancer. Organoids are 3D multicellular structures consisting of various organ-specific cell types that self-assemble into structures recapitulating *in vivo* tissue architecture. Importantly, organoid cultures have the potential to provide more accurate representations of tissue physiology than 2D monolayer cultures, including for modeling development, studying interactions with the tumor microenvironment, and assessing response to drug treatments (Clevers, 2016; Duval et al., 2017; Imamura et al., 2015; Luca et al., 2013). Intestinal organoid systems are particularly well-characterized and have become commonly utilized tools for investigating intestinal stem cell and cancer biology. Intestinal organoids can be produced from isolated intestinal stem cells or from stem cell-containing intestinal crypts derived from murine models (Barker et al., 2007; Miyoshi and Stappenbeck, 2013; Sato et al., 2009, 2011). These intestinal organoids are self-renewing (enabling long-term propagation and expansion), and they recapitulate *in vivo* architecture with self-assembling crypt-villus structures consisting of diverse intestinal cell types (Sato et al., 2009). Moreover, intestinal organoids are amenable to genetic manipulation and can be transformed into tumor organoids, which serve as critical research tools for understanding intestinal tumor progression (Drost et al., 2015). Intestinal tumor organoids can also be derived from patient tumor samples and are used for drug screening and personalized therapy design (Es et al., 2018; van de Wetering et al., 2015).

`

In addition to 3D intestinal organoid systems, GEMMs and transplant models of intestinal cancers are invaluable for investigations into intestinal cancer biology. To phenocopy human colon tumors, most of which exhibit aberrant Wnt/β-catenin signaling, several GEMMs have been constructed in which tumor initiation is driven by overactivation of Wnt/β-catenin signaling. One of the first GEMMs of intestinal cancer was the *Apc*^{min} model, which carries a germline mutation in *Apc* and exhibits multiple neoplasias in the intestine before death at around 120 days of age (Moser et al., 1990). Despite the shortened lifespan, this model has been used extensively to study early intestinal tumorigenesis and provided confirmation that intestinal tumorigenesis can be recapitulated in mice through overactive Wnt/β-catenin signaling. In addition to the *Apc*^{min} model, GEMMs of intestinal cancer have been generated in which *Apc* is conditionally deleted in the intestinal epithelium or specifically in the intestinal stem cells, both of which lead to robust initiation of intestinal adenomas particularly when combined with additional mutations in *Kras* and *Trp53* (Barker et al., 2007, 2009; Roper and Hung, 2012).

However, a major drawback to these GEMMs of intestinal cancer is that the tumors are predominantly restricted to the small intestine, while human intestinal cancers primarily occur in the colon (Bürtin et al., 2020; Roper and Hung, 2012). This has spurred the development of autochthonous colon cancer models as well as orthotopic transplant models in which tumor induction occurs in the colons of mice. For example, Roper and colleagues developed a colonoscopy-based injection method to deliver virus or transformed intestinal organoids into the colon epithelium of mice, leading to efficient generation of tumors in the distal mouse colon (Roper et al., 2018). Notably, transplantation of *Apc*$^{-/-}$;*Kras*$^{G12D/+}$;*Trp53*$^{-/-}$ colon organoids result in adenomas that advance to invasive carcinomas and metastasize to the liver, closely reflecting human disease progression (Roper et al., 2018). This transplant model offers a powerful platform to elucidate the mechanisms driving intestinal cancer tumor progression, including allowing interrogation of candidate genes.

`

Cellular plasticity and epigenetic regulation in colon cancer

As one of the fastest renewing tissues in the body, the intestinal epithelium is highly permissive to cellular plasticity, particularly under stress conditions and during tumorigenesis. Under homeostatic conditions, $LGR5^+$ actively cycling stem cells in the bottom of the intestinal crypt self-renew and proliferate to generate transit-amplifying cells (Barker et al., 2007). These cells then differentiate into the specialized cell types of the intestinal epithelium, including absorptive enterocytes, mucus-secreting goblet cells, and Paneth cells that contribute to the stem cell niche. However, a number of studies have demonstrated that following acute injury and loss of the stem cell compartment, multiple cell types, including committed secretory progenitors as well as terminally differentiated Paneth and enteroendocrine cells, can dedifferentiate and replace the $LGR5^+$ stem cell pool (van Es et al., 2012; Schmitt et al., 2018; Tian et al., 2011; Yan et al., 2012, 2017; Yu et al., 2018). These findings emphasize the highly dynamic nature of intestinal epithelial cells, where the reversion of lineage-committed cells into stem cells contributes to regeneration and cellular plasticity.

As in the non-transformed context, colon cancer is characterized by plasticity with dynamic transitions between CSCs and non-CSCs. Xenotransplantation and lineage tracing experiments have identified several putative markers for intestinal CSCs, including expression of CD133 and LGR5 (Kemper et al., 2012; Nakanishi et al., 2013; O'Brien et al., 2007b; Ricci-Vitiani et al., 2007b; Schepers et al., 2012; Vermeulen et al., 2008). Using LGR5 expression as a surrogate marker for CSCs, two groups independently demonstrated that depletion of $LGR5^+$ CSCs resulted in rapid replenishment of the stem cell pool by $LGR5^-$ non-CSCs (Shimokawa et al., 2017; de Sousa e Melo et al., 2017). de Sousa E Melo and colleagues utilized $Apc^{-/-}$; $Kras^{G12D/+}$;$Trp53^{-/-}$ tumor organoids in which exposure to diphtheria toxin selectively ablates $LGR5^+$ stem cells (de Sousa e Melo et al., 2017). These organoids formed tumors upon transplantation into recipient mice, and following administration of diphtheria toxin, $LGR5^+$ cells were ablated specifically in the tumors, and intestinal tumor growth stalled (de Sousa e Melo et

`

al., 2017). Interestingly, withdrawal of diphtheria toxin treatment led to rapid tumor regrowth and re-emergence of a $LGR5^+$ population, indicating that the $LGR5^+$ CSC state can be regenerated from $LGR5^-$ cells (de Sousa e Melo et al., 2017). In another study, Shimokawa and colleagues designed a CRISPR/Cas9 knock-in approach to conditionally and selectively ablate $LGR5^+$ cells in intestinal tumors (Shimokawa et al., 2017). The authors observed that upon elimination of $LGR5^+$ CSCs, post-mitotic tumor cells expressing KRT20 (which is a marker for terminal intestinal differentiation) can repopulate the $LGR5^+$ CSC pool (Shimokawa et al., 2017). These studies underscore the dynamic nature of intestinal tumor cells and the importance of understanding plasticity while designing CSC-targeting therapeutic agents.

While the existence of CSC plasticity is becoming increasingly evident, the molecular mechanisms underlying such plasticity are not yet clearly elucidated. Although overactivation of the Wnt/β-catenin signaling pathway is a hallmark of colon cancers, intratumorally heterogeneous expression of nuclear β-catenin (indicating Wnt signaling activation) is observed in colon cancer patient samples (Brabletz et al., 1998). Staining of nuclear β-catenin is particularly strong in colon cancer cells invading into neighboring stromal tissue, indicating that Wnt signaling, pro-invasive or metastatic programs, and cellular plasticity are intricately linked (Brabletz et al., 1998; Fodde and Brabletz, 2007). Indeed, a recent study identified a phenotypically plastic, stem-like, metastatic, and chemo-resistant population of colon cancer cells with high EMT activation in combination with enhanced Wnt signaling (Sacchetti et al., 2021). Furthermore, there is evidence that the intestinal tumor microenvironment may play a critical role in governing colon CSC plasticity. For example, fibroblasts in the stroma secrete growth factors that promote Wnt signaling and tumorigenicity in colon tumor cells (Lenos et al., 2018; Vermeulen et al., 2010b).

In conjunction with the accumulation of genetic alterations, modulations in epigenetic regulation are major contributors to colon tumorigenicity. As observed in other cancers, CRC is

`

characterized by global hypomethylation with hypermethylation at specific sites, including the promoter regions of key tumor suppressors, such as *CKDN2A*, *APC*, and the mismatch repair gene *hMLH1*, and such epigenetic alterations can drive uncontrolled proliferation and genomic instability (Bihl et al., 2012; Hiltunen et al., 1997; Lee et al., 2004). Notably, a subset of colorectal cancers is characterized by a CpG island methylator phenotype (CIMP) in which overactivity by DNA methyltransferases results in concordant hypermethylation at the promoters of multiple tumor suppressor genes (Toyota et al., 1999). Along with modulations in DNA methylation, colon cancers frequently present with aberrant expression of histone modifiers that are associated with altered colon tumorigenicity. For example, the histone modifiers EZH2 and KDM2B are overexpressed in patient colon cancer tumors, and downregulation of these proteins inhibit cell migration, invasion, and expression of intestinal CSC markers (Sanches et al., 2021). Efforts to carefully elucidate the epigenetic states in colon cancer progression are underway, with several recent studies utilizing single cell sequencing techniques to dissect the epigenomic landscape of colon tumor cells (della Chiara et al., 2021; Meir et al., 2020).

Targeting BMI1 in colon cancer

BMI1 is heavily implicated in both normal intestinal stem cell biology and intestinal tumorigenesis. BMI1 is expressed throughout the intestinal crypt, with particularly high expression in cells in the "+4 position" from the bottom of the crypt (Itzkovitz et al., 2012; Sangiorgi and Capecchi, 2008). Although BMI1 was originally proposed as a marker of intestinal stem cells, further studies showed that BMI1 more likely marks a reserve population of quiescent intestinal stem cells that proliferate and replace actively cycling $LGR5^{+}$ intestinal stem cells upon injury (Yan et al., 2012, 2017). Germline BMI1 loss impairs proliferation of crypt cells and alters the frequency of secretory and absorptive cells, underscoring BMI1's role in stem cell function (López-Arribillaga et al., 2015).

`

BMI1 is overexpressed in human colon tumors, and multiple studies, including research from our lab, have demonstrated an oncogenic role for BMI1 in colon tumorigenesis. Labeling of BMI1-expressing intestinal tumor cells in an inflammation-induced model of sporadic intestinal cancer revealed that a subset of $BMI1^{+}$ cells is capable of clonal expansion, suggesting a possible role for BMI1 in colon tumor propagation (Yanai et al., 2017). Our lab demonstrated that concurrent deletion of *Bmi1* and the tumor suppressor *Apc* specifically in the embryonic intestinal epithelium results in smaller and fewer tumors in a $p19^{ARF}$-dependent manner (Maynard et al., 2014). Such findings indicate a pro-tumorigenic role of BMI1 in small intestinal tumors. However, whether and how BMI1 supports tumorigenesis in the colon cancer context in unclear. Particularly given the poor prognosis of colon cancer patients with metastatic disease, it is of interest to determine whether BMI1 loss can affect tumorigenic processes in advanced colon cancer. In Chapter 3 of this thesis, I will discuss our findings in genetically ablating *Bmi1* in both transformed colon tumor organoids as well as established colon tumors.

V. REMAINING QUESTIONS

While synthesizing the wealth of knowledge regarding epigenetic regulators and cancer, it is evident that: (1) epigenetic regulation is inextricably intertwined with tumorigenic processes, including acquisition of intratumoral heterogeneity, cancer stem-like features, and cellular plasticity, and (2) perturbation of epigenetic regulator activity can have profound, context-dependent effects on tumor development. BMI1 serves as an example of an epigenetic regulator in which loss or overexpression can significantly alter cancer development. The prevailing hypothesis in the field is that loss of BMI1 activity can compromise self-renewal and maintenance of CSCs, the putative cellular drivers of tumor progression, metastatic spreading, and therapy resistance, primarily through derepression of the *Cdkn2a* locus and induction of apoptosis, cell cycle arrest, and/or senescence. Although many studies have established the

`

importance of BMI1 function during embryogenesis, there is a critical lack of knowledge of BMI1's role in established tumors in the adult context. Understanding the context-dependent roles of BMI1 is essential, especially given the significant interest in developing and utilizing pharmacological inhibitors of BMI1 (Cao et al., 2011).

In this thesis, I describe our interrogations into the functions of BMI1 in two epithelial tumor types, lung cancer and colon cancer. Our data show that deletion of *Bmi1* at the initiation of LUAD causes tumor suppression, proliferative impairment, and lifespan extension. In contrast, deletion of *Bmi1 in vivo* in existing lung or colon tumors is not tumor suppressive. Moreover, we reveal an unexpected role of BMI1 as a potential tumor suppressor in existing lung cancer through restraining cells from dedifferentiation, a critical step in the development of malignancy. Collectively, these findings argue that BMI1 inhibitors will at best be ineffective and may actually be harmful to cancer patient in certain contexts.

`

VI. REFERENCES

Abdouh, M., Hanna, R., el Hajjar, J., Flamier, A., and Bernier, G. (2016). The polycomb repressive complex 1 protein BMI1 is required for constitutive heterochromatin formation and silencing in mammalian somatic cells. Journal of Biological Chemistry *291*, 182–197.

Alajez, N. (2016). Significance of BMI1 and FSCN1 expression in colorectal cancer. Saudi Journal of Gastroenterology *22*.

Al-Hajj, M., Wicha, M.S., Benito-Hernandez, A., Morrison, S.J., and Clarke, M.F. (2003). Prospective identification of tumorigenic breast cancer cells. Proceedings of the National Academy of Sciences *100*.

Alzrigat, M., Párraga, A.A., Majumder, M.M., Ma, A., Jin, J., Österborg, A., Nahi, H., Nilsson, K., Heckman, C.A., Öberg, F., et al. (2017). The polycomb group protein BMI-1 inhibitor PTC-209 is a potent anti-myeloma agent alone or in combination with epigenetic inhibitors targeting EZH2 and the BET bromodomains. Oncotarget *8*, 103731–103743.

Andor, N., Graham, T.A., Jansen, M., Xia, L.C., Aktipis, C.A., Petritsch, C., Ji, H.P., and Maley, C.C. (2016). Pan-cancer analysis of the extent and consequences of intratumor heterogeneity. Nature Medicine *22*.

Bannister, A.J., and Kouzarides, T. (2011). Regulation of chromatin by histone modifications. Cell Research *21*.

Barker, N., van Es, J.H., Kuipers, J., Kujala, P., van den Born, M., Cozijnsen, M., Haegebarth, A., Korving, J., Begthel, H., Peters, P.J., et al. (2007). Identification of stem cells in small intestine and colon by marker gene Lgr5. Nature *449*.

Barker, N., Ridgway, R.A., van Es, J.H., van de Wetering, M., Begthel, H., van den Born, M., Danenberg, E., Clarke, A.R., Sansom, O.J., and Clevers, H. (2009). Crypt stem cells as the cells-of-origin of intestinal cancer. Nature *457*.

Becker, M., Korn, C., Sienerth, A.R., Voswinckel, R., Luetkenhaus, K., Ceteci, F., and Rapp, U.R. (2009). Polycomb group protein Bmi1 is required for growth of RAF driven non-small-cell lung cancer. PLoS ONE *4*, 1–10.

Bedard, P.L., Hansen, A.R., Ratain, M.J., and Siu, L.L. (2013). Tumour heterogeneity in the clinic. Nature *501*.

Bednar, F., Schofield, H.K., Collins, M.A., Yan, W., Zhang, Y., Shyam, N., Eberle, J.A., Almada, L.L., Olive, K.P., Bardeesy, N., et al. (2015). Bmi1 is required for the initiation of pancreatic cancer through an Ink4a-independent mechanism. Carcinogenesis *36*.

Begicevic, R.-R., and Falasca, M. (2017). ABC Transporters in Cancer Stem Cells: Beyond Chemoresistance. International Journal of Molecular Sciences *18*.

Belinsky, S.A., Nikula, K.J., Palmisano, W.A., Michels, R., Saccomanno, G., Gabrielson, E., Baylin, S.B., and Herman, J.G. (1998). Aberrant methylation of p16INK4a is an early event in lung cancer and a potential biomarker for early diagnosis. Proceedings of the National Academy of Sciences *95*.

`

Bihl, M.P., Foerster, A., Lugli, A., and Zlobec, I. (2012). Characterization of CDKN2A(p16) methylation and impact in colorectal cancer: systematic analysis using pyrosequencing. Journal of Translational Medicine *10*.

Bolomsky, A., Schlangen, K., Schreiner, W., Zojer, N., and Ludwig, H. (2016). Targeting of BMI-1 with PTC-209 shows potent anti-myeloma activity and impairs the tumour microenvironment. Journal of Hematology and Oncology *9*, 1–13.

Bolomsky, A., Muller, J., Stangelberger, K., Lejeune, M., Duray, E., Breid, H., Vrancken, L., Pfeiffer, C., Hübl, W., Willheim, M., et al. (2020). The anti-mitotic agents PTC-028 and PTC596 display potent activity in pre-clinical models of multiple myeloma but challenge the role of BMI-1 as an essential tumour gene. British Journal of Haematology 1–14.

Borah, A., Raveendran, S., Rochani, A., Maekawa, T., and Kumar, D.S. (2015). Targeting self-renewal pathways in cancer stem cells: clinical implications for cancer therapy. Oncogenesis *4*.

Brabletz, T., Jung, A., Hermann, K., Günther, K., Hohenberger, W., and Kirchner, T. (1998). Nuclear Overexpression of the Oncoprotein β-Catenin in Colorectal Cancer is Localized Predominantly at the Invasion Front. Pathology - Research and Practice *194*.

Bruggeman, S.W.M., Valk-Lingbeek, M.E., van der Stoop, P.P.M., Jacobs, J.J.L., Kieboom, K., Tanger, E., Hulsman, D., Leung, C., Arsenijevic, Y., Marino, S., et al. (2005). Ink4a and Arf differentially affect cell proliferation and neural stem cell self-renewal in Bmi1-deficient mice. Genes & Development *19*.

Bruggeman, S.W.M., Hulsman, D., Tanger, E., Buckle, T., Blom, M., Zevenhoven, J., van Tellingen, O., and van Lohuizen, M. (2007). Bmi1 Controls Tumor Development in an Ink4a/Arf-Independent Manner in a Mouse Model for Glioma. Cancer Cell *12*, 328–341.

Bürtin, F., Mullins, C.S., and Linnebacher, M. (2020). Mouse models of colorectal cancer: Past, present and future perspectives. World Journal of Gastroenterology *26*.

Camolotto, S.A., Pattabiraman, S., Mosbruger, T.L., Jones, A., Belova, V.K., Orstad, G., Streiff, M., Salmond, L., Stubben, C., Kaestner, K.H., et al. (2018). FoxA1 and FoxA2 drive gastric differentiation and suppress squamous identity in NKX2-1-negative lung cancer. ELife *7*, 1–28.

Cao, L., Bombard, J., Cintron, K., Sheedy, J., Weetall, M.L., and Davis, T.W. (2011). BMI1 as a novel target for drug discovery in cancer. Journal of Cellular Biochemistry *112*, 2729–2741.

Cao, R., Tsukada, Y., and Zhang, Y. (2005). Role of Bmi-1 and Ring1A in H2A Ubiquitylation and Hox Gene Silencing. Molecular Cell *20*.

Chaffer, C.L., and Weinberg, R.A. (2015). How Does Multistep Tumorigenesis Really Proceed? Cancer Discovery *5*.

Chaffer, C.L., Brueckmann, I., Scheel, C., Kaestli, A.J., Wiggins, P.A., Rodrigues, L.O., Brooks, M., Reinhardt, F., Su, Y., Polyak, K., et al. (2011). Normal and neoplastic nonstem cells can spontaneously convert to a stem-like state. Proceedings of the National Academy of Sciences *108*.

`

Chaffer, C.L., Marjanovic, N.D., Lee, T., Bell, G., Kleer, C.G., Reinhardt, F., D'Alessio, A.C., Young, R.A., and Weinberg, R.A. (2013). Poised Chromatin at the ZEB1 Promoter Enables Breast Cancer Cell Plasticity and Enhances Tumorigenicity. Cell *154*.

Chatoo, W., Abdouh, M., David, J., Champagne, M.P., Ferreira, J., Rodier, F., and Bernier, G. (2009). The polycomb group gene Bmi1 regulates antioxidant defenses in neurons by repressing p53 pro-oxidant activity. Journal of Neuroscience *29*, 529–542.

Chatterjee, A., Rodger, E.J., and Eccles, M.R. (2018). Epigenetic drivers of tumourigenesis and cancer metastasis. Seminars in Cancer Biology *51*.

Chen, D., Wu, M., Li, Y., Chang, I., Yuan, Q., Ekimyan-Salvo, M., Deng, P., Yu, B., Yu, Y., Dong, J., et al. (2017). Targeting BMI1+ Cancer Stem Cells Overcomes Chemoresistance and Inhibits Metastases in Squamous Cell Carcinoma. Cell Stem Cell *20*, 621–634.e6.

Chen, M.-W., Hua, K.-T., Kao, H.-J., Chi, C.-C., Wei, L.-H., Johansson, G., Shiah, S.-G., Chen, P.-S., Jeng, Y.-M., Cheng, T.-Y., et al. (2010). H3K9 Histone Methyltransferase G9a Promotes Lung Cancer Invasion and Metastasis by Silencing the Cell Adhesion Molecule Ep-CAM. Cancer Research *70*.

della Chiara, G., Gervasoni, F., Fakiola, M., Godano, C., D'Oria, C., Azzolin, L., Bonnal, R.J.P., Moreni, G., Drufuca, L., Rossetti, G., et al. (2021). Epigenomic landscape of human colorectal cancer unveils an aberrant core of pan-cancer enhancers orchestrated by YAP/TAZ. Nature Communications *12*.

Clevers, H. (2016). Modeling Development and Disease with Organoids. Cell *165*.

Collisson, E.A., Campbell, J.D., Brooks, A.N., Berger, A.H., Lee, W., Chmielecki, J., Beer, D.G., Cope, L., Creighton, C.J., Danilova, L., et al. (2014). Comprehensive molecular profiling of lung adenocarcinoma: The cancer genome atlas research network. Nature *511*, 543–550.

Concepcion, C.P., Ma, S., LaFave, L.M., Bhutkar, A., Liu, M., DeAngelo, L.P., Kim, J.Y., del Priore, I., Schoenfeld, A.J., Miller, M., et al. (2021). SMARCA4 inactivation promotes lineage-specific transformation and early metastatic features in the lung. Cancer Discovery.

di Croce, L., and Helin, K. (2013). Transcriptional regulation by Polycomb group proteins. Nature Structural & Molecular Biology *20*.

Curtis, S.J., Sinkevicius, K.W., Li, D., Lau, A.N., Roach, R.R., Zamponi, R., Woolfenden, A.E., Kirsch, D.G., Wong, K.K., and Kim, C.F. (2010). Primary tumor genotype is an important determinant in identification of lung cancer propagating cells. Cell Stem Cell *7*, 127–133.

David, H. (1988). Rudolf Virchow and Modern Aspects of Tumor Pathology. Pathology - Research and Practice *183*.

Desai, A., Webb, B., and Gerson, S.L. (2014). CD133+ cells contribute to radioresistance via altered regulation of DNA repair genes in human lung cancer cells. Radiotherapy and Oncology *110*.

`

Dey, A., Xiong, X., Crim, A., Dwivedi, S.K.D., Mustafi, S.B., Mukherjee, P., Cao, L., Sydorenko, N., Baiazitov, R., Moon, Y.-C., et al. (2018). Evaluating the Mechanism and Therapeutic Potential of PTC-028, a Novel Inhibitor of BMI-1 Function in Ovarian Cancer. Molecular Cancer Therapeutics *17*.

Douglas, D., Hsu, J.H.-R., Hung, L., Cooper, A., Abdueva, D., van Doorninck, J., Peng, G., Shimada, H., Triche, T.J., and Lawlor, E.R. (2008). BMI-1 promotes ewing sarcoma tumorigenicity independent of CDKN2A repression. Cancer Research *68*.

Dovey, J.S., Zacharek, S.J., Kim, C.F., and Lees, J.A. (2008). Bmi1 is critical for lung tumorigenesis and bronchioalveolar stem cell expansion. Proceedings of the National Academy of Sciences *105*.

Drost, J., van Jaarsveld, R.H., Ponsioen, B., Zimberlin, C., van Boxtel, R., Buijs, A., Sachs, N., Overmeer, R.M., Offerhaus, G.J., Begthel, H., et al. (2015). Sequential cancer mutations in cultured human intestinal stem cells. Nature *521*.

Du, J., Li, Y., Li, J., and Zheng, J. (2010). Polycomb group protein Bmi1 expression in colon cancers predicts the survival. Medical Oncology *27*.

Duma, N., Santana-Davila, R., and Molina, J.R. (2019). Non–Small Cell Lung Cancer: Epidemiology, Screening, Diagnosis, and Treatment. Mayo Clinic Proceedings *94*.

Duval, K., Grover, H., Han, L.-H., Mou, Y., Pegoraro, A.F., Fredberg, J., and Chen, Z. (2017). Modeling Physiological Events in 2D vs. 3D Cell Culture. Physiology *32*.

Es, H.A., Montazeri, L., Aref, A.R., Vosough, M., and Baharvand, H. (2018). Personalized Cancer Medicine: An Organoid Approach. Trends in Biotechnology *36*.

van Es, J.H., Sato, T., van de Wetering, M., Lyubimova, A., Yee Nee, A.N., Gregorieff, A., Sasaki, N., Zeinstra, L., van den Born, M., Korving, J., et al. (2012). Dll1+ secretory progenitor cells revert to stem cells upon crypt damage. Nature Cell Biology *14*.

Esteller, M., Corn, P.G., Baylin, S.B., and Herman, J.G. (2001). A gene hypermethylation profile of human cancer. Cancer Research *61*.

Facchino, S., Abdouh, M., Chatoo, W., and Bernier, G. (2010). BMI1 confers radioresistance to normal and cancerous neural stem cells through recruitment of the DNA damage response machinery. Journal of Neuroscience *30*, 10096–10111.

Fearon, E.R. (2011). Molecular Genetics of Colorectal Cancer. Annual Review of Pathology: Mechanisms of Disease *6*.

Fearon, E.R., and Vogelstein, B. (1990). A genetic model for colorectal tumorigenesis. Cell *61*.

Felip, E., Altorki, N., Zhou, C., Csőszi, T., Vynnychenko, I., Goloborodko, O., Luft, A., Akopov, A., Martinez-Marti, A., Kenmotsu, H., et al. (2021). Adjuvant atezolizumab after adjuvant chemotherapy in resected stage IB–IIIA non-small-cell lung cancer (IMpower010): a randomised, multicentre, open-label, phase 3 trial. The Lancet *398*, 1344–1357.

Felsenfeld, G. (2014). A Brief History of Epigenetics. Cold Spring Harbor Perspectives in Biology *6*.

`

Ferretti, R., Bhutkar, A., McNamara, M.C., and Lees, J.A. (2016). BMI1 induces an invasive signature in melanoma that promotes metastasis and chemoresistance. Genes & Development *30*.

Flamier, A., Abdouh, M., Hamam, R., Barabino, A., Patel, N., Gao, A., Hanna, R., and Bernier, G. (2020). Off-target effect of the BMI1 inhibitor PTC596 drives epithelial-mesenchymal transition in glioblastoma multiforme. Npj Precision Oncology *4*.

Flavahan, W.A., Gaskell, E., and Bernstein, B.E. (2017). Epigenetic plasticity and the hallmarks of cancer. Science *357*.

Fodde, R., and Brabletz, T. (2007). Wnt/β-catenin signaling in cancer stemness and malignant behavior. Current Opinion in Cell Biology *19*.

Ganesh, K., Stadler, Z.K., Cercek, A., Mendelsohn, R.B., Shia, J., Segal, N.H., and Diaz, L.A. (2019). Immunotherapy in colorectal cancer: rationale, challenges and potential. Nature Reviews Gastroenterology & Hepatology *16*.

Gerlinger, M., Rowan, A.J., Horswell, S., Larkin, J., Endesfelder, D., Gronroos, E., Martinez, P., Matthews, N., Stewart, A., Tarpey, P., et al. (2012). Intratumor Heterogeneity and Branched Evolution Revealed by Multiregion Sequencing. New England Journal of Medicine *366*.

Gil, J., and O'Loghlen, A. (2014). PRC1 complex diversity: where is it taking us? Trends in Cell Biology *24*.

Ginjala, V., Nacerddine, K., Kulkarni, A., Oza, J., Hill, S.J., Yao, M., Citterio, E., van Lohuizen, M., and Ganesan, S. (2011). BMI1 is recruited to DNA breaks and contributes to DNA damage-induced H2A ubiquitination and repair. Molecular and Cellular Biology *31*.

Goldberg, A.D., Allis, C.D., and Bernstein, E. (2007). Epigenetics: A Landscape Takes Shape. Cell *128*.

Greger, V., Passarge, E., Hopping, W., Messmer, E., and Horsthemke, B. (1989). Epigenetic changes may contribute to the formation and spontaneous regression of retinoblastoma. Human Genetics *83*.

Guo, B.-H., Feng, Y., Zhang, R., Xu, L.-H., Li, M.-Z., Kung, H.-F., Song, L.-B., and Zeng, M.-S. (2011). Bmi-1 promotes invasion and metastasis, and its elevated expression is correlated with an advanced stage of breast cancer. Molecular Cancer *10*.

Gupta, M., Concepcion, C.P., Fahey, C.G., Keshishian, H., Bhutkar, A., Brainson, C.F., Sanchez-Rivera, F.J., Pessina, P., Kim, J.Y., Simoneau, A., et al. (2020). BRG1 Loss Predisposes Lung Cancers to Replicative Stress and ATR Dependency. Cancer Research *80*.

el Hajjar, J., Chatoo, W., Hanna, R., Nkanza, P., Tétreault, N., Tse, Y.C., Wong, T.P., Abdouh, M., and Bernier, G. (2019). Heterochromatic genome instability and neurodegeneration sharing similarities with Alzheimer's disease in old Bmi1+/− mice. Scientific Reports *9*.

Hanahan, D., and Weinberg, R.A. (2011). Hallmarks of Cancer: The Next Generation. Cell *144*.

`

Haraguchi, N., Ishii, H., Mimori, K., Tanaka, F., Ohkuma, M., Kim, H.M., Akita, H., Takiuchi, D., Hatano, H., Nagano, H., et al. (2010). CD13 is a therapeutic target in human liver cancer stem cells. Journal of Clinical Investigation *120*.

Herbst, R.S., Giaccone, G., de Marinis, F., Reinmuth, N., Vergnenegre, A., Barrios, C.H., Morise, M., Felip, E., Andric, Z., Geater, S., et al. (2020). Atezolizumab for First-Line Treatment of PD-L1–Selected Patients with NSCLC. New England Journal of Medicine *383*, 1328–1339.

Hiltunen, M.O., Alhonen, L., Koistinaho, J., Myöhänen, S., Pääkkönen, M., Marin, S., Kosma, V.M., and Jänne, J. (1997). Hypermethylation of the APC (adenomatous polyposis coli) gene promoter region in human colorectal carcinoma. International Journal of Cancer *70*.

Hu, T., Kitano, A., Luu, V., Dawson, B., Hoegenauer, K.A., Lee, B.H., and Nakada, D. (2019). Bmi1 Suppresses Adipogenesis in the Hematopoietic Stem Cell Niche. Stem Cell Reports *13*.

Hurt, E.M., Kawasaki, B.T., Klarmann, G.J., Thomas, S.B., and Farrar, W.L. (2008). CD44+CD24− prostate cells are early cancer progenitor/stem cells that provide a model for patients with poor prognosis. British Journal of Cancer *98*.

Imamura, Y., Mukohara, T., Shimono, Y., Funakoshi, Y., Chayahara, N., Toyoda, M., Kiyota, N., Takao, S., Kono, S., Nakatsura, T., et al. (2015). Comparison of 2D- and 3D-culture models as drug-testing platforms in breast cancer. Oncology Reports *33*.

Issa, J.-P. (2004). CpG island methylator phenotype in cancer. Nature Reviews Cancer *4*, 988–993.

Itzkovitz, S., Lyubimova, A., Blat, I.C., Maynard, M., van Es, J., Lees, J., Jacks, T., Clevers, H., and van Oudenaarden, A. (2012). Single-molecule transcript counting of stem-cell markers in the mouse intestine. Nature Cell Biology *14*.

Iwama, A., Oguro, H., Negishi, M., Kato, Y., Morita, Y., Tsukui, H., Ema, H., Kamijo, T., Katoh-Fukui, Y., Koseki, H., et al. (2004). Enhanced Self-Renewal of Hematopoietic Stem Cells Mediated by the Polycomb Gene Product Bmi-1. Immunity *21*.

Jackson, E.L., Willis, N., Mercer, K., Bronson, R.T., Crowley, D., Montoya, R., Jacks, T., and Tuveson, D.A. (2001). Analysis of lung tumor initiation and progression using conditional expression of oncogenic K-ras. Genes & Development *15*.

Jackson, E.L., Olive, K.P., Tuveson, D.A., Bronson, R., Crowley, D., Brown, M., and Jacks, T. (2005). The Differential Effects of Mutant p53 Alleles on Advanced Murine Lung Cancer. Cancer Research *65*, 10280–10288.

Jacobs, J.J.L., Kieboom, K., Marino, S., DePinho, R.A., and van Lohuizen, M. (1999a). The oncogene and Polycomb-group gene bmi-1 regulates cell proliferation and senescence through the ink4a locus. Nature *397*.

Jacobs, J.J.L., Scheijen, B., Voncken, J.W., Kieboom, K., Berns, A., and van Lohuizen, M. (1999b). Bmi-1 collaborates with c-Myc in tumorigenesis by inhibiting c-Myc- induced apoptosis via INK4a/ARF. Genes and Development *13*, 2678–2690.

`

Johnson, L., Mercer, K., Greenbaum, D., Bronson, R.T., Crowley, D., Tuveson, D.A., and Jacks, T. (2001). Somatic activation of the K-ras oncogene causes early onset lung cancer in mice. Nature *410*.

Jones, B.A., Varambally, S., and Arend, R.C. (2018). Histone Methyltransferase EZH2: A Therapeutic Target for Ovarian Cancer. Molecular Cancer Therapeutics *17*.

Kandoth, C., McLellan, M.D., Vandin, F., Ye, K., Niu, B., Lu, C., Xie, M., Zhang, Q., McMichael, J.F., Wyczalkowski, M.A., et al. (2013). Mutational landscape and significance across 12 major cancer types. Nature *502*.

Kemper, K., Prasetyanti, P.R., de Lau, W., Rodermond, H., Clevers, H., and Medema, J.P. (2012). Monoclonal Antibodies Against Lgr5 Identify Human Colorectal Cancer Stem Cells. Stem Cells *30*.

Keum, N., and Giovannucci, E. (2019). Global burden of colorectal cancer: emerging trends, risk factors and prevention strategies. Nature Reviews Gastroenterology & Hepatology *16*.

Kim, K.H., and Roberts, C.W.M. (2016). Targeting EZH2 in cancer. Nature Medicine *22*.

Kim, J.H., Yoon, S.Y., Kim, C.-N., Joo, J.H., Moon, S.K., Choe, I.S., Choe, Y.-K., and Kim, J.W. (2004). The Bmi-1 oncoprotein is overexpressed in human colorectal cancer and correlates with the reduced p16INK4a/p14ARF proteins. Cancer Letters *203*.

Kleer, C.G., Cao, Q., Varambally, S., Shen, R., Ota, I., Tomlins, S.A., Ghosh, D., Sewalt, R.G.A.B., Otte, A.P., Hayes, D.F., et al. (2003). EZH2 is a marker of aggressive breast cancer and promotes neoplastic transformation of breast epithelial cells. Proceedings of the National Academy of Sciences *100*.

Kleinsmith, L.J., and Pierce, G.B. (1964). Multipotentiality of single embryonal carcinoma cells. Cancer Research *24*.

Kreso, A., van Galen, P., Pedley, N.M., Lima-Fernandes, E., Frelin, C., Davis, T., Cao, L., Baiazitov, R., Du, W., Sydorenko, N., et al. (2014). Self-renewal as a therapeutic target in human colorectal cancer. Nature Medicine *20*, 29–36.

Kwon, M., and Berns, A. (2013). Mouse models for lung cancer. Molecular Oncology *7*.

LaFave, L.M., Kartha, V.K., Ma, S., Meli, K., del Priore, I., Lareau, C., Naranjo, S., Westcott, P.M.K., Duarte, F.M., Sankar, V., et al. (2020). Epigenomic State Transitions Characterize Tumor Progression in Mouse Lung Adenocarcinoma. Cancer Cell *38*, 212–228.e13.

Längst, G., and Manelyte, L. (2015). Chromatin Remodelers: From Function to Dysfunction. Genes *6*.

Lapidot, T., Sirard, C., Vormoor, J., Murdoch, B., Hoang, T., Caceres-Cortes, J., Minden, M., Paterson, B., Caligiuri, M.A., and Dick, J.E. (1994). A cell initiating human acute myeloid leukaemia after transplantation into SCID mice. Nature *367*.

Lathia, J.D., Mack, S.C., Mulkearns-Hubert, E.E., Valentim, C.L.L., and Rich, J.N. (2015). Cancer stem cells in glioblastoma. Genes & Development *29*.

`

Lawson, D.A., Bhakta, N.R., Kessenbrock, K., Prummel, K.D., Yu, Y., Takai, K., Zhou, A., Eyob, H., Balakrishnan, S., Wang, C.-Y., et al. (2015). Single-cell analysis reveals a stem-cell program in human metastatic breast cancer cells. Nature *526*.

Le, D.T., Durham, J.N., Smith, K.N., Wang, H., Bartlett, B.R., Aulakh, L.K., Lu, S., Kemberling, H., Wilt, C., Luber, B.S., et al. (2017). Mismatch repair deficiency predicts response of solid tumors to PD-1 blockade. Science *357*.

Lee, C.K., Wu, Y.-L., Ding, P.N., Lord, S.J., Inoue, A., Zhou, C., Mitsudomi, T., Rosell, R., Pavlakis, N., Links, M., et al. (2015). Impact of Specific Epidermal Growth Factor Receptor (EGFR) Mutations and Clinical Characteristics on Outcomes After Treatment With EGFR Tyrosine Kinase Inhibitors Versus Chemotherapy in EGFR-Mutant Lung Cancer: A Meta-Analysis. Journal of Clinical Oncology *33*.

Lee, S., Hwang, K.S., Lee, H.J., Kim, J.-S., and Kang, G.H. (2004). Aberrant CpG island hypermethylation of multiple genes in colorectal neoplasia. Laboratory Investigation *84*.

Lemjabbar-Alaoui, H., Hassan, O.U., Yang, Y.-W., and Buchanan, P. (2015). Lung cancer: Biology and treatment options. Biochimica et Biophysica Acta (BBA) - Reviews on Cancer *1856*.

Lenos, K.J., Miedema, D.M., Lodestijn, S.C., Nijman, L.E., van den Bosch, T., Romero Ros, X., Lourenço, F.C., Lecca, M.C., van der Heijden, M., van Neerven, S.M., et al. (2018). Stem cell functionality is microenvironmentally defined during tumour expansion and therapy response in colon cancer. Nature Cell Biology *20*.

Lessard, J., and Sauvageau, G. (2003). Bmi-1 determines the proliferative capacity of normal and leukaemic stem cells. Nature *423*.

Lessard, J., Baban, S., and Sauvageau, G. (1998). Stage-specific expression of polycomb group genes in human bone marrow cells. Blood *91*.

Lim, Z.-F., and Ma, P.C. (2019). Emerging insights of tumor heterogeneity and drug resistance mechanisms in lung cancer targeted therapy. Journal of Hematology & Oncology *12*.

Liu, J., Cao, L., Chen, J., Song, S., Lee, I.H., Quijano, C., Liu, H., Keyvanfar, K., Chen, H., Cao, L.Y., et al. (2009). Bmi1 regulates mitochondrial function and the DNA damage response pathway. Nature *459*, 387–392.

Liu, S., Cong, Y., Wang, D., Sun, Y., Deng, L., Liu, Y., Martin-Trevino, R., Shang, L., McDermott, S.P., Landis, M.D., et al. (2014). Breast Cancer Stem Cells Transition between Epithelial and Mesenchymal States Reflective of their Normal Counterparts. Stem Cell Reports *2*.

van Lohuizen, M., Verbeek, S., Scheljen, B., Wientjens, E., van der Guidon, H., and Berns, A. (1991a). Identification of cooperating oncogenes in Eμ-myc transgenic mice by provirus tagging. Cell *65*, 737–752.

van Lohuizen, M., Frasch, M., Wientjens, E., and Berns, A. (1991b). Sequence similarity between the mammalian bmi-1 proto-oncogene and the Drosophila regulatory genes Psc and Su(z)2. Nature *353*.

`

López-Arribillaga, E., Rodilla, V., Pellegrinet, L., Guiu, J., Iglesias, M., Roman, A.C., Gutarra, S., González, S., Muñoz-Cánoves, P., Fernández-Salguero, P., et al. (2015). Bmi1 regulates murine intestinal stem cell proliferation and self-renewal downstream of Notch. Development (Cambridge) *142*, 41–50.

Loubiere, V., Papadopoulos, G.L., Szabo, Q., Martinez, A.-M., and Cavalli, G. (2020). Widespread activation of developmental gene expression characterized by PRC1-dependent chromatin looping. Science Advances *6*.

Luca, A.C., Mersch, S., Deenen, R., Schmidt, S., Messner, I., Schäfer, K.-L., Baldus, S.E., Huckenbeck, W., Piekorz, R.P., Knoefel, W.T., et al. (2013). Impact of the 3D Microenvironment on Phenotype, Gene Expression, and EGFR Inhibition of Colorectal Cancer Cell Lines. PLoS ONE *8*.

van der Lugt, N.M.T., Domen, J., Linders, K., van Roon, M., Robanus-Maandag, E., te Riele, H., van der Valk, M., Deschamps, J., Sofroniew, M., van Lohuizen, M., et al. (1994). Posterior transformation, neurological abnormalities, and severe hematopoietic defects in mice with a targeted deletion of the bmi-1 proto- oncogene. Genes and Development *8*, 757–769.

van der Lugt, N.M.T., Alkema, M., Berns, A., and Deschamps, J. (1996). The Polycomb-group homolog Bmi-1 is a regulator of murine Hox gene expression. Mechanisms of Development *58*.

Marjanovic, N.D., Hofree, M., Chan, J.E., Canner, D., Wu, K., Trakala, M., Hartmann, G.G., Smith, O.C., Kim, J.Y., Evans, K.V., et al. (2020). Emergence of a High-Plasticity Cell State during Lung Cancer Evolution. Cancer Cell *38*, 229–246.e13.

Marley, A.R., and Nan, H. (2016). Epidemiology of colorectal cancer. International Journal of Molecular Epidemiology and Genetics *7*.

Martins-Neves, S.R., Paiva-Oliveira, D.I., Wijers-Koster, P.M., Abrunhosa, A.J., Fontes-Ribeiro, C., Bovée, J.V.M.G., Cleton-Jansen, A.-M., and Gomes, C.M.F. (2016). Chemotherapy induces stemness in osteosarcoma cells through activation of Wnt/β-catenin signaling. Cancer Letters *370*.

Masliah-Planchon, J., Bièche, I., Guinebretière, J.-M., Bourdeaut, F., and Delattre, O. (2015). SWI/SNF Chromatin Remodeling and Human Malignancies. Annual Review of Pathology: Mechanisms of Disease *10*.

Maughan, T.S., Adams, R.A., Smith, C.G., Meade, A.M., Seymour, M.T., Wilson, R.H., Idziaszczyk, S., Harris, R., Fisher, D., Kenny, S.L., et al. (2011). Addition of cetuximab to oxaliplatin-based first-line combination chemotherapy for treatment of advanced colorectal cancer: results of the randomised phase 3 MRC COIN trial. The Lancet *377*.

Maynard, M.A., Ferretti, R., Hilgendorf, K.I., Perret, C., Whyte, P., and Lees, J.A. (2014). Bmi1 is required for tumorigenesis in a mouse model of intestinal cancer. Oncogene *33*.

McFadden, D.G., Politi, K., Bhutkar, A., Chen, F.K., Song, X., Pirun, M., Santiago, P.M., Kim-Kiselak, C., Platt, J.T., Lee, E., et al. (2016). Mutational landscape of EGFR-, MYC-, and Kras-driven genetically engineered mouse models of lung adenocarcinoma. Proceedings

of the National Academy of Sciences of the United States of America *113*, E6409–E6417.

Medema, J.P. (2013). Cancer stem cells: The challenges ahead. Nature Cell Biology *15*, 338–344.

Meir, Z., Mukamel, Z., Chomsky, E., Lifshitz, A., and Tanay, A. (2020). Single-cell analysis of clonal maintenance of transcriptional and epigenetic states in cancer cells. Nature Genetics *52*.

Melling, N., Thomsen, E., Tsourlakis, M.C., Kluth, M., Hube-Magg, C., Minner, S., Koop, C., Graefen, M., Heinzer, H., Wittmer, C., et al. (2015). Overexpression of enhancer of zeste homolog 2 (EZH2) characterizes an aggressive subset of prostate cancers and predicts patient prognosis independently from pre- and postoperatively assessed clinicopathological parameters. Carcinogenesis *36*.

Mercer, T.R., and Mattick, J.S. (2013). Structure and function of long noncoding RNAs in epigenetic regulation. Nature Structural & Molecular Biology *20*.

Merlo, A., Herman, J.G., Mao, L., Lee, D.J., Gabrielson, E., Burger, P.C., Baylin, S.B., and Sidransky, D. (1995). 5′ CpG island methylation is associated with transcriptional silencing of the tumour suppressor p16/CDKN2/MTS1 in human cancers. Nature Medicine *1*.

Miyoshi, H., and Stappenbeck, T.S. (2013). In vitro expansion and genetic modification of gastrointestinal stem cells in spheroid culture. Nature Protocols *8*.

Molofsky, A. v., Pardal, R., Iwashita, T., Park, I.-K., Clarke, M.F., and Morrison, S.J. (2003). Bmi-1 dependence distinguishes neural stem cell self-renewal from progenitor proliferation. Nature *425*.

Molofsky, A. v, He, S., Bydon, M., Morrison, S.J., and Pardal, R. (2005). Bmi-1 promotes neural stem cell self-renewal and neural development but not mouse growth and survival by repressing the p16Ink4a and p19Arf senescence pathways. Genes & Development *19*.

Moore, L.D., Le, T., and Fan, G. (2013). DNA Methylation and Its Basic Function. Neuropsychopharmacology *38*.

Morrisey, E.E., and Hogan, B.L.M. (2010). Preparing for the First Breath: Genetic and Cellular Mechanisms in Lung Development. Developmental Cell *18*, 8–23.

Moser, A.R., Pitot, H.C., and Dove, W.F. (1990). A Dominant Mutation That Predisposes to Multiple Intestinal Neoplasia in the Mouse. Science *247*.

Nakanishi, Y., Seno, H., Fukuoka, A., Ueo, T., Yamaga, Y., Maruno, T., Nakanishi, N., Kanda, K., Komekado, H., Kawada, M., et al. (2013). Dclk1 distinguishes between tumor and normal stem cells in the intestine. Nature Genetics *45*.

Nowell, P.C. (1976). The Clonal Evolution of Tumor Cell Populations. Science *194*.

Nuovo, G.J., Plaia, T.W., Belinsky, S.A., Baylin, S.B., and Herman, J.G. (1999). In situ detection of the hypermethylation-induced inactivation of the p16 gene as an early event in oncogenesis. Proceedings of the National Academy of Sciences *96*.

`

O'Brien, C.A., Pollett, A., Gallinger, S., and Dick, J.E. (2007a). A human colon cancer cell capable of initiating tumour growth in immunodeficient mice. Nature *445*.

O'Brien, C.A., Pollett, A., Gallinger, S., and Dick, J.E. (2007b). A human colon cancer cell capable of initiating tumour growth in immunodeficient mice. Nature *445*.

Oguro, H., Iwama, A., Morita, Y., Kamijo, T., van Lohuizen, M., and Nakauchi, H. (2006). Differential impact of Ink4a and Arf on hematopoietic stem cells and their bone marrow microenvironment in Bmi1-deficient mice. Journal of Experimental Medicine *203*.

Oguro, H., Yuan, J., Ichikawa, H., Ikawa, T., Yamazaki, S., Kawamoto, H., Nakauchi, H., and Iwama, A. (2010). Poised Lineage Specification in Multipotential Hematopoietic Stem and Progenitor Cells by the Polycomb Protein Bmi1. Cell Stem Cell *6*.

Park, I., Qian, D., Kiel, M., Becker, M.W., Pihalja, M., Weissman, I.L., Morrison, S.J., and Clarke, M.F. (2003). Bmi-1 is required for maintenance of adult self-renewing haematopoietic stem cells. Nature *423*.

Pengelly, A.R., Kalb, R., Finkl, K., and Müller, J. (2015). Transcriptional repression by PRC1 in the absence of H2A monoubiquitylation. Genes & Development *29*.

Pietersen, A.M., Evers, B., Prasad, A.A., Tanger, E., Cornelissen-Steijger, P., Jonkers, J., and van Lohuizen, M. (2008). Bmi1 Regulates Stem Cells and Proliferation and Differentiation of Committed Cells in Mammary Epithelium. Current Biology *18*.

Piotrowska, Z., Niederst, M.J., Karlovich, C.A., Wakelee, H.A., Neal, J.W., Mino-Kenudson, M., Fulton, L., Hata, A.N., Lockerman, E.L., Kalsy, A., et al. (2015). Heterogeneity Underlies the Emergence of EGFRT790 Wild-Type Clones Following Treatment of T790M-Positive Cancers with a Third-Generation EGFR Inhibitor. Cancer Discovery *5*.

Quintana, E., Shackleton, M., Sabel, M.S., Fullen, D.R., Johnson, T.M., and Morrison, S.J. (2008). Efficient tumour formation by single human melanoma cells. Nature *456*.

Rao, C. v., and Yamada, H.Y. (2013). Genomic Instability and Colon Carcinogenesis: From the Perspective of Genes. Frontiers in Oncology *3*.

Ricci-Vitiani, L., Lombardi, D.G., Pilozzi, E., Biffoni, M., Todaro, M., Peschle, C., and de Maria, R. (2007a). Identification and expansion of human colon-cancer-initiating cells. Nature *445*.

Ricci-Vitiani, L., Lombardi, D.G., Pilozzi, E., Biffoni, M., Todaro, M., Peschle, C., and de Maria, R. (2007b). Identification and expansion of human colon-cancer-initiating cells. Nature *445*.

Roper, J., and Hung, K.E. (2012). Priceless GEMMs: genetically engineered mouse models for colorectal cancer drug development. Trends in Pharmacological Sciences *33*.

Roper, J., Tammela, T., Akkad, A., Almeqdadi, M., Santos, S.B., Jacks, T., and Yilmaz, Ö.H. (2018). Colonoscopy-based colorectal cancer modeling in mice with CRISPR-Cas9 genome editing and organoid transplantation. Nature Protocols *13*.

Rowbotham, S.P., Li, F., Dost, A.F.M., Louie, S.M., Marsh, B.P., Pessina, P., Anbarasu, C.R., Brainson, C.F., Tuminello, S.J., Lieberman, A., et al. (2018). H3K9 methyltransferases

and demethylases control lung tumor-propagating cells and lung cancer progression. Nature Communications *9*.

Rycaj, K., and Tang, D.G. (2015). Cell-of-Origin of Cancer versus Cancer Stem Cells: Assays and Interpretations. Cancer Research *75*.

Sacchetti, A., Teeuwssen, M., Verhagen, M., Joosten, R., Xu, T., Stabile, R., van der Steen, B., Watson, M.M., Gusinac, A., Kim, W.K., et al. (2021). Phenotypic plasticity underlies local invasion and distant metastasis in colon cancer. ELife *10*.

Sanches, J.G.P., Song, B., Zhang, Q., Cui, X., Yabasin, I.B., Ntim, M., Li, X., He, J., Zhang, Y., Mao, J., et al. (2021). The Role of KDM2B and EZH2 in Regulating the Stemness in Colorectal Cancer Through the PI3K/AKT Pathway. Frontiers in Oncology *11*.

Sanchez-Rivera, F.J., Papagiannakopoulos, T., Romero, R., Tammela, T., Bauer, M.R., Bhutkar, A., Joshi, N.S., Subbaraj, L., Bronson, R.T., Xue, W., et al. (2014). Rapid modelling of cooperating genetic events in cancer through somatic genome editing. Nature *516*, 428–431.

Sangiorgi, E., and Capecchi, M.R. (2008). Bmi1 is expressed in vivo in intestinal stem cells. Nature Genetics *40*.

Sato, T., Vries, R.G., Snippert, H.J., van de Wetering, M., Barker, N., Stange, D.E., van Es, J.H., Abo, A., Kujala, P., Peters, P.J., et al. (2009). Single Lgr5 stem cells build crypt-villus structures in vitro without a mesenchymal niche. Nature *459*.

Sato, T., Stange, D.E., Ferrante, M., Vries, R.G.J., van Es, J.H., van den Brink, S., van Houdt, W.J., Pronk, A., van Gorp, J., Siersema, P.D., et al. (2011). Long-term Expansion of Epithelial Organoids From Human Colon, Adenoma, Adenocarcinoma, and Barrett's Epithelium. Gastroenterology *141*.

Schepers, A.G., Snippert, H.J., Stange, D.E., van den Born, M., van Es, J.H., van de Wetering, M., and Clevers, H. (2012). Lineage tracing reveals Lgr5+ stem cell activity in mouse intestinal adenomas. Science (New York, N.Y.) *337*.

Schmitt, M., Schewe, M., Sacchetti, A., Feijtel, D., van de Geer, W.S., Teeuwssen, M., Sleddens, H.F., Joosten, R., van Royen, M.E., van de Werken, H.J.G., et al. (2018). Paneth Cells Respond to Inflammation and Contribute to Tissue Regeneration by Acquiring Stem-like Features through SCF/c-Kit Signaling. Cell Reports *24*.

Schoenfeld, A.J., Bandlamudi, C., Lavery, J.A., Montecalvo, J., Namakydoust, A., Rizvi, H., Egger, J., Concepcion, C.P., Paul, S., Arcila, M.E., et al. (2020). The Genomic Landscape of SMARCA4 Alterations and Associations with Outcomes in Patients with Lung Cancer. Clinical Cancer Research *26*.

Schwitalla, S., Fingerle, A.A., Cammareri, P., Nebelsiek, T., Göktuna, S.I., Ziegler, P.K., Canli, O., Heijmans, J., Huels, D.J., Moreaux, G., et al. (2013). Intestinal Tumorigenesis Initiated by Dedifferentiation and Acquisition of Stem-Cell-like Properties. Cell *152*.

Selamat, S.A., Galler, J.S., Joshi, A.D., Fyfe, M.N., Campan, M., Siegmund, K.D., Kerr, K.M., and Laird-Offringa, I.A. (2011). DNA Methylation Changes in Atypical Adenomatous Hyperplasia, Adenocarcinoma In Situ, and Lung Adenocarcinoma. PLoS ONE *6*.

`

Shimokawa, M., Ohta, Y., Nishikori, S., Matano, M., Takano, A., Fujii, M., Date, S., Sugimoto, S., Kanai, T., and Sato, T. (2017). Visualization and targeting of LGR5+ human colon cancer stem cells. Nature *545*.

Smith, Z.D., and Meissner, A. (2013). DNA methylation: roles in mammalian development. Nature Reviews Genetics *14*.

Smith, B.A., Balanis, N.G., Nanjundiah, A., Sheu, K.M., Tsai, B.L., Zhang, Q., Park, J.W., Thompson, M., Huang, J., Witte, O.N., et al. (2018). A Human Adult Stem Cell Signature Marks Aggressive Variants across Epithelial Cancers. Cell Reports *24*.

Snyder, E.L., Watanabe, H., Magendantz, M., Hoersch, S., Chen, T.A., Wang, D.G., Crowley, D., Whittaker, C.A., Meyerson, M., Kimura, S., et al. (2013). Nkx2-1 Represses a Latent Gastric Differentiation Program in Lung Adenocarcinoma. Molecular Cell *50*, 185–199.

Song, L.-B., Li, J., Liao, W.-T., Feng, Y., Yu, C.-P., Hu, L.-J., Kong, Q.-L., Xu, L.-H., Zhang, X., Liu, W.-L., et al. (2009). The polycomb group protein Bmi-1 represses the tumor suppressor PTEN and induces epithelial-mesenchymal transition in human nasopharyngeal epithelial cells. Journal of Clinical Investigation *119*.

de Sousa e Melo, F., Kurtova, A. v., Harnoss, J.M., Kljavin, N., Hoeck, J.D., Hung, J., Anderson, J.E., Storm, E.E., Modrusan, Z., Koeppen, H., et al. (2017). A distinct role for Lgr5+ stem cells in primary and metastatic colon cancer. Nature *543*.

Sulaiman, S., Arafat, K., Iratni, R., and Attoub, S. (2019). PTC-209 Anti-Cancer Effects Involved the Inhibition of STAT3 Phosphorylation. Frontiers in Pharmacology *10*.

Sullivan, I., and Planchard, D. (2016). ALK inhibitors in non-small cell lung cancer: the latest evidence and developments. Therapeutic Advances in Medical Oncology *8*.

Sung, H., Ferlay, J., Siegel, R.L., Laversanne, M., Soerjomataram, I., Jemal, A., and Bray, F. (2021). Global Cancer Statistics 2020: GLOBOCAN Estimates of Incidence and Mortality Worldwide for 36 Cancers in 185 Countries. CA: A Cancer Journal for Clinicians *71*.

Sutherland, K.D., Song, J.Y., Kwon, M.C., Proost, N., Zevenhoven, J., and Berns, A. (2014). Multiple cells-of-origin of mutant K-Ras-induced mouse lung adenocarcinoma. Proceedings of the National Academy of Sciences of the United States of America *111*, 4952–4957.

Tavares, L., Dimitrova, E., Oxley, D., Webster, J., Poot, R., Demmers, J., Bezstarosti, K., Taylor, S., Ura, H., Koide, H., et al. (2012). RYBP-PRC1 Complexes Mediate H2A Ubiquitylation at Polycomb Target Sites Independently of PRC2 and H3K27me3. Cell *148*.

Thakur, B., and Ray, P. (2017). Cisplatin triggers cancer stem cell enrichment in platinum-resistant cells through NF-κB-TNFα-PIK3CA loop. Journal of Experimental & Clinical Cancer Research *36*.

The Cancer Genome Atlas Network (2012). Comprehensive molecular characterization of human colon and rectal cancer. Nature *487*.

`

Tian, H., Biehs, B., Warming, S., Leong, K.G., Rangell, L., Klein, O.D., and de Sauvage, F.J. (2011). A reserve stem cell population in small intestine renders Lgr5-positive cells dispensable. Nature *478*.

Titford, M. (2010). Rudolf Virchow: Cellular Pathologist. Laboratory Medicine *41*.

Toyota, M., Ahuja, N., Ohe-Toyota, M., Herman, J.G., Baylin, S.B., and Issa, J.-P.J. (1999). CpG island methylator phenotype in colorectal cancer. Proceedings of the National Academy of Sciences *96*.

Turdo, A., Veschi, V., Gaggianesi, M., Chinnici, A., Bianca, P., Todaro, M., and Stassi, G. (2019). Meeting the Challenge of Targeting Cancer Stem Cells. Frontiers in Cell and Developmental Biology *7*.

van de Wetering, M., Francies, H.E., Francis, J.M., Bounova, G., Iorio, F., Pronk, A., van Houdt, W., van Gorp, J., Taylor-Weiner, A., Kester, L., et al. (2015). Prospective Derivation of a Living Organoid Biobank of Colorectal Cancer Patients. Cell *161*.

Vermeulen, L., Todaro, M., de Sousa Mello, F., Sprick, M.R., Kemper, K., Perez Alea, M., Richel, D.J., Stassi, G., and Medema, J.P. (2008). Single-cell cloning of colon cancer stem cells reveals a multi-lineage differentiation capacity. Proceedings of the National Academy of Sciences *105*.

Vermeulen, L., de Sousa E Melo, F., van der Heijden, M., Cameron, K., de Jong, J.H., Borovski, T., Tuynman, J.B., Todaro, M., Merz, C., Rodermond, H., et al. (2010a). Wnt activity defines colon cancer stem cells and is regulated by the microenvironment. Nature Cell Biology *12*.

Vermeulen, L., de Sousa E Melo, F., van der Heijden, M., Cameron, K., de Jong, J.H., Borovski, T., Tuynman, J.B., Todaro, M., Merz, C., Rodermond, H., et al. (2010b). Wnt activity defines colon cancer stem cells and is regulated by the microenvironment. Nature Cell Biology *12*.

Vessoni, A.T., Filippi-Chiela, E.C., Lenz, G., and Batista, L.F.Z. (2020). Tumor propagating cells: drivers of tumor plasticity, heterogeneity, and recurrence. Oncogene *39*.

Visvader, J.E., and Lindeman, G.J. (2012). Cancer Stem Cells: Current Status and Evolving Complexities. Cell Stem Cell *10*.

Vonlanthen, S., Heighway, J., Altermatt, H.J., Gugger, M., Kappeler, A., Borner, M.M., van Lohuizen, M., and Betticher, D.C. (2001). The bmi-1 oncoprotein is differentially expressed in non-small cell lung cancer and correlates with INK4A-ARF locus expression. British Journal of Cancer *84*, 1372–1376.

Vrzalikova, K., Skarda, J., Ehrmann, J., Murray, P.G., Fridman, E., Kopolovic, J., Knizetova, P., Hajduch, M., Klein, J., Kolek, V., et al. (2008). Prognostic value of Bmi-1 oncoprotein expression in NSCLC patients: a tissue microarray study. Journal of Cancer Research and Clinical Oncology *134*, 1037–1042.

Wan, L., Li, X., Shen, H., and Bai, X. (2013). Quantitative analysis of EZH2 expression and its correlations with lung cancer patients' clinical pathological characteristics. Clinical and Translational Oncology *15*.

`

Wang, H., Wang, L., Erdjument-Bromage, H., Vidal, M., Tempst, P., Jones, R.S., and Zhang, Y. (2004). Role of histone H2A ubiquitination in Polycomb silencing. Nature *431*.

Wang, X., Zhao, H., Lv, L., Bao, L., Wang, X., and Han, S. (2016). Prognostic Significance of EZH2 Expression in Non-Small Cell Lung Cancer: A Meta-analysis. Scientific Reports *6*.

Wang, X., Ricciuti, B., Nguyen, T., Li, X., Rabin, M.S., Awad, M.M., Lin, X., Johnson, B.E., and Christiani, D.C. (2021). Association between Smoking History and Tumor Mutation Burden in Advanced Non–Small Cell Lung Cancer. Cancer Research *81*.

Wei, J., Zhai, L., Xu, J., and Wang, H. (2006). Role of Bmi1 in H2A Ubiquitylation and Hox Gene Silencing. Journal of Biological Chemistry *281*.

Westcott, P.M.K., Halliwill, K.D., To, M.D., Rashid, M., Rust, A.G., Keane, T.M., Delrosario, R., Jen, K.Y., Gurley, K.E., Kemp, C.J., et al. (2015). The mutational landscapes of genetic and chemical models of Kras-driven lung cancer. Nature *517*, 489–492.

Winslow, M.M., Dayton, T.L., Verhaak, R.G.W., Kim-Kiselak, C., Snyder, E.L., Feldser, D.M., Hubbard, D.D., Dupage, M.J., Whittaker, C.A., Hoersch, S., et al. (2011). Suppression of lung adenocarcinoma progression by Nkx2-1. Nature *473*, 101–104.

Xie, Y.-H., Chen, Y.-X., and Fang, J.-Y. (2020). Comprehensive review of targeted therapy for colorectal cancer. Signal Transduction and Targeted Therapy *5*.

Xu, X., Rock, J.R., Lu, Y., Futtner, C., Schwab, B., Guinney, J., Hogan, B.L.M., and Onaitis, M.W. (2012). Evidence for type II cells as cells of origin of K-Ras - Induced distal lung adenocarcinoma. Proceedings of the National Academy of Sciences of the United States of America *109*, 4910–4915.

Yan, K.S., Chia, L.A., Li, X., Ootani, A., Su, J., Lee, J.Y., Su, N., Luo, Y., Heilshorn, S.C., Amieva, M.R., et al. (2012). The intestinal stem cell markers Bmi1 and Lgr5 identify two functionally distinct populations. Proceedings of the National Academy of Sciences of the United States of America *109*.

Yan, K.S., Gevaert, O., Zheng, G.X.Y., Anchang, B., Probert, C.S., Larkin, K.A., Davies, P.S., Cheng, Z., Kaddis, J.S., Han, A., et al. (2017). Intestinal Enteroendocrine Lineage Cells Possess Homeostatic and Injury-Inducible Stem Cell Activity. Cell Stem Cell *21*.

Yanai, H., Atsumi, N., Tanaka, T., Nakamura, N., Komai, Y., Omachi, T., Tanaka, K., Ishigaki, K., Saiga, K., Ohsugi, H., et al. (2017). Intestinal cancer stem cells marked by Bmi1 or Lgr5 expression contribute to tumor propagation via clonal expansion. Scientific Reports *7*.

Yang, M.-H., Hsu, D.S.-S., Wang, H.-W., Wang, H.-J., Lan, H.-Y., Yang, W.-H., Huang, C.-H., Kao, S.-Y., Tzeng, C.-H., Tai, S.-K., et al. (2010). Bmi1 is essential in Twist1-induced epithelial–mesenchymal transition. Nature Cell Biology *12*.

Yao, Q., Chen, Y., and Zhou, X. (2019). The roles of microRNAs in epigenetic regulation. Current Opinion in Chemical Biology *51*.

`

Yu, S., Tong, K., Zhao, Y., Balasubramanian, I., Yap, G.S., Ferraris, R.P., Bonder, E.M., Verzi, M.P., and Gao, N. (2018). Paneth Cell Multipotency Induced by Notch Activation following Injury. Cell Stem Cell *23*.

Zacharek, S.J., Fillmore, C.M., Lau, A.N., Gludish, D.W., Chou, A., Ho, J.W.K., Zamponi, R., Gazit, R., Bock, C., Jäger, N., et al. (2011). Lung stem cell self-renewal relies on BMI1-dependent control of expression at imprinted loci. Cell Stem Cell *9*, 272–281.

Zencak, D., Lingbeek, M., Kostic, C., Tekaya, M., Tanger, E., Hornfeld, D., Jaquet, M., Munier, F.L., Schorderet, D.F., van Lohuizen, M., et al. (2005). Bmi1 loss produces an increase in astroglial cells and a decrease in neural stem cell population and proliferation. The Journal of Neuroscience : The Official Journal of the Society for Neuroscience *25*.

Zhang, F., Sui, L., and Xin, T. (2008). Correlations of BMI-1 expression and telomerase activity in ovarian cancer tissues. Experimental Oncology *30*.

Zhang, H., Qi, J., Reyes, J.M., Li, L., Rao, P.K., Li, F., Lin, C.Y., Perry, J.A., Lawlor, M.A., Federation, A., et al. (2016). Oncogenic Deregulation of EZH2 as an Opportunity for Targeted Therapy in Lung Cancer. Cancer Discovery *6*.

Zheng, Y., de la Cruz, C.C., Sayles, L.C., Alleyne-Chin, C., Vaka, D., Knaak, T.D., Bigos, M., Xu, Y., Hoang, C.D., Shrager, J.B., et al. (2013). A Rare Population of CD24+ITGB4+Notchhi Cells Drives Tumor Propagation in NSCLC and Requires Notch3 for Self-Renewal. Cancer Cell.

Zhou, W., Zhu, P., Wang, J., Pascual, G., Ohgi, K.A., Lozach, J., Glass, C.K., and Rosenfeld, M.G. (2008). Histone H2A Monoubiquitination Represses Transcription by Inhibiting RNA Polymerase II Transcriptional Elongation. Molecular Cell *29*.

Zhou, Y., Wang, L., Vaseghi, H.R., Liu, Z., Lu, R., Alimohamadi, S., Yin, C., Fu, J.-D., Wang, G.G., Liu, J., et al. (2016). Bmi1 Is a Key Epigenetic Barrier to Direct Cardiac Reprogramming. Cell Stem Cell *18*.

CHAPTER 2: Inactivation of *Bmi1* in established lung adenocarcinoma activates tumor promoting gene programs and not tumor suppression

Rachit Neupane*, Elaine Y. Kuo*, Daniel L. Karl*, Paul S. Danielian*, Sofia Hu, Charlie Whittaker, Vincent L. Butty, Roderick T. Bronson, Peter M.K. Westcott, and Jacqueline A. Lees

Contribution:
*These authors contributed equally to this work
R.N., E.Y.K, and P.S.D. conducted the mouse experiments in Figures 3-5.
D.L.K. and P.S.D. conducted the mouse experiments in Figures 1-2.
S.H., C.W., and V.B. analyzed the gene expression data.
P.M.K.W. contributed to tumor grading data in Figure 3.
R.N., E.Y.K, D.L.K., P.S.D., and J.A.L designed the study and analyzed the data.
R.N., E.Y.K, D.L.K., P.S.D., and J.A.L wrote the chapter.

ABSTRACT

Cancer is characterized by dedifferentiation, heterogeneity, and plasticity. A subset of tumor cells, termed cancer stem cells (CSCs), can initiate tumor growth, promote metastasis, and drive post-treatment relapse. Thus, there is strong interest in targeting CSCs as a therapeutic strategy for cancer. B lymphoma Mo-MLV insertion region 1 homolog (BMI1) is a prime candidate because it enables stem cell self-renewal and is upregulated in cancer. Here, we use genetically engineered mouse models to determine the consequences of genetic ablation of *Bmi1* in lung adenocarcinomas (LUAD), which accounts for 40% of lung cancer cases. Deletion of *Bmi1* at LUAD initiation causes proliferative impairment, tumor suppression, and significant lifespan extension. In stark contrast, *Bmi1* deletion in established LUAD does not impair tumor progression, CSC numbers, CSC capacity, or metastatic potential. Instead, *Bmi1* deletion induces upregulation of transcriptional programs associated with LUAD dedifferentiation and progression. We conclude that BMI1 inhibition would be ineffective, and potentially dangerous, as an LUAD treatment.

INTRODUCTION

Cancer is the second leading cause of deaths worldwide, and its incidence and mortality rates are projected to grow rapidly (Sung et al., 2021). Cancer is a highly dynamic disease, characterized by intratumoral heterogeneity and plasticity (Dagogo-Jack and Shaw, 2018; Hanahan and Weinberg, 2011). Subpopulations of phenotypically distinct cancer cells can exist within a single tumor, and at least some cancer cells have the ability to switch between different states (Chaffer et al., 2011; Meacham and Morrison, 2013). Although genetic heterogeneity can be a hallmark of specific subpopulations, the plasticity of cancer cells is largely achieved through epigenetic regulation (Flavahan et al., 2017). Because epigenetic changes are reversible, they play a critical role in tumor development, allowing cells to switch back and forth between various states in ways that enable progression to more aggressive disease. Examples of these include epithelial to mesenchymal transitions (EMT), which can enable cell motility and migration, and dedifferentiation into more progenitor- or precursor-like states (Chaffer and Weinberg, 2015; Skrypek et al., 2017).

It is postulated that a specific subset of tumor cells, alternately named cancer stem cells (CSCs), tumor-initiating cells (TICs) or tumor-propagating cells (TPCs), is able to initiate and support tumor growth, yield metastatic lesions, and be resistant to therapy, enabling relapse after treatment (Medema, 2013; Vessoni et al., 2020; Visvader and Lindeman, 2012). Consequently, a “holy grail” for cancer treatment is to identify methods to specifically target and eradicate CSCs. CSC populations have been identified for many solid tumors including glioma, breast, colon, prostate and lung cancers (Al-Hajj et al., 2003; Curtis et al., 2010; Hurt et al., 2008; Lathia et al., 2015; Lau et al., 2014; O’Brien et al., 2007; Ricci-Vitiani et al., 2007; Zheng et al., 2013). CSCs can be maintained through asymmetric division and self-renewal, in an analogous manner to normal stem cells, and also be created from non-CSC tumor cells via state switching and acquisition of stem-like properties (Visvader and Lindeman, 2012). Indeed, it

appears that tumor cells can dynamically switch between CSC and non-CSC states (Chaffer and Weinberg, 2015). This model suggests that CSC-targeting treatments may need to be repeated, or combined with standard therapies to simultaneously target both CSCs and non-CSCs, but it does not diminish their potential value.

In the goal of targeting CSCs, considerable attention has been focused on BMI1. BMI1 is a Polycomb group RING factor (PCGF) protein and functions as a regulatory component of the epigenetic regulator Polycomb Repressive Complex 1 (Cao et al., 2005; Gil and O'Loghlen, 2014; van Lohuizen et al., 1991a). BMI1 was first identified via its ability to cooperate with *c-myc* in driving B-cell lymphomagenesis (van Lohuizen et al., 1991b), and subsequent studies found that it is upregulated in most tumor types and its expression correlates with poor prognosis (Siddique and Saleem, 2012). Analyses of germline *Bmi1*$^{-/-}$ mice revealed key roles for BMI1 in normal development, particularly in maintaining the self-renewal capacity of both hematopoietic and neural stem cells, which largely depend upon BMI1's ability to silence the *Cdkn2a* locus (Jacobs et al., 1999a; Lessard and Sauvageau, 2003; van der Lugt et al., 1994; Molofsky et al., 2003; Oguro et al., 2006; Park et al., 2003). *Cdkn2a* encodes two key tumor suppressors, p16^{INK4A}, which promotes the activity of pRB, thus causing cell cycle arrest, and p19^{ARF} (p14^{ARF} in humans), which allows for p53 accumulation, thus inducing cell cycle arrest, senescence or apoptosis (Lowe and Sherr, 2003). Importantly, BMI1 was found to be highly expressed in numerous adult stem cell populations and lowly expressed in post-mitotic tissues (Iwama et al., 2004; Lessard et al., 1998; Molofsky et al., 2005; Park et al., 2004; Yan et al., 2012). Moreover, a plethora of studies showed that BMI1 loss frequently impaired adult stem cell function and also curtailed tumorigenesis in response to oncogenic triggers (Dovey et al., 2008; Lessard and Sauvageau, 2003; Maynard et al., 2014; Molofsky et al., 2005; Park et al., 2003; Zacharek et al., 2011). Importantly, in many, but not all, cases derepression of *Cdkn2a* played a major role in both stem cell and tumor impairments. These observations led to the prevailing view that BMI1 is a key stem cell regulator, acting largely via *Cdkn2a* repression.

BMI1 has also been documented to have many other important molecular functions. It controls the silencing of core developmental regulators and thus influences embryonal patterning and lineage specification (Cao et al., 2005; van der Lugt et al., 1996). It also affects the integrity of the genome in various ways. BMI1 accumulates at repetitive DNA sequences and localizes to sites of DNA damage, and BMI1 loss causes a deficiency in constitutive heterochromatin formation and delays DNA damage recognition and repair (Abdouh et al., 2016; Barabino et al., 2016; Facchino et al., 2010; Ginjala et al., 2011). Furthermore, BMI1 associates with DNA replication regulators, and loss of BMI1 can cause replication stress and fork stalling (Agherbi et al., 2009; Sanchez et al., 2020).

BMI1 also suppresses the formation of reactive oxygen species (ROS) and supports mitochondrial function (Bednar et al., 2015; Chatoo et al., 2009; Liu et al., 2009). Additionally, BMI1 enables cell migration, invasion, and metastasis through various mechanisms including promoting the epithelial-mesenchymal transition (Douglas et al., 2008; Ferretti et al., 2016; Yang et al., 2010). Notably, as with *Cdkn2a* repression, these non-canonical functions of BMI1 are tumor-enabling, either demonstrated or theoretical. Given BMI1's well-established function in stem cell maintenance, and its widespread reactivation in tumors, BMI1 has long been considered an excellent candidate for targeting CSCs and companies are developing BMI1 inhibitors (Cao et al., 2011).

Despite this push towards clinical applications, most of the data on BMI1's roles come from analyses of germline *Bmi1*$^{-/-}$ mice, in which BMI1 is absent throughout embryogenesis, or from transplantation assays of various cell lines. In this study, we use genetically engineered mouse models (GEMMs) that allow us to probe the consequences of *Bmi1* deletion at either the time of tumor initiation or, to model the best-case outcome for BMI1 inhibition in patients, in established tumors. We chose to conduct these studies in lung adenocarcinoma (LUAD), driven by oncogenic *Kras*^{G12D} with or without *Trp53* inactivation, for several reasons. Lung cancer is the second most commonly diagnosed cancer, with LUAD being the most frequent subtype, and the

5-year survival rate is only 10-20% as patients commonly present with advanced, metastatic disease (Duma et al., 2019; Sung et al., 2021). Thus, there is strong need to identify viable targets for therapy. BMI1 is upregulated in human lung tumors, and its expression is associated with LUAD progression and inversely correlated with $p16^{INK4A}$ and $p14^{ARF}$ levels (Vonlanthen et al., 2001; Vrzalikova et al., 2008). Moreover, by breeding a spontaneously activating $Kras^{G12D}$ allele into germline $Bmi1^{-/-}$ mice, we had previously shown that the embryonal absence of BMI1 blocks LUAD progression at an early stage, and this is due to *Cdkn2a* derepression (Dovey et al., 2008). Additionally, we, and others, had established that $Bmi1^{-/-}$ bronchioalveolar stem cells (BASCs) display proliferation and self-renewal defects which reflect derepression of *Cdkn2a*, as well as another CDK inhibitor, p57 (Dovey et al., 2008, Zacharek et al., 2011). Our data in this current study show that deletion of *Bmi1* at the time of LUAD initiation also yields tumor suppression, defined by a clear proliferation defect, but there is no evidence of *Cdkn2a* derepression. In contrast, and disappointingly from a therapeutic standpoint, we find that deletion of *Bmi1* in existing tumors fails to suppress tumor progression and metastasis, nor does BMI1 loss impair CSC function, as judged by transplantation assays. Moreover, BMI1 loss in established tumors causes upregulation of transcriptional programs associated with LUAD dedifferentiation and progression, raising concerns that inhibition of *Bmi1* in patients might act to promote, rather than inhibit, lung cancer progression.

RESULTS

Loss of BMI1 at tumor initiation suppresses LUAD progression in mouse models independent of Trp53

Our first goal was to determine the consequences of deleting *Bmi1* at the time of LUAD initiation. To achieve this, we crossed conditional *Bmi1* alleles (Maynard et al., 2014) into the K and KP LUAD mouse models, which carry an inducible oncogenic form of KRAS (Jackson et al., 2001) without (K model) or with homozygous *Trp53*^{fl} conditional alleles (KP model) (Jonkers et al., 2001). Intratracheal delivery of a lentivirus that induces constitutive expression of Cre recombinase is known to yield sporadic activation of oncogenic KRAS, and coincident mutation of *Trp53* in the KP model, resulting in the launch of numerous tumors (Jackson et al., 2005). Addition of *Bmi1*$^{fl/fl}$ into this model should allow concomitant *Bmi1* deletion. To assess the efficacy of *Bmi1* loss, we induced tumors in K and KP mice that were *Bmi1*$^{+/+}$ or *Bmi1*$^{fl/fl}$ and harvested the lungs 24 or 20 weeks later for immunohistological analyses (Figure S1; data not shown). BMI1 staining was detected in the vast majority of *Bmi1*$^{+/+}$ tumors for both K (n = 129/130) and KP (n = 126/128) models in a widespread manner (Figure S1A). Gratifyingly, in the *Bmi1*$^{fl/fl}$ context, almost all K (n = 154/155) and KP (n = 118/119) tumors lacked any BMI1-postive tumor cells (Figure S1A). Tumor infiltrating stromal and immune cells continued to stain positive for BMI1, accounting for the rare BMI1 signal in the *Bmi1*$^{fl/fl}$ tumors, and serving as a positive control (Figure S1A). This, and subsequent tumor analyses, fully validated our ability to effectively delete *Bmi1* and unequivocally established that BMI1 is not absolutely required for either K or KP mutant LUAD formation.

We then asked whether BMI1 loss has any effect on K or KP mutant tumors. To begin, we generated cohorts of K mice that were *Bmi1*$^{+/+}$, *Bmi1*$^{fl/+}$ or *Bmi1*$^{fl/fl}$, infected them with lentiviral Cre, and tracked their survival over time (Figure 1A). This revealed a significant increase in the median survival of *Bmi1*$^{fl/fl}$ animals versus the *Bmi1*$^{+/+}$ controls (66%; p = 0.0004)

and also the *Bmi1*$^{fl/+}$ animals (52%; p = 0.026), which displayed an intermediate phenotype (Figure 1A). Thus, mutation of *Bmi1* at tumor initiation has a tumor suppressive effect on KRAS^{G12D}-driven LUAD that is dose-dependent.

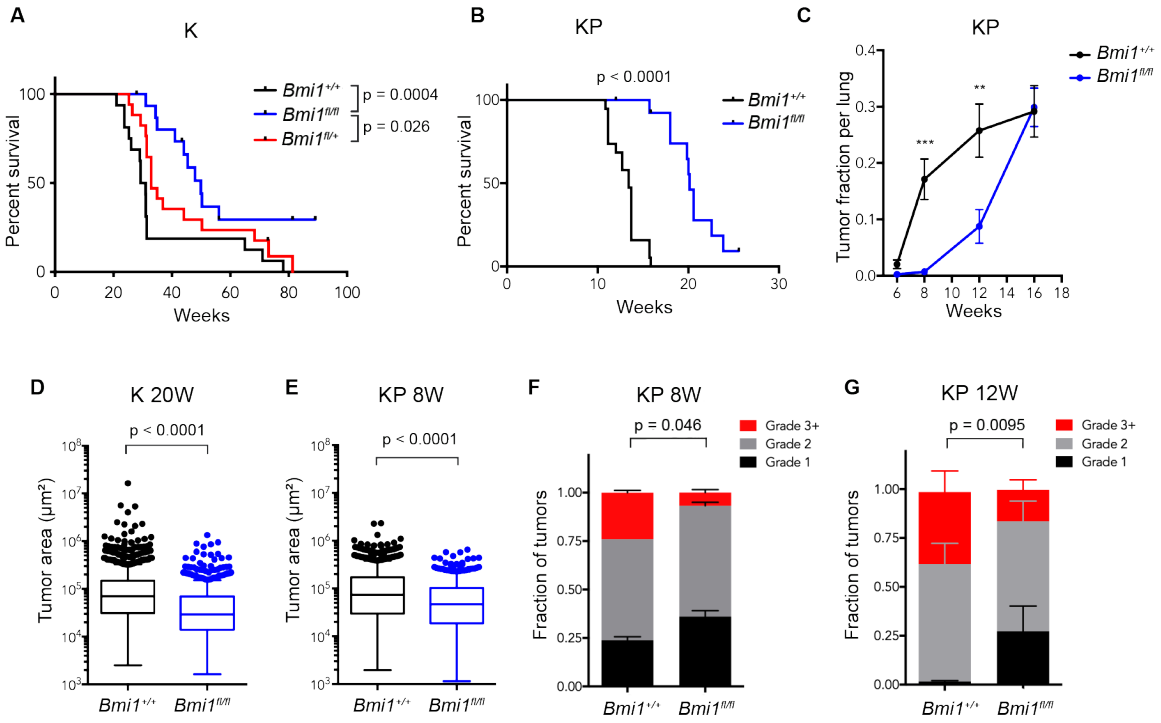

Figure 1. Deletion of *Bmi1* at LUAD initiation extends lifespan, decreases tumor sizes, and reduces fraction of high-grade tumors. **A)** Kaplan-Meier curves for *Kras*$^{LSL\text{-}G12D/+}$ (K) mice that were *Bmi1*$^{+/+}$ (n = 16); *Bmi1*$^{+/fl}$ (n = 17) and *Bmi1*$^{fl/fl}$ (n = 16) post tumor induction with intratracheal delivery of lentiviral Cre. Significantly increased survival was observed in *Bmi1*$^{fl/fl}$ versus *Bmi1*$^{+/+}$ (p = 0.0004) and *Bmi1*$^{fl/fl}$ versus *Bmi1*$^{+/fl}$ (p = 0.026). Statistical significance was determined by Wilcoxon test**. B)** Kaplan-Meier curves for *Kras*$^{LSL\text{-}G12D/+}$;*Trp53*$^{fl/fl}$ (KP) mice post tumor induction showed a significant increase in survival for *Bmi1*$^{fl/fl}$ (n = 14) versus *Bmi1*$^{+/+}$ (n = 19) animals (p ≤ 0.0001) by Wilcoxon test. **C)** Tumor fraction/lung was quantified for KP mice of the indicated numbers and *Bmi1* status at: 6W (3 *Bmi1*$^{+/+}$, 5 *Bmi1*$^{fl/fl}$), 8W (5 *Bmi1*$^{+/+}$, 5 *Bmi1*$^{fl/fl}$), 12W (4 *Bmi1*$^{+/+}$, 6 *Bmi1*$^{fl/fl}$) and 16W (5 *Bmi1*$^{+/+}$, 7 *Bmi1*$^{fl/fl}$) post tumor induction. By Student's t-test, *Bmi1*$^{fl/fl}$ animals had significantly lower tumor burden at 8W (***p = 0.0018) and 12W (**p = 0.012). **D,E)** Individual tumor areas were significantly lower in the *Bmi1* deficient tumors, compared to *Bmi1* wildtype controls, for both: **D)** K mice 20W post infection (*Bmi1*$^{fl/fl}$ = 7 mice, 698 tumors; *Bmi1*$^{+/+}$ = 6 mice, 1156 tumors) and **E)** KP mice 8W post infection (*Bmi1*$^{fl/fl}$ = 5 mice, 514 tumors; *Bmi1*$^{+/+}$ = 4 mice, 493 tumors) as determined by Student's t-test. Box plots generated using the Tukey method. **F,G)** Analysis of the fraction of tumors by grade showed a significant shift towards lower grades for *Bmi1* deficient tumors, compared to *Bmi1* wildtype controls, for KP mice at both: **F)** 8W post infection (*Bmi1*$^{fl/fl}$ = 5 mice, 301 tumors; *Bmi1*$^{+/+}$ = 5 mice, 156 tumors) and **G)** 12W post infection (*Bmi1*$^{fl/fl}$ = 5 mice; 183 tumors, *Bmi1*$^{+/+}$ = 4 mice, 203 tumors) as determined by MANOVA test.

If this suppression was mediated through activation of $p19^{ARF}$, as is seen with germline *Bmi1* loss in oncogenic KRAS-driven LUAD (Becker et al., 2009; Dovey et al., 2008; Zacharek et al., 2011), we predicted that this survival benefit would be *Trp53*-dependent. To address this, we also examined cohorts of KP mice that were $Bmi1^{+/+}$ or $Bmi1^{fl/fl}$ (Figure 1B). Unexpectedly, BMI1 loss also significantly increased median survival of KP mutant mice (50%; $p < 0.0001$; Figure 1B). Indeed, the degree of life extension in the KP model (50%; $p < 0.0001$) was remarkably similar to that seen in the K model (66%; $p = 0.0004$; Figure 1A, 1B). Thus, we conclude that *Bmi1* deletion at tumor initiation has a suppressive effect that is irrespective of the initial *Trp53* status.

To further explore the nature of this tumor suppression, we examined how total tumor burden changed over time. For this analysis, we used the KP model, as the time course of tumor onset is more consistent than the K model. $Bmi1^{+/+}$ and $Bmi1^{fl/fl}$ KP mice were infected with lentiviral Cre and 4-5 animals harvested at each of 4 time points, ending at 16 weeks when the $Bmi1^{+/+}$ animals began to exhibit morbidity (Figure 1C). The overall tumor burden was dramatically lower in $Bmi1^{fl/fl}$ animals, versus $Bmi1^{+/+}$ controls, at both the 8-week ($p = 0.0018$) and 12-week ($p = 0.012$) timepoints (Figure 1C). However, this difference was eliminated by 16 weeks post-infection (Figure 1C). These findings argue that BMI1 loss has an initial suppressive effect, but this is eventually overcome.

The presence of numerous tumors per mouse is a well-known feature of both K and KP models. Thus, lower total tumor burden and increased survival could result from a reduced ability of *Bmi1*-deficient tumors to initiate and/or impairment in tumor development and progression. To address the first possibility, we quantified tumors in lung sections collected at early post-infection time points for both K (8 weeks) and KP (6 week) models. We observed no significant difference in tumor numbers in $Bmi1^{fl/fl}$ mice versus $Bmi1^{+/+}$ littermates in either K or KP models (Figure S1B, C), indicating that BMI1 loss does not suppress tumor initiation. Given this finding, we next examined tumor size at early (8 weeks) and late (20 weeks) time points for

both K and KP models (Figure 1D,E and S1D,E). BMI1 loss significantly reduced average tumor size in the K model at 20 weeks (2.5-fold, $p < 0.0001$; Figure 1D) and the KP model at both 8 (1.4-fold, $p < 0.0001$; Figure 1E) and 20 (4.5-fold, $p=0.0047$; Figure S1E) weeks, with the K model at 8 weeks trending in the same direction, but not reaching significance (Figure S1D). Moreover, parallel analyses showed that the fraction of higher-grade tumors was significantly lower in the KP *Bmi1*$^{fl/fl}$ mice, compared to *Bmi1*$^{+/+}$ controls, at both 8 ($p < 0.05$) and 12 ($p< 0.01$) weeks (Figure 1F,G). Notably, BMI1 loss did not prevent transition to grade 3, or occasionally even higher-grade tumors, in the KP model, but it did reduce their occurrence. In the K animals, there was also a shift towards lower grade tumors for *Bmi1*$^{fl/fl}$ mice relative to *Bmi1*$^{+/+}$ controls, although this altered tumor distribution did not reach statistical significance, likely reflecting the greater stochasticity of this model (Figure S1F, G). However, we did detect a significant difference in the number of grade 3 tumors at 20 weeks in the K animals ($p = 0.045$), as these were detected at reasonable frequency in *Bmi1*$^{+/+}$ mice but essentially absent in *Bmi1*$^{fl/fl}$ mice (Figure S1F). Taken together, these data show that *Bmi1* deletion at tumor initiation extends lifespan by restraining both the size and progression of LUAD in a *Trp53*-independent manner.

BMI1 loss at tumor initiation induces proliferation and cell cycle progression defects in LUAD

We then considered the underlying basis for this tumor progression defect. BMI1 is known to repress the transcription of core cell cycle inhibitors (Park et al., 2004), including p27, p57 and both genes of the *Cdkn2a* locus, p16^{INK4A} and p19^{ARF}. Thus, we isolated mRNA from KP mutant tumors that were *Bmi1*$^{fl/fl}$ or *Bmi1*$^{+/+}$ and classified as grade 2 and conducted qRT-PCR (Figure S2A). The level of *Bmi1* mRNA was significantly lower in the *Bmi1*$^{fl/fl}$ mice, compared to *Bmi1*$^{+/+}$ controls (Figure S2A). However, the *Bmi1* mutant tumors showed no significant derepression of *Ink4a*, *Cdkn1b* (p27) or *Cdkn1c* (p57) (Figure S2A), in stark contrast to the upregulation of these genes in K mutant tumors with germline *Bmi1* deletion (Dovey et al., 2008). We also examine p19^{ARF} expression by immunohistochemistry. In both K and KP

models, $p19^{ARF}$ staining was only observed in grade 3 areas of tumors, in agreement with prior studies (Feldser et al., 2010; Muzumdar et al., 2016), and no significant difference was observed between *Bmi1*$^{fl/fl}$ and *Bmi1*$^{+/+}$ tumors (Figure S2B). Immunological staining of p21 was also comparable between *Bmi1*$^{fl/fl}$ and *Bmi1*$^{+/+}$ tumors (data not shown). We then screened for derepression of heterochromatic repeat sequences, as this has been reported to result from BMI1 loss in normal tissues and could interfere with DNA replication (Abdouh et al., 2016; Barabino et al., 2016). Specifically, we generated cDNA from the total RNA of 4 *Bmi1*$^{fl/fl}$ and 4 *Bmi1*$^{+/+}$ KP tumors, and using qRT-PCR, we showed that these tumors had no statistically significant difference in the expression levels of Line, Line-1, Sine, SineB2, major satellite or minor satellite repeat sequences (Figure S2C).

Having ruled out these well-known BMI1 roles, we turned to the unbiased approach of mRNA sequencing to understand the tumor progression defect. For this, we isolated numerous tumors from KP mice that were *Bmi1*$^{fl/fl}$ (n = 5 mice) or *Bmi1*$^{+/+}$ (n = 7 mice). We used a portion of the tumor for histological analyses to establish their grade and confirmed the absence or presence of BMI1 by immunohistochemical staining. Based on these analyses, we selected grade 2 and grade 3 tumors with minimal stromal contamination (n = 11-12 for each genotype) and used the remaining tumor portion to generate RNA and conduct high throughput transcriptional analysis using a Digital Gene Expression (HT-DGE) strategy (Soumillon et al., 2014). We performed differential gene expression analysis using DESeq2 (Love et al., 2014) to identify genes that were differentially expressed (fold change > 2; FDR q value < 0.05) between the different genotypes and tumor grades. This identified a gene expression signature that segregated the *Bmi1*$^{fl/fl}$ and *Bmi1*$^{+/+}$ tumors, as illustrated by a heat-map with hierarchical clustering (Figure 2A). In agreement with our qPCR and immunological analyses above, none of the cell cycle inhibitors p21, p27 and $p16^{INK4A}$/$p19^{ARF}$ were significantly upregulated in *Bmi1*$^{fl/fl}$ tumors, although we did see a modest but significant increase in p57 (*Cdkn1c*) transcripts (Figure S2D), which differed from our prior qRT-PCR analyses of tumors (Figure S2A). We

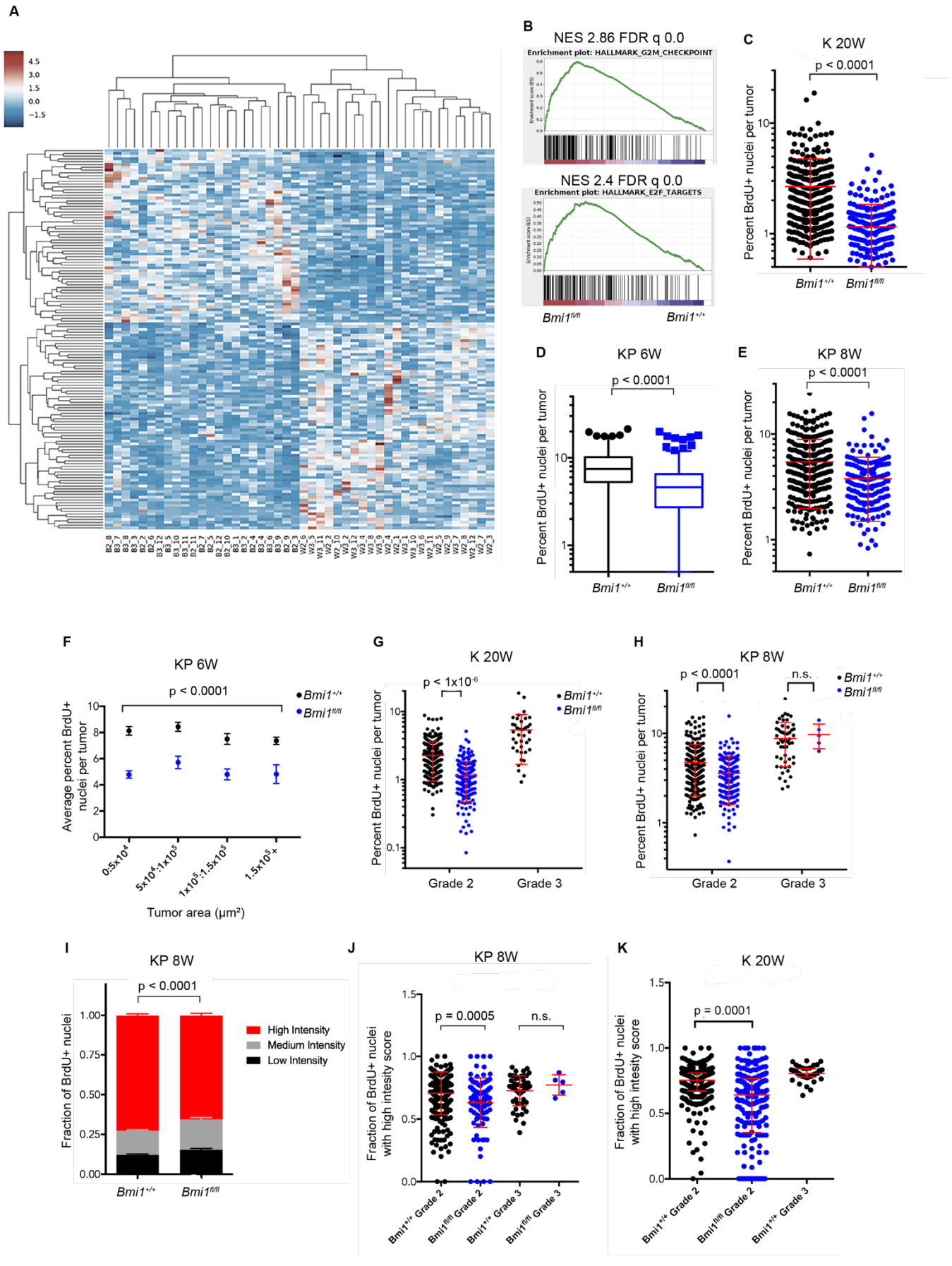
A
4.5
3.0
1.5
0.0
−1.5
B
NES 2.86 FDR q 0.0
Enrichment plot: HALLMARK_G2M_CHECKPOINT
NES 2.4 FDR q 0.0
Enrichment plot: HALLMARK_E2F_TARGETS
Bmi1fl/fl
Bmi1+/+
C
K 20W
p < 0.0001
Percent BrdU+ nuclei per tumor
Bmi1+/+
Bmi1fl/fl
D
KP 6W
p < 0.0001
Percent BrdU+ nuclei per tumor
Bmi1+/+
Bmi1fl/fl
E
KP 8W
p < 0.0001
Percent BrdU+ nuclei per tumor
Bmi1+/+
Bmi1fl/fl
F
KP 6W
p < 0.0001
Bmi1+/+
Bmi1fl/fl
Average percent BrdU+ nuclei per tumor
0:5x10⁴
5x10⁴:1x10⁵
1x10⁵:1.5x10⁵
1.5x10⁵+
Tumor area (μm²)
G
K 20W
p < 1x10⁻⁶
Bmi1+/+
Bmi1fl/fl
Percent BrdU+ nuclei per tumor
Grade 2
Grade 3
H
KP 8W
p < 0.0001
n.s.
Bmi1+/+
Bmi1fl/fl
Percent BrdU+ nuclei per tumor
Grade 2
Grade 3
I
KP 8W
p < 0.0001
High Intensity
Medium Intensity
Low Intensity
Fraction of BrdU+ nuclei
Bmi1+/+
Bmi1fl/fl
J
KP 8W
p = 0.0005
n.s.
Fraction of BrdU+ nuclei with high intesity score
Bmi1+/+ Grade 2
Bmi1fl/fl Grade 2
Bmi1+/+ Grade 3
Bmi1fl/fl Grade 3
K
K 20W
p = 0.0001
Fraction of BrdU+ nuclei with high intesity score
Bmi1+/+ Grade 2
Bmi1fl/fl Grade 2
Bmi1+/+ Grade 3

Figure 2. BMI1 loss at LUAD initiation induces defects in proliferation and cell cycle progression. **A)** Heatmap and dendrogram of significantly differentially expressed genes (≥ 2 fold; q < 0.05) for *Bmi1*$^{+/+}$ grade 2 (labeled W2, n=11) and grade 3 (W3, n=12) and *Bmi1*$^{fl/fl}$ grade 2 (B2, n=12) and grade 3 (B3, n=11) tumors. **B)** GSEA analyses showed significant upregulation of G2/M checkpoint and E2F target gene sets in *Bmi1*$^{fl/fl}$ versus *Bmi1*$^{+/+}$ tumors. **C-E)** Graphs of percent BrdU-positive nuclei/tumor showing mean and SD values, and p values (Student's t-test) for: **C)** K mice at 20W post tumor induction (*Bmi1*$^{+/+}$ n = 5 mice, 300 tumors*; Bmi1*$^{fl/fl}$ n = 6 mice, 210 tumors); **D)** KP mice 6W (*Bmi1*$^{+/+}$ n = 6 mice, 443 tumors; *Bmi1*$^{fl/fl}$ n = 6 mice, 259 tumors) and **E)** KP mice 8W (*Bmi1*$^{+/+}$ n = 5 mice, 300 tumors; *Bmi1*$^{fl/fl}$ n = 5 mice, 155 tumors). **F)** Average percent BrdU-positive nuclei for KP 6W tumors (from **D**) binned by size. Error bars = SD, p values determined by Student's t-test. **G,H)** Analysis of percent BrdU-positive nuclei by tumor grade with p values (Student's t-test) for: **G)** K mice 20W post tumor induction (*Bmi1*$^{+/+}$ n = 6 mice, 256 grade 2 and 39 grade 3 and above tumors; *Bmi1*$^{fl/fl}$ n = 6 mice, 209 grade 2 and 0 grade 3 and above tumors); and **H)** KP mice 8W post tumor induction (*Bmi1*$^{+/+}$ n = 5 mice, 247 grade 2 tumors and 52 grade 3; *Bmi1*$^{fl/fl}$ n = 5 mice, 151 grade 2 tumors, and 5 grade 3 and above tumors). **I)** Graph shows distribution of low, medium and high intensity nuclear BrdU staining in tumors from *Bmi1*$^{+/+}$ (n = 5 mice, 301 tumors) versus *Bmi1*$^{fl/fl}$ (n = 5 mice, 156 tumors) KP mice at 8W post induction. p value determined by MANOVA. **J,K)** Graphs show fraction of BrdU positive nuclei with high intensity score in grade 2 or grade 3 tumors from: **J)** KP mice 8W post tumor induction (*Bmi1*$^{+/+}$ n = 5 mice, 249 grade 2 tumors, 52 grade 3 and above tumors; *Bmi1*$^{fl/fl}$ n = 5 mice, 104 grade 2 tumors, 5 grade 3 and above tumors); and **K)** K mice at 20W post tumor induction (*Bmi1*$^{+/+}$ n = 6 mice, 225 grade 2 tumors, 39 grade 3 and above tumors; *Bmi1*$^{fl/fl}$ n = 6 mice, 209 grade 2 tumors, no grade 3 and above tumors). p values determined by Student's t-test.

performed gene set enrichment analyses (GSEA) and identified the Hallmark gene sets G2/M checkpoint (normalized enrichment score (NES) = 2.86; FDR q value < $1x10^{-4}$) and E2F targets (NES score = 2.4; FDR q value < $1x10^{-4}$) as highly significantly enriched in the *Bmi1*$^{fl/fl}$ tumors (Figure 2B). We then considered only the grade 2 or grade 3 tumors and found that these two data sets were still significantly enriched in the *Bmi1*$^{fl/fl}$ samples (Figure S2E). Notably, these gene programs were enriched in grade 2 (G2/M checkpoint NES = 2.64, FDR q value < $1x10^{-4}$, and E2F targets NES = 2.33, FDR q value < $1x10^{-4}$) versus grade 3 tumors (G2/M checkpoint NES = 1.76, FDR q value = 0.005, and E2F targets NES = 1.49, FDR q value= 0.05) suggesting that this phenotype weakened with tumor progression (Figure S2E).

G2/M checkpoint and E2F targets are both associated with cell cycle regulation. In theory, higher levels of these genes in *Bmi1*$^{fl/fl}$ tumors could reflect either an increase in proliferating cells or defects in cell cycle progression that cause persistence of S-phase and/or G2/M populations. Since loss of BMI1 impairs tumor size and progression, we suspected the latter hypothesis. To distinguish between the two possibilities, we examined the level of DNA replication in *Bmi1*$^{fl/fl}$ and *Bmi1*$^{+/+}$ tumors at various times post-initiation by assessing BrdU

incorporation via immunohistochemistry (Figure S2F). Immune infiltrating cells were identified by co-staining for the pan-immune cell marker CD45, and eliminated from this analysis. This quantification showed a highly significant reduction ($p < 0.0001$) in the average percentage of BrdU-positive cells in *Bmi1*$^{fl/fl}$ tumors for both K (20 weeks = 1.4 fold) and KP (6 weeks = 1.6 fold; 8 weeks = 1.4 fold) models (Figure 2C-E). We wondered whether these proliferation differences were an indirect consequence of the reduced mean size of *Bmi1*$^{fl/fl}$ tumors, compared to their *Bmi1*$^{+/+}$ controls. Thus, using an early KP time point to give a large range of tumor sizes, we binned tumors by size and found that the proliferation index was significantly lower ($p < 0.0001$) in *Bmi1*$^{fl/fl}$ for every single size bin (Figure 2F and S2G). Thus, the reduction in proliferation is independent of tumor size.

Since our tumor sequencing analyses identified the G2/M checkpoint and E2F targets data sets as significantly different between *Bmi1*$^{fl/fl}$ and *Bmi1*$^{+/+}$ samples in both grade 2 and grade 3 tumors, we also determined the proliferation index by grade in both the K (20 weeks) and KP (8 weeks) models. Consistent with their rarity, no *Bmi1*$^{fl/fl}$ grade 3 tumors were observed in the K mice (Figure 2G). In contrast, grade 2 tumors were plentiful for both genotypes and BrdU incorporation was 2-fold lower ($p < 1x10^{-6}$) in the *Bmi1*$^{fl/fl}$ samples (Figure 2G). In the KP model, BrdU incorporation in grade 2 tumors was also significantly lower (1.3 fold, $p < 0.0001$) for *Bmi1*$^{fl/fl}$ tumors (Figure 2H), indicating that this is independent of *Trp53* status. The KP model did yield a small number of *Bmi1*$^{fl/fl}$ grade 3 tumors, and the level of BrdU incorporation was not significantly different from that of the *Bmi1*$^{+/+}$ controls (Figure 2H).

In addition to showing that BMI1 loss reduced the fraction of dividing cells, the BrdU incorporation data also revealed evidence of cell cycle progression defects. Specifically, we quantified the intensity of nuclear BrdU immunohistochemistry staining in grade 2 tumors using an automated software that binned them into low, medium or high categories and found that the distribution showed a significant downward shift towards lower intensity staining in KP *Bmi1*$^{fl/fl}$ tumors (Figure 2I). This trended in the same direction in the K model, but did not reach

significance (Figure S2H). We also considered the intensity of BrdU incorporation by tumor grade, examining the fraction of BrdU-positive nuclei/tumor with the highest intensity score in grade 2 or grade 3 tumors (Figure 2J, K). The fraction of tumor cells displaying this high intensity staining was significantly lower for *Bmi1*$^{fl/fl}$ tumors that were grade 2 in both the KP (8 weeks post-induction, p = 0.0005) and K (20 weeks post-induction, p = 0.0001) models (Figure 2J-K), supporting an impairment in S-phase progression. This difference was not apparent in grade 3 tumors (KP model; Figure 2J). Taken together, these data, along with the elevated expression of G2/M checkpoint and E2F target genes in *Bmi1*$^{fl/fl}$ versus *Bmi1*$^{+/+}$ samples (with higher enrichment in grade 2 than grade 3 tumors) and reduced percentage of dividing cells (which is only significant in grade 2 tumors), strongly suggest that BMI1 loss induces cell cycle progression defects and proliferative impairments that are clearly apparent in grade 2 tumors, but are resolved or bypassed in the rare tumors that achieve the transition to grade 3.

BMI1 loss in established LUAD tumors does not suppress tumor progression

Due to prior studies that stress the importance of BMI1 in cancer and stem cell function, there is significant focus on the generation of BMI1 inhibitors for patient treatment (Cao et al., 2011). However, a significant portion of LUAD have already acquired grade 3 status, or higher, at the time of diagnoses. Our data above show that BMI1 was largely dispensable for higher grade KP mutant tumors, at least when it was absent from initiation and therefore providing opportunity for adaptation. However, it seemed entirely plausible that acute deletion of *Bmi1* within existing tumors might yield a different outcome. To assess this possibility, we generated a second transgenic model, focusing on the KP context, that allows the timings of tumor launch and *Bmi1* deletion to be temporally separated. Specifically, we generated mice harboring our *Bmi1*$^{fl/fl}$ alleles, as well as oncogenic *Kras* (Young et al., 2011) and *Trp53* conditional deletion (Lee et al., 2012) alleles that are regulated by the FLP recombinase, and both *Rosa26-CAG-FSF-CreERT2* (Schönhuber et al., 2014) and *Rosa26-CAG-LSL-tdTomato* (Madisen et al.,

2010) alleles. We then validated this model by generating mice that were *Kras*$^{FSF\text{-}G12D/+}$; *Trp53*$^{frt/frt}$; *Rosa26-CAG-FSF-CreERT2; Rosa26-CAG-LSL-tdTomato* and either *Bmi1*$^{+/+}$or *Bmi1*$^{fl/fl}$ and introducing adenovirus expressing FLPo recombinase by intratracheal delivery to launch KP mutant tumors that also express CreERT2 (herein called KPCreER; Figure S3A). We screened these animals periodically by micro computed tomography to detect the presence of significant tumor load and then treated them with vehicle or tamoxifen. Tamoxifen administration should activate CreERT2, triggering loss of BMI1 specifically in the *Bmi1*$^{fl/fl}$ animals and allowing expression of the tdTomato fluorescent marker in all animals (Figure S3A). To assess this new inducible model, we first examined mice without tamoxifen treatment and found that less than 2% of cells expressed tdTomato, on average, indicating that the background recombination rate is low (data not shown). We then compared tumors from *Bmi1*$^{+/+}$ or *Bmi1*$^{fl/fl}$ KPCreER mice that received tamoxifen (Figure S3B). As with our prior model, immunohistochemical staining showed BMI1 was broadly expressed in the *Bmi1*$^{+/+}$ tumors and almost fully eliminated in the *Bmi1*$^{fl/fl}$ tumors, except in infiltrating immune cells (Figure S3B). Moreover, tdTomato expression was broadly activated in both genotypes (Figure S3B). Notably, the universal activation of the tdTomato allele means that both *Bmi1* genotypes are subjected to the induction of DNA breaks and presumably any associated DNA damage response.

Having validated this model, we then examined the effect of acute *Bmi1* loss on LUAD. For this, we launched two separate KPCreER cohorts, both containing similar numbers of *Bmi1*$^{+/+}$ and *Bmi1*$^{fl/fl}$ animals, in which tumors had been initiated by intratracheal intubation of either $1x10^7$ pfu (cohort A) or $2.5x10^7$ pfu (cohort B) of adenovirus that induce FLPo expression. All mice were injected with tamoxifen at 13 or 9 weeks post launch, respectively. These times were selected in order to generate a large spectrum of tumor sizes and grades, including significant representation of grade 3 tumors. The lungs were then harvested via necropsy at 3, 14 and 45 days (D) post tamoxifen treatment to capture short- and long-term effects of *Bmi1* deletion, and tdTomato expression and *Bmi1* loss (where relevant) were confirmed by

immunohistochemistry (data not shown). We then examined various tumor properties using 3 or more animals for each genotype and time point, which corresponded to approximately 150 tumors per condition for both cohorts A (Figure 3) and B (Figure S3C). Analysis of cleaved caspase 3 levels by immunohistochemical staining detected little apoptosis in any of the samples, with no significant difference observed between the *Bmi1*$^{fl/fl}$ and *Bmi1*$^{+/+}$ genotypes (data not shown). In contrast, our assessment of proliferation revealed variable results; the level of BrdU-positive nuclei/area did not differ significantly between *Bmi1*$^{fl/fl}$ and *Bmi1*$^{+/+}$ for two conditions [Cohort A D14 (Figure 3A) and Cohort B D14 (Figure S3Ci)], but was significantly reduced in *Bmi1*$^{fl/fl}$ tumors for three of the conditions [Cohort A D45 (Figure 3A) and Cohort B D3 and D45 (Figure S3Ci)] and elevated in *Bmi1*$^{fl/fl}$ tumors for one condition [Cohort A D3 (Figure 3A)]. Notably, as well as being inconsistent, the proliferation differences did not translate into tumor impairment. First, the numbers of tumors were not significantly different between *Bmi1*$^{fl/fl}$ and *Bmi1*$^{+/+}$ animals at D3, D14 or D45 for either cohort (Figure 3B, Figure S3Cii). Second, the total tumor burden was significantly higher, not lower, for *Bmi1*$^{fl/fl}$ in cohort B, D14 ($p=0.0074$; Figure S3Ciii), and trended higher, but not statistically significant, for all of the other conditions [cohort A: D3, D14 and D45 (Figure 3C) and cohort B: D3 and D45 (Figure S3Ciii)]. Finally, the distributions of tumor grades were not significantly different between the two genotypes at D3, D14 or D45 for either cohort (Figure 3D, Figure S3Civ). Thus, we conclude that *Bmi1* inactivation in existing tumors does not yield appreciable tumor suppression.

Ablation of BMI1 in established LUAD tumors promotes expression of tumorigenic programs

We next asked whether loss of BMI1 altered the transcriptional profile of KPCreER tumors. To address this, we isolated tumors cells by FACS (based upon tdTomato-positive staining and the absence of hematopoietic cell lineage markers) from the dissociated lungs of four animals of each genotype from cohort B D3, D14 and D45 post-tamoxifen time points and performed bulk mRNA sequencing. Because these animals all have numerous tumors, of

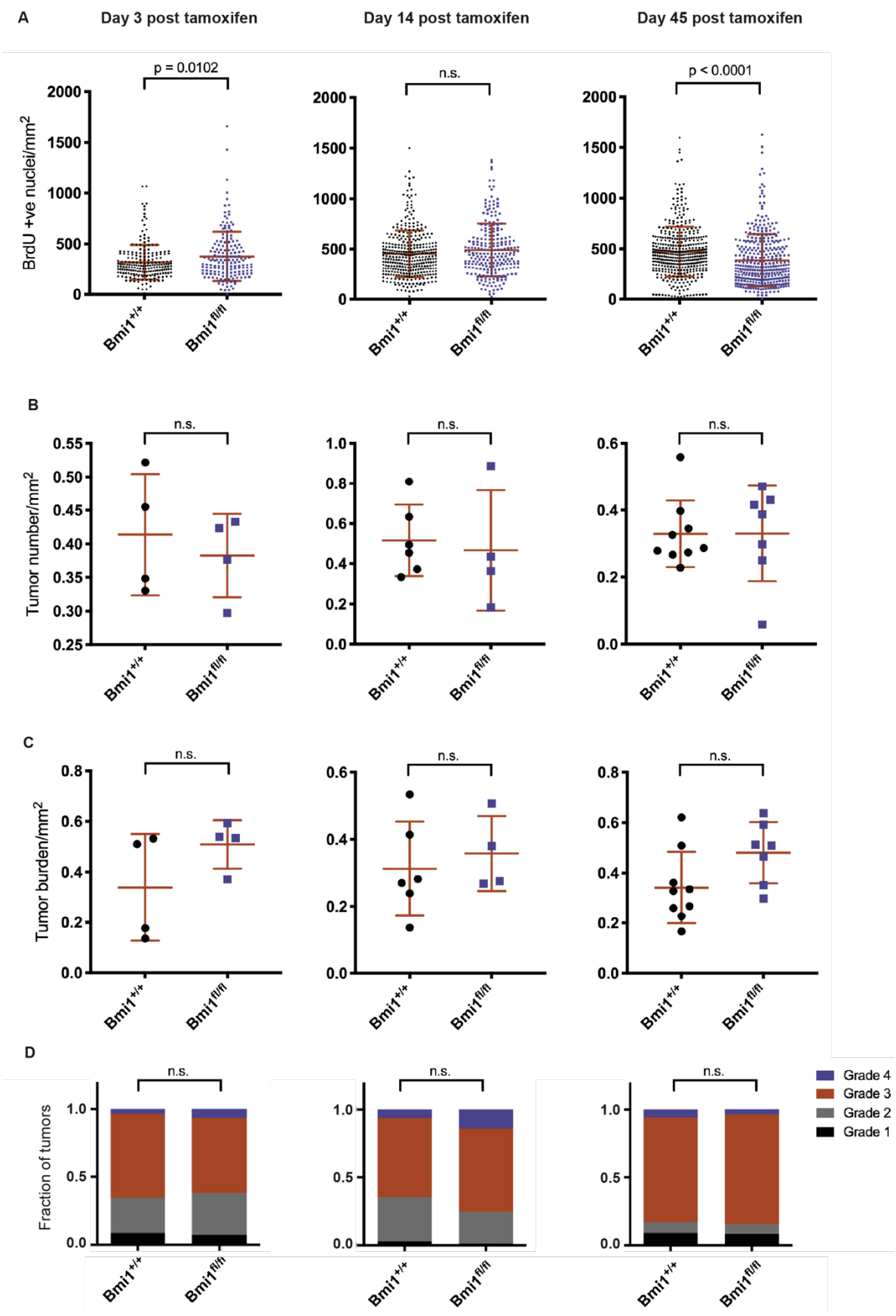
A
Day 3 post tamoxifen
Day 14 post tamoxifen
Day 45 post tamoxifen
p = 0.0102
n.s.
p < 0.0001
BrdU +ve nuclei/mm2
2000
1500
1000
500
0
Bmi1+/+
Bmi1fl/fl
B
n.s.
Tumor number/mm2
0.55
0.50
0.45
0.40
0.35
0.30
0.25
1.0
0.8
0.6
0.4
0.2
0.0
C
Tumor burden/mm2
D
Fraction of tumors
1.0
0.5
0.0
Grade 4
Grade 3
Grade 2
Grade 1

Figure 3. Acute *Bmi1* deletion in established LUAD tumors does not strongly impair tumor progression. Mice bearing KPCreER $Bmi1^{+/+}$ versus $Bmi1^{fl/fl}$ tumors (Cohort A) were harvested 3 days ($Bmi1^{+/+}$ n=4, $Bmi1^{fl/fl}$ n=4), 14 days ($Bmi1^{+/+}$ n=6, $Bmi1^{fl/fl}$ n=4), or 45 days ($Bmi1^{+/+}$ n=9, $Bmi1^{fl/fl}$ n=7) after tamoxifen treatment, which induced *Bmi1* deletion. **A-C**) Graphs with the mean +/- one SD shown for: **A**) Number of BrdU positive nuclei per mm^2 per tumor. Each point represents one tumor (Day 3 n = 205 $Bmi1^{+/+}$, 167 $Bmi1^{fl/fl}$; Day 14 n = $Bmi1^{+/+}$ 358, $Bmi1^{fl/fl}$ 234; and Day 45 n = $Bmi1^{+/+}$ 407, $Bmi1^{fl/fl}$ 355) and p values were determined using unpaired Student's t-test. **B**) Average tumor number/mm^2 of lung/animal. p values were determined by Mann Whitney test. **C**) Average tumor burden/mm^2 of lung/animal. p values determined using unpaired Student's t-test with Welch's correction. **D**) Graphs show tumor grade distribution/animal, with p values determined by ANOVA.

various sizes and grades, this approach should minimize "jackpot" tumor events, and instead provide a holistic view of gene expression changes. The resulting data were analyzed using DESeq2 to identify significant differentially expressed (DE) genes between the $Bmi1^{fl/fl}$ and $Bmi1^{+/+}$ KPCreER tumor cell populations, as judged by fold change > 2, q-value < 0.05. In the D3 samples, no significantly DE genes were identified (Figure S3D). This was not particularly surprising, as we had anticipated that there would be a phenotypic lag between the deletion of *Bmi1* and any related gene expression changes. Indeed, we selected the D3 time point as a baseline control with this in mind, thinking that it would precede any concerted *Bmi1*-regulated gene expression changes, but be sufficiently removed from any transcriptional DNA damage responses caused by the Cre recombinase. Importantly, we did detect significant DE genes in both the D14 and D45 samples (Figure S3D), supporting a phenotypic lag and establishing that *Bmi1* loss did affect the transcriptome, whether directly or indirectly. Notably, as with deletion of *Bmi1* at initiation, we did not observe significant derepression of the *Cdkn2a* locus following acute BMI1 loss (data not shown).

To identify differentially regulated pathways between KPCreER $Bmi1^{fl/fl}$ and $Bmi1^{+/+}$ tumors in the D14 and D45 samples, we performed gene set enrichment analysis (GSEA; Mootha et al., 2003; Subramanian et al., 2005) against the C2 gene set collection in the molecular signatures database (MSigDB). Since BMI1 is an epigenetic repressor, we looked for gene sets that were upregulated in $Bmi1^{fl/fl}$ tumor cells, compared to $Bmi1^{+/+}$ controls, focusing specifically on ones enriched at both D14 and D45 timepoints to identify programs that resulted

from *Bmi1* loss and were stable over time. Five gene sets fulfilled these criteria (Figure S3E). Strikingly, one of these gene sets was targets of HNF4α, which regulates gastrointestinal differentiation and had been previously shown to characterize the dedifferentiation of lung adenocarcinoma tumor cells to a more embryonic-like state (Snyder et al., 2013), while a second gene set was associated with gastric cancers (Figure S3E). The lung originates from the anterior foregut during embryogenesis (Morrisey and Hogan, 2010), and expression of HNF4α and other gastrointestinal markers indicates dedifferentiation of LUAD cells and is a hallmark of LUAD progression (Snyder et al., 2013). These gene sets were not significantly enriched in the D3 samples, indicating that the changes were a consequence of long-term loss of BMI1 (Figure S3D).

We conducted additional analyses to explore the notion that BMI1 loss promotes dedifferentiation of the KPCreER tumors. For this, we took advantage of a prior study by Synder and coworkers (Snyder et al., 2013), which deleted a marker of low grade KP mutant LUAD, the pulmonary transcription factor NKX2.1, demonstrated that this drove tumor progression, and identified lung, lung/gut, and gut gene signatures that characterized increasing states of progression. We performed unsupervised hierarchical clustering on the expression of these three gene sets in our samples. Notably, the lung/gut and gut signatures were highly enriched in all four of the D45 and two of the D14 $Bmi1^{fl/fl}$ samples, relative to any other sample, including all $Bmi1^{+/+}$ samples (Figure 4A). To further extend this analysis, we generated two larger, high confidence gene sets, comprised of genes that were significantly upregulated or downregulated ($\log_2$ fold change > 2, $p < 0.01$) in the NKX2.1-deficient tumors using data from Snyder et al., 2013. We appended these gene sets to the MSigDb C2 collection and ran GSEA on our D45 samples. Strikingly, genes upregulated by *Nkx2.1* deletion were significantly enriched in the $Bmi1^{fl/fl}$ samples (NES = 6.62, FDR q value < 10^{-6}) while genes downregulated by *Nkx2.1* deletion were significantly enriched for $Bmi1^{+/+}$ (NES = 3.30, FDR q value < 10^{-6}; Figure S3F).

Collectively, these data show that loss of *Bmi1* in existing tumors resulted in derepression of gene expression programs associated with the embryonic gastric lineage and previously linked to dedifferentiation and progression of KP mutant LUAD.

These bulk sequencing data suggest that the *Bmi1* deficient tumors follow the normal dedifferentiation trajectory of KP mutant LUAD, but in an enabled manner. To further explore this notion, we used single cell RNA sequencing to compare the identity and relative distribution of subpopulations from *Bmi1*$^{fl/fl}$ versus *Bmi1*$^{+/+}$ tumors. For this, tdTomato-positive tumor cells were isolated from the lungs of *Bmi1*$^{fl/fl}$ and *Bmi1*$^{+/+}$ KPCreER mice at 52 days post tamoxifen injection, prepared for sequencing using the Seqwell method (Gierahn et al., 2017), and the resulting data were processed using Seurat v3 (Satija et al., 2015). Uniform manifold approximation (UMAP) was used to reduce the dimensionality of the dataset and visualize the cells in 2D space (Figure 4B). Unsupervised clustering identified 15 clusters in this UMAP (Figure 4B), with *Bmi1*$^{+/+}$ and *Bmi1*$^{fl/fl}$ cells represented in all 15 clusters (Figure 4B, S4A). However, there were clear differences in their distribution, which reflects global differences in transcriptional profiles (Figure S4A). *Bmi1*$^{+/+}$ cells were significantly overrepresented in clusters in the bottom left quadrant of the UMAP (i.e. clusters 1, 3 and 5), while *Bmi1*$^{fl/fl}$ cells were predominantly located in clusters in the top right quadrant of the UMAP (e.g. clusters 11-15; Figure S4A).

We then characterized the identity of the 15 clusters (Figure 4C, S4B; see Materials and Methods). As part of these analyses, we scored each single cell for expression of the aforementioned lung, lung-gut and gut lineage signatures (Snyder et al., 2013) in every *Bmi1*$^{fl/fl}$ and *Bmi1*$^{+/+}$ cell by summing normalized transcript counts for each gene in the signature. These analyses showed a clear lung-to-gut axis across the UMAPs (Figure 4C), with the lung signature being enriched in the bottom left quadrant (which was enriched for *Bmi1*$^{+/+}$ cells) and the gut signature being enriched in the top right quadrant (which was enriched for *Bmi1*$^{fl/fl}$ cells). Consistent with these findings, all three signatures showed significant differences in their

distribution between the *Bmi1*$^{+/+}$ and *Bmi1*$^{fl/fl}$ populations ($p < 2 \times 10^{-16}$), with the lung signature being under-represented, and the lung-gut and gut lineage signatures both over-represented in the *Bmi1*$^{fl/fl}$ cells compared to the wildtype controls (Figure 4D). We also conducted GSEA using

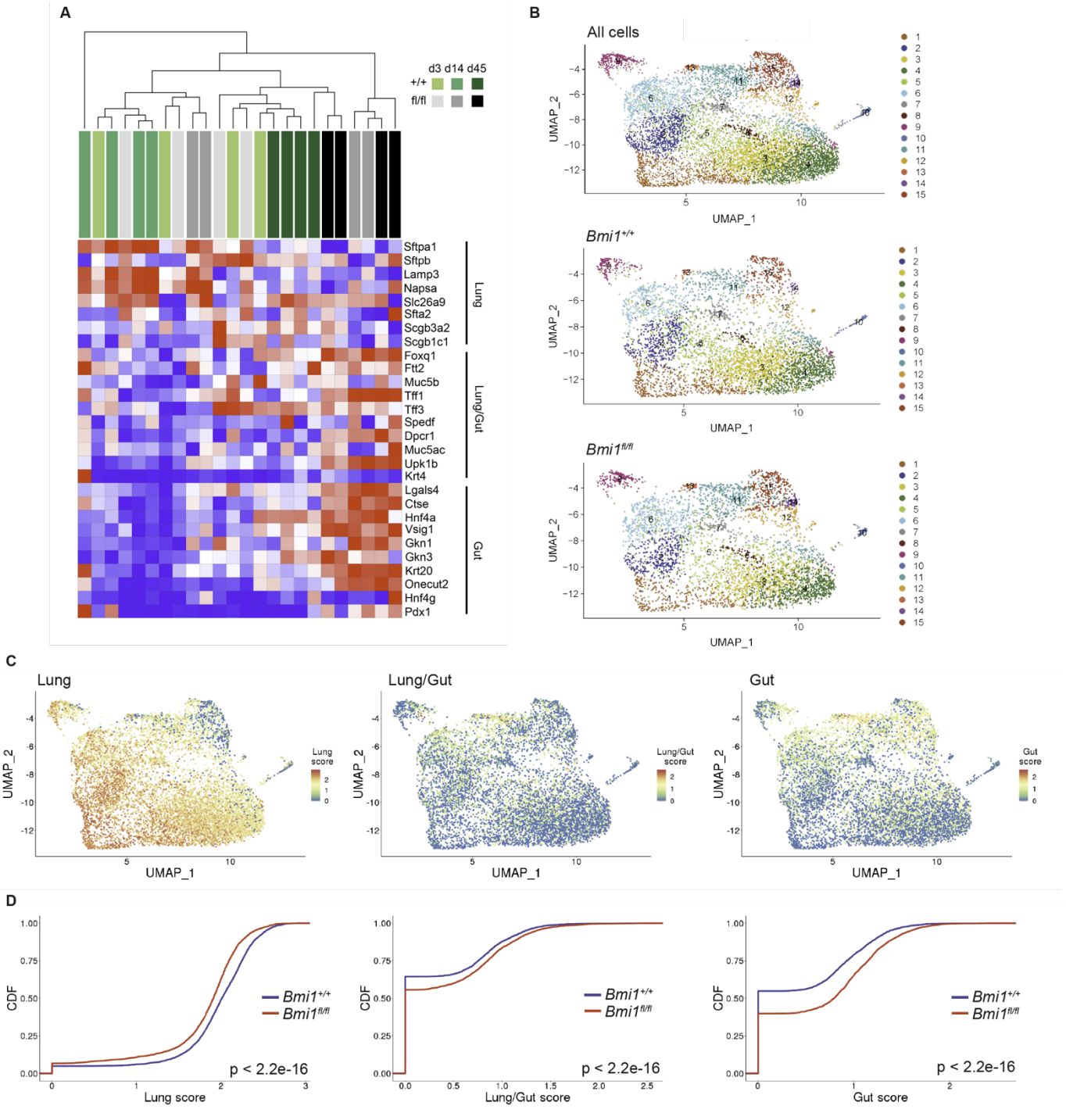

Figure 4. Acute ablation of *Bmi1* in established LUAD tumors promotes acquisition of gut lineage programs. **A**) Unsupervised hierarchical clustering of bulk tumor sequencing data from TdTomato-positive tumor cells collected day 3, 14 or 45 after tamoxifen injection (n=4 animals/genotype/timepoint) using the lung, lung/gut, and gut gene sets (Snyder et al., 2013) **B**) UMAP projections and clustering of single-cell transcriptional profiles from 9457 single TdTomato-positive tumor cells collected from $Bmi1^{+/+}$ (4941 cells) and $Bmi1^{fl/fl}$ (4516 cells) KPCreER animals 52 days after tamoxifen treatment. Images of all (top), $Bmi1^{+/+}$ (middle), and $Bmi1^{fl/fl}$ (bottom) cells projected onto a shared UMAP. **C, D**) The lung, lung-gut and gut signatures (Snyder et al. 2013) were scored in each $Bmi1^{+/+}$ and $Bmi1^{fl/fl}$ cell by summing normalized transcript counts over each gene in the signature, and shown: **C)** projected onto the shared UMAP, or **D)** as cumulative distribution functions, with significance established by the Kolmogorov-Smirnov test.

several other reported lung cell signatures (Marjanovic et al., 2020; Montoro et al., 2018; Plasschaert et al., 2018) and identified enrichment for gut lineage markers in clusters 11-15 (Figure S4B). Thus, collectively, our bulk and single cell RNA sequencing analyses indicate that BMI1 loss promotes transition through the normal LUAD dedifferentiation trajectory and facilitates acquisition of gut lineage programs that are traditionally associated with tumor progression.

We next investigated whether BMI1 loss impacts tumorigenesis in ways beyond this dedifferentiation phenotype. We examined the tumor-propagating cell (TPC) frequency (as a functional proxy for CSC frequency) and metastatic potential of *Bmi1* mutant lung tumors because BMI1 has been previously shown to play a positive role in both processes (Ferretti et al., 2016; Kreso et al., 2014). We used a gene set for metastasis (Winslow et al., 2011) and two for lung TPC markers [denoted TPC A (Lau et al., 2014) and TPC B (Zheng et al., 2013)] and scored each cell for these signatures by summing the normalized transcript counts for each gene in the signature. These analyses revealed significant differences in their distribution between the two genotypes (Figure 5A), with the tMet ($p = 7.6 \times 10^{-10}$), TPC A ($p = 2.4 \times 10^{-11}$) and TPC B ($p = 3.5 \times 10^{-4}$) signatures all showing higher scores in the $Bmi1^{fl/fl}$ than $Bmi1^{+/+}$ cells, suggesting that BMI1 loss was promoting metastatic programs and tumor-propagating ability. To test this functionally, we launched $Bmi1^{fl/fl}$ and $Bmi1^{+/+}$ KPCreER tumors with adenoviral FLPo ($1x10^7$ pfu), waited 60-65 days before tamoxifen treatment, and then examined these animals

74 days after tamoxifen treatment. Notably, 58% (7/12) of the *Bmi1*$^{fl/fl}$ animals exhibited metastases in the mediastinal lymph nodes, the plural cavity or both locations, in contrast to

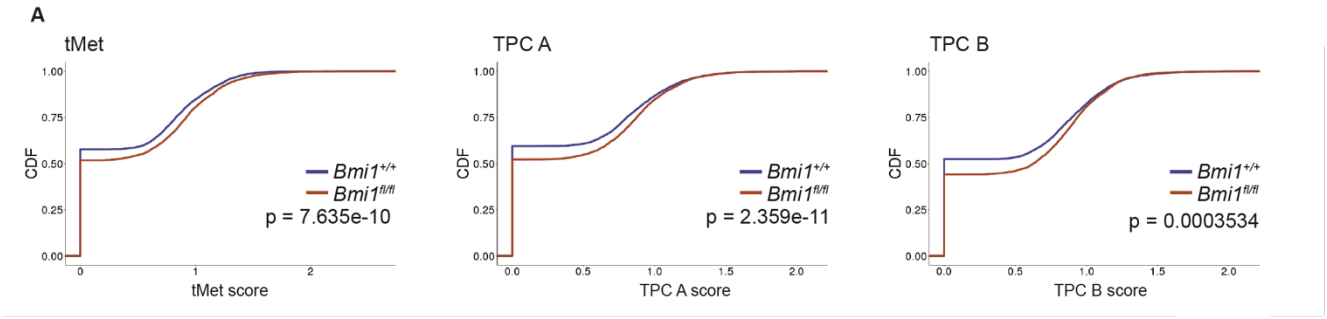

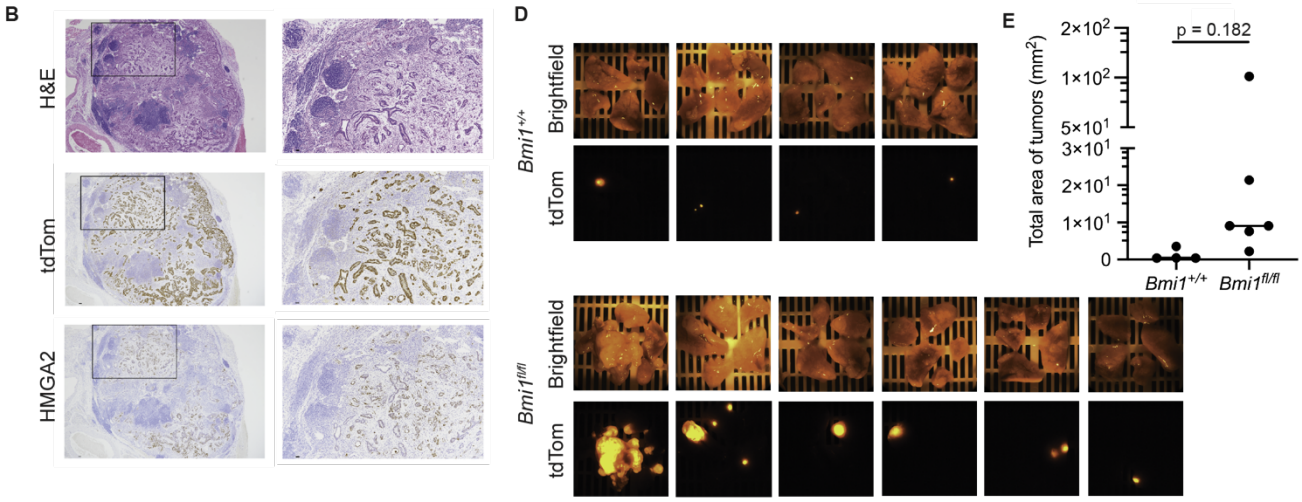

C

	500 cells	2000 cells	5000 cells	CSC frequency
Bmi1$^{+/+}$	1/10	4/9	7/9	**1/3485**
Bmi1$^{fl/fl}$	1/10	6/9	7/8	**1/2325**

Figure 5. BMI1 loss in established LUAD tumors promotes acquisition of gene expression programs associated with metastasis and tumor propagation, but does not increase formation of metastases or alter representation of cancer stem cells (CSCs). **A**) Scores were calculated for gene set signatures associated with metastasis (tMet, left panel), or for two different sets of lung tumor-propagating cell (TPC) markers, denoted TPC A (middle panel) or TPC B (right panel) in for each cell by summing the normalized transcript counts for each gene in the signature. The graphs show cumulative distribution functions for *Bmi1*$^{+/+}$ versus *Bmi1*$^{fl/fl}$ cells, with significance established using the Kolmogorov-Smirnov test. **B**) Representative example of histochemical (H & E) and immunohistochemical staining for tdTomato and HMGA2 (brown stain) in a metastatic lesion in a lymph node of a *Bmi1*$^{fl/fl}$ animal analyzed at day 74 post tamoxifen injection. Inset boxes in the left column represent the area shown in the higher power images in the right column. Nuclei are counterstained (blue), scale bars represent 50μm, left column and 25μm, right column. **C**) Quantification of CSC frequency in *Bmi1*$^{+/+}$ and *Bmi1*$^{fl/fl}$ tumors, after serial transplantation and limiting dilution analysis, using ELDA method (Hu and Smyth, 2009). Differences in CSC frequencies are not significant, as determined by Chi-squared test. **D)** Brightfield and tdTomato (tdTom) fluorescence images of lungs of mice transplanted with 2000 *Bmi1*$^{+/+}$ or *Bmi1*$^{fl/fl}$ tumor cells. **E)** Quantification of total tumor area of mice transplanted with 2000 *Bmi1*$^{+/+}$ or *Bmi1*$^{fl/fl}$ tumor cells, as assessed by tdTom fluorescence.

only 25% (4/16) *Bmi1*$^{+/+}$ mice. Their lung origin was confirmed by expression of both tdTomato and the dedifferentiation marker, HMGA2 (Figure 5B). Although this increase was not statistically significant ($p = 0.121$, Fisher's exact test), we can certainly conclude that BMI1 loss in existing LUAD tumors does not impair their metastatic ability. We also used this cohort to assess the effects of BMI1 loss on CSC frequency by limiting dilution. Specifically, we isolated tumor cells from three *Bmi1*$^{+/+}$ and three *Bmi1*$^{fl/fl}$ mice by FACS for the tdTomato marker and transplanted various cell numbers into recipient mice. The frequency of tumor formation allowed us to calculate the CSC frequency, which was slightly higher (but not statistically significant) for the *Bmi1*$^{fl/fl}$ cells compared to the *Bmi1*$^{+/+}$ controls ($p = 0.34$; Figure 5C). Additionally, analyses of the tumors from mice receiving 2000 cells showed that *Bmi1*$^{fl/fl}$ cells yielded larger tumors, though this difference was not statistically significant ($p = 0.182$, Figure 5D-E). Taken together, these data indicate that loss of BMI1 in established LUAD does not impair the progression of the primary tumors, the representation of CSCs or the formation of metastases, but instead enables acquisition of gene expression programs that enhance all three of these processes.

DISCUSSION

In this study, we used GEMMs to assess the consequences of *Bmi1* deletion in the context of LUAD driven by oncogenic KRAS^{G12D}. Within this single model, we find that BMI1 loss has profoundly different effects, based on the timing of its deletion. We see tumor suppression in two different settings, germline *Bmi1* absence (Dovey et al., 2008) or deletion at tumor initiation, but this arises through different mechanisms. Specifically, *Cdkn2a* activation plays a key role in the germline *Bmi1*$^{-/-}$ mice (Dovey et al., 2008) but is not observed in our initiation model (or in the established tumor setting), consistent with the latter being unaffected by *Trp53* status. The observed differential *Cdkn2a* dependence likely reflects the starting state of the *Cdkn2a* locus. During embryogenesis, *Cdkn2a* is not detectably expressed in almost all tissues,

and BMI1 is key for repression of this locus (Jacobs et al., 1999b; McKeller et al., 2002; Zindy et al., 1997). Thus, in germline *Bmi1*$^{-/-}$ mice, the *Cdkn2a* locus remains unsilenced, and presumably easily triggered by oncogenic conditions. In contrast, *Cdkn2a* is appropriately silenced in our *Bmi1*$^{fl/fl}$ conditional model, and subsequent induction of BMI1 loss does not lead to its activation. Our findings are entirely consistent with another study, reporting *Cdkn2a*-independent tumor suppression after *Bmi1* deletion at the initiation of pancreatic cancer (Bednar et al., 2015). Collectively, these refute the dream hypothesis that BMI1 loss/inhibition will serve to activate *Cdkn2a* and thereby trigger senescence or apoptosis.

Despite the lack of *Cdkn2a* involvement, *Bmi1* deletion at LUAD initiation does cause a significant proliferation defect. This is accompanied by upregulation of cell cycle-associated GSEA signatures, E2F target gene and G2/M arrest, and a reduction in the fraction of tumor cells showing high levels of BrdU incorporation. The simplest explanation for these observations is that BMI1 loss impairs S-phase progression, causing accumulation of cells displaying cell cycle defects. These fit with several studies showing that BMI1 associates with both the replication and DNA damage response machineries and is required for efficient replication fork progression and DNA damage repair (Agherbi et al., 2009; Sanchez et al., 2020). Importantly, the proliferation defects we observe appear sufficient to reduce tumor sizes and impair tumor progression. Interestingly, some *Bmi1*-deficient tumors do manage to transition to grade 3, at least in the KP model. These grade 3 tumors still show upregulation of E2F target gene and G2/M checkpoint GSEA signatures, but to a lesser extent than the grade 2 setting, and this no longer correlates with proliferative impairment. This suggests that tumors somehow overcome the deleterious effects of BMI1 loss. Notably, grade 3 tumors have a higher proliferative index than their grade 2 counterparts, in the *Bmi1* wildtype context, and prior studies have reported that LUAD progression is accompanied by increased MAPK signaling, which could enable this elevated proliferation (Feldser et al., 2010). It seems likely that the proliferative impairment in grade 2 *Bmi1*$^{fl/fl}$ tumors creates a major hurdle for transition to grade 3. One possibility is that a

compensatory mechanism must occur to allow this leap. However, if this does exist, it cannot diverge significantly from the normal disease trajectory, or must occur at the post-transcriptional level, as GSEA did not reveal any obvious adaptation signature that distinguished *Bmi1*$^{fl/fl}$ grade 3 from either *Bmi1*$^{fl/fl}$ grade 2 or *Bmi1*$^{+/+}$ grade 3. The alternative possibility is that the grade 2 to grade 3 transition occurs via the same stochastic mechanism(s) in *Bmi1*$^{fl/fl}$ as *Bmi1*$^{+/+}$ tumors, and the resulting proliferative boost somehow mitigates the deleterious effects of BMI1 loss. Notably, regardless of the mechanism, for both K and KP models, deletion of *Bmi1* at initiation delays but does not completely block tumor progression.

The most important aspect of our study is the effect of *Bmi1* deletion in established tumors. Since considerable efforts are being made to develop BMI1 inhibitors, our goal was to use genetic *Bmi1* ablation to determine the best possible response in LUAD. We conducted this analysis at time points when the tumors were predominantly grade 3 or higher, because patients commonly present with advanced disease (Duma et al., 2019; Lim and Ma, 2019). *Bmi1* inactivation was highly efficient, but the phenotype effects were extremely disappointing from a potential therapeutic standpoint. Specifically, we observed no significant effect on the number, size, overall burden, or grade representation of tumors, even 6+ weeks after *Bmi1* deletion. We wondered whether additional time was required for *Bmi1* deletion to have an effect, and thus launched fewer tumors and waited 10+ weeks post-ablation. Even with this longer time frame, the frequency of metastatic events was actually higher in the *Bmi1* mutants, although not significantly. Furthermore, transplantation experiments showed that CSC representation was unaltered, and the tumors arising from *Bmi1*$^{fl/fl}$ cells were significantly larger than their *Bmi1*$^{+/+}$ counterparts. Thus, *Bmi1* deletion yielded no material tumor suppression, even after many rounds of cell division. Even more concerning, our bulk and single cell sequencing data both showed that BMI1 loss increased the frequency of cells acquiring gene expression signatures that are hallmarks of LUAD progression, particularly the previously reported lung/gut and gut signatures (Snyder et al., 2013). In other words, the *Bmi1*$^{fl/fl}$ tumor cells follow the normal

dedifferentiation trajectory for LUAD, but in an enhanced manner. It is an open question how this occurs. However, we favor the notion that *Bmi1* loss causes gene derepression, perhaps stochastically, and thus provides a larger evolutionary landscape that allows positive selection for cells bearing the desirable, tumor-enabling signature.

Notably, the tumor promoting effects are similar to those seen with other epigenetic regulators, such as EED, a PRC2 component, or G9a, a H3K9 histone methyltransferase. In both cases, loss of these proteins can cause more aggressive tumors, which exhibit increased expression of previously established markers of tumor progression (Avgustinova et al., 2018; Rowbotham et al., 2018; Serresi et al., 2016). Interestingly, this tumor promoting effect of EED loss was also seen in LUAD (Serresi et al., 2016), and thus disruption of either PRC1 or PRC2 Polycomb Repressive Complexes promotes acquisition of the gastric signature and tumor acceleration. Taken together, these findings suggest that targeting of epigenetic regulators needs to be approached with caution. At a minimum, our data argue that inhibition of BMI1 will be ineffective in the treatment of LUAD and could well yield adverse effects for these patients.

SUPPLEMENTAL FIGURES

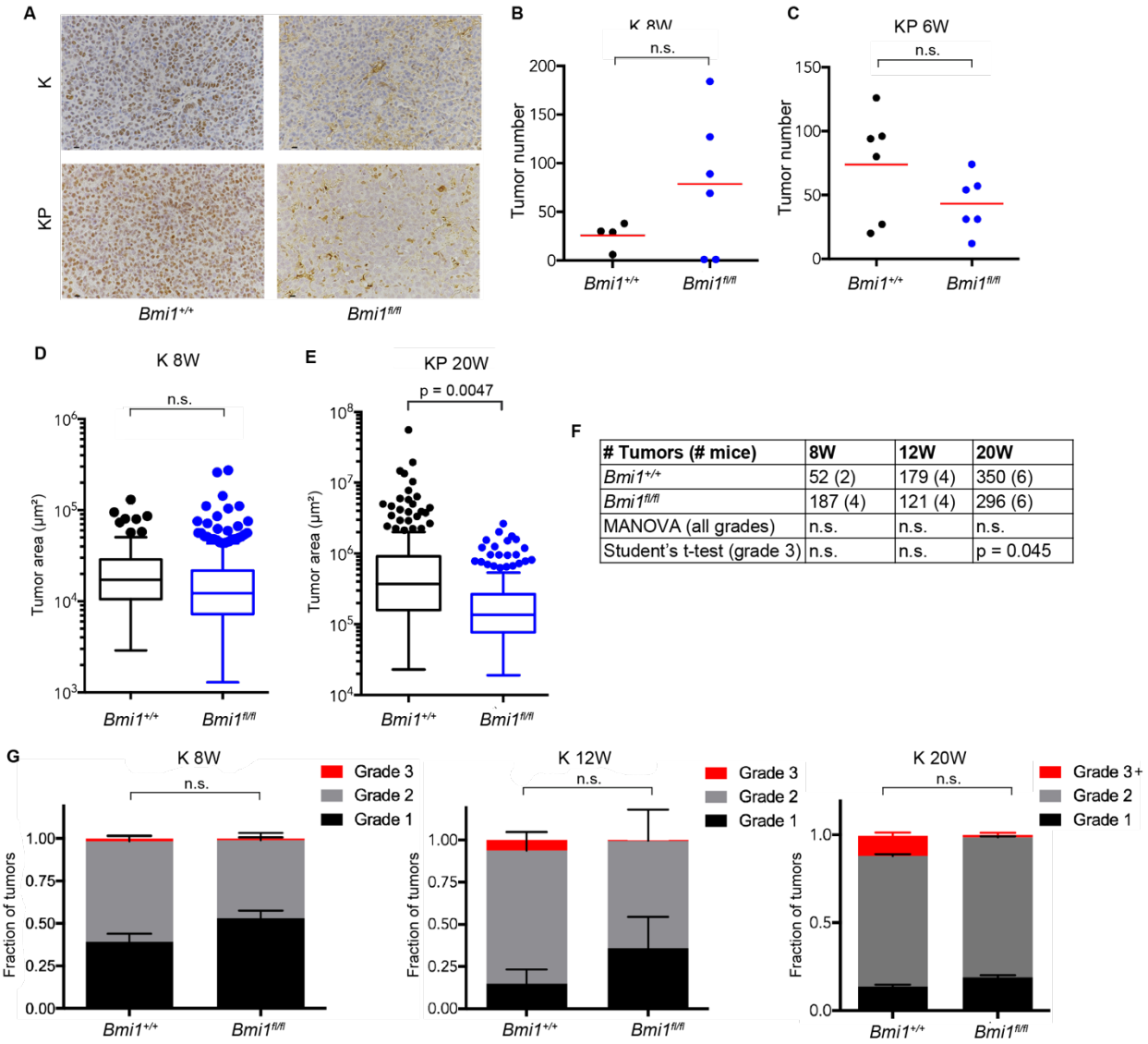

Figure S1. BMI1 loss does not suppress LUAD tumor initiation. **A)** Immunohistochemistry for BMI1 (brown), with counterstained nuclei (light blue) in representative *Bmi1*$^{+/+}$ and *Bmi1*$^{fl/fl}$ tumors from K and KP models, at 24 and 20 weeks post infection, respectively. All BMI-positive cells in the *Bmi1*$^{fl/fl}$ samples are non-tumor derived cell types. Scale bar = 25μm. **B,C)** *Bmi1* mutation does not significantly alter the number of LUAD induced per mouse in either **B)** K (8 weeks post-tumor induction) or **C)** KP (6 weeks post-tumor induction) models, as judged by Student's t-test. **D)** In the K model at the 8 weeks post-tumor induction, there was no significant difference in the average tumor area between *Bmi1*$^{+/+}$ (n = 4 mice, 103 tumors) and *Bmi1*$^{fl/fl}$ (n = 6 mice, 471 tumors) tumors, as judged by Student's t-test. **E)** In the KP model at 20 weeks post-tumor induction, the average tumor area was significantly smaller for *Bmi1*$^{fl/fl}$ (n = 5 mice, 141 tumors) versus *Bmi1*$^{+/+}$ (n = 5 mice, 216 tumors), as judged by Student's t-test. **F)** The indicated number of mice and tumors from K *Bmi1*$^{+/+}$ or *Bmi1*$^{fl/fl}$ mice at 8, 12 and 20 weeks post tumor induction were used to identify tumor grade by histological analyses. **F,G)** The distribution of grade 1, 2 and 3 tumors was not significantly different (MANOVA test) but trended towards lower grades in the *Bmi1* mutant tumors, while the frequency of grade 3 tumors was significantly lower (Student's t-test) in *Bmi1*$^{fl/fl}$ tumors versus *Bmi1*$^{+/+}$ controls at 20 weeks post induction.

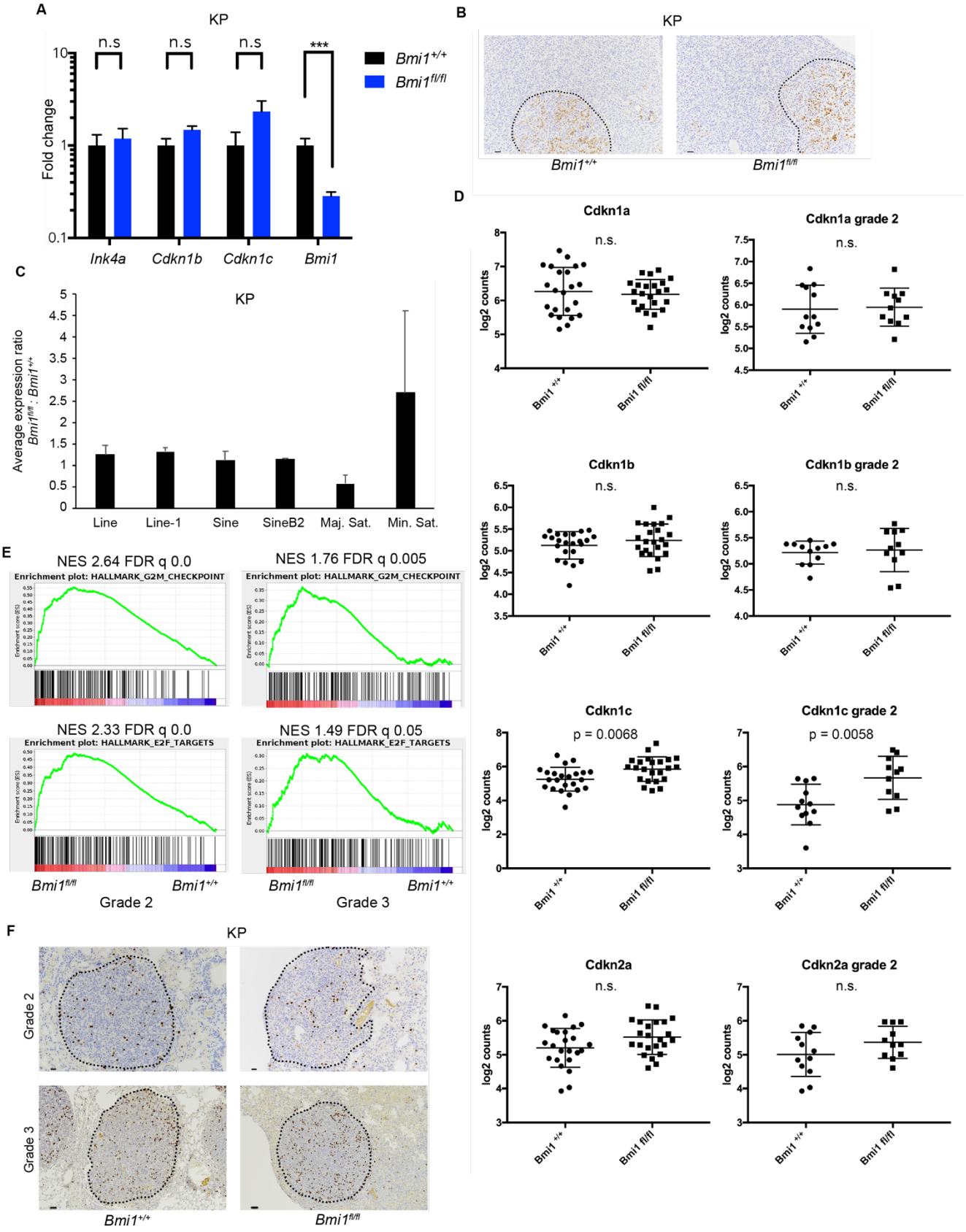

Figure S2 (continued on next page)

G

Bins (μm^2)	p values	# of *Bmi1*$^{+/+}$ tumors	# of *Bmi1*$^{fl/fl}$ tumors
$<5x10^4$	<0.000001	175	171
$5x10^4$ - $1x10^5$	0.000011	106	50
$1x10^5$ – $1.5x10^5$	0.000659	59	19
$>1.5x10^5$	0.00052	103	19

H

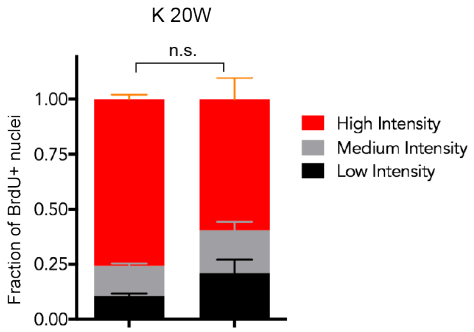

Figure S2. BMI1 loss affects progression through the cell cycle. **A)** RNA from 6-8 grade 2 KP tumors for each genotype was used for qRT-PCR quantification of mRNA transcript levels for the indicated cell cycle inhibitors, which all showed no significant differences between *Bmi1*$^{+/+}$ and *Bmi1*$^{fl/fl}$, and for *Bmi1*, which was significantly reduced in *Bmi1*$^{fl/fl}$ tumors. *** $p < 0.001$, as judged by Student's t-test. **B)** Representative immunohistochemical staining for $p19^{ARF}$ showed expression (brown stain) restricted to grade 3 areas of tumors (outlined) with no significant difference between *Bmi1*$^{+/+}$ and *Bmi1*$^{fl/fl}$ tumors. Nuclei are counterstained blue, scale bar = 25mm. **C)** RNA from grade 2 KP tumors which were *Bmi1*$^{+/+}$ (n = 4) or *Bmi1*$^{fl/fl}$ (n = 4) was used for qRT-PCR quantification of transcript levels of the indicated repetitive elements. The graph shows the ratio of transcript levels in *Bmi1*$^{fl/fl}$ over *Bmi1*$^{+/+}$, none of which were significantly different between the two genotypes, as judged by Student's t-test. **D)** Transcript levels from the sequenced tumors (log2 transformed blind variance stabilized counts from the HT-DGEseq) for the indicated CDK inhibitors including *Cdkn2a* ($p16^{INK4A}$, $p19^{ARF}$), *Cdkn1a* (p21) and *Cdkn1b* (p27), which showed no significant difference between *Bmi1*$^{+/+}$ and *Bmi1*$^{fl/fl}$ tumors, and *Cdkn1c* (p57), which showed a significant but modest, < 1.8 fold increase. Graphs on the left show all tumors, and those on the right show grade 2 tumors only. Each point represents a tumor, p value determined by Student's t-test. **E)** GSEA analyses of sequencing data showed significant upregulation of G2/M checkpoint and E2F target gene sets in *Bmi1*$^{fl/fl}$ versus *Bmi1*$^{+/+}$ for grade 2 tumors but less significantly for grade 3 tumors. **F)** Representative images of immunohistochemical staining for BrdU (brown stain) in KP *Bmi1*$^{+/+}$ and *Bmi1*$^{fl/fl}$ tumors that are grade 2 or 3. Nuclei are counterstained blue, scale bar for grade 2 = 20mm, and grade 3 = 50mm**. G)** Table showing the indicated tumor size bins, number of tumors analyzed from Figure 2F, statistical analyses of the proliferation rates. p values determined by Student's t-test. **H)** Graph shows distribution of low, medium and high intensity nuclear BrdU staining in tumors from *Bmi1*$^{+/+}$ (n = 6 mice, 203 tumors) versus *Bmi1*$^{fl/fl}$ (n = 6 mice, 206 tumors) K mice at 20W post induction. Trend is towards lower intensity but was not significant, as judged by one-way ANOVA.

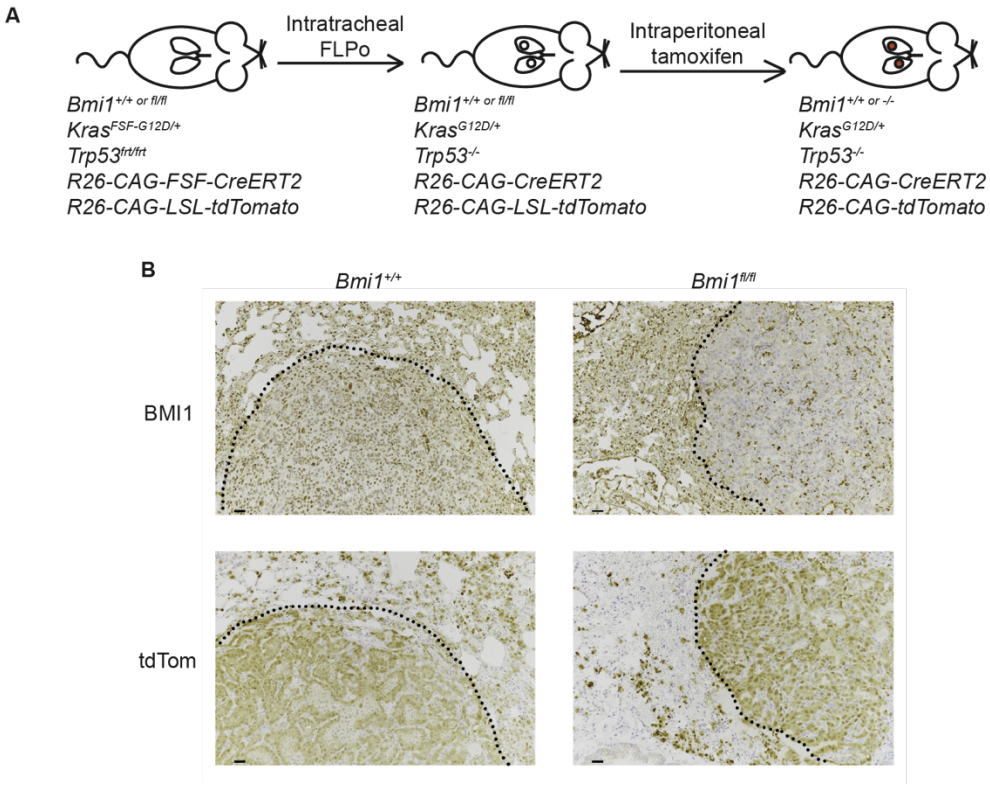

Figure S3 (continued on next page)

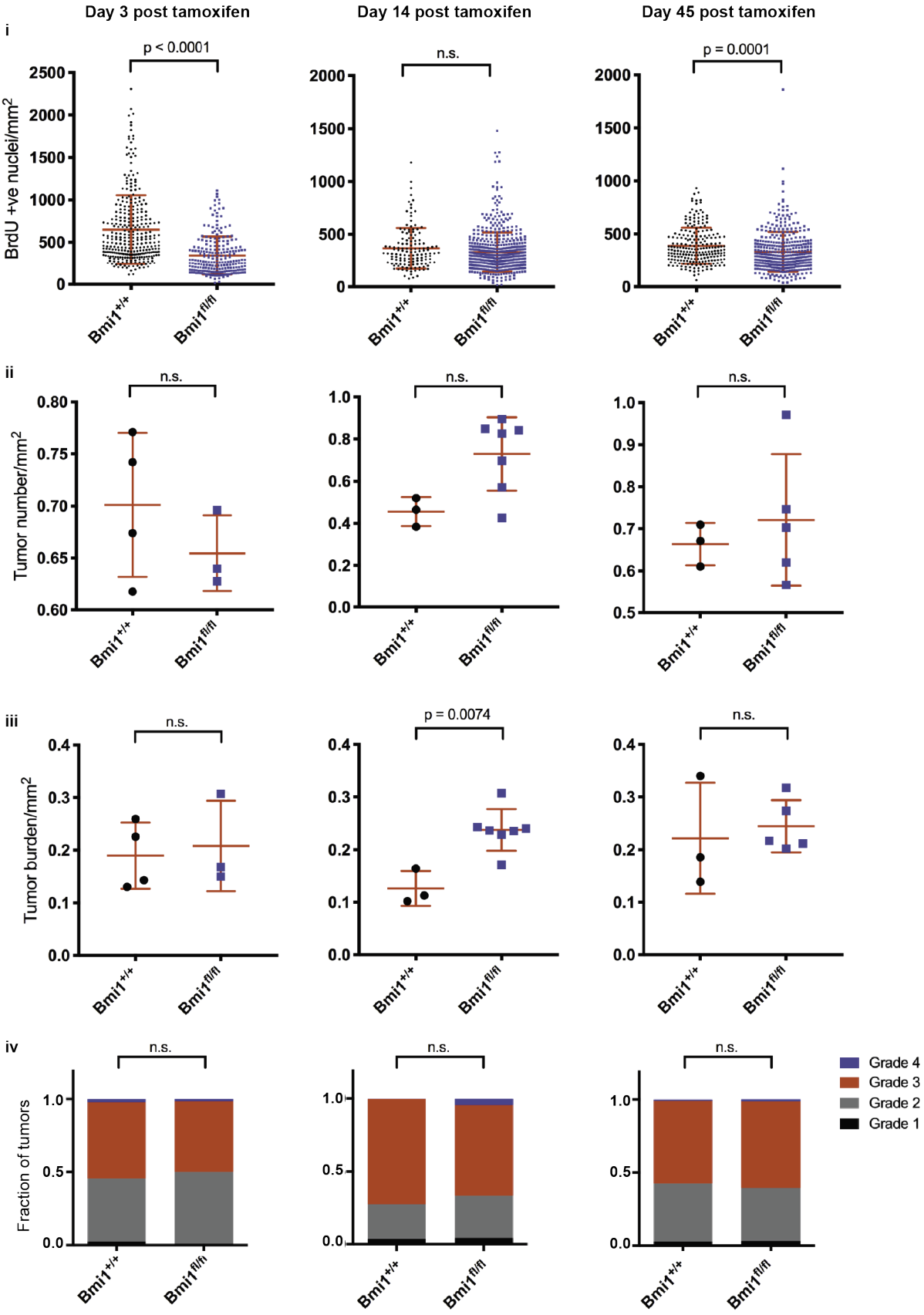

Figure S3 (continued on next page)

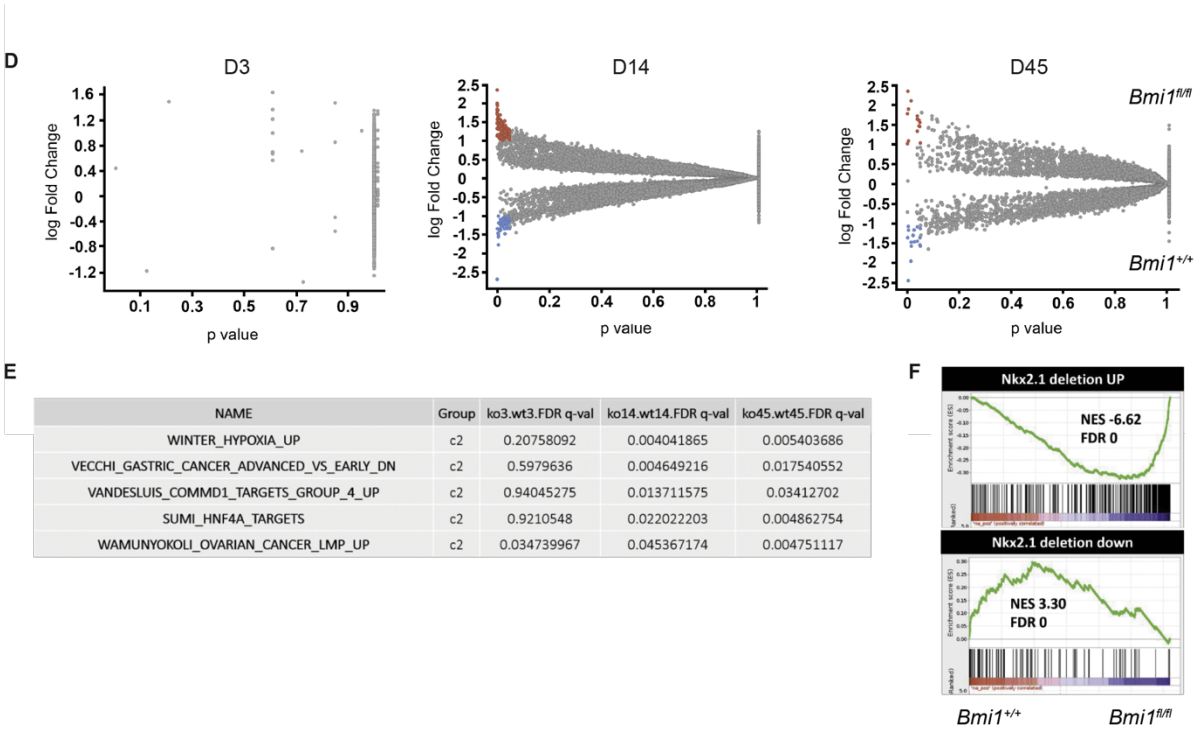

NAME	Group	ko3.wt3.FDR q-val	ko14.wt14.FDR q-val	ko45.wt45.FDR q-val
WINTER_HYPOXIA_UP	c2	0.20758092	0.004041865	0.005403686
VECCHI_GASTRIC_CANCER_ADVANCED_VS_EARLY_DN	c2	0.5979636	0.004649216	0.017540552
VANDESLUIS_COMMD1_TARGETS_GROUP_4_UP	c2	0.94045275	0.013711575	0.03412702
SUMI_HNF4A_TARGETS	c2	0.9210548	0.022022203	0.004862754
WAMUNYOKOLI_OVARIAN_CANCER_LMP_UP	c2	0.034739967	0.045367174	0.004751117

Figure S3. Schematic and characterization of acute *Bmi1* deletion in established LUAD tumors. **A**) Lung tumors were launched by intratracheal infusion of adenovirus expressing FLPo recombinase, which deleted *Trp53* and activated expression of oncogenic KRAS^{G12D} and CreERT2 by deleting the *FRT* flanked stop cassettes. Following tumor establishment, intraperitoneal injection of tamoxifen induced Cre-mediated deletion of the *loxP* flanked stop cassette, inducing expression of tdTomato and loss of BMI1 in *Bmi1*$^{fl/fl}$ animals. **B**) Immunohistochemical staining of representative *Bmi1*$^{+/+}$ and *Bmi1*$^{fl/fl}$ tumors from tamoxifen-treated mice. Tumors are demarked by the dotted line. Adjacent sections stained for BMI1 (upper panels) and tdTomato (tdTom; lower panels) indicate that BMI1 expression is lost only from *Bmi1*$^{fl/fl}$ tumor cells, but is still expressed in tumor infiltrating cells. All tumors express tdTomato. Nuclei are counterstained (blue), scale bars = 25μm. **C)** Acute *Bmi1* deletion in established LUAD tumors does not considerably impair tumor progression. Mice bearing KPCreER *Bmi1*$^{+/+}$ versus *Bmi1*$^{fl/fl}$ tumors (Cohort B) were harvested 3 days (*Bmi1*$^{+/+}$ n=4, *Bmi1*$^{fl/fl}$ n=4), 14 days (*Bmi1*$^{+/+}$ n=3, *Bmi1*$^{fl/fl}$ n=7) or 45 days (*Bmi1*$^{+/+}$ n=3, *Bmi1*$^{fl/fl}$ n=5) after tamoxifen treatment, which induces *Bmi1* deletion. **Ci-Ciii**) Graphs with the mean +/- one SD shown for: **Ci**) Number of BrdU-positive nuclei per mm^2 per tumor. Each point represents one tumor (Day 3 n = 306 *Bmi1*$^{+/+}$, 224 *Bmi1*$^{fl/fl}$; Day 14 n = *Bmi1*$^{+/+}$ 134, *Bmi1*$^{fl/fl}$ 552; and Day 45 n = *Bmi1*$^{+/+}$ 223, *Bmi1*$^{fl/fl}$ 387) and p values determined using unpaired Student's t-test. **Cii**) Average tumor number/mm^2 of lung/animal. p values determined by Mann Whitney test. **Ciii**) Average tumor burden/mm^2 of lung/animal. p values determined using an unpaired Student's t-test with Welch's correction. **Civ**) Graphs show tumor grade distribution/animal, with p values determined by ANOVA. **D)** Scatterplots of gene expression differences determined by DESeq2 analyses between *Bmi1*$^{+/+}$ and *Bmi1*$^{fl/fl}$ tumor samples at Day (D) 3, 14, and 45 after tamoxifen treatment. (n = 4 animals of each genotype per timepoint). Differentially expressed genes (logFC > 1, FDR <0.05) upregulated in *Bmi1*$^{fl/fl}$ or *Bmi1*$^{+/+}$ samples are highlighted in red or blue, respectively. **E)** Table listing five gene sets enriched in both Day 14 and Day 45 *Bmi1*$^{fl/fl}$ tumor samples relative to *Bmi1*$^{+/+}$ tumor samples following GSEA analysis performed using pre-ranked genes from the DESeq2 analysis and MSigDB C2 collection (FDR q value < 0.05). **F)** GSEA plots showing that genes upregulated following loss of NKX2.1 are enriched in *Bmi1*$^{fl/fl}$ tumors whilst, conversely, *Bmi1*$^{+/+}$ tumors are enriched for downregulated genes.

A

Cluster	# Bmi1$^{+/+}$ cells	# Bmi1$^{fl/fl}$ cells	Fraction Bmi1$^{+/+}$	Fraction Bmi1$^{fl/fl}$	OR	Fisher's
1	476	320	9.6%	7.1%	0.72	8.37E-06
2	448	379	9.1%	8.4%	0.92	0.26
3	1094	743	22.1%	16.5%	0.69	2.89E-12
4	770	694	15.6%	15.4%	0.98	0.78
5	734	501	14.9%	11.1%	0.72	6.13E-08
6	312	408	6.3%	9.0%	1.47	6.47E-07
7	117	95	2.4%	2.1%	0.89	0.40
8	45	73	0.9%	1.6%	1.79	2.14E-03
9	164	165	3.3%	3.7%	1.10	0.40
10	52	49	1.1%	1.1%	1.03	0.92
11	374	569	7.6%	12.6%	1.76	3.77E-16
12	98	148	2.0%	3.3%	1.67	9.70E-05
13	21	46	0.4%	1.0%	2.41	7.89E-04
14	18	63	0.4%	1.4%	3.87	3.56E-08
15	218	263	4.4%	5.8%	1.34	1.97E-03

B

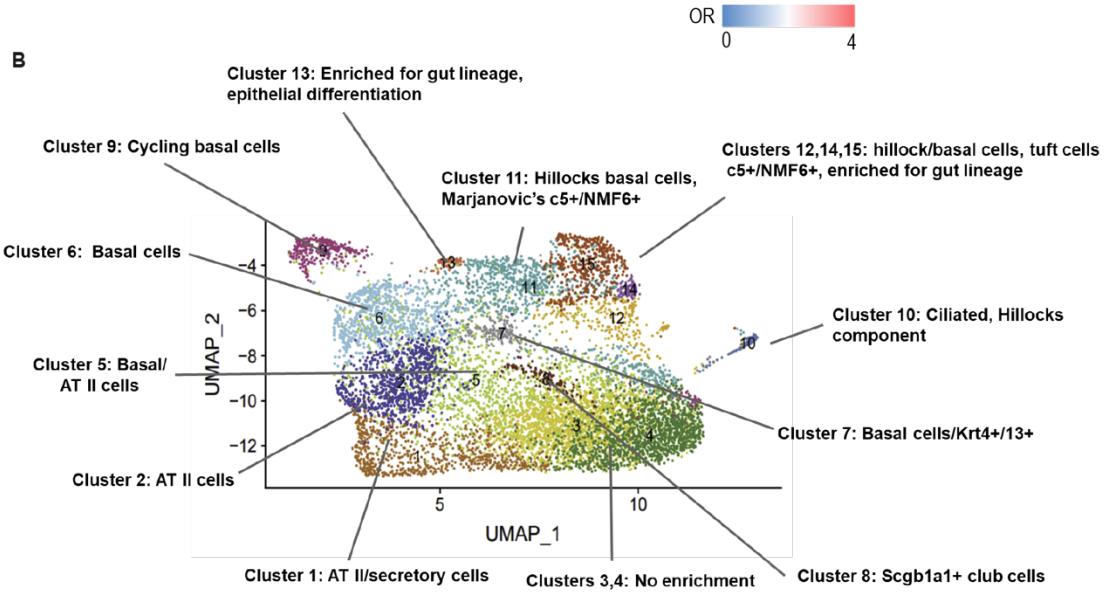

Figure S4. Characterization of *Bmi1*$^{+/+}$ and *Bmi1*$^{fl/fl}$ LUAD tumor cells using single cell RNA sequencing. **A)** Number and proportion of *Bmi1*$^{+/+}$ and *Bmi1*$^{fl/fl}$ cells in each cluster. The odds-ratio (OR) of *Bmi1*$^{fl/fl}$ cell representation in each cluster was calculated and evaluated using Fisher's exact test and the resulting p values are shown. **B)** Cell-type characterization of clusters within the UMAP plot determined by running GSEA with gene signatures derived from (Marjanovic et al., 2020; Montoro et al., 2018; Plasschaert et al., 2018).

MATERIALS AND METHODS

Viral production

Lentiviral backbone PGK-Cre plasmid was a gift from Tyler Jacks (MIT; modified from Addgene plasmid 17408). Lentiviral particles were generated by transfection of 293T cells using TransIT-LT1 (Mirus 2305) with lentiviral backbone plasmid and packaging vectors pCMV-dR8.2 (gag/pol, Addgene plasmid 8455) and pCMV-VSV-G (Addgene plasmid 8454). Supernatant was collected at 48 and 72 hours after transfection, concentrated at 25,000 r.p.m with an Optima L-100 XP ultra-centrifuge (Beckman Coulter), and resuspended in Opti-Mem (Thermo Fisher 31985062). Viral titer was determined using 3TZ reporter cells (DuPage, Dooley and Jacks, 2009). Adenoviral particles expressing FLPo were purchased from Vector Biolabs (Ad CMV FLPo, 1775).

Mouse strains and tumor initiation

Animal studies were approved by the Committee for Animal Care, and conducted in compliance with the Animal Welfare Act Regulations and other federal statutes relating to animals and experiments involving animals and adheres to the principles set forth in the Guide for the Care and Use of Laboratory Animals, 8th ed. National Research Council, 2011 (institutional animal welfare assurance no. A3125–01).

Mice harboring *Kras*$^{LSL\text{-}G12D/+}$ (Jackson et al., 2001), *Kras*$^{FSF\text{-}G12D/+}$ (Jackson laboratories #023590), *Trp53*^{fl} (Jonkers et al., 2001) (Jackson laboratories stock #008462), *Trp53*^{frt} (Lee et al., 2012) (Jackson laboratories stock #017767), *Bmi1*^{fl} (Maynard et al., 2014) (Jackson laboratories stock #028572), *Rosa26-CAG-FSF-CreERT2* (Schönhuber et al., 2014) and *Rosa26-CAG-LSL-tdTomato* (Madisen et al., 2010) (Jackson laboratories stock #007914) alleles are as described. PCR based genotyping was conducted as described in the cited references apart from *Bmi1* genotyping which used the following primers:

GGTTCCTCTTCATACATGACG and GACATACCCAATACTTTC (wild-type allele 279bp, floxed allele 313bp products) and the Rosa26-CAG-FSF-CreERT2 genotyping: GATAGTGAAACAGGGGCAATGG and TCTGCCAGGTTGGTCAGTAAGC (263bp product). All animals were maintained on a mixed C57BL/6J x 129SvJ x Balb/c background.

Tumors were initiated via intratracheal intubation with lentivirus or adenovirus expressing Cre or FLPo recombinases, as described (DuPage et al., 2009). K mice were infected with $5x10^4$ lentiviral particles per mouse. KP mice were infected with 10^5 or 10^4 lentiviral particles per mouse. For experiments with K and KP mice, littermates were used as controls. KPCreER mice were infected with $1x10^7$ pfu or $2.5x10^7$ pfu, as specified in the text. Tamoxifen (Sigma Aldrich, T5648) was administered via intraperitoneal injection (10mg/ml in corn oil, Sigma C8267) at 0.1g/kg once a day for four days. The tumor burden in live animals was examined by micro-Computerized Tomography using an eXplore CT-120 whole mouse micro computed tomography imager (GE Healthcare) and MicroView Software (Parallax Innovations).

Histology and tumor grading

Where required, BrdU (Sigma 85002) in medical grade PBS was dosed at 30mg/kg and injected 1 hour before euthanasia. Following necropsy lungs were perfused with formalin and fixed in formalin overnight. Tissue was washed in PBS then transferred to 70% ethanol, embedded in paraffin, and 4 micron sections were cut. Lung sections were stained with haematoxylin and eosin in a Thermo Gemini stainer and coverslips added using the Thermo Consul cover slipper. Images were captured using Leica Aperio AT2 Digital Slide Scanner and Aperio ImageScope Software. Tumor burden was measured as the fraction of tumor tissue per total lung area in a section. Tumor and lung areas were determined using Aperio ImageScope Software v12.3.0.5056.

For experiments with K and KP mice, tumors arising in mice were classified into 3 grades with the assistance of a board-certified veterinary pathologist. Grade 1 tumors displayed

minimal pleomorphism and include atypical adenomatous hyperplasias or small adenomas. Grade 2 adenomas were larger and exhibited uniform nuclei that are sometime slightly enlarged. Grade 3 tumors were identified as adenocarcinomas with severe nuclear atypia and cellular pleomorphism.

For the studies using KPCreER mice, a deep learning neural network-based software, provided by Aiforia was used to quantify tumor burden and tumor grade distribution (LaFave et al., 2020). Tumor size, tumor number, and tumor proliferation rate was quantified using open source QuPath software (Bankhead et al., 2017). An algorithm to detect tumors was trained using a subset of tumors from our samples. A manual quality assessment was made post classification of the tumors by the software. Following tumor detection, tumor proliferation rate was measured in the QuPath program by calculating the number of BrdU positive nuclei per mm^2 of tumor area. Graphical software PRISM and functions in MATLAB were used to generate graphs and perform statistical tests.

Immunohistochemistry

Immunohistochemistry (IHC) was performed using the following antibodies: BMI1(1:100, Millipore F6 05-637), BrdU (1:100, Abcam ab6326), CD45 (1:100, Abcam ab10558), HMGA2 (1:2000, Biocheck 59170AP), Cleaved Caspase 3 (1:200, Cell Signaling 9661), $p19^{ARF}$ (1:100, Santa Cruz sc-32748), and HNF4α (1:1000 Cell Signaling 3113). Images were captured using a Leica Aperio AT2 Digital Slide Scanner and Aperio ImageScope Software v12.3.0.5056 or on a Nikon Eclipse microscope with a DS Ri2 camera and NIS Elements Software.

IHC was performed on Thermo Autostainer 360 machine for many of the listed antibodies. Heat induced epitope retrieval procedure using Thermo citrate buffer pH=6.0 was performed on the pre-treatment module and slides subsequently treated with Biocare rodent block, primary antibody, and anti-mouse (Biocare), anti-rat (Vector Labs), or anti-rabbit (Vector Labs) HRP-polymer and developed with Thermo Ultra DAB. Slides were counterstained with

haematoxylin in a Thermo Gemini stainer and coverslips added using the Thermo Consul cover slipper.

IHC for all other antibodies was performed as follows: Rehydrated slides were washed in PBS 0.15% Triton X-100 (Sigma Aldrich T9284) followed by inactivation of endogenous peroxidases by incubation with 3% H2O2 (VWR MK524002) in PBS. Antigen retrieval was performed by heating in a 1250 W microwave for 6 min at 60% power followed by three rounds of 4 min at 40% power using a solution 8.2 mM sodium citrate, 1.8 mM citric acid, pH 6.0. Slides were blocked with PBS containing 5% of the appropriate serum and incubated overnight with the primary antibody diluted in PBS 0.15% Triton X-100 or this buffer alone or a non- specific antiserum as controls. Secondary antibodies (Vectastain ABC kits, Vector laboratories, PK-6100) were diluted 1:200 in PBS containing 0.4% of the appropriate blocking serum and detected using a DAB substrate following the manufacturer's instructions (Vector Laboratories, SK-4100). For BMI1 staining, a MOM kit (Vector Laboratories, BMK-2202) was used according to the manufacturer's instructions and an UltraVision LP Detection System (Thermo Fisher, TL060HD) for staining. Slides were counterstained with haematoxylin in a Thermo Gemini stainer and coverslips added using the Thermo Consul cover slipper.

Unless otherwise specified a minimum of 4 sections from 4 independent age, cohort and timepoint matched animals of each genotype were stained.

For experiments with K and KP tumors, quantification of positive nuclei and intensity scoring for BrdU was performed on tumors using Aperio ImageScope Software v12.3.0.5056 analysis algorithm Nuclear v9 with the following algorithm inputs:

Version	9.1
View Width	1000
View Height	1000
Overlap Size	100
Image Zoom	1
Classifier	None

Class List	
Classifier Neighborhood	0
Pixel Size (um)	0.504
Averaging Radius (um)	1
Averaging Radius (Pixels)	2
Curvature Threshold	2
Segmentation Type	0

Threshold Type	2
Lower Intensity Threshold	0
Upper Intensity Threshold	214
Min Nuclear Size (um^2)	10
Min Nuclear Size (Pixels)	39
Max Nuclear Size (um^2)	1.00E+06
Max Nuclear Size (Pixels)	3.94E+06
Min Roundness	0.2
Min Compactness	0
Min Elongation	5E-02
Remove Light Objects	0
Weak(1+) Threshold	210
Moderate(2+) Threshold	188
Strong(3+) Threshold	162
Black Threshold	0
Edge Trim	Weighted
Markup Image Type	Analysis
Nuclear Red OD	0.696858
Nuclear Green OD	0.643073
Nuclear Blue OD	0.317563
Positive Red OD	0.244583
Positive Green OD	0.509334
Positive Blue OD	0.825081
Color(3) Red OD	0
Color(3) Green OD	0
Color(3) Blue OD	0
Clear Area Intensity	233

Use Mode	Analysis/Tuning
Classifier Type	IHCNuclear
Classifier Definition File	IHCNuclearTraining
Display Plots	Yes

RNA isolation and qRT-PCR

Isolated tumors from mouse lungs were bisected. Half of the tumor was fixed for histology as described above, and half snap frozen in liquid nitrogen and stored in -80C. Grade 2 tumors were pulverized using Geno/Grinder 2010 (SPEX SamplePrep) and RNA was extracted from frozen powder using TRIZOL Reagent (Invitrogen 15596026) and spun to remove non-soluble fraction. Following addition of chloroform and centrifugation per manufacturer's protocol, RNA was purified from the aqueous phase using an RNeasy Mini Kit (Qiagen 74106) including an on column DNAse I incubation step (Qiagen 79254). cDNA was generated using Superscript III RT (Invitrogen 18080044) per manufacturer. Real-Time quantitative PCR reactions were performed using Fast SYBR Green PCR Master Mix (Thermo Fisher 4385616) and a Step One Plus Real-Time PCR System (Applied Biosystem). All gene expression was shown relative to 18S and normalized to the average value of *Bmi1*$^{+/+}$ tumors. Primers qPCR were as follows (F: forward primer, R: reverse primer):

18S F	CGTCTGCCCTATCAACTTTGC
18S R	CTTGGATGTGGTAGCCGTTTC
BMI1 F	CAAAACCAGAACACTCCTGAA
BMI1 R	TCTTCTTCTCTTCATCTCATTTTTGA
$p16^{INK4A}$ F	GCGGGCACTGCTGGAAG
$p16^{INK4A}$ R	CGTTGCCCATCATCATCACC
p57 F	CGAACGACTTCTTCGCCAA
p57 R	ACGCCTTGTTCTCCTGCG
p27 F	TTGGTGGACCAAATGCCTGACT
p27 R	AATCTTCTGCAGCAGGTCGCTT

For analyses of repeat sequence expression, four *Bmi1*$^{+/+}$ wild type and four *Bmi1*$^{fl/fl}$ KP grade 2 tumor RNA samples were treated with Dnase I (Thermo Fisher 18068015) and then used to generate cDNA and the transcript levels analyzed as described above using Ubiquitin transcript levels for normalization and the listed primer pairs. Samples without reverse transcriptase added were used to rule out contaminating genomic DNA.

LINE F	TGGCTTGTGCTGTAAGATCG
LINE R	TCTGTTGGTGGTCTTTTTGTC
SINE F	GAGCACACCCATGCACATAC
SINE R	AAAGGCATGCACCTCTACCACC
Minor Satellite F	TTGGAAACGGGATTTGTAGA
Minor Satellite R	CGGTTTCCAACATATGTGTTTT
Major Satellite F	GGCGAGAAAACTGAAAATCACG
Major Satellite R	CTTGCCATATTCCACGTCCT
LINE-1 F	AGTGCAGAGTTCTATCAGACCTTC
LINE-1 R	AACCTACTTGGTCAGGATGGATG
Sineb2 F	GAGCACCTGACTGCTCTTCC
Sineb2 R	ACACACCAGAAGAGGGCATC
Ubiquitin R	GCAAGTGGCTAGAGTGCAGAGTAA
Ubiquitin F	TGGCTATTAATTATTCGGTCTGCAT

All primers were purchased from Sigma Aldrich.

Bulk RNA sequencing and analysis of K and KP tumors

For experiments with K and KP tumors, mRNA from individual tumors were isolated as described above and checked for quality and purity using a 2100 BioAnalyzer (Agilent). 48 tumors were selected for Digital Gene Expression (DGE) based on purity of sample as measured by histology and RNA quality. RNA was processed for DGE as described (Soumillon et al., 2014). Briefly, 20ng of RNA was converted to cDNA, and enriched for polyA. Individual transcripts marked with unique molecular identifiers (UMI) and barcoded by tumor. cDNA was then tagmented using Nextera XT (Illumina) to enrich for 3' fragments for sequencing. Samples

were sequenced in 40 nucleotide reads with paired ends using a HiSeq 2000 (Illumina). After sequencing, samples were de-convoluted by barcode and collapsed by UMI+40 nucleotide stranded read. Reads were aligned to mm9 version of the mouse genome using tophat 2.0.4 with segment length of 16 and filtered for Q30 quality mapping. Mapped reads were annotated to UCSC mm9 annotated genes and counted using HTseq. Raw expression counts were upper-quartile normalized to a count of 2000 (Bullard et al., 2010).

Differential expression analysis was performed in a biased manner to directly compare gene expression between two subgroups of the HT-DGEseq samples as indicated. Specifically, raw counts were processed for differential expression and principal component analysis using DEseq2 v1.10.1 (Love, Huber and Anders, 2014). Differential expression (DE) gene signature was developed by filtering for fold 1.5 change and Benjamini Hochberg adjusted p value of 0.05. Preranked gene set enrichment analysis (GSEA) using Hallmark gene sets was performed on DE signatures sorted by fold change as described in (Mootha et al., 2003; Subramanian et al., 2005). Data were analyzed through the use of QIAGEN's Ingenuity® Pathway Analysis (IPA®, QIAGEN Redwood City).

Lung tumor cell isolation from KPCreER tumors

Mice were sacrificed, and lungs were perfused with PBS. Lungs were then chopped using sterilized razor blade and incubated at 37C for 1 hour in 2mg/ml collagenase/dispase (Sigma Aldrich, 11097113001) and 0.1mg/mL DNase I in DMEM (Worthington Biomedical LS002138). The cells were then filtered through 70μm filter and red blood cells were lysed using ACK lysis buffer (Thermo Fisher A1049201). Following a wash, the cells were incubated with APC-conjugated antibodies against CD45 (eBioscience 17-0451-82), CD31 (BioLegend 102510), and Ter119 (BD Biosciences 557909) for 20 minutes in ice. After a spin and a wash, the cells were resuspended in PBS+10% FBS (Hyclone SH30910.03) with DAPI (BD

Pharmingen 564907) for FACS sorting. Cells were sorted using BD FACS Aria Cell Sorter for the DAPI-negative, APC-negative, and tdTomato-positive populations.

Bulk RNA sequencing and differential expression analysis for KPCreER tumors

10000 tumor cells were isolated using the FACS sorting method described and sorted directly into Trizol (Thermo Fisher 15596026) in an Eppendorf tube coated with FBS. Chloroform extraction was performed on the mix and the aqueous phase was collected for RNA. RNA was then extracted using the RNeasy Micro Kit (Qiagen 74034). The quality of RNA was analyzed using AATI FEMTO Pulse analyzer. Samples were then prepared for sequencing using Kapa mRNA Hyperprep (Roche 08098093702), and sequenced using HiSeq2000 (Illumina).

Differentially expressed genes were analyzed using DESeq2 package (Love et al., 2014). Preranked gene list using output from DeSeq2 was used to run gene set enrichment analysis (Subramanian et al., 2005). Additional gene sets curated were appended to the C2 gene sets in the molecular signature database v6.2. Unsupervised hierarchical clustering was performed using Morpheus software from Broad Institute (https://software.broadinstitute.org/morpheus).

Single cell RNA sequencing and analysis of KPCreER tumors

Tumor cells from KPCreER mice were isolated using the FACS sorting method described above and prepared for single cell RNA sequencing using the SeqWell pipeline described (Gierahn et al., 2017). Paired-end sequencing reads were processed using an analytical pipeline derived from the DropSeq pipeline v. 1.12, as described in (Gierahn et al., 2017). Briefly, reads were converted to a bam file using picard v. 2.9.0-1-gf5b9f50-SNAPSHOT, tagged with cell and transcript barcodes, and subsequently sequencing adapters and polyadenosine tracts were trimmed. Upon regenerating fastq files, reads were aligned with

STAR v. 2.5.3a (Dobin et al., 2013) against the murine GRCh/38 assembly Gencode M15 release. Genomic features of the aligned reads were annotated, including gene and exon of origin when relevant. Bead synthesis errors were assessed and when possible, altered unique molecular identifiers (UMIs) were repaired. Cell barcode abundance was tallied and gene expression was called for the top 2000 cell barcodes.

Count matrices of genes x cells were imported in the R v. 3.5.1 statistical environment and Seurat v.3 beta was used as the primary analytical package (Satija et al., 2015). Count matrices were merged into a single Seurat object. Normalization to ten thousand transcript per cell barcodes was run on each sample individually, and variable features were identified using the vst method based on the top 2000 feature. The samples were then integrated using Seurat's IntegrateData procedure, using 2000 anchors (Butler et al., 2018). Subsequently, dimensionality reduction using principal component analysis, visualization in UMAP embeddings and cluster identification based on the Louvain algorithm for nearest-neighbor identification were all based on the integrated dataset, while differential expression analysis was run on non-integrated data. Briefly, the top 20 principal components were used to build the kNN graph, considering 10 nearest neighbors. The resulting graph was partitioned using a shared nearest neighbor (SNN) modularity optimization-based clustering algorithm at resolution 0.8 to identify clusters. Iterative visualizations and plotting of QC metrics led to the exclusion of cells with low-transcript and high-mitochondrial content, eventually resulting in 9457 cells (with more than 200 UMIs and 200 genes per cell) and 7196 genes being retained for downstream analysis.

In addition to cluster identification on the integrated object, genotype-specific data integration was performed on the remaining cells to verify the robustness of cluster calls. Upon inspection of the data, cells in the merged object falling in the neighborhood of some *Bmi1*$^{fl/fl}$-specific subclusters (clusters 11-15) were manually apportioned to these clusters. Proportions of cells from either genotype in each cluster were tallied and compared using the Fisher's exact

test for biases in cell representation in each given cluster iteratively against the rest of the cells, pooled by genotype.

Functional signatures were retrieved from the literature (Lau et al., 2014; Snyder et al., 2013; Winslow et al., 2011; Zheng et al., 2013). Each signature was scored in each cell by summing transcript counts normalized per 10K transcripts over each gene present in the signature.

To determine cell type assignment and enrichment for functional pathways within each cluster, cluster-specific markers were identified using the FindAllMarker function, with logfc.threshold=-20 and the Wilcoxon test for significance. Resulting outputs were converted to rank files. Gene set enrichment analysis (implemented in GSEA desktop version, v4.1.0) (Mootha et al., 2003; Subramanian et al., 2005), was performed to gauge the enrichment of different lung cell signatures reported in (Marjanovic et al., 2020; Montoro et al., 2018; Plasschaert et al., 2018), running the algorithm in pre-ranked mode with the log2FC column as the ranking metric, with a weighted scoring scheme, normalizing by meandiv, restricting the analysis to gene sets sizes between 5 and 2000 genes. Additionally, gene ontology analysis of clusters 3, 4, 13, 14 and 15 was performed in GSEA pre-ranked mode against MsigDB 7.0 C5 using the pre-built orthology converting table based on the official gene symbol as the key. 1000 permutations were run for p-value estimation.

ACKNOWLEDGEMENTS

We thank: Anna Kuperman, Lynn Liu, Stephanie Riocci and Jenny Tadros; the Koch Institute Swanson Biotechnology Center, particularly the Histology, Flow Cytometry, Integrated Genomics and Bioinformatics, and the Preclinical Modeling, Imaging and Testing core facilities for technical help; Tyler Jacks, Dieter Saur, and David Kirsch for transgenic alleles and reagents; and members of the Lees and Jacks' laboratories for advice and discussions. Funding was provided by a Transcend grant from Janssen Pharmaceuticals, the MIT Stem Cell Initiative, and P01-CA042063-31 (NIH NCI) to J.A.L, as well the Koch Institute Support (core) Grant P30-CA14051 (NCI). E.Y.K. received support from Ludwig Center for Molecular Oncology Fund and NIH Pre-Doctoral Training Grant GM007287. D.L.K. received support from an NSF pre-doctoral fellowship. S.H. received support from NIH 1F30CA260739-01. J.A.L. is the Virginia and D.K. Ludwig Professor for Cancer Research at the Koch Institute at MIT.

REFERENCES

Abdouh, M., Hanna, R., el Hajjar, J., Flamier, A., and Bernier, G. (2016). The polycomb repressive complex 1 protein BMI1 is required for constitutive heterochromatin formation and silencing in mammalian somatic cells. Journal of Biological Chemistry *291*, 182–197.

Agherbi, H., Gaussmann-Wenger, A., Verthuy, C., Chasson, L., Serrano, M., and Djabali, M. (2009). Polycomb mediated epigenetic silencing and replication timing at the INK4a/ARF locus during senescence. PLoS ONE *4*, 1–10.

Al-Hajj, M., Wicha, M.S., Benito-Hernandez, A., Morrison, S.J., and Clarke, M.F. (2003). Prospective identification of tumorigenic breast cancer cells. Proceedings of the National Academy of Sciences *100*.

Avgustinova, A., Symeonidi, A., Castellanos, A., Urdiroz-Urricelqui, U., Solé-Boldo, L., Martín, M., Pérez-Rodríguez, I., Prats, N., Lehner, B., Supek, F., et al. (2018). Loss of G9a preserves mutation patterns but increases chromatin accessibility, genomic instability and aggressiveness in skin tumours. Nature Cell Biology *20*.

Bankhead, P., Loughrey, M.B., Fernández, J.A., Dombrowski, Y., McArt, D.G., Dunne, P.D., McQuaid, S., Gray, R.T., Murray, L.J., Coleman, H.G., et al. (2017). QuPath: Open source software for digital pathology image analysis. Scientific Reports *7*, 16878.

Barabino, A., Plamondon, V., Abdouh, M., Chatoo, W., Flamier, A., Hanna, R., Zhou, S., Motoyama, N., Hébert, M., Lavoie, J., et al. (2016). Loss of Bmi1 causes anomalies in retinal development and degeneration of cone photoreceptors. Development (Cambridge) *143*, 1571–1584.

Becker, M., Korn, C., Sienerth, A.R., Voswinckel, R., Luetkenhaus, K., Ceteci, F., and Rapp, U.R. (2009). Polycomb group protein Bmi1 is required for growth of RAF driven non-small-cell lung cancer. PLoS ONE *4*, 1–10.

Bednar, F., Schofield, H.K., Collins, M.A., Yan, W., Zhang, Y., Shyam, N., Eberle, J.A., Almada, L.L., Olive, K.P., Bardeesy, N., et al. (2015). Bmi1 is required for the initiation of pancreatic cancer through an Ink4a-independent mechanism. Carcinogenesis *36*.

Butler, A., Hoffman, P., Smibert, P., Papalexi, E., and Satija, R. (2018). Integrating single-cell transcriptomic data across different conditions, technologies, and species. Nature Biotechnology.

Cao, L., Bombard, J., Cintron, K., Sheedy, J., Weetall, M.L., and Davis, T.W. (2011). BMI1 as a novel target for drug discovery in cancer. Journal of Cellular Biochemistry *112*, 2729–2741.

Cao, R., Tsukada, Y., and Zhang, Y. (2005). Role of Bmi-1 and Ring1A in H2A Ubiquitylation and Hox Gene Silencing. Molecular Cell *20*.

Chaffer, C.L., and Weinberg, R.A. (2015). How Does Multistep Tumorigenesis Really Proceed? Cancer Discovery *5*.

Chaffer, C.L., Brueckmann, I., Scheel, C., Kaestli, A.J., Wiggins, P.A., Rodrigues, L.O., Brooks, M., Reinhardt, F., Su, Y., Polyak, K., et al. (2011). Normal and neoplastic nonstem cells

can spontaneously convert to a stem-like state. Proceedings of the National Academy of Sciences *108*.

Chatoo, W., Abdouh, M., David, J., Champagne, M.P., Ferreira, J., Rodier, F., and Bernier, G. (2009). The polycomb group gene Bmi1 regulates antioxidant defenses in neurons by repressing p53 pro-oxidant activity. Journal of Neuroscience *29*, 529–542.

Curtis, S.J., Sinkevicius, K.W., Li, D., Lau, A.N., Roach, R.R., Zamponi, R., Woolfenden, A.E., Kirsch, D.G., Wong, K.K., and Kim, C.F. (2010). Primary tumor genotype is an important determinant in identification of lung cancer propagating cells. Cell Stem Cell *7*, 127–133.

Dagogo-Jack, I., and Shaw, A.T. (2018). Tumour heterogeneity and resistance to cancer therapies. Nature Reviews Clinical Oncology *15*.

Dobin, A., Davis, C.A., Schlesinger, F., Drenkow, J., Zaleski, C., Jha, S., Batut, P., Chaisson, M., and Gingeras, T.R. (2013). STAR: Ultrafast universal RNA-seq aligner. Bioinformatics.

Douglas, D., Hsu, J.H.-R., Hung, L., Cooper, A., Abdueva, D., van Doorninck, J., Peng, G., Shimada, H., Triche, T.J., and Lawlor, E.R. (2008). BMI-1 promotes ewing sarcoma tumorigenicity independent of CDKN2A repression. Cancer Research *68*.

Dovey, J.S., Zacharek, S.J., Kim, C.F., and Lees, J.A. (2008). Bmi1 is critical for lung tumorigenesis and bronchioalveolar stem cell expansion. Proceedings of the National Academy of Sciences *105*.

Duma, N., Santana-Davila, R., and Molina, J.R. (2019). Non–Small Cell Lung Cancer: Epidemiology, Screening, Diagnosis, and Treatment. Mayo Clinic Proceedings *94*.

DuPage, M., Dooley, A.L., and Jacks, T. (2009). Conditional mouse lung cancer models using adenoviral or lentiviral delivery of Cre recombinase. Nature Protocols *4*, 1064–1072.

Facchino, S., Abdouh, M., Chatoo, W., and Bernier, G. (2010). BMI1 confers radioresistance to normal and cancerous neural stem cells through recruitment of the DNA damage response machinery. Journal of Neuroscience *30*, 10096–10111.

Feldser, D.M., Kostova, K.K., Winslow, M.M., Taylor, S.E., Cashman, C., Whittaker, C.A., Sanchez-Rivera, F.J., Resnick, R., Bronson, R., Hemann, M.T., et al. (2010). Stage-specific sensitivity to p53 restoration during lung cancer progression. Nature *468*, 572–575.

Ferretti, R., Bhutkar, A., McNamara, M.C., and Lees, J.A. (2016). BMI1 induces an invasive signature in melanoma that promotes metastasis and chemoresistance. Genes & Development *30*.

Flavahan, W.A., Gaskell, E., and Bernstein, B.E. (2017). Epigenetic plasticity and the hallmarks of cancer. Science *357*.

Gierahn, T.M., Wadsworth, M.H., Hughes, T.K., Bryson, B.D., Butler, A., Satija, R., Fortune, S., Christopher Love, J., and Shalek, A.K. (2017). Seq-Well: Portable, low-cost rna sequencing of single cells at high throughput. Nature Methods.

Gil, J., and O'Loghlen, A. (2014). PRC1 complex diversity: where is it taking us? Trends in Cell Biology *24*.

Ginjala, V., Nacerddine, K., Kulkarni, A., Oza, J., Hill, S.J., Yao, M., Citterio, E., van Lohuizen, M., and Ganesan, S. (2011). BMI1 is recruited to DNA breaks and contributes to DNA damage-induced H2A ubiquitination and repair. Molecular and Cellular Biology *31*.

Hanahan, D., and Weinberg, R.A. (2011). Hallmarks of Cancer: The Next Generation. Cell *144*.

Hu, Y., and Smyth, G.K. (2009). ELDA: Extreme limiting dilution analysis for comparing depleted and enriched populations in stem cell and other assays. Journal of Immunological Methods *347*, 70–78.

Hurt, E.M., Kawasaki, B.T., Klarmann, G.J., Thomas, S.B., and Farrar, W.L. (2008). CD44+CD24− prostate cells are early cancer progenitor/stem cells that provide a model for patients with poor prognosis. British Journal of Cancer *98*.

Iwama, A., Oguro, H., Negishi, M., Kato, Y., Morita, Y., Tsukui, H., Ema, H., Kamijo, T., Katoh-Fukui, Y., Koseki, H., et al. (2004). Enhanced Self-Renewal of Hematopoietic Stem Cells Mediated by the Polycomb Gene Product Bmi-1. Immunity *21*.

Jackson, E.L., Willis, N., Mercer, K., Bronson, R.T., Crowley, D., Montoya, R., Jacks, T., and Tuveson, D.A. (2001). Analysis of lung tumor initiation and progression using conditional expression of oncogenic K-ras. Genes & Development *15*.

Jackson, E.L., Olive, K.P., Tuveson, D.A., Bronson, R., Crowley, D., Brown, M., and Jacks, T. (2005). The Differential Effects of Mutant p53 Alleles on Advanced Murine Lung Cancer. Cancer Research *65*, 10280–10288.

Jacobs, J.J.L., Scheijen, B., Voncken, J.W., Kieboom, K., Berns, A., and van Lohuizen, M. (1999a). Bmi-1 collaborates with c-Myc in tumorigenesis by inhibiting c-Myc- induced apoptosis via INK4a/ARF. Genes and Development *13*, 2678–2690.

Jacobs, J.J.L., Kieboom, K., Marino, S., DePinho, R.A., and van Lohuizen, M. (1999b). The oncogene and Polycomb-group gene bmi-1 regulates cell proliferation and senescence through the ink4a locus. Nature *397*.

Jonkers, J., Meuwissen, R., van der Gulden, H., Peterse, H., van der Valk, M., and Berns, A. (2001). Synergistic tumor suppressor activity of BRCA2 and p53 in a conditional mouse model for breast cancer. Nature Genetics.

Kreso, A., van Galen, P., Pedley, N.M., Lima-Fernandes, E., Frelin, C., Davis, T., Cao, L., Baiazitov, R., Du, W., Sydorenko, N., et al. (2014). Self-renewal as a therapeutic target in human colorectal cancer. Nature Medicine *20*, 29–36.

Lathia, J.D., Mack, S.C., Mulkearns-Hubert, E.E., Valentim, C.L.L., and Rich, J.N. (2015). Cancer stem cells in glioblastoma. Genes & Development *29*.

Lau, A.N., Curtis, S.J., Fillmore, C.M., Rowbotham, S.P., Mohseni, M., Wagner, D.E., Beede, A.M., Montoro, D.T., Sinkevicius, K.W., Walton, Z.E., et al. (2014). Tumor-propagating cells and Yap/Taz activity contribute to lung tumor progression and metastasis. EMBO Journal *33*, 468–481.

Lee, C.L., Moding, E.J., Huang, X., Li, Y., Woodlief, L.Z., Rodrigues, R.C., Ma, Y., and Kirsch, D.G. (2012). Generation of primary tumors with Flp recombinase in FRT-flanked p53 mice. DMM Disease Models and Mechanisms *5*, 397–402.

Lessard, J., and Sauvageau, G. (2003). Bmi-1 determines the proliferative capacity of normal and leukaemic stem cells. Nature *423*.

Lessard, J., Baban, S., and Sauvageau, G. (1998). Stage-specific expression of polycomb group genes in human bone marrow cells. Blood *91*.

Lim, Z.-F., and Ma, P.C. (2019). Emerging insights of tumor heterogeneity and drug resistance mechanisms in lung cancer targeted therapy. Journal of Hematology & Oncology *12*.

Liu, J., Cao, L., Chen, J., Song, S., Lee, I.H., Quijano, C., Liu, H., Keyvanfar, K., Chen, H., Cao, L.Y., et al. (2009). Bmi1 regulates mitochondrial function and the DNA damage response pathway. Nature *459*, 387–392.

van Lohuizen, M., Frasch, M., Wientjens, E., and Berns, A. (1991a). Sequence similarity between the mammalian bmi-1 proto-oncogene and the Drosophila regulatory genes Psc and Su(z)2. Nature *353*.

van Lohuizen, M., Verbeek, S., Scheljen, B., Wientjens, E., van der Guidon, H., and Berns, A. (1991b). Identification of cooperating oncogenes in Eμ-myc transgenic mice by provirus tagging. Cell *65*, 737–752.

Love, M.I., Huber, W., and Anders, S. (2014). Moderated estimation of fold change and dispersion for RNA-seq data with DESeq2. Genome Biology.

Lowe, S.W., and Sherr, C.J. (2003). Tumor suppression by Ink4a–Arf: progress and puzzles. Current Opinion in Genetics & Development *13*, 77–83.

van der Lugt, N.M.T., Domen, J., Linders, K., van Roon, M., Robanus-Maandag, E., te Riele, H., van der Valk, M., Deschamps, J., Sofroniew, M., van Lohuizen, M., et al. (1994). Posterior transformation, neurological abnormalities, and severe hematopoietic defects in mice with a targeted deletion of the bmi-1 proto- oncogene. Genes and Development *8*, 757–769.

van der Lugt, N.M.T., Alkema, M., Berns, A., and Deschamps, J. (1996). The Polycomb-group homolog Bmi-1 is a regulator of murine Hox gene expression. Mechanisms of Development *58*.

Madisen, L., Zwingman, T.A., Sunkin, S.M., Oh, S.W., Zariwala, H.A., Gu, H., Ng, L.L., Palmiter, R.D., Hawrylycz, M.J., Jones, A.R., et al. (2010). A robust and high-throughput Cre reporting and characterization system for the whole mouse brain. Nature Neuroscience *13*, 133–140.

Marjanovic, N.D., Hofree, M., Chan, J.E., Canner, D., Wu, K., Trakala, M., Hartmann, G.G., Smith, O.C., Kim, J.Y., Evans, K.V., et al. (2020). Emergence of a High-Plasticity Cell State during Lung Cancer Evolution. Cancer Cell *38*, 229–246.e13.

Maynard, M.A., Ferretti, R., Hilgendorf, K.I., Perret, C., Whyte, P., and Lees, J.A. (2014). Bmi1 is required for tumorigenesis in a mouse model of intestinal cancer. Oncogene *33*.

McKeller, R.N., Fowler, J.L., Cunningham, J.J., Warner, N., Smeyne, R.J., Zindy, F., and Skapek, S.X. (2002). The Arf tumor suppressor gene promotes hyaloid vascular regression during mouse eye development. Proceedings of the National Academy of Sciences *99*, 3848–3853.

Meacham, C.E., and Morrison, S.J. (2013). Tumour heterogeneity and cancer cell plasticity. Nature *501*.

Medema, J.P. (2013). Cancer stem cells: The challenges ahead. Nature Cell Biology *15*, 338–344.

Molofsky, A. v., Pardal, R., Iwashita, T., Park, I.-K., Clarke, M.F., and Morrison, S.J. (2003). Bmi-1 dependence distinguishes neural stem cell self-renewal from progenitor proliferation. Nature *425*.

Molofsky, A. v, He, S., Bydon, M., Morrison, S.J., and Pardal, R. (2005). Bmi-1 promotes neural stem cell self-renewal and neural development but not mouse growth and survival by repressing the p16Ink4a and p19Arf senescence pathways. Genes & Development *19*.

Montoro, D.T., Haber, A.L., Biton, M., Vinarsky, V., Lin, B., Birket, S.E., Yuan, F., Chen, S., Leung, H.M., Villoria, J., et al. (2018). A revised airway epithelial hierarchy includes CFTR-expressing ionocytes. Nature.

Mootha, V.K., Daly, M.J., Patterson, N., Mesirov, J.P., Golub, T.R., Tamayo, P., Spiegelman, B., and Groop, L.C. (2003). PGC-1α-responsive genes involved in oxidative phosphorylation are coordinately downregulated in human diabetes. Nature Genetics.

Morrisey, E.E., and Hogan, B.L.M. (2010). Preparing for the First Breath: Genetic and Cellular Mechanisms in Lung Development. Developmental Cell *18*, 8–23.

Muzumdar, M.D., Dorans, K.J., Chung, K.M., Robbins, R., Tammela, T., Gocheva, V., Li, C.M.-C., and Jacks, T. (2016). Clonal dynamics following p53 loss of heterozygosity in Kras-driven cancers. Nature Communications *7*, 12685.

O'Brien, C.A., Pollett, A., Gallinger, S., and Dick, J.E. (2007). A human colon cancer cell capable of initiating tumour growth in immunodeficient mice. Nature *445*.

Oguro, H., Iwama, A., Morita, Y., Kamijo, T., van Lohuizen, M., and Nakauchi, H. (2006). Differential impact of Ink4a and Arf on hematopoietic stem cells and their bone marrow microenvironment in Bmi1-deficient mice. Journal of Experimental Medicine *203*.

Park, I., Qian, D., Kiel, M., Becker, M.W., Pihalja, M., Weissman, I.L., Morrison, S.J., and Clarke, M.F. (2003). Bmi-1 is required for maintenance of adult self-renewing haematopoietic stem cells. Nature *423*.

Park, I.K., Morrison, S.J., and Clarke, M.F. (2004). Bmi1, stem cells, and senescence regulation. Journal of Clinical Investigation.

Plasschaert, L.W., Žilionis, R., Choo-Wing, R., Savova, V., Knehr, J., Roma, G., Klein, A.M., and Jaffe, A.B. (2018). A single-cell atlas of the airway epithelium reveals the CFTR-rich pulmonary ionocyte. Nature.

Ricci-Vitiani, L., Lombardi, D.G., Pilozzi, E., Biffoni, M., Todaro, M., Peschle, C., and de Maria, R. (2007). Identification and expansion of human colon-cancer-initiating cells. Nature *445*.

Rowbotham, S.P., Li, F., Dost, A.F.M., Louie, S.M., Marsh, B.P., Pessina, P., Anbarasu, C.R., Brainson, C.F., Tuminello, S.J., Lieberman, A., et al. (2018). H3K9 methyltransferases

and demethylases control lung tumor-propagating cells and lung cancer progression. Nature Communications *9*.

Sanchez, A., de Vivo, A., Tonzi, P., Kim, J., Huang, T.T., and Kee, Y. (2020). Transcription-replication conflicts as a source of common fragile site instability caused by BMI1-RNF2 deficiency. PLoS Genetics *16*, e1008524.

Satija, R., Farrell, J.A., Gennert, D., Schier, A.F., and Regev, A. (2015). Spatial reconstruction of single-cell gene expression data. Nature Biotechnology.

Schönhuber, N., Seidler, B., Schuck, K., Veltkamp, C., Schachtler, C., Zukowska, M., Eser, S., Feyerabend, T.B., Paul, M.C., Eser, P., et al. (2014). A next-generation dual-recombinase system for time- and host-specific targeting of pancreatic cancer. Nature Medicine *20*, 1340–1347.

Serresi, M., Gargiulo, G., Proost, N., Siteur, B., Cesaroni, M., Koppens, M., Xie, H., Sutherland, K.D., Hulsman, D., Citterio, E., et al. (2016). Polycomb Repressive Complex 2 Is a Barrier to KRAS-Driven Inflammation and Epithelial-Mesenchymal Transition in Non-Small-Cell Lung Cancer. Cancer Cell *29*, 17–31.

Siddique, H.R., and Saleem, M. (2012). Role of BMI1, a Stem Cell Factor, in Cancer Recurrence and Chemoresistance: Preclinical and Clinical Evidences. STEM CELLS *30*.

Skrypek, N., Goossens, S., de Smedt, E., Vandamme, N., and Berx, G. (2017). Epithelial-to-Mesenchymal Transition: Epigenetic Reprogramming Driving Cellular Plasticity. Trends in Genetics *33*.

Snyder, E.L., Watanabe, H., Magendantz, M., Hoersch, S., Chen, T.A., Wang, D.G., Crowley, D., Whittaker, C.A., Meyerson, M., Kimura, S., et al. (2013). Nkx2-1 Represses a Latent Gastric Differentiation Program in Lung Adenocarcinoma. Molecular Cell *50*, 185–199.

Soumillon, M., Cacchiarelli, D., Semrau, S., van Oudenaarden, A., and Mikkelsen, T.S. (2014). Characterization of directed differentiation by high-throughput single-cell RNA-Seq. BioRxiv.

Subramanian, A., Tamayo, P., Mootha, V.K., Mukherjee, S., Ebert, B.L., Gillette, M.A., Paulovich, A., Pomeroy, S.L., Golub, T.R., Lander, E.S., et al. (2005). Gene set enrichment analysis: A knowledge-based approach for interpreting genome-wide expression profiles. Proceedings of the National Academy of Sciences *102*, 15545–15550.

Sung, H., Ferlay, J., Siegel, R.L., Laversanne, M., Soerjomataram, I., Jemal, A., and Bray, F. (2021). Global Cancer Statistics 2020: GLOBOCAN Estimates of Incidence and Mortality Worldwide for 36 Cancers in 185 Countries. CA: A Cancer Journal for Clinicians *71*.

Vessoni, A.T., Filippi-Chiela, E.C., Lenz, G., and Batista, L.F.Z. (2020). Tumor propagating cells: drivers of tumor plasticity, heterogeneity, and recurrence. Oncogene *39*.

Visvader, J.E., and Lindeman, G.J. (2012). Cancer Stem Cells: Current Status and Evolving Complexities. Cell Stem Cell *10*.

Vonlanthen, S., Heighway, J., Altermatt, H.J., Gugger, M., Kappeler, A., Borner, M.M., van Lohuizen, M., and Betticher, D.C. (2001). The bmi-1 oncoprotein is differentially

expressed in non-small cell lung cancer and correlates with INK4A-ARF locus expression. British Journal of Cancer *84*, 1372–1376.

Vrzalikova, K., Skarda, J., Ehrmann, J., Murray, P.G., Fridman, E., Kopolovic, J., Knizetova, P., Hajduch, M., Klein, J., Kolek, V., et al. (2008). Prognostic value of Bmi-1 oncoprotein expression in NSCLC patients: a tissue microarray study. Journal of Cancer Research and Clinical Oncology *134*, 1037–1042.

Winslow, M.M., Dayton, T.L., Verhaak, R.G.W., Kim-Kiselak, C., Snyder, E.L., Feldser, D.M., Hubbard, D.D., Dupage, M.J., Whittaker, C.A., Hoersch, S., et al. (2011). Suppression of lung adenocarcinoma progression by Nkx2-1. Nature *473*, 101–104.

Yan, K.S., Chia, L.A., Li, X., Ootani, A., Su, J., Lee, J.Y., Su, N., Luo, Y., Heilshorn, S.C., Amieva, M.R., et al. (2012). The intestinal stem cell markers Bmi1 and Lgr5 identify two functionally distinct populations. Proceedings of the National Academy of Sciences of the United States of America *109*.

Yang, M.-H., Hsu, D.S.-S., Wang, H.-W., Wang, H.-J., Lan, H.-Y., Yang, W.-H., Huang, C.-H., Kao, S.-Y., Tzeng, C.-H., Tai, S.-K., et al. (2010). Bmi1 is essential in Twist1-induced epithelial–mesenchymal transition. Nature Cell Biology *12*.

Young, N.P., Crowley, D., and Jacks, T. (2011). Uncoupling cancer mutations reveals critical timing of p53 loss in sarcomagenesis. Cancer Research *71*, 4040–4047.

Zacharek, S.J., Fillmore, C.M., Lau, A.N., Gludish, D.W., Chou, A., Ho, J.W.K., Zamponi, R., Gazit, R., Bock, C., Jäger, N., et al. (2011). Lung stem cell self-renewal relies on BMI1-dependent control of expression at imprinted loci. Cell Stem Cell *9*, 272–281.

Zheng, Y., de la Cruz, C.C., Sayles, L.C., Alleyne-Chin, C., Vaka, D., Knaak, T.D., Bigos, M., Xu, Y., Hoang, C.D., Shrager, J.B., et al. (2013). A Rare Population of CD24+ITGB4+Notchhi Cells Drives Tumor Propagation in NSCLC and Requires Notch3 for Self-Renewal. Cancer Cell.

Zindy, F., Quelle, D.E., Roussel, M.F., and Sherr, C.J. (1997). Expression of the p16INK4a tumor suppressor versus other INK4 family members during mouse development and aging. Oncogene *15*, 203–211.

CHAPTER 3: Loss of BMI1 in established colon tumors does not suppress tumor progression

Elaine Y. Kuo, Pedro N. Pozo, Paul S. Danielian, Shinya Imada, Colin E. Fowler, Charlie Whittaker, Rachit Neupane, and Jacqueline A. Lees

Contribution:
E.Y.K. conducted all tumor organoid and mouse experiments.
P.N.P, P.S.D., and S.I. assisted with mouse experiments.
C.E.F. and C.W. conducted gene expression analyses.
R.N. assisted with design of the study.
E.Y.K. and J.A.L. designed the study, analyzed the data, and wrote the chapter.

ABSTRACT

Cancer is a highly dynamic and heterogeneous disease, and tumor recurrence following treatment represents a critical clinical challenge. Increasing evidence suggests that a subset of tumor cells, called cancer stem cells (CSCs), initiate and support tumor growth, promote metastatic spreading, and drive relapse following chemotherapy. The epigenetic regulator B lymphoma Mo-MLV insertion region 1 homolog (BMI1) has emerged as a candidate therapeutic target for CSCs because of its overexpression in cancer and function in maintaining tissue stem cell function. To interrogate the role of BMI1 in colon cancer proliferation and progression, we developed colon tumor organoids and mouse models in which transformation and BMI1 loss are temporally controlled. We determine that BMI1 loss does not induce proliferative impairments, nor suppress tumor growth, in established *Apc, Kras,* and *Trp53* mutant colon cancer. Our findings suggest that under certain conditions, BMI1 inhibition may be an ineffective treatment for colon cancer.

INTRODUCTION

Colorectal cancer (CRC) is the third most commonly diagnosed cancer and the second leading cause of cancer morbidity in the world (Sung et al., 2021). Sporadic CRC is widely accepted to develop in a stepwise manner with the accumulation of key genetic alterations (Fearon and Vogelstein, 1990). A vast majority of early colon adenomas demonstrate aberrant activation of the Wnt signaling pathway, such as loss of the tumor suppressor *Apc* and deregulation of the proto-oncogene β-catenin (Fearon and Vogelstein, 1990; Schatoff et al., 2017). As the adenomas progress to more aggressive adenocarcinomas, other mutations, such as oncogenic activation of KRAS and loss of p53, are commonly observed (Armaghany et al., 2012; Fearon, 2011). Despite substantial characterization of the genetic mutations associated with CRC tumor development, and success in early detection and treatment, there remains a need to develop effective therapies that prevent progression and recurrence of the disease.

There is extensive evidence that cancers, including CRC, are highly heterogeneous and may contain a subpopulation of cells, termed cancer stem cells (CSCs), that exhibit core characteristics of normal stem cells, including the ability to indefinitely self-renew and give rise to phenotypically diverse tumor cells (Kreso and Dick, 2014; Munro et al., 2018; O'Brien et al., 2007; Zeuner et al., 2014). Importantly, these CSCs can drive metastatic spreading, and persistence of these cells following chemotherapy can cause relapse (Alison et al., 2011; Dylla et al., 2008; Liu et al., 2014). Thus, there is significant interest in identifying and targeting proteins that regulate CSC function (Yang et al., 2020).

One candidate protein for specifically targeting cancer stem cells is BMI1, an epigenetic regulator and proto-oncogene critical for normal stem cell function (van Lohuizen et al., 1991). BMI1 is a member of the Polycomb repressive complex 1 (PRC1), which mediates monoubiquitination of H2AK119, leading to transcriptional repression (Cao et al., 2005; Kallin et al., 2009). BMI1 is known to influence cell cycle progression through repression of *Cdkn2a,*

which encodes the cell cycle regulators $p16^{INK4A}$ and $p19^{ARF}$, thereby preventing cell cycle arrest and/or apoptosis (Jacobs et al., 1999b, 1999a). In addition, BMI1 regulates genes involved in development and differentiation, DNA damage response, epithelial-to-mesenchymal transition programs, and regulation of reactive oxygen species (Biehs et al., 2013; Cao et al., 2005; Ginjala et al., 2011; Ismail et al., 2010; Liu et al., 2009; Yang et al., 2010). In a wide variety of tissue compartments, BMI1 is highly expressed in the stem cells and is critical for stem cell maintenance and function, as germline loss of BMI1 results in decreased self-renewal ability, due to derepression of *Cdkn2a*, as well as altered differentiation patterns, due to derepression of lineage-specific genes and activation of alternative lineage programs (Bruggeman et al., 2005; Lessard and Sauvageau, 2003; Leung et al., 2004; Park et al., 2003; Zencak et al., 2005).

In addition to its role in normal stem cell biology, BMI1 is commonly overexpressed in a number of tumor contexts, including CRC, and its expression correlates with poor prognosis (Du et al., 2010; Li et al., 2010; Tateishi et al., 2006). Over the past two decades, many studies have demonstrated the role of BMI1 in promoting tumorigenic processes, such as impairing tumor initiation and progression (largely through derepression of *Cdkn2a*) and promoting metastasis (Bednar et al., 2015; Chen et al., 2017; Douglas et al., 2008; Dovey et al., 2008; Ferretti et al., 2016; Lessard and Sauvageau, 2003; Molofsky et al., 2005; Oguro et al., 2006). Specifically in the CRC context, we have previously demonstrated that in mouse models of intestinal cancer, germline deletion of *Bmi1* suppresses progression and maintenance of intestinal adenomas in a $p19^{ARF}$-dependent manner (Maynard et al., 2014).

Given the importance of BMI1 in normal stem cell biology, as well as its overexpression in cancer, there is significant interest in deploying BMI1 inhibition to induce derepression of $p16^{INK4A}$ and $p19^{ARF}$ and thus cell cycle arrest and/or apoptosis in CSCs (Dey et al., 2018; Kreso et al., 2014). However, many of these studies demonstrating BMI1's pro-tumorigenic roles relied on genetic ablation of *Bmi1* during embryogenesis at or prior to tumor initiation, which is not reflective of clinical settings, or usage of pharmacological inhibitors with poor pharmacokinetics

or off-target effects (Bolomsky et al., 2020; Eberle-Singh et al., 2019; Kim et al., 2014; Kreso et al., 2014). To determine the maximal possible impact of BMI1 inhibition, we have developed mouse models in which we can elucidate the effects of BMI1 loss in established tumors in the adult context. In Chapter 2 of this thesis, we demonstrated that BMI1 loss in non-small cell lung cancer is not tumor suppressive, but rather promotes dedifferentiation and pro-metastatic gene programs. In this chapter, we investigate the consequences of *Bmi1* deletion in transformed organoids and established tumors in mouse models of CRC. Our data show that genetic ablation of *Bmi1* does not impair CRC proliferation or tumor growth, arguing that BMI1 is likely to be an ineffective target for the treatment of CRC.

RESULTS

To assess the effects of BMI1 loss in established colon tumors in the adult context, we constructed 3D tumor organoid systems and mouse models in which transformation and conditional *Bmi1* deletion can be independently controlled. We chose to begin our studies with ablation of *Bmi1* in *Apc*$^{-/-}$*; Kras*$^{G12D/+}$*;* and *Trp53*$^{-/-}$ (abbreviated to AKP) mutant colon cells to understand the effects of BMI1 loss in progressed colon tumors. Furthermore, investigating BMI1 loss in this mutational background mirrors our studies in *Kras*$^{G12D/+}$*;Trp53*$^{-/-}$ lung tumors, enabling comparison between the two different epithelial tumor tissue types. For *in vitro* studies on *Bmi1* deletion in AKP colon tumor cells, we took advantage of the emergence of 3D culture technologies and derived colon tumor organoids, which have been demonstrated to more closely recapitulate physiological conditions than 2D monolayer conditions (Drost and Clevers, 2018).

Our general strategy was to delete *Bmi1 in vitro* in 3D tumor organoids and assess for proliferative defects. Furthermore, we orthotopically transplanted colon tumor organoids into recipient mice and subsequently induced BMI1 loss in established colon tumors. We utilized

Bmi1-wildtype mice (*Bmi1*$^{+/+}$) or mice in which core functions of *Bmi1* (encoded by exons 4-8) are flanked by loxP sites (Maynard et al., 2014). *Bmi1*$^{+/+}$ and *Bmi1*$^{fl/fl}$ genotypes were combined with *Kras* (*Kras*$^{FSF\text{-}G12D/+}$) and *Trp53* (*Trp53*$^{frt/frt}$) alleles, in which oncogenic *Kras*^{G12D} expression and *Trp53* deletion can be induced by the FLPo recombinase activity (Lee et al., 2012; Young et al., 2011), as well as *Rosa26-CAG-Frt-STOP-Frt-CreERT2* (Madisen et al., 2010) and *Rosa26-CAG-Lox-STOP-Lox-tdTomato* (Schönhuber et al., 2014) alleles (Figure 1A). Colon crypts were isolated from these transgenic mice and cultured in basement membrane matrix (Matrigel) to form 3D organoids. These were infected with lentivirus expressing FlpO, Cas9, a guide RNA against *Apc* (sgApc), and GFP, followed by withdrawal of Wnt and other growth factors to select for *Bmi1*$^{+/+}$ or *Bmi1*$^{fl/fl}$ AKP tumor organoids expressing tamoxifen-inducible Cre recombinase and GFP. Subsequent treatment with 4-hydroxytamoxifen (4-OHT) and fluorescent-activated cell sorting (FACS) for the induced tdTomato expression allowed isolation of *Bmi1*$^{+/+}$ or *Bmi1*-null (*Bmi1*$^{-/-}$) AKP tumor organoids (Figure 1A). To control for line-to-line variability, we independently generated three *Bmi1*$^{+/+}$ AKP (denoted as *Bmi1*$^{+/+}$ AKP #1 - #3) and three *Bmi1*$^{fl/fl}$ AKP (denoted as *Bmi1*$^{fl/fl}$ AKP #1 - #3) tumor organoid lines from a total of six mice (one tumor organoid line per mouse). We confirmed that we can robustly delete *Bmi1* with this system, as addition of 4-OHT in *Bmi1*$^{fl/fl}$ AKP tumor organoids led to loss of BMI1 protein (Figure 1B, S1A).

Deletion of Bmi1 *in AKP tumor organoids* in vitro *does not impair proliferation*

BMI1 loss *in vitro* is commonly characterized with induction of cell cycle arrest, cellular senescence, and/or apoptosis, which results primarily from derepression of the canonical BMI1 targets, p16^{INK4A} and p19^{ARF} (Bruggeman, 2005; Jacobs et al., 1999a; Molofsky et al., 2005). Thus, to understand whether BMI1 deletion alters cell cycle progression, we treated *Bmi1*$^{+/+}$ and *Bmi1*$^{fl/fl}$ AKP colon tumor organoids with vehicle (-4-OHT) or 4-OHT (+4-OHT) to generate *Bmi1*$^{+/+}$ or *Bmi1*$^{-/-}$ AKP tumor organoids. We then treated the tumor organoids with 5-ethynyl-2'-deoxyuridine (EdU), which is incorporated into the DNA of cells undergoing DNA replication,

and stained the tumor organoids for EdU incorporation and DAPI to determine cell cycle profiles. We showed that BMI1 loss does not significantly alter the distribution of G0/G1, S, and G2/M populations (Figure 1C, S1B). This indicated that BMI1 loss was not significantly affecting cell cycle phasing.

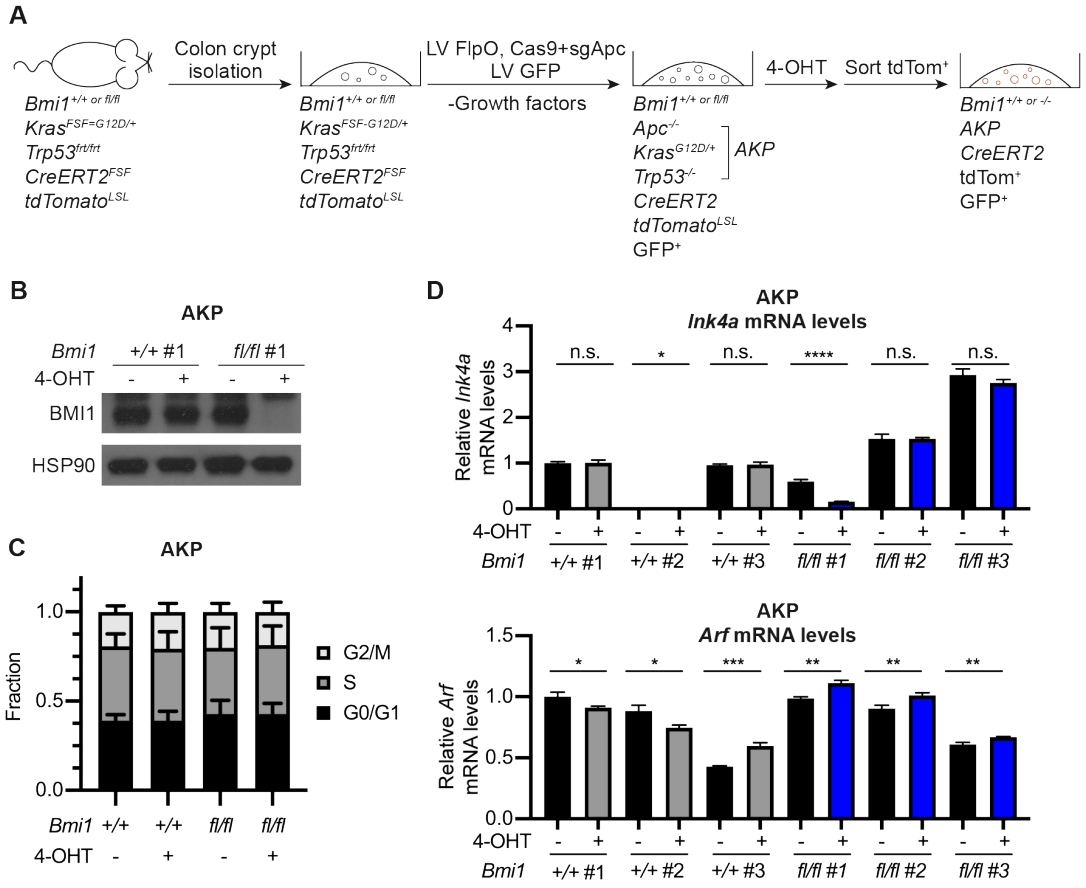

Figure 1. *In vitro* deletion of *Bmi1* in AKP colon tumor organoids does not alter cell cycle phasing nor *Ink4a* and *Arf* expression. **A)** Schematic for generation of *Apc*$^{-/-}$;*Kras*$^{G12D/+}$;*Trp53*$^{-/-}$ (AKP) tumor organoids and conditional deletion of *Bmi1 in vitro*. Colon crypts were isolated from mice and cultured in Matrigel to form 3D organoids. Lentiviral infection with FlpO, sgApc, Cas9, and GFP resulted in deletion of *Apc* and expression of GFP, as well as activation of oncogenic *Kras*, deletion of *Trp53*, and expression of tamoxifen inducible Cre recombinase (CreERT2) through deletion of the *FRT* flanked stop cassettes. Withdrawal of Wnt selected for AKP tumor organoids. Treatment of these AKP tumor organoids with 4-hydroxytamoxifen (4-OHT) induced Cre-mediated deletion of the *loxP* flanked stop cassettes, resulting in tdTomato expression and loss of BMI1 in *Bmi1*$^{fl/fl}$ tumor organoids. **B)** Immunoblot of BMI1 protein expression in *Bmi1*$^{+/+}$ AKP #1 and *Bmi1*$^{fl/fl}$ AKP #1 tumor organoids treated with EtOH vehicle control (-4-OHT) or 4-OHT (+4-OHT). **C)** Fraction of *Bmi1*$^{+/+}$ AKP #1 - #3 and *Bmi1*$^{fl/fl}$ AKP #1 - #3 tumor organoid cells in G0/G1, S, and G2/M cell cycle phases, as assayed by EdU incorporation. Cells were pulse-labeled with EdU for 45 min. before harvest. Mean and S.D. are shown. $p > 0.05$ by ANOVA. **D)** Relative mRNA levels of *Ink4a* (top panel) and *Arf* (bottom panel) in AKP tumor organoids, as determined by qRT-PCR. All samples were normalized to *Bmi1*$^{+/+}$ AKP #1 -4-OHT levels. Mean and S.D. are shown. Statistical significance was determined with unpaired Student's t-test. n.s. $p > 0.05$, * $p < 0.05$, ** $p < 0.01$, *** $p < 0.001$, **** $p < 0.0001$.

We next performed real-time quantitative reverse transcription PCR (qRT-PCR) to quantify the mRNA levels of *Ink4a* and *Arf* (which encode $p16^{INK4A}$ and $p19^{ARF}$, respectively). To compare mRNA transcript levels across the different tumor organoid lines, we arbitrarily chose to normalize mRNA levels to the $Bmi1^{+/+}$ AKP #1 -4-OHT condition (Figure 1D). In the absence of 4-OHT (i.e. when the $Bmi1^{+/+}$ and $Bmi1^{fl/fl}$ AKP lines were all still *Bmi1* wildtype), there was some variation in the basal levels of *Ink4a* and *Arf* mRNA (Figure 1D). After 4-OHT treatment, some samples showed alterations that were scored as significant, but these were all very modest (Figure 1D). For *Ink4a*, the signal was actually downregulated in one of the $Bmi1^{fl/fl}$ AKP samples and not significantly altered in the other two. In the case of *Arf*, the change did not exceed 1.1-fold for any of the three $Bmi1^{fl/fl}$ lines. Moreover, the largest (1.4-fold), and most significant, change was observed in a $Bmi1^{+/+}$ line. Given the well-established role of BMI1 loss in promoting *Ink4a* and *Arf* derepression, these findings were unexpected. We wondered whether this was a feature of the 3D growth conditions. To address this, we generated 2D monolayer cultures from the six AKP tumor organoid lines and re-examined *Ink4a* and *Arf* mRNA levels by qRT-PCR (Figure S1C). Under these conditions, the basal (i.e. -4-OHT) levels of both *Ink4a* and *Arf* were clearly higher in all six of the AKP samples, compared to the 3D growth conditions (Figure S1C). Despite this higher starting point, again the addition of 4-OHT yielded minor changes in *Ink4a* and *Arf* mRNA, which were inconsistent with regard to direction and/or genotype. Thus, we conclude that BMI1 loss has little to no impact on either cell cycle profiles or *Ink4a* and *Arf* expression of the AKP lines. These findings were unexpected, given the well-established role of BMI1 in altering cell cycle progression through derepression of $p16^{INK4A}$ and $p19^{ARF}$.

We also asked whether BMI1 loss alters proliferation and CSC frequency. For this, we performed tumor organoid formation assays for $Bmi1^{+/+}$ AKP #1 & #2 and $Bmi1^{fl/fl}$ AKP #1 & #2 tumor organoid lines and used the numbers and sizes of tumor organoids formed as proxies for proliferation and stemness. In each case, tumor organoids were plated and treated with either

vehicle or 4-OHT for 5 days (Figure 2A). The organoids were then dissociated, sorted using FACS for tdTom$^-$GFP$^+$ cells (for vehicle-treated tumor organoids) or tdTom$^+$GFP$^+$ cells (for 4-OHT-treated tumor organoids) and plated as single cells in Matrigel (Figure 2A, S2A). Seven days after plating, the numbers and areas of tumor organoids formed were quantified (Figure 2A). To test the possibility that proliferative defects and stem cell exhaustion only become evident after a prolonged period of time, we repeated the sorting and plating process twice more for a total of three sorts (Figure 2A).

For all colon tumor organoid lines surveyed, whether *Bmi1*$^{+/+}$ or *Bmi1*$^{fl/fl}$, the numbers of tumor organoids formed, and their gross morphologies, were not significantly different between -4-OHT and +4-OHT conditions (Figure 2B, S2B-C). This was true even following serial passaging, suggesting that BMI1 loss does not greatly impair cancer stem cell frequency (Figure 2B, Figure S2B-C). The distribution of tumor organoid sizes was scored as significantly different for all samples, irrespective of their genotype and passage. We believe that this is a product of the very large sample sizes, and not a true indication of strong phenotypic effects. Indeed, one of the 4-OHT-treated *Bmi1*$^{fl/fl}$ lines (#1) was slightly smaller, on average, but the other (#2) was larger (Figure 2C, S2D). This suggests that BMI1 loss largely does not materially compromise proliferation (Figure 2C, S2D). Taken together, the tumor organoid formation and serial passaging assays indicate that BMI1 loss does not adversely affect proliferative ability or CSC frequency of colon tumor cells.

We also performed a competitive growth assay to determine whether BMI1 loss confers a more subtle growth advantage or disadvantage in AKP colon tumor cells. *Bmi1*$^{+/+}$ and *Bmi1*$^{fl/fl}$ AKP tumor organoids were treated with vehicle (resulting in tdTom$^-$GFP$^+$ cells) or 4-OHT (resulting in tdTom$^+$GFP$^+$ cells) for five days. For each line, tumor organoids from each treatment group were then dissociated, combined, and then passaged every 5 days (Figure 2D).

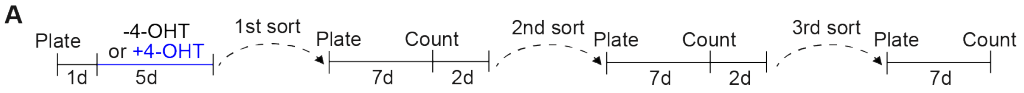
A
Plate
-4-OHT
or +4-OHT
1d
5d
1st sort
Plate
Count
7d
2d
2nd sort
Plate
Count
7d
2d
3rd sort
Plate
Count
7d

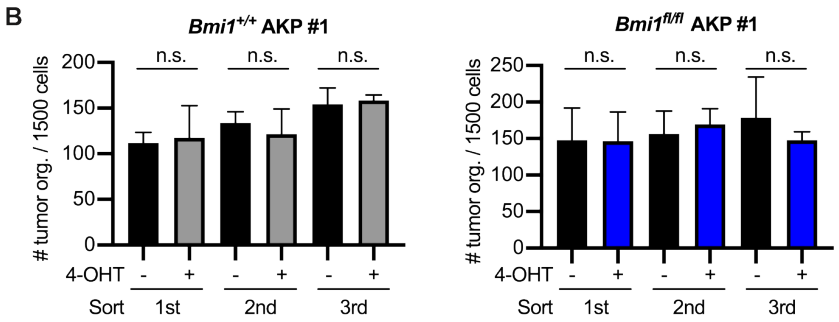
B
Bmi1+/+ AKP #1
Bmi1fl/fl AKP #1
tumor org. / 1500 cells
n.s.
4-OHT
Sort
1st
2nd
3rd

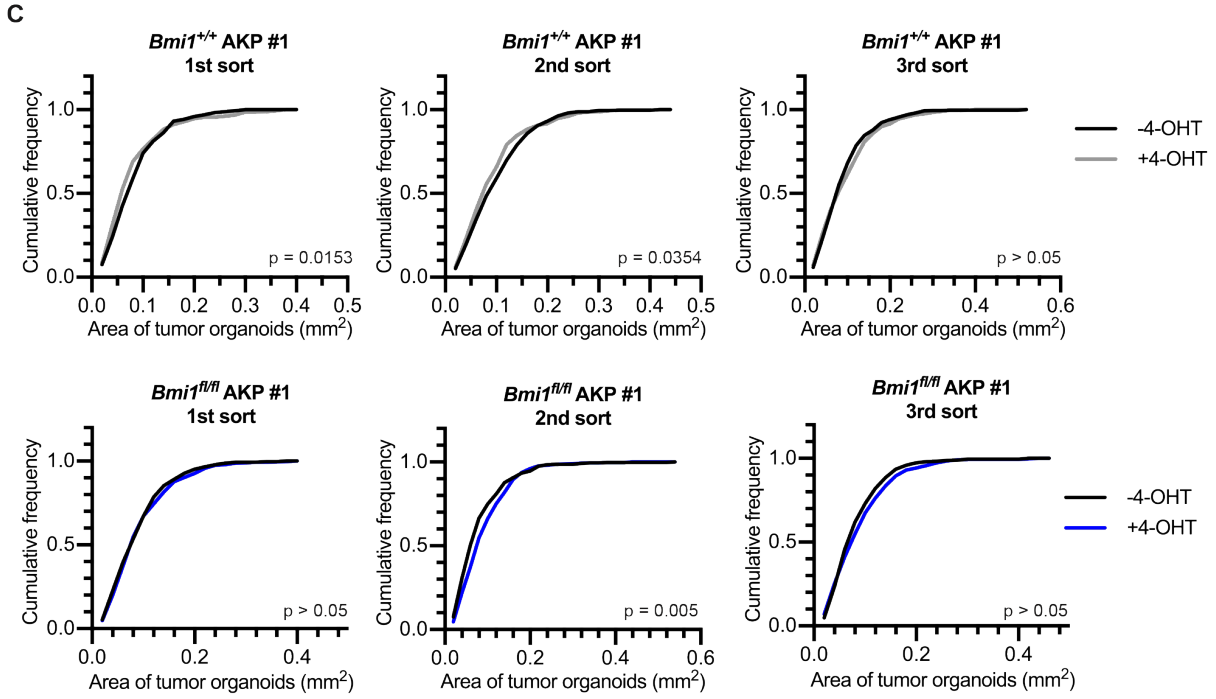
C
Bmi1+/+ AKP #1
1st sort
2nd sort
3rd sort
Bmi1fl/fl AKP #1
Cumulative frequency
Area of tumor organoids (mm2)
p = 0.0153
p = 0.0354
p > 0.05
p = 0.005
-4-OHT
+4-OHT

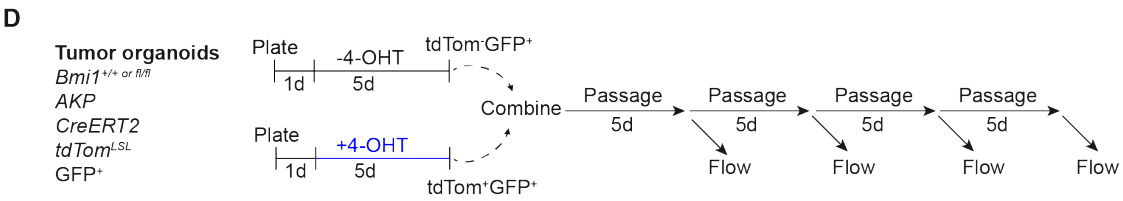
D
Tumor organoids
Bmi1+/+ or fl/fl
AKP
CreERT2
tdTomLSL
GFP+
Plate
-4-OHT
+4-OHT
1d
5d
tdTom-GFP+
tdTom+GFP+
Combine
Passage
5d
Flow

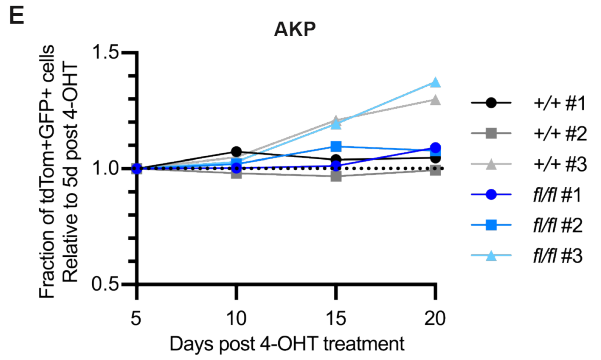
E
AKP
Fraction of tdTom+GFP+ cells
Relative to 5d post 4-OHT
Days post 4-OHT treatment
+/+ #1
+/+ #2
+/+ #3
fl/fl #1
fl/fl #2
fl/fl #3

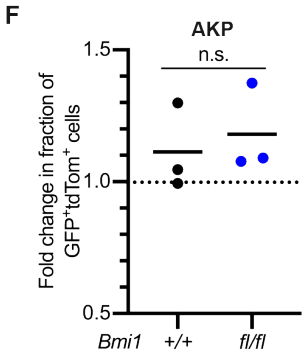
F
AKP
n.s.
Fold change in fraction of
GFP+tdTom+ cells
Bmi1
+/+
fl/fl

Figure 2. BMI1 loss does not impact proliferation of AKP tumor organoids. **A)** Schematic for AKP tumor organoid formation assay with serial passaging. Tumor organoids were plated and treated with EtOH vehicle control (-4-OHT) or 50nM 4-OHT (+4-OHT) for 5 days. The tumor organoids were then dissociated, sorted using FACS for live $tdTom^{+}GFP^{-}$ cells (for -4-OHT tumor organoids) or live $tdTom^{+}GFP^{+}$ cells (for +4-OHT tumor organoids) and plated as single cells in Matrigel. The numbers and areas of tumor organoids were quantified 7 days after sorting. The sorting, plating, and quantification processes were repeated twice more for a total of three sorts. **B)** Quantification of the number of $Bmi1^{+/+}$ AKP #1 and $Bmi1^{fl/fl}$ AKP #1 tumor organoids formed from 1500 cells plated. Blue bars represent the condition where BMI1 is lost (i.e. $Bmi1^{fl/fl}$ cells +4-OHT). Mean and S.D. are shown, and significance was determined using unpaired Student's t-test. n.s. $p > 0.05$. **C)** Cumulative distribution functions of $Bmi1^{+/+}$ AKP #1 and $Bmi1^{fl/fl}$ AKP #1 tumor organoid areas. Significance was determined using Kolmogorov-Smirnov test. **D)** Schematic of competition assay. $Bmi1^{+/+}$ AKP #1 - #3 and $Bmi1^{fl/fl}$ AKP #1 - #3 tumor organoids were treated either -4-OHT or +4-OHT. These tumor organoids were combined and passaged, and samples were collected at every passage for analysis by flow cytometry. **E)** Fraction of $tdTom^{+}GFP^{+}$ cells at each time point, as determined by flow cytometry. **F)** Fold change in the percentage of $tdTom^{+}GFP^{+}$ cells between time point 2 and time point 5. Mean is shown, and statistical significance was determined using unpaired Student's t-test. n.s. $p > 0.05$.

At every passage, samples were collected for flow cytometry to assess the representation of $tdTom^{-}GFP^{+}$ vs $tdTom^{+}GFP^{+}$ cells (Figure 2D). For example, if BMI1 loss conferred a growth disadvantage, we would expect a decrease in the relative representation of $tdTom^{+}GFP^{+}$ cells. For all three $Bmi1^{fl/fl}$ AKP tumor organoid lines, we did not observe a significant change in the representation of $tdTom^{+}GFP^{+}$ cells, suggesting that BMI1 loss does not impact proliferation of AKP tumor cells (Figure 2E-F).

Acute ablation of Bmi1 *in established AKP colon tumors does not impair tumor growth*

To understand the effects of BMI1 loss *in vivo*, we orthotopically transplanted the colon tumor organoid lines into recipient mice, ablated *Bmi1* specifically in the colon tumors, and assessed for changes in gene expression and tumor growth kinetics. To induce colon tumors, we performed colonoscopy-mediated injection of colon tumor organoids into the submucosa of the distal colons of recipient mice (Roper et al., 2018). As we sought to understand the effects of BMI1 loss at multiple time points, mice were transplanted with two doses (either 1000 or 150 tumor organoids) of $Bmi1^{+/+}$ AKP #1 or $Bmi1^{fl/fl}$ AKP #1 tumor organoids (Figure 3A). After confirmation of tumor establishment via colonoscopy (Figure S3A), mice were injected intraperitoneally with tamoxifen to induce tdTomato expression in all mice and *Bmi1* deletion in

Bmi1$^{fl/fl}$ mice (Figure 3A). Tumors from mice injected with 1000 tumor organoids were then harvested at 3 days post tamoxifen ("early time point"), while tumors from mice that received 150 tumor organoids were collected 4-5 weeks post tamoxifen ("late time point"; Figure 3A). Using immunohistochemical staining, we verified that BMI1 is expressed in the *Bmi1*$^{+/+}$ AKP tumors and that BMI1 protein was effectively lost in the *Bmi1*$^{fl/fl}$ tumors at both early and late time points (Figure 3B). Notably, pathological examination showed that all of the AKP colon tumors, regardless of *Bmi1* status, were highly aggressive and high grade and there was, if any, little morphological difference between *Bmi1*$^{+/+}$ and *Bmi1*$^{fl/fl}$ tumors.

Having confirmed efficient BMI1 loss, we sought to understand whether *Bmi1* ablation affected the transcriptional profiles of the AKP tumors. At the time of harvest, we dissociated the colon tumors (n = 3 per genotype per time point), sorted for tdTom^{+}GFP^{+} tumor cells, and performed bulk RNA-sequencing and differential gene analyses with DESeq2 (Figure 3A, S3B; Love et al., 2014). When we performed supervised hierarchical clustering based on gene expression, we observed that the *Bmi1*$^{+/+}$ samples clustered away from the *Bmi1*$^{fl/fl}$ samples (Figure S3C). As the *Bmi1*$^{+/+}$ and *Bmi1*$^{fl/fl}$ tumor organoids were independently derived from separate mice, this could reflect either line-to-line variability or genotype-specific effects. *Bmi1*$^{fl/fl}$ early time point samples segregated away from *Bmi1*$^{fl/fl}$ late time point samples (Figure S3C). We examined the gene expression of canonical BMI1 targets and proliferation markers. Similar to *in vitro Bmi1* deletion, BMI1 loss did not induce upregulation of *Ink4a* and *Arf* mRNA transcripts (Figure 3C). As a marker for proliferation, we examined *Pcna* mRNA transcript levels and also PCNA protein levels by immunohistochemical staining and did not observe altered levels (Figure 3C-D). This strongly suggests that BMI1 loss does not affect proliferation of the colon tumor cells *in vivo*, mirroring our *in vitro* findings.

We previously discovered that BMI1 loss in established lung adenocarcinoma does not yield significant proliferation defects, but rather promotes dedifferentiation and expression of pro-metastatic gene programs (see Chapter 2 of the thesis). To determine whether BMI1 loss

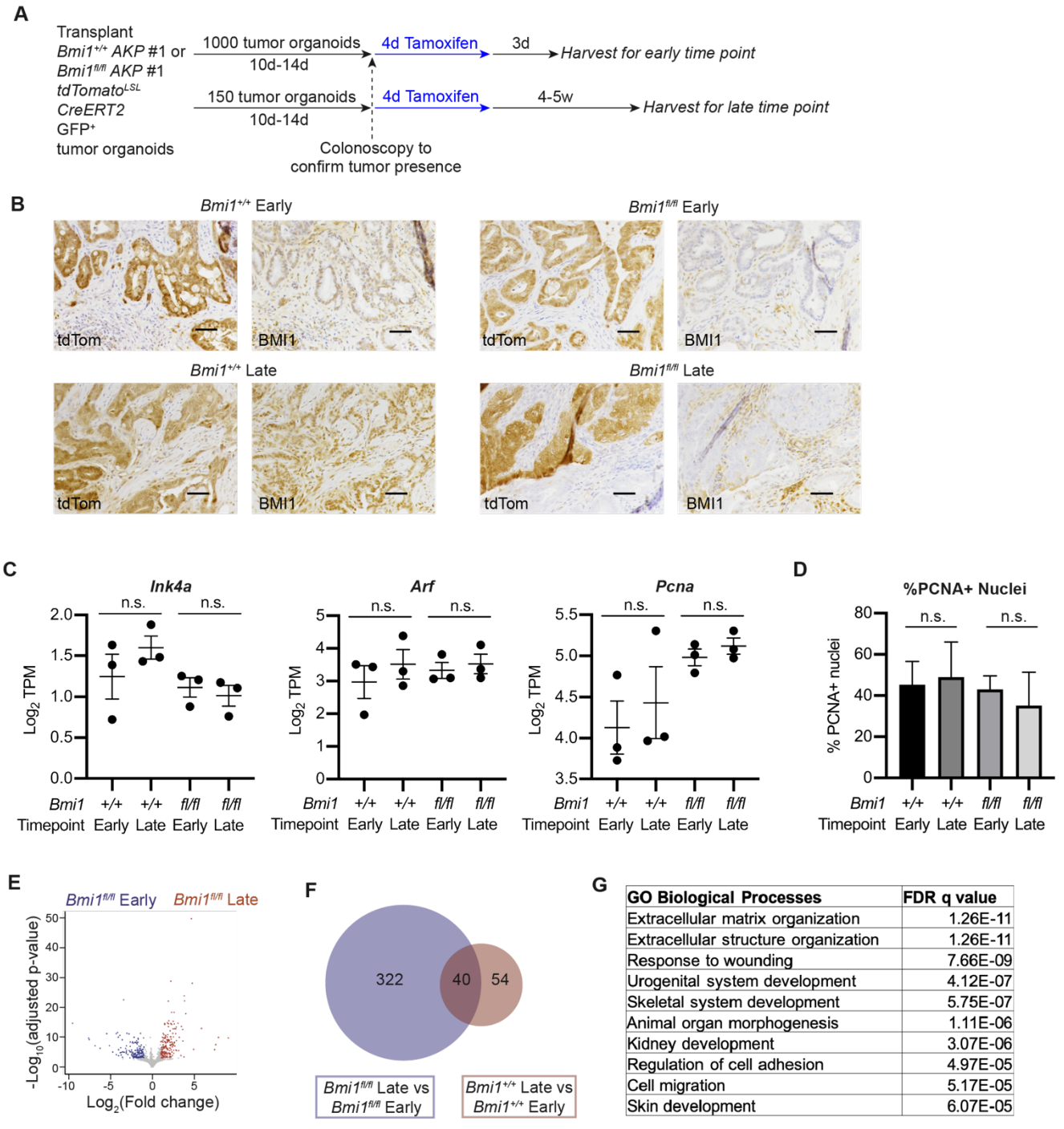

GO Biological Processes	FDR q value
Extracellular matrix organization	1.26E-11
Extracellular structure organization	1.26E-11
Response to wounding	7.66E-09
Urogenital system development	4.12E-07
Skeletal system development	5.75E-07
Animal organ morphogenesis	1.11E-06
Kidney development	3.07E-06
Regulation of cell adhesion	4.97E-05
Cell migration	5.17E-05
Skin development	6.07E-05

Figure 3. *In vivo* deletion of *Bmi1* in AKP colon tumors and transcriptional profiling of tumor cells. **A)** Schematic for *Bmi1* deletion in established AKP colon tumors. Using colonoscopy-mediated injection, mice were transplanted with 1000 or 150 *Bmi1*$^{+/+}$ AKP #1 or *Bmi1*$^{fl/fl}$ AKP #1 tumor organoids. Following confirmation of tumor presence by colonoscopy, all mice received daily intraperitoneal injections of tamoxifen (dose: 0.1g tamoxifen per kg mouse) for 4 days. Following 3 days of rest, mice that received the 1000 tumor organoid dose were euthanized, and colon tumors were collected for histology and bulk RNA-seq (early time point). Mice that received the 150 tumor organoid dose were euthanized and colon tumors were collected for histology and bulk RNA-seq 4-5 weeks after tamoxifen injection (late time point). **B)** Immunohistochemical staining of representative *Bmi1*$^{+/+}$ and *Bmi1*$^{fl/fl}$ tumors from tamoxifen-

treated mice. Adjacent sections stained for BMI1 and tdTomato indicate that BMI1 expression is lost only from *Bmi1*$^{fl/fl}$ tumor cells, but is present in *Bmi1*$^{+/+}$ tumor cells and in tumor infiltrating cells. Scale bar represents 50μm. **C)** mRNA transcript levels for *Ink4a, Arf*, and *Pcna* of cells isolated from colon tumors (n=3 mice per genotype per time point). Mean and S.D. are shown, and statistical significance was determined using unpaired Student's t-test. **D)** Percentage of PCNA^{+} nuclei, as determined by immunohistochemical staining, in the AKP tumors. Mean and S.D. are shown, and statistical significance was determined using unpaired Student's t-test. n.s. $p > 0.05$. **E)** Scatterplot of differentially expressed genes between *Bmi1*$^{fl/fl}$ early and *Bmi1*$^{fl/fl}$ late samples, as determined by DESeq2 analyses (n=3 mice per time point; $\log_2$FC > 1, FDR q value < 0.05; Love et al. 2014). Genes upregulated in *Bmi1*$^{fl/fl}$ early or *Bmi1*$^{fl/fl}$ late samples are highlighted in blue or red, respectively. **F)** Venn diagram depicting the number of genes that are commonly or uniquely differentially expressed between *Bmi1*$^{fl/fl}$ early and *Bmi1*$^{fl/fl}$ late samples versus *Bmi1*$^{+/+}$ early and *Bmi1*$^{+/+}$ late samples. **G)** Gene sets significantly enriched in *Bmi1*$^{fl/fl}$ late samples relative to *Bmi1*$^{fl/fl}$ early samples, as determined by Gene Ontology analyses using the 322 uniquely differentially expressed genes represented in Figure 3F.

induces similar gene programs in the AKP colon cancer context, we identified and analyzed the genes differentially between *Bmi1*$^{fl/fl}$ early and *Bmi1*$^{fl/fl}$ late time points. Our previous studies in the lung cancer context have indicated that at an early time point (3 days after the last tamoxifen dose), BMI1 protein was no longer detectable by immunohistochemistry, but the gene expression changes resulting from BMI1 loss have not yet materialized (see Chapter 2 of the thesis). Therefore, we considered the gene expression of *Bmi1*$^{fl/fl}$ early time point tumors (3 days post-tamoxifen) as basal level and used it for comparison with *Bmi1*$^{fl/fl}$ late time point tumors. We identified 362 genes differentially expressed between *Bmi1*$^{fl/fl}$ early and late time point samples, of which 200 are upregulated and 162 are downregulated in the *Bmi1*$^{fl/fl}$ late samples (Figure 3E). 40 of these genes were also differentially expressed between *Bmi1*$^{+/+}$ early and *Bmi1*$^{+/+}$ late samples, and thus we hypothesize that these result from tumor growth and progression, rather than BMI1 loss (Figure 3F). To identify differentially regulated pathways specific to BMI1 loss, we performed Gene Ontology analysis on the remaining 322 BMI1 loss-specific genes, and this identified a number of biological processes related tumorigenesis and metastasis, such as extracellular matrix organization, regulation of cell adhesion, and developmental programs (Figure 3G). Our findings suggest that although there is no proliferative defect or derepression of *Cdnk2a* upon BMI1 loss, *Bmi1* ablation may alter the transcriptional profiles of AKP tumors, particularly modifying the expression of programs known to influence cancer progression.

Despite our results indicating no difference in the levels of the proliferation marker PCNA, we sought to directly test whether that BMI1 loss impairs tumor growth. To achieve this, we used three-dimensional (3D) ultrasound imaging and reconstruction of the distal colon, a minimally invasive method that enables quantitative and longitudinal monitoring of tumor growth (Freeling and Rezvani, 2016). We transplanted mice with 150 *Bmi1*$^{fl/fl}$ AKP #1 tumor organoids and performed 3D ultrasound imaging to first confirm tumor establishment and then track tumor growth following vehicle or tamoxifen treatment (Figure 4A, S4A). We observed that some colon tumors grew as solid masses, while other tumors were cystic with areas of fluid, inflammation, and/or cell debris, as indicated by dark regions in the ultrasound images (Figure S4B). Although further replicates are required to characterize these two different tumor morphologies, we evenly assigned tumors of both types to vehicle or tamoxifen treatment. To understand how BMI1 loss impacts the growth of specifically solid tumor regions, we excluded the cystic regions and only quantified the cell-based volumes (Figure S4B). Colon tumors of vehicle- and tamoxifen-treated mice grew at similar rates, suggesting that BMI1 loss does not impair tumor growth (Figure 4B-C).

To understand whether BMI1 loss may impact CSC frequency, we dissociated the colon tumors of four vehicle-treated and four tamoxifen-treated mice, sorted and isolated tdTom^{+}GFP^{+} colon tumor cells, and plated them as single cells in Matrigel to assess for tumor organoid formation ability. The number of tumor organoids formed was not significantly different between vehicle-treated and tamoxifen-treated tumors, suggesting that *Bmi1* status does not impact CSC frequency (Figure 4D). Overall, our results indicate that BMI1 loss does not impair progression of AKP colon cancer. These findings differ from our previous studies establishing the significant tumor suppressive effects of BMI1 loss in the embryonic *Bmi1* knock-out setting (Maynard et al., 2014), but align with our previous studies on *Bmi1* deletion in established adult lung tumors (see Chapter 2 of the thesis).

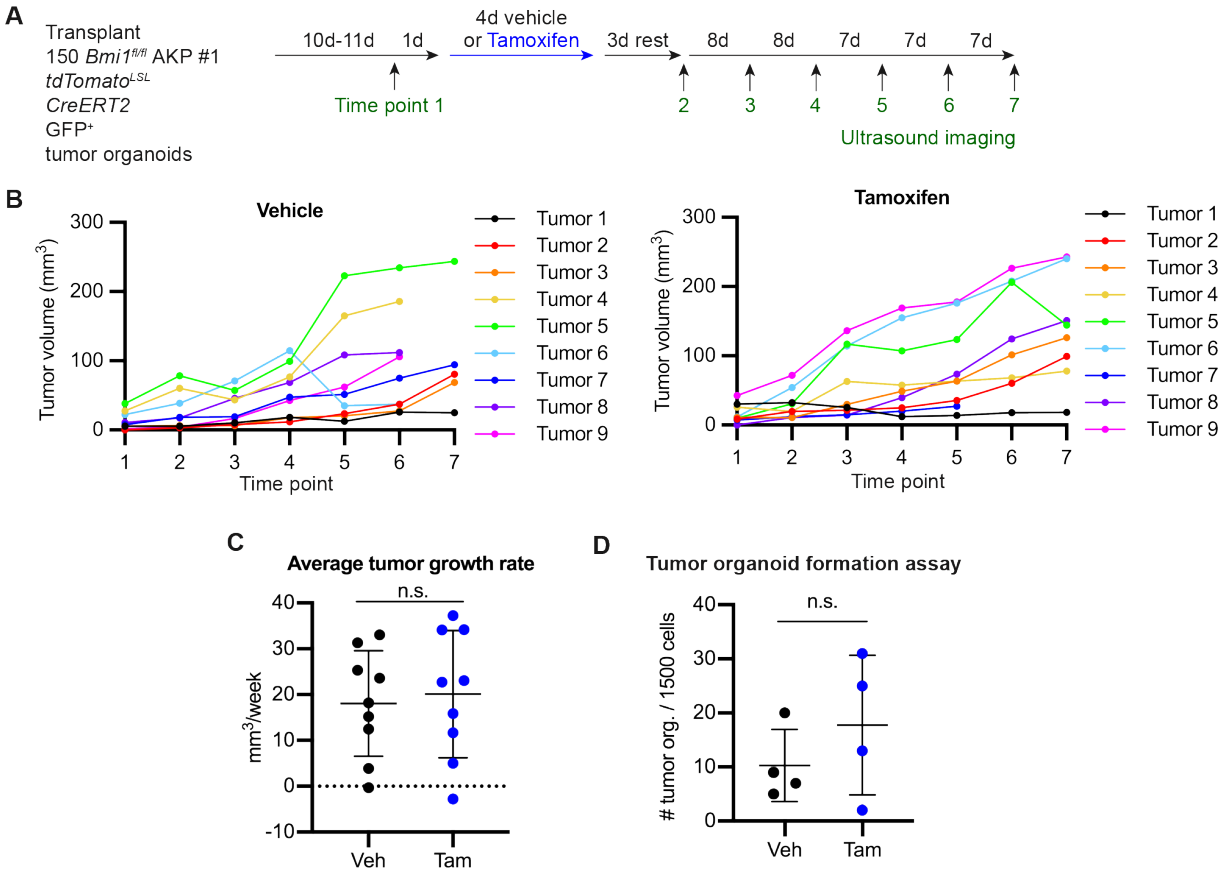

Figure 4. BMI1 loss in established AKP colon tumors does not suppress tumor growth.
A) Schematic for *Bmi1* deletion in established AKP colon tumors and longitudinal tracking of tumor growth. 150 *Bmi1*$^{fl/fl}$ AKP #1 tumor organoids were transplanted into the colons of recipient mice via colonoscopy-mediated injection. Following confirmation of tumor establishment by 3D ultrasound imaging at time point 1, mice received daily intraperitoneal injections of corn oil vehicle control or tamoxifen (dose: 0.1g tamoxifen per kg mouse) for 4 days. Following 3 days of rest, colon tumors were imaged every 7-8 days using 3D ultrasound imaging. **B)** Tumor volumes of 9 tumors from a total of 8 vehicle-treated mice (left) and 9 tumors from a total of 8 tamoxifen-treated mice (right) at each time point, as determined by ultrasound imaging and reconstruction. **C)** Average weekly growth rate of the colon tumors between time point 2 and the final time point prior to euthanasia. Mean and S.D. are shown, and statistical significance was determined using unpaired Student's t-test. n.s. $p > 0.05$. **D)** Number of tumor organoids formed after isolating and culturing 1500 single cells from vehicle-treated or tamoxifen-treated colon tumors. Mean and S.D. are shown, and statistical significance was determined using unpaired Student's t-test. n.s. $p > 0.05$.

Deletion of Bmi1 *in* Apc$^{-/-}$;Kras$^{G12D/+}$ *(AK) colon tumor organoids and established AK tumors may reduce proliferation and suppress tumor growth*

Since the tumor suppressor p53 functions downstream of the canonical BMI1 target *Cdkn2a*, it seemed possible that any *Cdkn2a*-dependent effects of BMI1 loss were masked by

p53 loss in the AKP colon tumor setting. Therefore, we sought to generate a colon cancer model in which *Trp53* is wildtype to determine whether *Trp53* status affects tumor progression following BMI1 loss. To achieve this, we generated *Apc*$^{-/-}$;*Kras*$^{G12D/+}$ (AK) colon tumor organoids by utilizing a similar approach as the one taken to generate AKP colon tumor organoids, with the notable difference of using *Trp53*$^{+/+}$ rather than *Trp53*$^{fl/fl}$ alleles and a transgene with tamoxifen inducible Cre recombinase under the control of the mouse villin 1 promoter (Villin-CreERT2; Figure 5A; el Marjou et al., 2004). As with the AKP setting, we independently generated three biological replicates of *Bmi1*$^{+/+}$ AK tumor organoid lines (denoted as *Bmi1*$^{+/+}$ AK #1 - #3) and three biological replicates of *Bmi1*$^{fl/fl}$ AK tumor organoid lines (denoted as *Bmi1*$^{fl/fl}$ AK #1 - #3) to control for line-to-line variability. Using Western blot, we confirmed robust ablation of BMI1 protein in *Bmi1*$^{fl/fl}$ AK lines upon 4-OHT treatment (Figure 5B, Figure S5A).

We first investigated whether BMI1 loss in the AK mutational background induced cell cycle arrest or affected cell cycle phasing. To do so, we pulsed *Bmi1*$^{+/+}$ and *Bmi1*$^{fl/fl}$ AK tumor organoids with EdU and stained with DAPI to determine the frequency of cells in different cell cycle phases. We found that the cell cycle profiles were not significantly different upon BMI1 loss (Figure 5C, Figure S5B). Interestingly, we did observe upregulation of *Ink4a* mRNA levels (2.0 to 4.2-fold increase) in all three *Bmi1*$^{fl/fl}$ tumor organoid lines upon BMI1 loss, but this was insufficient to cause cell cycle arrest or even moderately alter the representation of G1 cells versus other cell cycle phases (Figure 5D, Figure S5C). We also used tumor organoid formation assays as methods to understand the impacts of BMI1 loss on AK tumor cell proliferation and CSC frequency (Figure 6A, Figure S6A). We observed that BMI1 loss did not affect the numbers of tumor organoids formed, their gross morphologies, nor the distributions of tumor organoid sizes, even following serial passaging (Figure 6B-C, Figure S6B-D). These results indicate that BMI1 loss does not impair proliferation or CSC frequency of AK colon tumor cells.

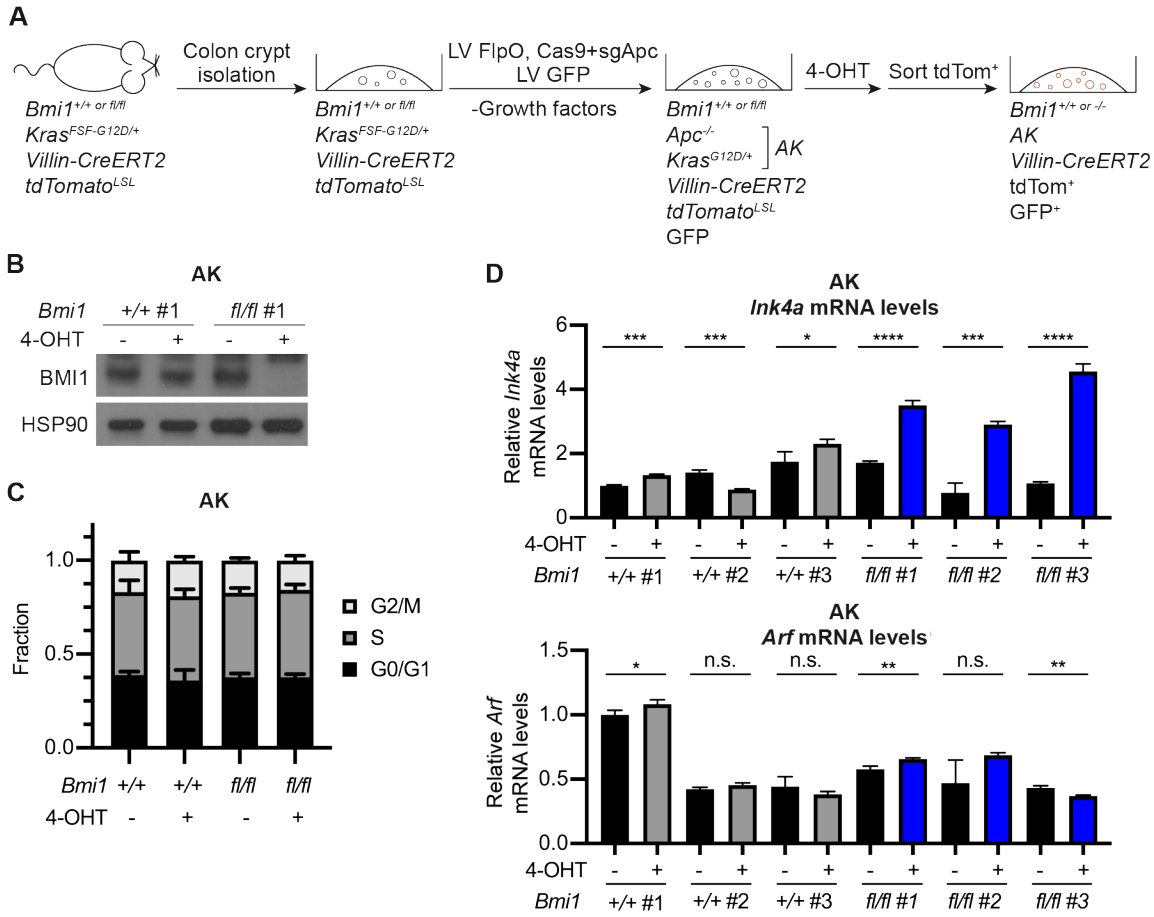

Figure 5. Deletion of *Bmi1* in AK tumor organoids does not alter cell cycle phasing but induces upregulation of *Ink4a* expression. **A)** Schematic for generation of *Apc*$^{-/-}$*; Kras*$^{G12D/+}$ (AK) tumor organoids and conditional deletion of *Bmi1 in vitro*. Colon crypts were isolated from mice and cultured in Matrigel to form 3D organoids. Lentiviral infection with FlpO, sgApc, Cas9, and GFP, followed by withdrawal of Wnt, resulted in deletion of *Apc* and expression of GFP, as well as activation of oncogenic *Kras*. Treatment of these AK tumor organoids with 4-hydroxytamoxifen (4-OHT) induced activation of Cre (expression of which is driven by the mouse villin 1 promoter), resulting in tdTomato expression and loss of BMI1 in *Bmi1*$^{fl/fl}$ tumor organoids. **B)** Immunoblot of BMI1 protein in *Bmi1*$^{+/+}$ AK #1 and *Bmi1*$^{fl/fl}$ AK #1 tumor organoids treated with EtOH vehicle control (-4-OHT) or 4-OHT (+4-OHT). **C)** Fraction of *Bmi1*$^{+/+}$ AK #1 - #3 and *Bmi1*$^{fl/fl}$ AK #1 - #3 tumor organoid cells in G0/G1, S, and G2/M cell cycle phases, as assayed by EdU incorporation. Cells were pulse-labeled with EdU for 1 hr. 30 min. before harvest. Mean and S.D. are shown. $p > 0.05$ as determined by ANOVA. **D)** Relative mRNA levels of *Ink4a* (top) and *Arf* (bottom) in AK tumor organoids, as determined by qRT-PCR. All samples were normalized to *Bmi1*$^{+/+}$ AK #1 -4-OHT levels. Mean and S.D. are shown, and statistical significance was determined with unpaired Student's t-test. n.s. $p > 0.05$, * $p < 0.05$, ** $p < 0.01$, *** $p < 0.001$, **** $p < 0.0001$.

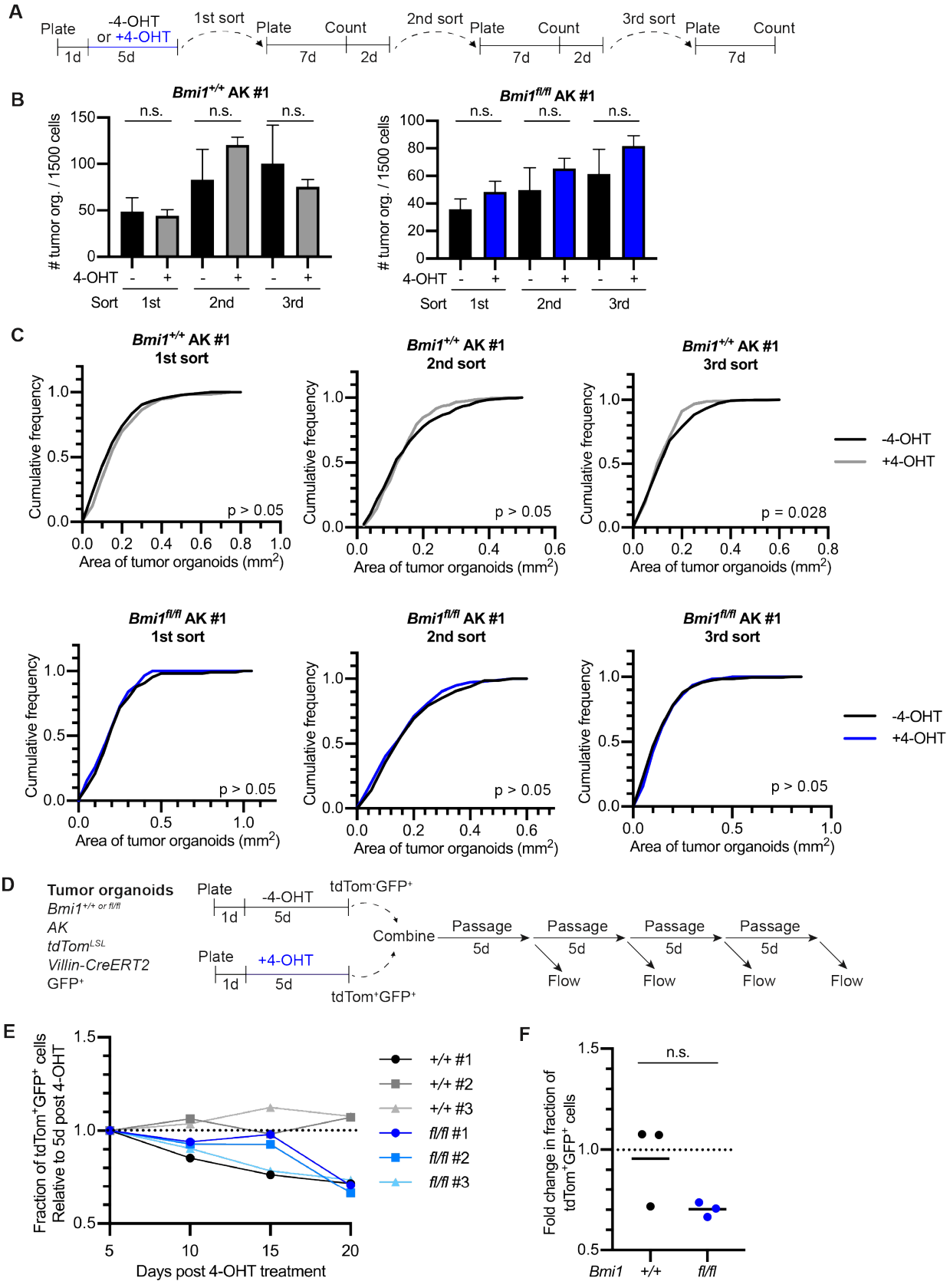
A
Plate
-4-OHT
or +4-OHT
1d
5d
1st sort
Plate
Count
7d
2d
2nd sort
Plate
Count
7d
2d
3rd sort
Plate
Count
7d
B
Bmi1+/+ AK #1
Bmi1fl/fl AK #1
tumor org. / 1500 cells
n.s.
4-OHT
Sort
1st
2nd
3rd
C
Bmi1+/+ AK #1
1st sort
2nd sort
3rd sort
Cumulative frequency
Area of tumor organoids (mm2)
p > 0.05
p = 0.028
-4-OHT
+4-OHT
Bmi1fl/fl AK #1
1st sort
2nd sort
3rd sort
D
Tumor organoids
Bmi1+/+ or fl/fl
AK
tdTomLSL
Villin-CreERT2
GFP+
Plate
-4-OHT
+4-OHT
1d
5d
tdTom-GFP+
tdTom+GFP+
Combine
Passage
5d
Flow
E
Fraction of tdTom+GFP+ cells
Relative to 5d post 4-OHT
Days post 4-OHT treatment
+/+ #1
+/+ #2
+/+ #3
fl/fl #1
fl/fl #2
fl/fl #3
F
Fold change in fraction of
tdTom+GFP+ cells
n.s.
Bmi1
+/+
fl/fl

Figure 6. BMI1 loss may confer a mild growth disadvantage in AK tumor organoids. **A)** Schematic for AK tumor organoid formation assay with serial passaging. AK tumor organoids were plated and treated with EtOH vehicle control (-4-OHT) or 50nM 4-OHT (+4-OHT) for 5 days. Tumor organoids were then dissociated, sorted using FACS for live $tdTom^{+}GFP^{-}$ cells (for -4-OHT tumor organoids) or live $tdTom^{+}GFP^{+}$ cells (for +4-OHT tumor organoids) and plated as single cells in Matrigel. The numbers and areas of tumor organoids were quantified 7 days after sorting. The sorting, plating, and quantification processes were repeated twice more for a total of 3 sorts. **B)** Quantification of the number of *Bmi1*$^{+/+}$ AK #1 and *Bmi1*$^{fl/fl}$ AK #1 tumor organoids formed from 1500 cells plated. Blue bars represent the condition where BMI1 is lost (i.e. *Bmi1*$^{fl/fl}$ cells +4-OHT). Mean and S.D. are shown, and significance was determined using unpaired Student's t-test. n.s. $p > 0.05$. **C)** Cumulative distribution functions of *Bmi1*$^{+/+}$ AK #1 and *Bmi1*$^{fl/fl}$ AK #1 tumor organoid areas. Significance was determined using Kolmogorov-Smirnov test. **D)** Schematic of competition assay. *Bmi1*$^{+/+}$ AK #1 - #3 and *Bmi1*$^{fl/fl}$ AK #1 - 3 tumor organoids were treated either -4-OHT or +4-OHT. These tumor organoids were combined and passaged, and samples were collected at every passage for analysis by flow cytometry. **E)** Fraction of $tdTom^{+}GFP^{+}$ cells at each time point, as determined by flow cytometry. **F)** Fold change in the percentage of $tdTom^{+}GFP^{+}$ cells between time point 2 and time point 5. Mean is shown, and statistical significance was determined using unpaired Student's t-test. n.s. $p > 0.05$.

We also performed competitive growth assays with AK tumor organoids, and interestingly, these raised the possibility of growth defects upon BMI1 loss. As with the AKP experiments, we treated AK tumor organoids with vehicle or 4-OHT, combined and passaged the cells, and then assessed for the representation of *Bmi1*$^{-/-}$ cells by expression of fluorescent markers and flow cytometry (Figure 6D). In the case of the *Bmi1*$^{+/+}$ AK lines, the relative frequency of $tdTom^{+}GFP^{+}$ cells remained relatively unchanged across the four time points for two lines, while the frequency decreased in the third *Bmi1*$^{+/+}$ AK line (Figure 6E). For the *Bmi1*$^{fl/fl}$ AK lines, the frequency of $tdTom^{+}GFP^{+}$ cells for all three decreased by the fourth time point (Figure 6E). Though the change in representation of $tdTom^{+}GFP^{+}$ cells over the four timepoints was not significantly different between *Bmi1*$^{+/+}$ and *Bmi1*$^{fl/fl}$ AK lines (Figure 6F), these results suggest, for the first time in the present study, the possibility of a growth disadvantage with BMI1 loss in transformed colon cancer cells. However, we note that this phenotype is not especially strong, and further replicates including additional passages, are required.

To assess the effects of BMI1 loss in AK colon tumors *in vivo*, we performed a pilot orthotopic transplant experiment using colonoscopy-mediated injection of AK tumor organoids into the colons of recipient mice (Figure 7A). We transplanted *Bmi1*$^{fl/fl}$ AK #1 tumor organoids into recipient mice, treated mice with either vehicle or tamoxifen, and tracked tumor growth. We

chose to transplant a high dose of 1000 AK tumor organoids, as establishment of AK tumors was known to be difficult with this transplant method (personal communication with Yilmaz Lab, MIT). Quantification of tumor volumes and longitudinal tracking was again achieved with 3D ultrasound imaging and reconstruction (Figure 7A; Freeling and Rezvani, 2016). Unfortunately, only three of the vehicle-treated mice survived until time point 6, as several mice were euthanized early in the study due to formation of large cystic masses (Figure 7B). Intriguingly, reductions in tumor volumes were observed in the majority of tamoxifen-treated mice, with complete tumor regression in one mouse (Figure 7B). These preliminary results suggest that BMI1 loss may be detrimental to the maintenance and growth of AK tumors, but more replicates of the transplant experiment are required to draw definitive conclusions.

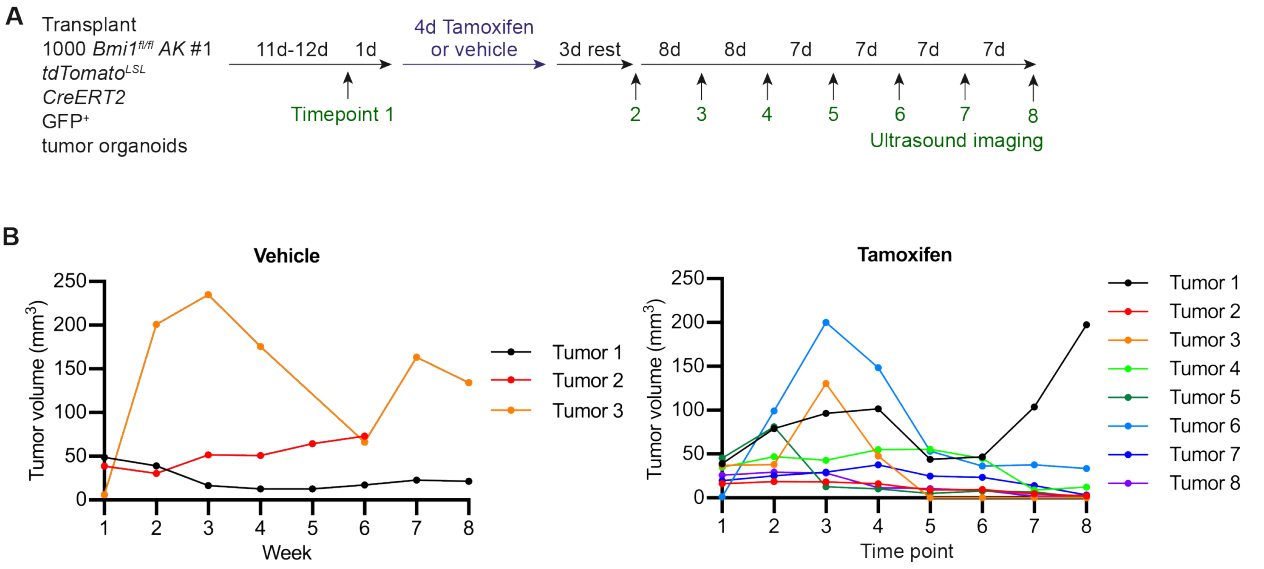

Figure 7. Longitudinal tracking of AK colon tumor growth following BMI1 loss. **A)** Schematic for *Bmi1* deletion in established AK colon tumors. 1000 *Bmi1*$^{fl/fl}$ AK #1 tumor organoids were transplanted into the colons of recipient mice via colonoscopy-mediated injection. Following confirmation of tumor establishment by 3D ultrasound imaging at time point 1, mice received daily intraperitoneal injections of tamoxifen (dose: 0.1g tamoxifen per kg mouse) or corn oil vehicle control for 4 days. After 3 days of rest, colon tumors were imaged every 7-8 days using 3D ultrasound imaging. **B)** Tumor volumes of 3 tumors from a total of 3 vehicle-treated mice (left) and 8 tumors from a total of 8 tamoxifen-treated mice (right) at each time point, as determined by 3D ultrasound imaging and reconstruction.

DISCUSSION

BMI1 has been widely studied for its oncogenic roles, leading to significant interest in targeting BMI1 as a cancer therapeutic. We and others have previously demonstrated that *Bmi1* deficiency in tumors causes proliferative impairment, particularly in the context of embryonic *Bmi1* ablation or deletion at tumor initiation, including in small intestinal tumors (Maynard et al., 2014). In contrast to these former studies, we now demonstrate that BMI1 loss in established colon AKP tumors in adult mice does not impair tumor maintenance or progression. We utilize 3D tumor organoids and determine that *Bmi1* deletion *in vitro* does not impact proliferation. Moreover, upon orthotopic transplant of the colon tumor organoids into mice, we demonstrate that BMI1 loss *in vivo* after AKP tumor establishment does not impair tumor growth kinetics. Our preliminary studies do suggest that BMI1 loss may be tumor suppressive in the AK colon tumor context. However, more replicates, especially of the *in vivo* tumor tracking experiment, are required. Overall, our data bear high resemblance to our findings in lung cancer, where BMI1 loss in established lung tumors in adult mice is not tumor suppressive.

We postulate several reasons as to why our observations on BMI1 loss in established adult tumors contrast sharply with previous studies, which have overwhelmingly found that BMI1 loss is detrimental to tumor progression largely through derepression of *Cdkn2a*. The first hypothesis is that in the adult context, BMI1 is dispensable for suppression of $p16^{INK4A}$ and $p19^{ARF}$. Much of the evidence linking BMI1 and *Cdkn2a* were uncovered using germline $Bmi1^{-/-}$ mice, indicating BMI1's critical role in suppressing *Cdkn2a* during embryogenesis. However, we hypothesize that in the adult context, loss of BMI1 is insufficient to induce upregulation of $p16^{INK4A}$ and $p19^{ARF}$, and the tumors are able to maintain proliferative capacity. The second hypothesis is that loss of an epigenetic regulator, such as BMI1, can greatly alter the chromatin landscape and promote plasticity, allowing tumors to quickly adapt to selection pressures. Our third hypothesis is that another Polycomb group protein is compensating for BMI1 loss. Indeed,

a recent study using a colitis-associated model of CRC demonstrated that combined loss of BMI1 with its homologue, MEL18, was significantly more tumor suppressive than knock out of BMI1 alone (Liu et al., 2017). More studies, such as chromatin profiling experiments, are required to elucidate the specific targets of BMI1 in the adult lung and colon contexts and how expression of these targets and the chromatin landscape change during tumorigenesis.

Our data also contrast with studies utilizing BMI1 inhibitors, where pharmacological inhibition using the compounds PTC-209, PTC-596, or PTC-028 potently suppress tumor progression in xenograft models (Dey et al., 2018; Elango et al., 2019; Kreso et al., 2014; Nishida et al., 2017; Sulaiman et al., 2019). We have determined that treatment with PTC-209 impairs proliferation equally well in *Bmi1*$^{+/+}$ and *Bmi1*$^{-/-}$ colon tumor organoids (data not shown). Other studies have also determined that PTC-596 and PTC-028 exert cytotoxic effects independent of *Bmi1* status (Bolomsky et al., 2016; Eberle-Singh et al., 2019; Flamier et al., 2020). Therefore, we believe that our mouse models offer a more robust system to directly interrogate BMI1 loss in tumors.

Taken altogether, we have demonstrated that BMI1 loss in established colon tumors of adult mice is not tumor suppressive, at least in the absence of functional p53. Our results caution against the use of BMI1 inhibition alone as a strategy for cancer treatment, and more studies are required to understand the specific timing and context in which BMI1 inhibition is effective.

SUPPLEMENTAL FIGURES

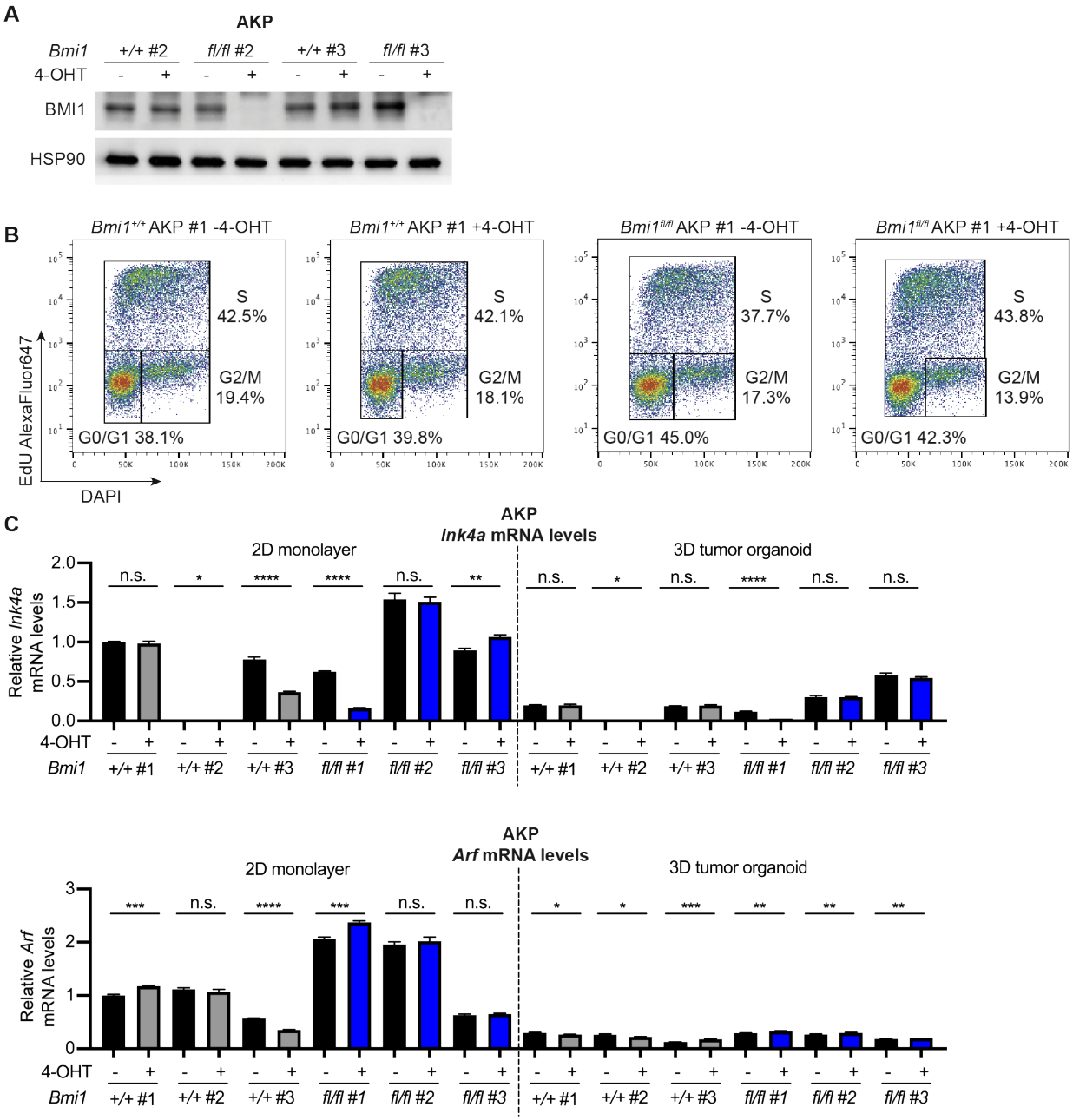

Figure S1. *In vitro* deletion of *BMI1* does not impact AKP tumor organoid cell cycle profiles and *Ink4a*/*Arf* expression. **A)** Immunoblot of BMI1 expression in *Bmi1*$^{+/+}$ AKP #2 & #3 and *Bmi1*$^{fl/fl}$ AKP #2 & #3 tumor organoids treated EtOH vehicle control (-4-OHT) or 4-OHT (+4-OHT). **B)** Representative analytical flow cytometry plots of *Bmi1*$^{+/+}$ AKP #1 and *Bmi1*$^{fl/fl}$ AKP #1 +/- 4-OHT pulsed with EdU (y-axis) and treated with DAPI (x-axis). Percentage of cells in each cell cycle phase is shown. **C)** Relative mRNA levels of *Ink4a* (top) and *Arf* (bottom) in AKP 2D monolayer cells and 3D tumor organoids, as determined by qRT-PCR. All samples were normalized to level of target expression in *Bmi1*$^{+/+}$ AKP #1 -4-OHT 2D monolayer cells. The data for 3D tumor organoids is equivalent to the data presented in Figure 1D and included as a comparison to the 2D monolayer condition. Mean and S.D. are shown. Statistical significance was determined by unpaired Student's t-test. n.s. $p > 0.05$, * $p < 0.05$, ** $p < 0.01$, *** $p < 0.001$, **** $p < 0.0001$.

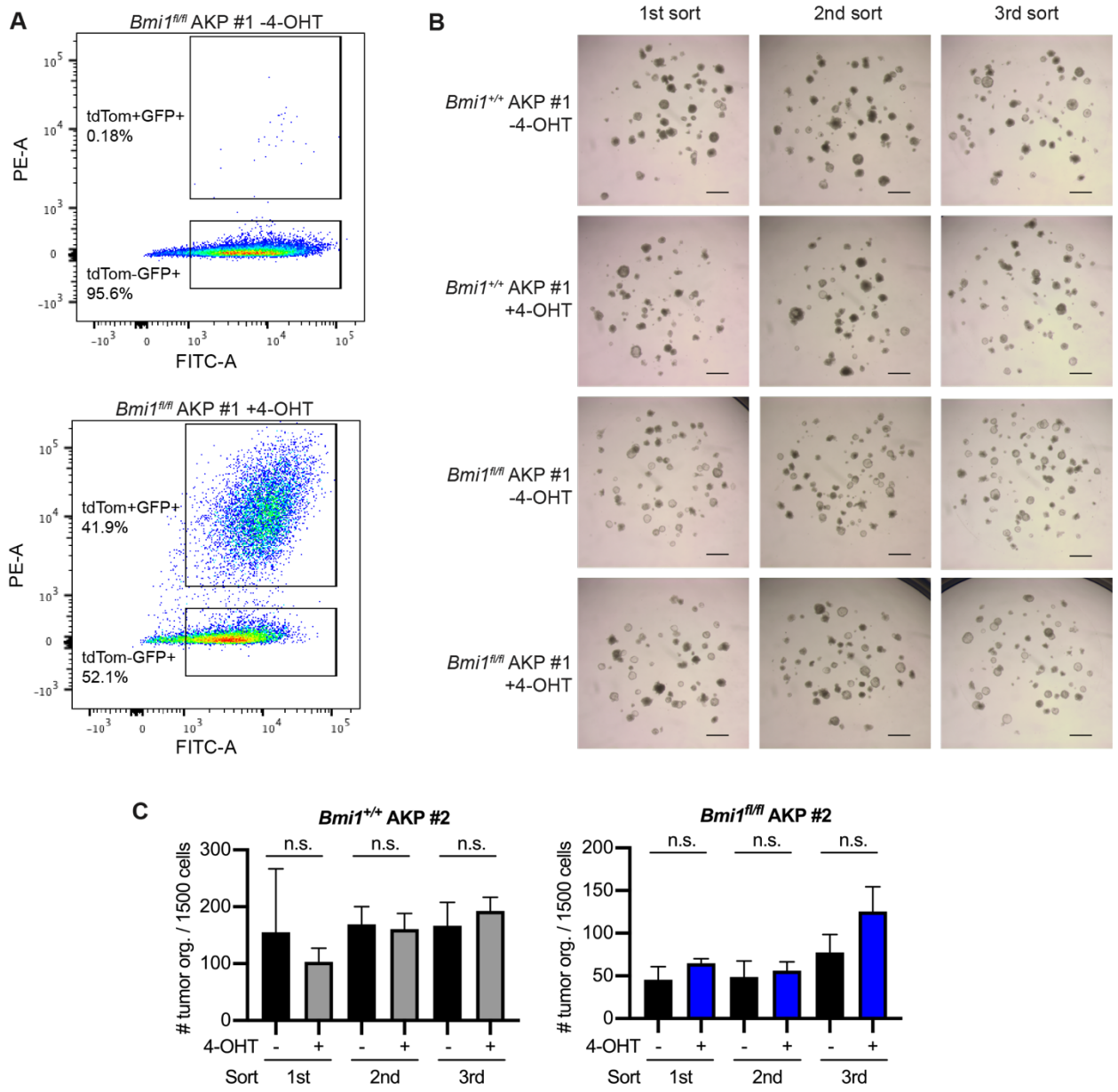

Figure S2 (continued on next page)

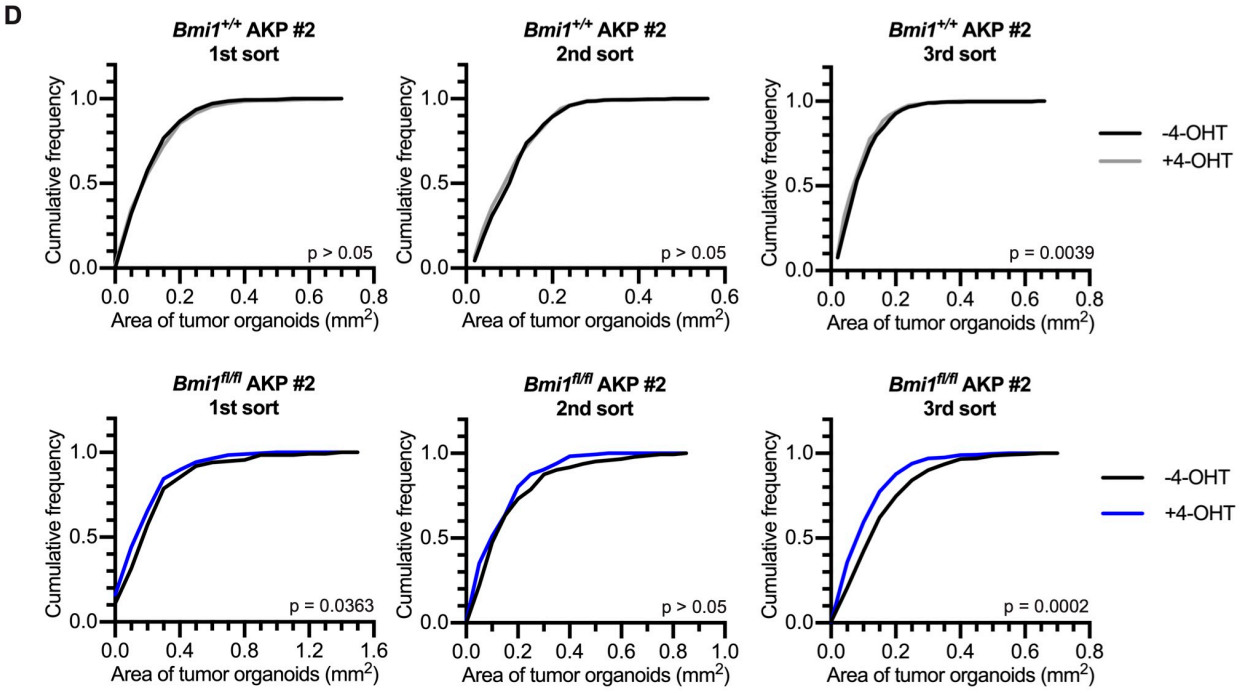

Figure S2. BMI1 loss does not alter proliferation of AKP tumor organoids through tumor organoid formation and serial passaging assays. **A)** Representative flow cytometry plots of tdTom^{+}GFP^{+} and tdTom^{+}GFP^{-} cells sorted for tumor organoid formation assays. **B)** Representative photos of *Bmi1*$^{+/+}$ AKP #1 and *Bmi1*$^{fl/fl}$ AKP #1 tumor organoids at each sort. Scale bar represents 1mm. **C)** Quantification of the number of *Bmi1*$^{+/+}$ AKP #2 and *Bmi1*$^{fl/fl}$ AKP #2 tumor organoids formed from 1500 cells plated. Blue bars represent the condition where BMI1 is lost (i.e. *Bmi1*$^{fl/fl}$ cells +4-OHT). Mean and S.D. are shown, and significance was determined using unpaired Student's t-test. n.s. $p > 0.05$. **D)** Cumulative distribution functions of *Bmi1*$^{+/+}$ AKP #2 and *Bmi1*$^{fl/fl}$ AKP #2 tumor organoid areas. Significance was determined using Kolmogorov-Smirnov test.

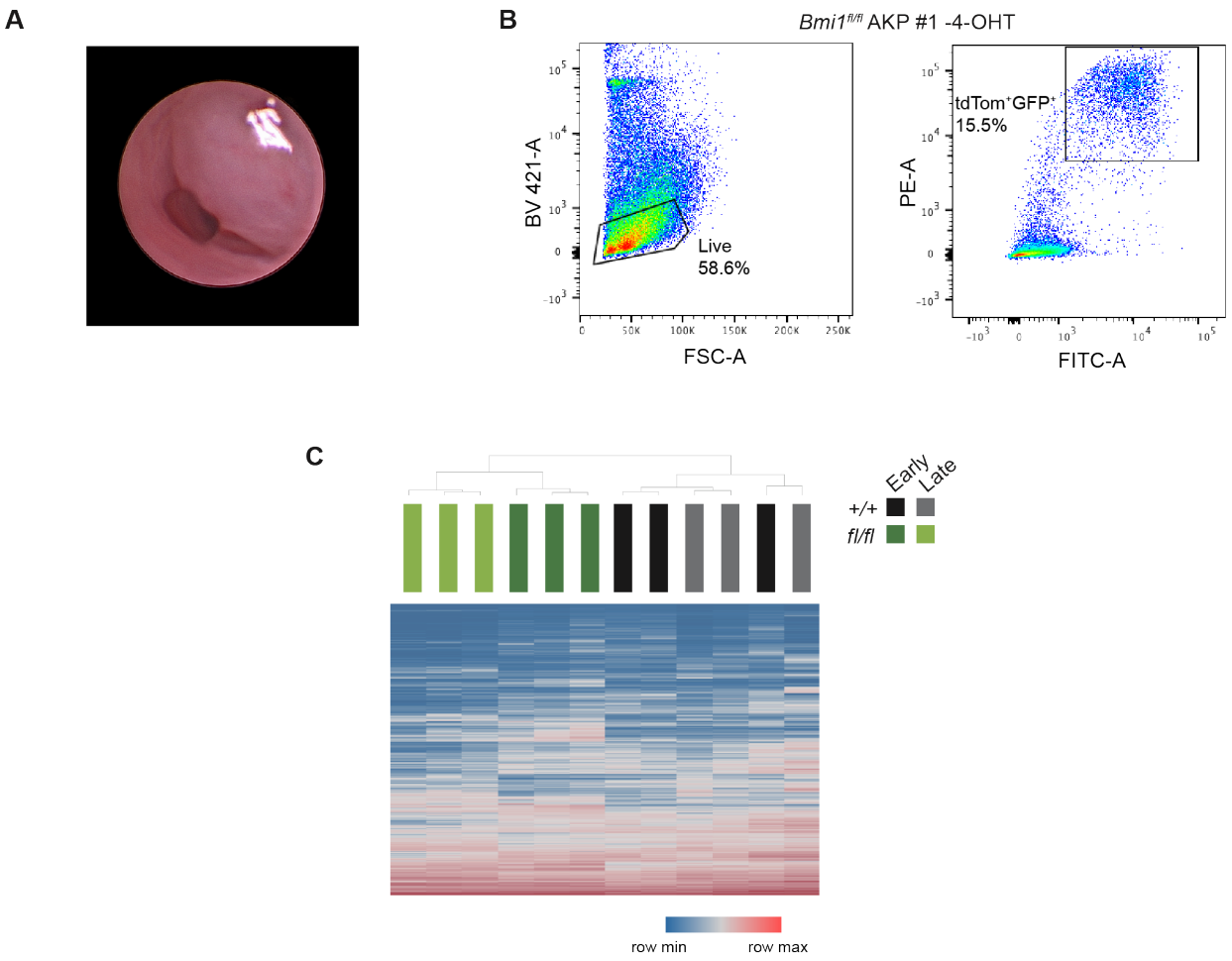

Figure S3. *In vivo* deletion of *Bmi1* in AKP colon tumors and transcriptional profiling of tumor cells. **A)** Representative colonoscopy image of a colon tumor generated by orthotopic transplant of tumor organoids into the submucosa of recipient mice. **B)** Representative flow cytometry plot of *Bmi1*$^{fl/fl}$ AKP #1 tumor cells, and tdTom^{+}GFP^{+} cells were isolated for bulk RNA-seq. **C)** Supervised hierarchical clustering of *Bmi1*$^{+/+}$ and *Bmi1*$^{fl/fl}$ early and late samples (n=3 mice per genotype per time point). Clustering was conducted using the 1863 genes that were differentially expressed (as determined by DESeq2) in at least one pairwise comparison (*Bmi1*$^{+/+}$ early vs *Bmi1*$^{+/+}$ late vs *Bmi1*$^{fl/fl}$ early vs *Bmi1*$^{fl/fl}$ late samples).

A

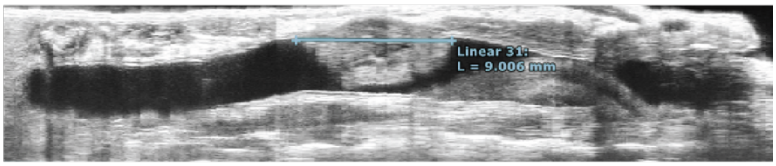

B

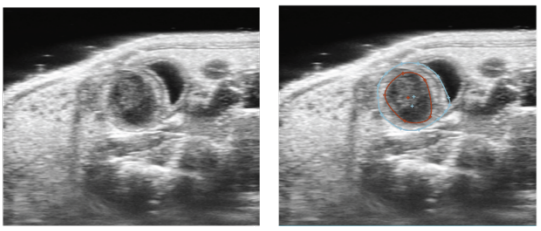

Figure S4. 3D ultrasound imaging and reconstruction of mouse colon. **A)** Representative sagittal colon slice acquired using ultrasound imaging and visualized with Vevo LAB software. The tumor length along the colon wall is highlighted in blue. **B)** Representative transverse colon slice depicting the colon tumor boundaries (blue) and a cystic region within the colon tumor (red).

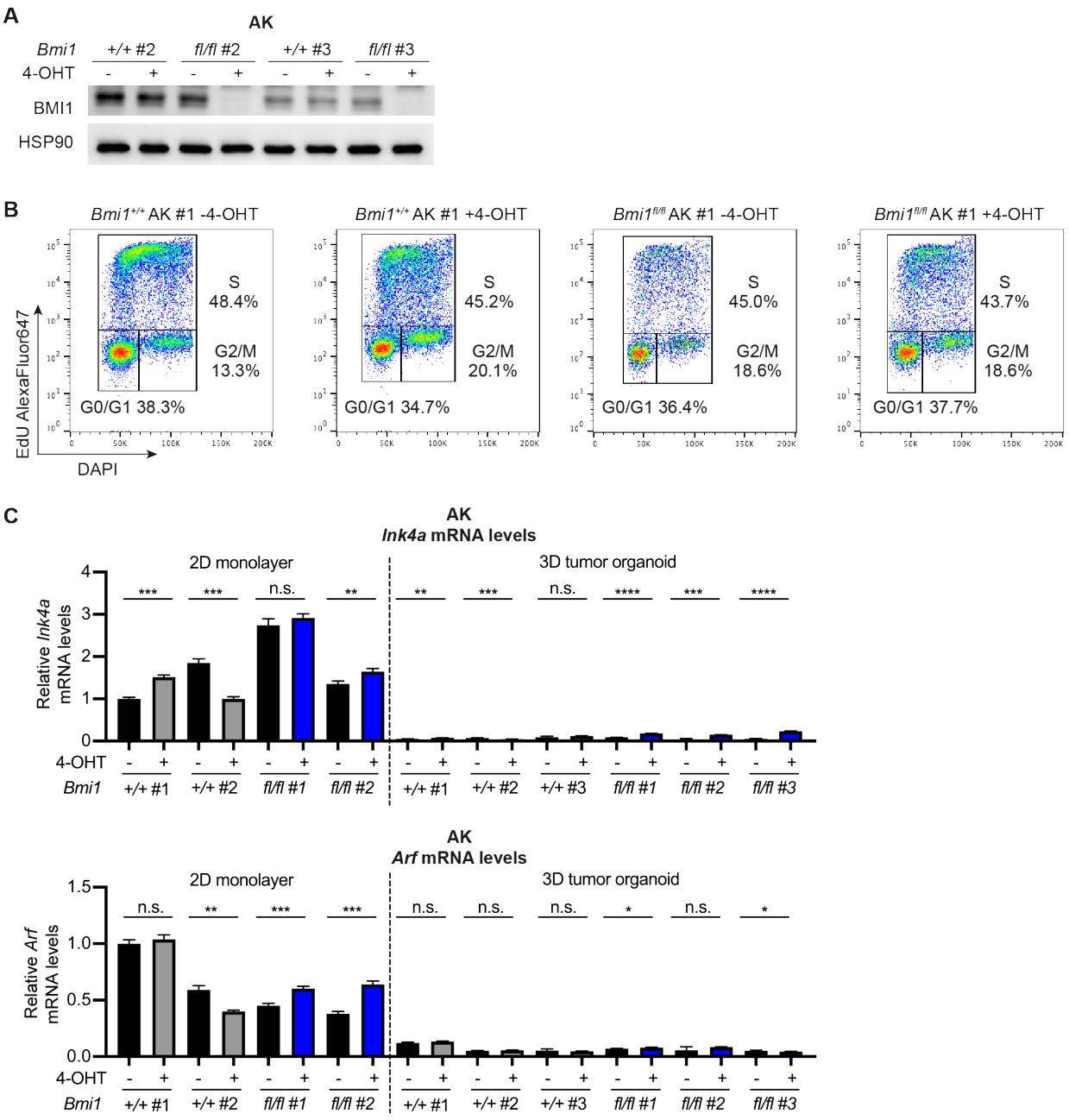

Figure S5. *In vitro* deletion of *BMI1* does not impact AK tumor organoid cell cycle profiles. **A)** Immunoblot of BMI1 expression in *Bmi1*$^{+/+}$ AK #2 & #3 and *Bmi1*$^{fl/fl}$ AK #2 & #3 tumor organoids treated EtOH vehicle control (-4-OHT) or 4-OHT (+4-OHT). **B)** Representative analytical flow cytometry plots of *Bmi1*$^{+/+}$ AK #1 and *Bmi1*$^{fl/fl}$ AK #1 +/- 4-OHT pulsed with EdU (y-axis) and treated with DAPI (x-axis). Percentage of cells in each cell cycle phase is shown. **C)** Relative mRNA levels of *Ink4a* (top) and *Arf* (bottom) in AK 2D monolayer cells and 3D tumor organoids, as determined by qRT-PCR. The data for 3D tumor organoids is equivalent to the data presented in Figure 5D and included as a comparison to the 2D monolayer condition. All samples were normalized to level of target expression in *Bmi1*$^{+/+}$ AK #1 -4-OHT 2D monolayer cells. Mean and S.D. are shown, and statistical significance was determined with unpaired Student's t-test. n.s. $p > 0.05$, * $p < 0.05$, ** $p < 0.01$, *** $p < 0.001$, **** $p < 0.0001$.

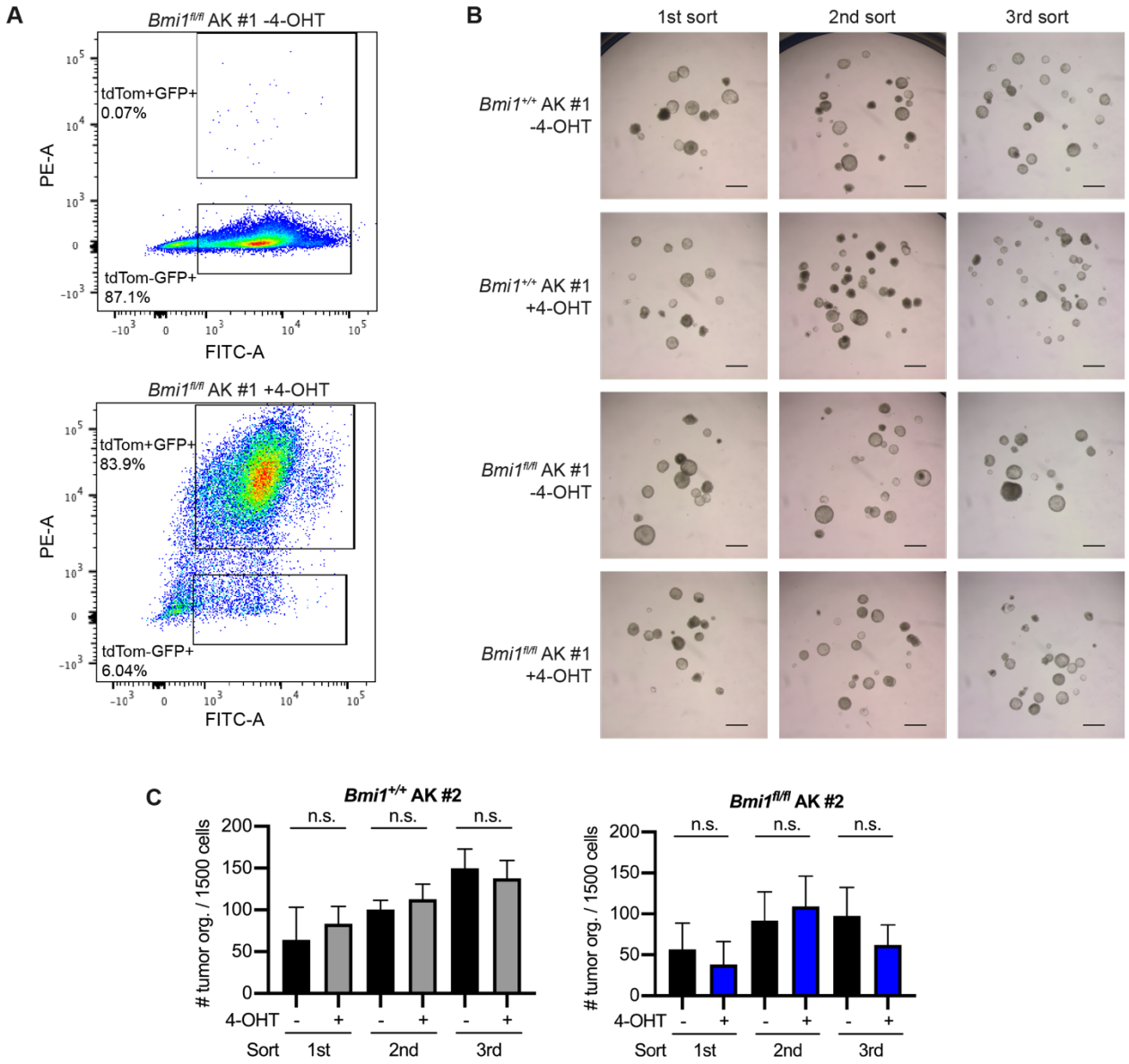

Figure S6 (continued on next page)

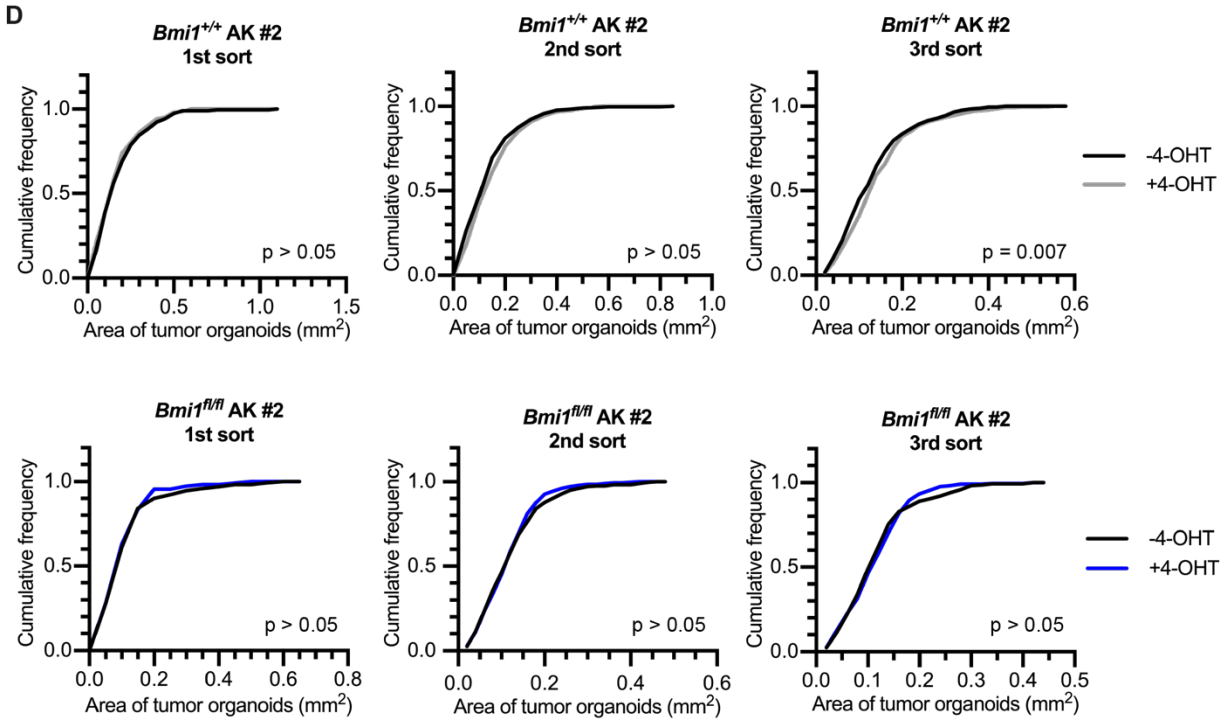

Figure S6. BMI1 loss does not impact AK tumor organoid proliferation as assayed by tumor organoid formation and serial passaging assays. **A)** Representative flow cytometry plots of tdTom^{+}GFP^{+} and tdTom^{+}GFP^{-} cells sorted for tumor organoid formation assays. **B)** Representative photos of *Bmi1*$^{+/+}$ AK #1 and *Bmi1*$^{fl/fl}$ AK #1 tumor organoids at each sort. Scale bar represents 1mm. **C)** Quantification of the number of *Bmi1*$^{+/+}$ AK #2 and *Bmi1*$^{fl/fl}$ AK #2 tumor organoids formed from 1500 cells plated. Blue bars represent the condition where BMI1 is lost (i.e. *Bmi1*$^{fl/fl}$ cells +4-OHT). Mean and S.D. are shown, and significance was determined using unpaired Student's t-test. n.s. $p > 0.05$. **D)** Cumulative distribution functions of *Bmi1*$^{+/+}$ AK #2 and *Bmi1*$^{fl/fl}$ AK #2 tumor organoid areas. Significance was determined using Kolmogorov-Smirnov test.

MATERIALS AND METHODS

Mouse models

Mice with the following alleles were used: *Bmi1*^{fl} (Maynard et al., 2014), *Kras*$^{FSF\text{-}G12D/+}$ (Jackson laboratories #023590), *Trp53*^{frt} (Lee et al., 2012; Jackson laboratories stock #017767), *Rosa26-CAG-FSF-CreERT2* (Schönhuber et al., 2014), *Rosa26-CAG-LSL-tdTomato* (Madisen et al., 2010; Jackson laboratories stock #007914), and *Villin-CreERT2* (el Marjou et al., 2004; Jackson laboratories #020282). PCR based genotyping was conducted as described in the cited references apart from *Bmi1* genotyping which used the following primers: GGTTCCTCTTCATACATGACG and GACATACCCAATACTTTC (wild-type allele 279bp, floxed allele 313bp products) and the Rosa26-CAG-FSF-CreERT2 genotyping: GATAGTGAAACAGGGGCAATGG and TCTGCCAGGTTGGTCAGTAAGC (263bp product). All animals were maintained on a mixed C57BL/6J x 129SvJ x Balb/c background.

Colon crypt isolation and generation of colon organoids

To isolate colon crypts, mice were euthanized and the colons were removed and flushed with cold PBS. Colons were manually chopped into 4-5 mm pieces, washed twice with cold PBS, and incubated in 5mM EDTA in PBS at 4C on a shaking rotor for 1 hour. The colon fragments were then washed twice with cold PBS, pipetted vigorously for 5 minutes, and pelleted by centrifugation. 200 colon crypt fragments were mixed with Wnt conditioned media (WRN media; Miyoshi and Stappenbeck, 2013), and the basement membrane matrix Matrigel (Corning 356231) was added such that Matrigel constituted 75% of the resulting mixture. 40μL of the crypt, media, and Matrigel mixture were added to one well of a 24-well plate and placed at 37C for 30 minutes. Following polymerization of Matrigel, 650μL of WRN media supplemented with 10μM Y-27632 (Stemcell Technologies #72302) was added to the well, and colon

organoids emerged by 48 hours after plating. Media was replaced with fresh WRN media (without Y-27632) every three days until transformation.

Lentiviral production

The lentiviral backbone pLL3.3 (gift from Tyler Jacks, MIT) was modified using Gibson cloning (Gibson et al., 2009) to include FlpO, Cas9, and a sgRNA against *Apc* (ggcactcaaaacgcttttga). The pHAGE PGK-GFP-IRES-LUC-W lentiviral vector (Wilson et al., 2010) was used to induce GFP expression. Lentiviral particles were generated by transfecting 293FT cells with the lentiviral vector, packaging plasmid psPAX2 (Addgene plasmid #12260), and envelope plasmid pMD2.G (Addgene plasmid #12259; Dull et al., 1998; Gibson et al., 2009) using TransIT-LT1 transfection reagent (Mirus Bio #MIR2304). Supernatant was collected at 2 days and 3 days post transfection, and concentrated by ultracentrifugation at 25000rpm for 2 hours.

Generation of tumor organoids

Starting 24 hours prior to infection, the colon organoids were incubated with 10μM of nicotinamide (Thermo Fisher Scientific #128271000) in WRN media. To dissociate the colon organoids, Matrigel with the embedded organoids were scraped from the plate, placed in an Eppendorf tube, mechanically dissociated for 20 seconds with vigorous pipetting, and incubated with TrypLE Express (Thermo Fisher Scientific #12604-013) for 45 sec at 37C. After addition of cold DMEM, the organoid fragments were pelleted by centrifugation and resuspended in L-WRN media with 10μM Y-27632, polybrene (Millipore Sigma #TR-1003-G), and lentivirus expressing FlpO, Cas9, and a sgRNA against *Apc* (detailed above). The organoid, media, and lentivirus mixture was pipetted onto Matrigel and incubated at 37C for 6 hours. Following viral incubation, the organoids were washed with PBS twice, and L-WRN media was added. After 4-5 days, the organoids were passaged through the dissociation process as described above, plated in fresh

Matrigel, and incubated in WRN media. After an additional 4-5 days, the organoids were passaged and switched to growth in minimal media comprising of: Advanced DMEM/F-12 (Thermo Fisher Scientific #12634010), B-27 supplement (Thermo Fisher Scientific #17504-044), L-glutamine (GE Healthcare #SH30034.01), and penicillin-streptomycin solution (Corning #30002CI). Growth in minimal media lacking Wnt selects for *Apc*-mutant tumor organoids (Drost et al., 2015; Matano et al., 2015; Schwank et al., 2013). Following transformation, colon tumor organoids were passaged every 4-5 days using fresh Matrigel and minimal media. Treatment with 10μM nutlin-3 (Cayman Chemical #10004372) was used to select for *p53*-mutant tumor organoids.

Tumor organoid formation assays

Colon tumor organoids were passaged as described above. 24 hours after plating, colon tumor organoids were incubated with minimal media with 50nM 4-hydroxytamoxifen (4-OHT; Millipore Sigma #H7904) or EtOH vehicle control for 5 days. Following incubation with 4-OHT, colon tumor organoids were dissociated as described above, placed in minimal media containing 10μM Y-27632, 10% FBS, and DAPI, and filtered through 35μm cell strainer (Corning #352235). Cells were sorted using BD FACS Aria Cell Sorter for DAPI-negative, tdTomato-positive, and/or GFP-positive populations. 1500 cells per sample were isolated, embedded in Matrigel, and plated into 3 wells (for 500 cells/well) with minimal media. Organoid numbers and sizes were quantified 7 days following the sort using ImageJ and Matlab. The dissociation, sorting, and plating process were repeated for the serial passaging experiments.

Quantitative real time PCR (qRT-PCR)

Total RNA was isolated and purified with RNeasy Plus Mini Kit (Qiagen #74134) following manufacturer's protocols. RNA was reverse transcribed into cDNA using SuperScript III First-Strand Synthesis System for RT-PCR (Invitrogen #18080-051). Real-time quantitative

PCR was conducted using Fast SYBR Green (Thermo Fisher Scientific #4385610) on a StepOnePlus Real-Time PCR System (Applied Biosystems). Data were analyzed using the ΔΔCt method, and relative mRNA levels were normalized to *Gapdh* levels. The following primers were used (F: forward primer, R: reverse primer):

Bmi1 F	5'- CAAAACCAGAACACTCCTGAA
Bmi1 R	5'- TCTTCTTCTCTTCATCTCATTTTTGA
Ink4a F	5'- GCGGGCACTGCTGGAAG
Ink4a R	5'- CGTTGCCCATCATCATCACC
Arf F (Matheu et al., 2007)	5'- GCCGCACCGGAATCCT
Arf R (Matheu et al., 2007)	5'- TTGAGCAGAAGAGCTGCTACGT
Gapdh F	5'- ATGGTGAAGGTCGGTGTGA
Gapdh R	5'- AATCTCCACTTTGCCACTGC

Western blot

Protein was extracted from colon tumor organoid cell pellets through incubation in RIPA buffer (150mM NaCl, 1% NP-40, 0.5% sodium deoxycholate, 0.1% SDS, 50mM Tris pH=8.0) supplemented with protease inhibitor (Roche #11836153001), and protein concentration was quantified by BCA assay (Thermo Fisher Scientific #23250). 20μg of protein was mixed with standard 4x Laemmli buffer and run on 4% SDS-polyacrylamide gels before transfer onto nitrocellulose membrane. Membranes were blocked with 5% milk in tris-buffered saline with 0.1% Tween-20, and immunoblotting was conducted using anti-HSP90 primary antibody (1:2000, BD610418), anti-BMI1 serum (generated in the Lees Lab), and HRP-conjugated anti-mouse secondary antibody (Cytiva #NA931). Signals were visualized with enhanced chemiluminescence (SuperSignal West Femto Maximum Sensitivity Substrate, Thermo Fisher #34095) and film or imaged with a BioRad ChemiDoc MP Imaging System.

Cell cycle profiling with EdU incorporation assay

Colon tumor organoids were passaged as described above. Four days following plating, the colon tumor organoids were incubated in minimal media containing 10μM 5-ethynyl-2'-

deoxyuridine (EdU; Sigma-Aldrich #T511285) for 45 minutes (AKP tumor organoids) or 90 minutes (AK tumor organoids). Tumor organoids were dissociated, incubated and washed with PBS + 1% BSA, and fixed with 4% formaldehyde (Electron Microscopy Sciences #15710). Following fixation, cells were washed with PBS, blocked with 1% BSA, and permeabilized with 0.5% Triton X-100 (Sigma-Aldrich #T9284). Cells were incubated with Click-IT labeling reaction solution, containing 1mM CuSO4, 1mM AlexaFluor 647 azide (ThermoFisher Scientific #A102777), and 100mM ascorbic acid, for 30 minutes. Cells were subsequently washed with PBS and treated with RNase A and DAPI. Cell cycle profiles of singlet cells (DNA content between 2N and 4N) were determined using flow cytometry with BD LSR II and FlowJo software.

In vitro *competition assay*

Two wells of each colon tumor organoid line were passaged and plated as described above. 24 hours after plating, 50nM 4-OHT or EtOH vehicle control was added to one well of each colon tumor organoid line. After 5 days, the two wells of each colon tumor organoid line were dissociated, combined, and plated. The tumor organoids were passaged four times, and at each passage, a portion of cells were analyzed for the representation of $tdTomato^+$ and GFP^+ cells using flow cytometry with BD LSR II and analysis with FlowJo software.

Colon tumor induction in vivo

48 hours after plating, tumor organoids were extracted from Matrigel through mechanical dissociation by pipetting, and the concentration of tumor organoids was determined through microscopy and manual counting. Tumor organoids were resuspended in Opti-MEM media (Thermo Fisher Scientific #31985062) with 10% Matrigel at the appropriate tumor organoid concentration. 50μL of the tumor organoid mixture were transplanted into the colon epithelium of recipient 16-20 week old female NCr nude mice (Taconic NCRNU-F sp/sp) via colonoscopy as

previously described in (Roper et al., 2018). Colonoscopy was performed 10-11 days after transplant to confirm tumor presence. Health and body conditions of mice were monitored at least once every three days, and mice were euthanized by carbon dioxide inhalation when poor body conditions were observed or the desired timepoints were reached, following Committee on Animal Care and MIT Department of Comparative Medicine protocols. Tamoxifen (Sigma-Aldrich T5648) was dissolved in corn oil (Sigma-Aldrich C8267), placed in a shaking incubator at 37C overnight, sterile-filtered, and stored at 4C. At the indicated time points, mice were dosed with 0.1g tamoxifen/kg for four days via intraperitoneal injection.

Histology and immunohistochemistry

Mice bearing colon tumors were euthanized, and colon tumors were extracted. Colon tumors were placed in formalin overnight. Tissue was washed in PBS then transferred to 70% ethanol, embedded in paraffin, and 4μm sections were cut. Immunohistochemical staining for proteins of interest was performed as follows: slides were deparaffinized and rehydrated using xylene, and antigen retrieval was performed by placing slides in a solution containing 10mM citric acid and in the decloaking chamber (BioCare Medical) at 125C for 10min. Tissues were permeabilize with 0.1% Tween-20 in PBS, and endogenous peroxidases were inactivated by incubation with 3% H2O2 (VWR MK524002) in PBS.

For immunohistochemical staining of BMI1, slides were blocked using the UltraVision LP Detection System (Thermo Fisher Scientific #TL060HD) following manufacturer's protocol. Slides were incubated with primary anti-BMI1 antibody (1:200, Millipore clone F6) diluted in Mouse-on-Mouse (M.O.M.) diluent (Vector Laboratories #BMK-2202) overnight at 4C. Following washes with PBS, incubation with secondary antibody and visualization was conducted using the UltraVision LP Detection System (Thermo Fisher Scientific #TL060HD) following manufacturer's instructions. Slides were counterstained with haematoxylin.

Immunohistochemical staining of PCNA was performed using M.O.M. ImmPRESS HRP Polymer kit (Vector Laboratories #MP-2400) following manufacturer protocols, and slides were counterstained with haematoxylin. Percentage of PCNA-positive cells was quantified using QuPath software (Bankhead et al., 2017).

Dissociation and isolation of colon tumor cells

Mice bearing colon tumors were euthanized, and colon tumors were manually extracted. Tumors were manually minced with a sterilized razor blade and placed in a shaking incubator at 37C for 30min. in 1mg/mL collagenase (Sigma #9407), 0.1mg/mL DNase I (Worthington Biomedical #LS002138), 0.36mM CaCl2, 5mM HEPES buffer, and Advanced DMEM/F12 (Thermo Fisher Scientific #1263401). Tumor cells were washed with PBS, strained through 70μm mesh, and resuspended in Advanced DMEM/F12 with 10μM Y-27632, 1% BSA, and DAPI. Immediately prior to sorting, cells were strained through a 35μm mesh. Cells were isolated using BD FACS Aria Cell Sorter for $DAPI^-$ and $tdTomato^+$ populations.

RNA isolation

Murine colon tumor cells were isolated as described above. For cell isolation, 4800 to 18000 live, TdTomato-expressing cells (per sample) were sorted using FACS directly into a DNA Lobind tube (Eppendorf #022431021) with 1mL of Trizol (Thermo Fisher Scientific #15596026). Samples were stored at -80C prior to RNA isolation. To isolate RNA, 200μL of chloroform were added to each sample, and the samples were briefly vortexed and allowed to sit at room temperature for 3 minutes. Samples were then centrifuged at 12000xg for 15 minutes at 4C, and the aqueous phase was removed and added into 1400μL of RLT buffer (Qiagen #74004) with 14μL of β-mercaptoethanol. After addition of 1000μL of 100% ethanol, the

samples were loaded into RNeasy Micro Kit columns (Qiagen #74004) and RNA was isolated following the manufacturer's protocol.

Bulk RNA sequencing and analysis

RNA from murine colon tumor cells were isolated as described above, and RNA quality was assessed using the AATI FemtoPulse Analyzer (Agilent). RNA sequencing libraries were prepared using Clontech SMARTer Stranded Total RNAseq Kit - Pico Input (Clontech ZapR) and sequenced using NextSeq500 (Illumina). Samples with at least 10 million reads were used for further analyses. Differentially expressed genes were analyzed using DESeq2 method (Love et al., 2014), and supervised hierarchical clustering (Ward's method) was performed using the 1863 genes that were differentially expressed in at least one pairwise comparison (*Bmi1*$^{+/+}$ early vs *Bmi1*$^{+/+}$ late vs *Bmi1*$^{fl/fl}$ early vs *Bmi1*$^{fl/fl}$ late samples). Differentially regulated pathways were identified using analyses with the Biological Processes Gene Ontology (GeneGO MetaCore).

Tumor tracking using 3-dimensional ultrasound imaging

Longitudinal tracking and quantification of murine colon tumor volumes was performed based methods described in (Freeling and Rezvani, 2016) Mice were transplanted with colon tumor organoids as described above and placed on a gel diet (Bio-Serv #NGB-2) throughout the duration of the study. Sixteen hours prior to imaging, food was withdrawn from the animals to reduce shadowing effects during imaging. To collect images of the mouse colon, mice were placed under anesthesia induced by isoflurane. Colons of the mice were subsequently flushed with PBS to remove feces. To provide enhanced contrast and visualization of the colon, mice received an intraperitoneal injection of medical grade 0.9% sodium chloride saline solution (ICU Medical #0990-7983-02), and ultrasound transmission gel (Parker Laboratories Aquasonic 100) was administered retrograde within the colon via the anus. Acquisition of ultrasound images and 3D colon reconstruction were achieved using the Vevo 3100 Micro-Ultrasound System with

550S and 250S transducers and Vevo LAB software (as described in Freeling and Rezvani, 2016). Mice were imaged weekly for 6-8 weeks until adverse body conditions were observed or the end of the experiment was reached. Tumor volumes were quantified using Vevo LAB software. To quantify the solid, cell-based volume of the tumor, cystic regions, which appear dark in ultrasound images, were gated and subtracted from the total tumor volume.

Animal studies were approved by the Committee for Animal Care, and conducted in compliance with the Animal Welfare Act Regulations and other federal statutes relating to animals and experiments involving animals and adheres to the principles set forth in the Guide for the Care and Use of Laboratory Animals, 8th ed. National Research Council, 2011 (institutional animal welfare assurance no. A3125–01).

ACKNOWLEDGEMENTS

We thank the Koch Institute Swanson Biotechnology Center, particularly the Histology, Flow Cytometry, Integrated Genomics and Bioinformatics, and the Preclinical Modeling, Imaging and Testing core facilities for technical help; Tyler Jacks for transgenic alleles and reagents; and members of the Lees laboratory for advice and discussions. Funding was provided by the MIT Stem Cell Initiative. E.Y.K. received support from Ludwig Center for Molecular Oncology Fund. EYK and C.E.F received support from the NIH Pre-Doctoral Training Grant GM007287. J.A.L. is the Virginia and D.K. Ludwig Professor for Cancer Research at the Koch Institute at MIT.

REFERENCES

Alison, M.R., Lim, S.M., and Nicholson, L.J. (2011). Cancer stem cells: problems for therapy? The Journal of Pathology *223*.

Armaghany, T., Wilson, J.D., Chu, Q., and Mills, G. (2012). Genetic alterations in colorectal cancer. Gastrointestinal Cancer Research : GCR *5*.

Bankhead, P., Loughrey, M.B., Fernández, J.A., Dombrowski, Y., McArt, D.G., Dunne, P.D., McQuaid, S., Gray, R.T., Murray, L.J., Coleman, H.G., et al. (2017). QuPath: Open source software for digital pathology image analysis. Scientific Reports *7*, 16878.

Bednar, F., Schofield, H.K., Collins, M.A., Yan, W., Zhang, Y., Shyam, N., Eberle, J.A., Almada, L.L., Olive, K.P., Bardeesy, N., et al. (2015). Bmi1 is required for the initiation of pancreatic cancer through an Ink4a-independent mechanism. Carcinogenesis *36*, 730–738.

Biehs, B., Hu, J.K.-H., Strauli, N.B., Sangiorgi, E., Jung, H., Heber, R.-P., Ho, S., Goodwin, A.F., Dasen, J.S., Capecchi, M.R., et al. (2013). BMI1 represses Ink4a/Arf and Hox genes to regulate stem cells in the rodent incisor. Nature Cell Biology *15*.

Bolomsky, A., Schlangen, K., Schreiner, W., Zojer, N., and Ludwig, H. (2016). Targeting of BMI-1 with PTC-209 shows potent anti-myeloma activity and impairs the tumour microenvironment. Journal of Hematology and Oncology *9*, 1–13.

Bolomsky, A., Muller, J., Stangelberger, K., Lejeune, M., Duray, E., Breid, H., Vrancken, L., Pfeiffer, C., Hübl, W., Willheim, M., et al. (2020). The anti-mitotic agents PTC-028 and PTC596 display potent activity in pre-clinical models of multiple myeloma but challenge the role of BMI-1 as an essential tumour gene. British Journal of Haematology 1–14.

Bruggeman, S.W.M. (2005). Ink4a and Arf differentially affect cell proliferation and neural stem cell self-renewal in Bmi1-deficient mice. Genes & Development *19*, 1438–1443.

Bruggeman, S.W.M., Valk-Lingbeek, M.E., van der Stoop, P.P.M., Jacobs, J.J.L., Kieboom, K., Tanger, E., Hulsman, D., Leung, C., Arsenijevic, Y., Marino, S., et al. (2005). Ink4a and Arf differentially affect cell proliferation and neural stem cell self-renewal in Bmi1-deficient mice. Genes & Development *19*.

Cao, R., Tsukada, Y., and Zhang, Y. (2005). Role of Bmi-1 and Ring1A in H2A Ubiquitylation and Hox Gene Silencing. Molecular Cell *20*.

Chen, D., Wu, M., Li, Y., Chang, I., Yuan, Q., Ekimyan-Salvo, M., Deng, P., Yu, B., Yu, Y., Dong, J., et al. (2017). Targeting BMI1+ Cancer Stem Cells Overcomes Chemoresistance and Inhibits Metastases in Squamous Cell Carcinoma. Cell Stem Cell *20*, 621–634.e6.

Dey, A., Xiong, X., Crim, A., Dwivedi, S.K.D., Mustafi, S.B., Mukherjee, P., Cao, L., Sydorenko, N., Baiazitov, R., Moon, Y.-C., et al. (2018). Evaluating the Mechanism and Therapeutic Potential of PTC-028, a Novel Inhibitor of BMI-1 Function in Ovarian Cancer. Molecular Cancer Therapeutics *17*.

Douglas, D., Hsu, J.H.-R., Hung, L., Cooper, A., Abdueva, D., van Doorninck, J., Peng, G., Shimada, H., Triche, T.J., and Lawlor, E.R. (2008). BMI-1 promotes ewing sarcoma tumorigenicity independent of CDKN2A repression. Cancer Research *68*.

Dovey, J.S., Zacharek, S.J., Kim, C.F., and Lees, J.A. (2008). Bmi1 is critical for lung tumorigenesis and bronchioalveolar stem cell expansion. Proceedings of the National Academy of Sciences *105*.

Drost, J., and Clevers, H. (2018). Organoids in cancer research. Nature Reviews Cancer *18*.

Drost, J., van Jaarsveld, R.H., Ponsioen, B., Zimberlin, C., van Boxtel, R., Buijs, A., Sachs, N., Overmeer, R.M., Offerhaus, G.J., Begthel, H., et al. (2015). Sequential cancer mutations in cultured human intestinal stem cells. Nature *521*, 43–47.

Du, J., Li, Y., Li, J., and Zheng, J. (2010). Polycomb group protein Bmi1 expression in colon cancers predicts the survival. Medical Oncology *27*.

Dull, T., Zufferey, R., Kelly, M., Mandel, R.J., Nguyen, M., Trono, D., and Naldini, L. (1998). A Third-Generation Lentivirus Vector with a Conditional Packaging System. Journal of Virology *72*, 8463–8471.

Dylla, S.J., Beviglia, L., Park, I.-K., Chartier, C., Raval, J., Ngan, L., Pickell, K., Aguilar, J., Lazetic, S., Smith-Berdan, S., et al. (2008). Colorectal Cancer Stem Cells Are Enriched in Xenogeneic Tumors Following Chemotherapy. PLoS ONE *3*.

Eberle-Singh, J.A., Sagalovskiy, I., Maurer, H.C., Sastra, S.A., Palermo, C.F., Decker, A.R., Kim, M.J., Sheedy, J., Mollin, A., Cao, L., et al. (2019). Effective delivery of a microtubule polymerization inhibitor synergizes with standard regimens in models of pancreatic ductal adenocarcinoma. Clinical Cancer Research *25*, 5548–5560.

Elango, R., Vishnubalaji, R., Manikandan, M., Binhamdan, S.I., Siyal, A.-A., Alshawakir, Y.A., Alfayez, M., Aldahmash, A., and Alajez, N.M. (2019). Concurrent targeting of BMI1 and CDK4/6 abrogates tumor growth in vitro and in vivo. Scientific Reports *9*.

Fearon, E.R. (2011). Molecular Genetics of Colorectal Cancer. Annual Review of Pathology: Mechanisms of Disease *6*.

Fearon, E.R., and Vogelstein, B. (1990). A genetic model for colorectal tumorigenesis. Cell *61*.

Ferretti, R., Bhutkar, A., McNamara, M.C., and Lees, J.A. (2016). BMI1 induces an invasive signature in melanoma that promotes metastasis and chemoresistance. Genes & Development *30*.

Flamier, A., Abdouh, M., Hamam, R., Barabino, A., Patel, N., Gao, A., Hanna, R., and Bernier, G. (2020). Off-target effect of the BMI1 inhibitor PTC596 drives epithelial-mesenchymal transition in glioblastoma multiforme. Npj Precision Oncology *4*.

Freeling, J.L., and Rezvani, K. (2016). Assessment of murine colorectal cancer by micro-ultrasound using three dimensional reconstruction and non-linear contrast imaging. Molecular Therapy - Methods & Clinical Development *3*.

Gibson, D.G., Young, L., Chuang, R.-Y., Venter, J.C., Hutchison, C.A., and Smith, H.O. (2009). Enzymatic assembly of DNA molecules up to several hundred kilobases. Nature Methods *6*, 343–345.

Ginjala, V., Nacerddine, K., Kulkarni, A., Oza, J., Hill, S.J., Yao, M., Citterio, E., van Lohuizen, M., and Ganesan, S. (2011). BMI1 is recruited to DNA breaks and contributes to DNA damage-induced H2A ubiquitination and repair. Molecular and Cellular Biology *31*.

Ismail, I.H., Andrin, C., McDonald, D., and Hendzel, M.J. (2010). BMI1-mediated histone ubiquitylation promotes DNA double-strand break repair. Journal of Cell Biology *191*.

Jacobs, J.J.L., Kieboom, K., Marino, S., DePinho, R.A., and van Lohuizen, M. (1999a). The oncogene and Polycomb-group gene bmi-1 regulates cell proliferation and senescence through the ink4a locus. Nature *397*.

Jacobs, J.J.L., Scheijen, B., Voncken, J.W., Kieboom, K., Berns, A., and van Lohuizen, M. (1999b). Bmi-1 collaborates with c-Myc in tumorigenesis by inhibiting c-Myc- induced apoptosis via INK4a/ARF. Genes and Development *13*, 2678–2690.

Kallin, E.M., Cao, R., Jothi, R., Xia, K., Cui, K., Zhao, K., and Zhang, Y. (2009). Genome-Wide uH2A Localization Analysis Highlights Bmi1-Dependent Deposition of the Mark at Repressed Genes. PLoS Genetics *5*.

Kim, M.J., Cao, L., Sheedy, J., Risher, N., Dumble, M., Lee, C.-S., Sydorenko, N., Baiazitov, R., Du, W., Moon, Y.-C., et al. (2014). Abstract 5517: PTC596-induced Bmi1 hyper-phosphorylation via Cdk1/2 activation resulting in tumor stem cell depletion. In Experimental and Molecular Therapeutics, (American Association for Cancer Research), p.

Kreso, A., and Dick, J.E. (2014). Evolution of the cancer stem cell model. Cell Stem Cell *14*.

Kreso, A., van Galen, P., Pedley, N.M., Lima-Fernandes, E., Frelin, C., Davis, T., Cao, L., Baiazitov, R., Du, W., Sydorenko, N., et al. (2014). Self-renewal as a therapeutic target in human colorectal cancer. Nature Medicine *20*, 29–36.

Lee, C.L., Moding, E.J., Huang, X., Li, Y., Woodlief, L.Z., Rodrigues, R.C., Ma, Y., and Kirsch, D.G. (2012). Generation of primary tumors with Flp recombinase in FRT-flanked p53 mice. DMM Disease Models and Mechanisms *5*, 397–402.

Lessard, J., and Sauvageau, G. (2003). Bmi-1 determines the proliferative capacity of normal and leukaemic stem cells. Nature *423*.

Leung, C., Lingbeek, M., Shakhova, O., Liu, J., Tanger, E., Saremaslani, P., van Lohuizen, M., and Marino, S. (2004). Bmi1 is essential for cerebellar development and is overexpressed in human medulloblastomas. Nature *428*.

Li, D., Tang, H., Fan, J., Yan, D., Zhou, C., Li, S., Wang, X., and Peng, Z. (2010). Expression level of Bmi-1 oncoprotein is associated with progression and prognosis in colon cancer. Journal of Cancer Research and Clinical Oncology *136*.

Liu, J., Cao, L., Chen, J., Song, S., Lee, I.H., Quijano, C., Liu, H., Keyvanfar, K., Chen, H., Cao, L.-Y., et al. (2009). Bmi1 regulates mitochondrial function and the DNA damage response pathway. Nature *459*.

Liu, S., Cong, Y., Wang, D., Sun, Y., Deng, L., Liu, Y., Martin-Trevino, R., Shang, L., McDermott, S.P., Landis, M.D., et al. (2014). Breast Cancer Stem Cells Transition between Epithelial and Mesenchymal States Reflective of their Normal Counterparts. Stem Cell Reports *2*.

Liu, X., Wei, W., Li, X., Shen, P., Ju, D., Wang, Z., Zhang, R., Yang, F., Chen, C., Cao, K., et al. (2017). BMI1 and MEL18 Promote Colitis-Associated Cancer in Mice via REG3B and STAT3. Gastroenterology *153*, 1607–1620.

van Lohuizen, M., Verbeek, S., Scheljen, B., Wientjens, E., van der Guidon, H., and Berns, A. (1991). Identification of cooperating oncogenes in Eμ-myc transgenic mice by provirus tagging. Cell *65*.

Love, M.I., Huber, W., and Anders, S. (2014). Moderated estimation of fold change and dispersion for RNA-seq data with DESeq2. Genome Biology.

Madisen, L., Zwingman, T.A., Sunkin, S.M., Oh, S.W., Zariwala, H.A., Gu, H., Ng, L.L., Palmiter, R.D., Hawrylycz, M.J., Jones, A.R., et al. (2010). A robust and high-throughput Cre reporting and characterization system for the whole mouse brain. Nature Neuroscience *13*, 133–140.

el Marjou, F., Janssen, K.-P., Chang, B.H.-J., Li, M., Hindie, V., Chan, L., Louvard, D., Chambon, P., Metzger, D., and Robine, S. (2004). Tissue-specific and inducible Cre-mediated recombination in the gut epithelium. Genesis (New York, N.Y. : 2000) *39*.

Matano, M., Date, S., Shimokawa, M., Takano, A., Fujii, M., Ohta, Y., Watanabe, T., Kanai, T., and Sato, T. (2015). Modeling colorectal cancer using CRISPR-Cas9–mediated engineering of human intestinal organoids. Nature Medicine *21*, 256–262.

Matheu, A., Maraver, A., Klatt, P., Flores, I., Garcia-Cao, I., Borras, C., Flores, J.M., Viña, J., Blasco, M.A., and Serrano, M. (2007). Delayed ageing through damage protection by the Arf/p53 pathway. Nature *448*, 375–379.

Maynard, M.A., Ferretti, R., Hilgendorf, K.I., Perret, C., Whyte, P., and Lees, J.A. (2014). Bmi1 is required for tumorigenesis in a mouse model of intestinal cancer. Oncogene *33*.

Miyoshi, H., and Stappenbeck, T.S. (2013). In vitro expansion and genetic modification of gastrointestinal stem cells in spheroid culture. Nature Protocols *8*, 2471–2482.

Molofsky, A. v, He, S., Bydon, M., Morrison, S.J., and Pardal, R. (2005). Bmi-1 promotes neural stem cell self-renewal and neural development but not mouse growth and survival by repressing the p16Ink4a and p19Arf senescence pathways. Genes & Development *19*.

Munro, M.J., Wickremesekera, S.K., Peng, L., Tan, S.T., and Itinteang, T. (2018). Cancer stem cells in colorectal cancer: a review. Journal of Clinical Pathology *71*.

Nishida, Y., Maeda, A., Kim, M.J., Cao, L., Kubota, Y., Ishizawa, J., AlRawi, A., Kato, Y., Iwama, A., Fujisawa, M., et al. (2017). The novel BMI-1 inhibitor PTC596 downregulates MCL-1 and induces p53-independent mitochondrial apoptosis in acute myeloid leukemia progenitor cells. Blood Cancer Journal *7*, e527–e527.

O'Brien, C.A., Pollett, A., Gallinger, S., and Dick, J.E. (2007). A human colon cancer cell capable of initiating tumour growth in immunodeficient mice. Nature *445*.

Oguro, H., Iwama, A., Morita, Y., Kamijo, T., van Lohuizen, M., and Nakauchi, H. (2006). Differential impact of Ink4a and Arf on hematopoietic stem cells and their bone marrow microenvironment in Bmi1-deficient mice. Journal of Experimental Medicine *203*.

Park, I., Qian, D., Kiel, M., Becker, M.W., Pihalja, M., Weissman, I.L., Morrison, S.J., and Clarke, M.F. (2003). Bmi-1 is required for maintenance of adult self-renewing haematopoietic stem cells. Nature *423*.

Roper, J., Tammela, T., Akkad, A., Almeqdadi, M., Santos, S.B., Jacks, T., and Yilmaz, Ö.H. (2018). Colonoscopy-based colorectal cancer modeling in mice with CRISPR-Cas9 genome editing and organoid transplantation. Nature Protocols *13*.

Schatoff, E.M., Leach, B.I., and Dow, L.E. (2017). WNT Signaling and Colorectal Cancer. Current Colorectal Cancer Reports *13*.

Schönhuber, N., Seidler, B., Schuck, K., Veltkamp, C., Schachtler, C., Zukowska, M., Eser, S., Feyerabend, T.B., Paul, M.C., Eser, P., et al. (2014). A next-generation dual-recombinase system for time- and host-specific targeting of pancreatic cancer. Nature Medicine *20*, 1340–1347.

Schwank, G., Koo, B.-K., Sasselli, V., Dekkers, J.F., Heo, I., Demircan, T., Sasaki, N., Boymans, S., Cuppen, E., van der Ent, C.K., et al. (2013). Functional Repair of CFTR by CRISPR/Cas9 in Intestinal Stem Cell Organoids of Cystic Fibrosis Patients. Cell Stem Cell *13*, 653–658.

Sulaiman, S., Arafat, K., Iratni, R., and Attoub, S. (2019). PTC-209 Anti-Cancer Effects Involved the Inhibition of STAT3 Phosphorylation. Frontiers in Pharmacology *10*.

Sung, H., Ferlay, J., Siegel, R.L., Laversanne, M., Soerjomataram, I., Jemal, A., and Bray, F. (2021). Global Cancer Statistics 2020: GLOBOCAN Estimates of Incidence and Mortality Worldwide for 36 Cancers in 185 Countries. CA: A Cancer Journal for Clinicians *71*.

Tateishi, K., Ohta, M., Kanai, F., Guleng, B., Tanaka, Y., Asaoka, Y., Tada, M., Seto, M., Jazag, A., Lianjie, L., et al. (2006). Dysregulated expression of stem cell factor Bmi1 in precancerous lesions of the gastrointestinal tract. Clinical Cancer Research : An Official Journal of the American Association for Cancer Research *12*.

Wilson, A.A., Murphy, G.J., Hamakawa, H., Kwok, L.W., Srinivasan, S., Hovav, A.-H., Mulligan, R.C., Amar, S., Suki, B., and Kotton, D.N. (2010). Amelioration of emphysema in mice through lentiviral transduction of long-lived pulmonary alveolar macrophages. Journal of Clinical Investigation *120*, 379–389.

Yang, L., Shi, P., Zhao, G., Xu, J., Peng, W., Zhang, J., Zhang, G., Wang, X., Dong, Z., Chen, F., et al. (2020). Targeting cancer stem cell pathways for cancer therapy. Signal Transduction and Targeted Therapy *5*.

Yang, M.-H., Hsu, D.S.-S., Wang, H.-W., Wang, H.-J., Lan, H.-Y., Yang, W.-H., Huang, C.-H., Kao, S.-Y., Tzeng, C.-H., Tai, S.-K., et al. (2010). Bmi1 is essential in Twist1-induced epithelial–mesenchymal transition. Nature Cell Biology *12*.

Young, N.P., Crowley, D., and Jacks, T. (2011). Uncoupling cancer mutations reveals critical timing of p53 loss in sarcomagenesis. Cancer Research *71*, 4040–4047.

Zencak, D., Lingbeek, M., Kostic, C., Tekaya, M., Tanger, E., Hornfeld, D., Jaquet, M., Munier, F.L., Schorderet, D.F., van Lohuizen, M., et al. (2005). Bmi1 loss produces an increase in astroglial cells and a decrease in neural stem cell population and proliferation. The Journal of Neuroscience : The Official Journal of the Society for Neuroscience *25*.

Zeuner, A., Todaro, M., Stassi, G., and de Maria, R. (2014). Colorectal cancer stem cells: from the crypt to the clinic. Cell Stem Cell *15*.

CHAPTER 4: Discussion and future directions

Review of BMI1 loss in lung and colon cancer

BMI1 is an epigenetic regulator critical for normal stem cell function and overexpressed in cancer. Given these observations, there is considerable interest in developing chemical inhibitors against this protein as cancer therapeutics. A number of studies have demonstrated that loss of BMI1 is highly tumor suppressive, concurrent with upregulation of the cell cycle regulators $p16^{INK4A}$ and $p19^{ARF}$, which induce cell cycle arrest and/or apoptosis (Dovey et al., 2008; Jacobs et al., 1999; Lessard and Sauvageau, 2003; Maynard et al., 2014). More recent studies have demonstrated oncogenic roles for BMI1 through pathways independent of $p16^{INK4A}$ and $p19^{ARF}$, including regulation of genome integrity, oxidative stress, and metastatic potential (Abdouh et al., 2016; Bednar et al., 2015; Chatoo et al., 2009; Facchino et al., 2010; Ferretti et al., 2016; el Hajjar et al., 2019; Liu et al., 2009; Song et al., 2009; Yang et al., 2010).

In this thesis, I present studies in two epithelial tumor types, lung adenocarcinoma (LUAD) and colon cancer, showing that the pro-tumorigenic effects of BMI1 activity is highly dependent on the context, and in certain settings, loss of BMI1 activity may promote tumorigenicity. When BMI1 was ablated concurrently with LUAD initiation, we observed increased survival and lower tumor burden in *Bmi1*$^{-/-}$ mice relative to *Bmi1*$^{+/+}$ mice without upregulation $p16^{INK4A}$ and $p19^{ARF}$ in the tumor tissues. We demonstrate that BMI1 loss induces cell cycle progression defects and proliferative impairment in low grade tumors. However, these proliferation defects were alleviated in tumors that achieved transition to grade 3, suggesting that BMI1 loss may be dispensable for tumor growth in aggressive, high-grade LUAD tumors.

To understand the role of BMI1 in high-grade LUAD tumors, as well as assess the clinical benefits of its inhibition in LUAD tumors, we constructed mouse models in which ablation of BMI1 occurred in established LUAD tumors at a time point where approximately half of the LUAD tumors have reached grade 3. In this setting, BMI1 loss did not substantially confer a negative impact on tumor growth, as assessed by tumor numbers, burden, and grades, nor was upregulation of $p16^{INK4A}$ and $p19^{ARF}$ observed. Rather, transcriptomic profiling by bulk RNA

sequencing and single cell RNA sequencing revealed an early upregulation of a latent gastric dedifferentiation program, elevated expression of genes associated with LUAD metastases, and increased frequency of cells expressing markers of LUAD tumor propagating cells, all of which are associated with LUAD progression (Lau et al., 2014; Snyder et al., 2013; Winslow et al., 2011; Zheng et al., 2013). Functional assays determined a slight, but not significant, increase in frequency of metastases and tumor-propagating cells in *Bmi1*$^{-/-}$ mice relative to *Bmi1*$^{+/+}$ mice. Overall, we have demonstrated that BMI1 loss in established LUAD tumors is dispensable for tumor progression, and rather, BMI1 loss induces acquisition of markers associated with LUAD tumor progression.

To elucidate whether such effects of BMI1 loss were restricted to the lung compartment, we constructed experimental mouse models of colon cancer where BMI1 is ablated in either transformed tumor organoids or in established colon tumors. Similar to our results in the established lung cancer context, BMI1 loss did not yield defects in proliferation of colon tumor organoids or *in vivo* tumor growth, nor did BMI1 loss induce upregulation of p16^{INK4A} and p19^{ARF}. We further showed that loss of BMI1 in established colon tumors induced expression of genes involved in developmental and metastatic programs, including cell adhesion and extracellular matrix organization.

Taken together, our findings indicate that the effects of BMI1 loss on tumor progression are highly dependent on both the setting and timing of BMI1 loss. Our data highlight the need to carefully dissect the effects of epigenetic regulator activity in various stages of tumorigenesis, especially given the increasing interest in targeting epigenetic regulators in the clinic. In the following sections, I aim to describe the implications of our findings in greater detail and explore potential methods to address outstanding questions.

Dual roles of epigenetic regulators as oncogenes and tumor suppressors

The observations that BMI1 deficiency was not deleterious to established tumor growth was surprising to us, given that numerous studies have demonstrated abrogation of tumorigenesis upon loss of BMI1 activity. BMI1 loss in a number of cancerous tissue types induced upregulation of $p16^{INK4A}$ and $p19^{ARF}$ expression, leading to proliferative impairments and hampering tumor development (Dovey et al., 2008; Jacobs et al., 1999; Lessard and Sauvageau, 2003; Maynard et al., 2014). Other studies have demonstrated a pro-oncogenic role for BMI1 in promotion of cell invasion and metastasis, as well as regulation of reactive oxygen species homeostasis (Bednar et al., 2015; Ferretti et al., 2016; Song et al., 2009; Yang et al., 2010). We now demonstrate that BMI1 loss can potentially exert pro-tumorigenic effects, particularly in established epithelial tumors, through modulating expression of developmental and metastatic programs. In addition, BMI1's canonical role of repressing $p16^{INK4A}$ and $p19^{ARF}$ expression appears to become dispensable for its effects on tumor development (to be elaborated upon in the next section).

In hindsight, the dual role of BMI1 as an oncogene and a tumor suppressor could have been anticipated. Other epigenetic regulators have been described as having either pro-tumorigenic or anti-tumorigenic functions, depending on the context. For example, both inactivating and activating mutations in Polycomb repressive complex 2 (PRC2) are frequently observed in human tumors, and even within the same tumor type, impaired PRC2 activity can both suppress and promote tumorigenesis (Kleer et al., 2003; Laugesen et al., 2016; Wassef et al., 2015). As another example, G9a is a histone methyltransferase widely described as an oncogene, leading to considerable interest into the development of G9a inhibitors (Casciello et al., 2015). However, a study using a model of squamous cell carcinoma demonstrated that although loss of G9a activity was initially tumor suppressive, G9a-depleted tumors became highly aggressive after a long latency period and were characterized by genomic instability (Avgustinova et al., 2018). Another study demonstrated that loss of G9a in *$Kras^{G12D};Trp53^{-/-}$*

GEMMs of LUAD enhanced tumor progression, including increased metastatic potential and tumor-propagating cell frequency (Rowbotham et al., 2018). These studies not only highlight that inhibition of a single epigenetic regulator can result in varying phenotypes depending on the cancer type but also underscore the need to understand the long-term effects of epigenetic regulator inhibition.

It is highly likely that epigenetic regulators have the potential to modulate expression of numerous target genes, and the loss of epigenetic marks or activity can deregulate various biological pathways and result in vastly different phenotypes depending on the setting, including the tissue type, cellular environment, and activated oncogenic signaling pathways. Our studies of BMI1 loss in LUAD indicate that the stage of tumor progression can be an influential determinant of epigenetic regulator activity. BMI1 ablation at the initiation of *Kras^{G12D};Trp53$^{-/-}$* LUAD was tumor suppressive through induction of proliferative impairment, while BMI1 loss in established grade 2/3 tumors initiated by the same mutations did not impair progression. Given the little overlap in gene sets enriched between the two experiments, we suspect that BMI1's targets fluctuate during LUAD progression, though careful characterization of BMI1 binding to target loci (such as through chromatin immunoprecipitation followed by sequencing) will be required. As interest grows for the development and clinical use of inhibitors targeting epigenetic regulators, our findings highlight the critical need to dissect the context-dependent roles and targets of epigenetic regulator activity in cancer.

Elucidating the role of BMI1 in maintaining Cdkn2a *repression during tumorigenesis*

Previous studies have overwhelmingly described a pro-oncogenic role for BMI1, particularly in repressing the *Cdkn2a* locus and thus preventing cell cycle arrest and apoptosis. We, along with many others, have demonstrated in a number of tissue contexts that the combination of BMI1 loss with tumor induction significantly abrogates cancer development concurrent with p16^{INK4A} and p19^{ARF} upregulation. In particular to lung and colon tumorigenesis,

the tissue types of interest in this thesis, induction of lung and colon cancer is greatly impeded in germline *Bmi1*$^{-/-}$ mice as compared to the *Bmi1*$^{+/+}$ mice, and such tumor suppressive effects were at least partially rescued with combination of p19^{ARF} loss (Dovey et al., 2008; Maynard et al., 2014). Such findings have led to the notion that BMI1 loss is detrimental to tumor growth because of induction of cell cycle arrest and apoptosis through the p16^{INK4A}-Rb and/or p19^{ARF}-p53 axes.

However, we have now demonstrated that BMI1 loss does not induce p16^{INK4A} and p19^{ARF} upregulation in several contexts, including in both *Trp53*$^{+/+}$ and *Trp53*$^{-/-}$ mutational backgrounds. We hypothesize that one reason for this discrepancy is the differential requirements for BMI1 in regulating p16^{INK4A} and p19^{ARF} during lung development as compared with tumorigenesis. During embryogenesis, BMI1 is crucial for repression of the *Cdkn2a* locus and preventing cell cycle arrest and apoptosis, both of which would greatly hamper organismal development. This function of BMI1 has been validated in a number of tissue compartments, where germline BMI1 loss induces proliferation defects that correlate with increased p16^{INK4A} and/or p19^{ARF} expression (Dovey et al., 2008; Iwama et al., 2004; Lessard and Sauvageau, 2003; Molofsky et al., 2003; Oguro et al., 2006; Park et al., 2003). In the adult context, we hypothesize that BMI1's role in actively repressing the *Cdkn2a* locus becomes dispensable, perhaps because the *Cdkn2a* locus is already properly silenced with a number of epigenetic mechanisms. Therefore, in the postnatal setting, other functions of BMI1, such as lineage specification and regulation of metastatic programs, become apparent and the predominant influences of tumor development. Our results are consistent with another study of pancreatic cancer, where knockdown of BMI1 did not alter expression of either p16^{INK4A} or p19^{ARF} (Bednar et al., 2015). To confirm the validity of our hypothesis, careful characterization of *Bmi1* knockdown or knockout in adult tissues and its effects on the *Cdkn2a* locus will be required.

Molecular mechanisms by which BMI1 loss drives lung dedifferentiation

Although we demonstrated through gene expression analyses that BMI1 loss in established lung tumors accelerates dedifferentiation to gastric and embryonal lineages, it is unclear how BMI1 loss mediates these effects. We postulate two methods by which BMI1 loss can drive early dedifferentiation in LUAD. The first hypothesis is that BMI1 loss leads to removal of transcriptionally repressive H2AK119ub marks, resulting in widespread destabilization of the chromatin environment and deregulation of a number of biological processes. Over time, pro-tumorigenic programs, namely those involved in lineage specification, metastasis, and tumor propagation, become selected for in the LUAD cells. Given that epigenetic regulation and plasticity are inextricably linked in both development and disease, it is not surprising that dysregulation of the epigenetic landscape could lead to genome-wide transcriptional instability and potentially promote tumor adaptation and growth. We can imagine a scenario where BMI1 loss generates intratumoral heterogeneity as different cells deregulate distinct biological processes and natural selection favors outgrowth of tumor cells endowed with the highest tumorigenicity, akin to Nowell's clonal evolution model of intratumoral heterogeneity (Nowell, 1976). To assess this possibility, epigenetic profiling of LUAD cells (such as through single cell ATAC-sequencing) shortly after and an extended period following BMI1 loss and overlaying the epigenomic data with our RNA-seq results would be enlightening. *In vivo* barcoding experiments, though currently technically challenging, would also uncover how BMI1 loss affects clonal evolution of LUAD cells.

Alternatively, but not exclusively, BMI1 may stabilize lung cell identity through directly binding to and inhibiting expression of non-pulmonary transcription factors. This possibility aligns with BMI1's role in normal stem cell biology in directing cell type specification and suppressing alterative lineage programs (Cao et al., 2005; van der Lugt et al., 1996; Oguro et al., 2010). To begin to address this, we performed SCENIC analyses (Aibar et al., 2017) with our single cell RNA sequencing data of *Bmi1*$^{+/+}$ and *Bmi1*$^{-/-}$ lung tumors. This method enables

reconstruction of gene regulatory networks using single cell transcriptomic data through transcription factor expression and binding motif analyses. We identified ONECUT2 as a transcription factor whose expression (and expression of its target genes) is significantly enriched in *Bmi1*$^{-/-}$ cells relative to *Bmi1*$^{+/+}$ cells (data not shown). ONECUT2 is a key regulator of hepatocyte, neural, and intestinal differentiation that becomes upregulated in late-stage LUAD tumors and following NKX2.1 loss (LaFave et al., 2020; Snyder et al., 2013). In addition, a recent study determined that overexpression of ONECUT2 promotes malignant growth, mediates metastasis, and induces expression of non-pulmonary genes in LUAD cells (Ma et al., 2019). Furthermore, our lab has demonstrated that BMI1 loss upregulates ONECUT2 expression in a non-epithelial tissue context (data not shown). Reflecting upon these findings, we hypothesize that BMI1 may restrain lung tumor cells within the pulmonary lineage through directly repressing *Onecut2* transcription in LUAD cells. To probe this possibility, a chromatin immunoprecipitation experiment to assess BMI1 binding to the promoter of *Onecut2* would be highly informative. As ONECUT2 becomes upregulated during the normal trajectory of LUAD progression (i.e. in the *Bmi1*$^{+/+}$ context), determination of how BMI1 occupancy at the *Onecut2* locus changes during LUAD development would be intriguing.

Comparison of BMI1 loss in colon cancer versus lung cancer context.

Our lab has previously demonstrated that embryonic deletion of *Bmi1*, either prior to, or concurrent with deletion of *Apc*, suppressed intestinal tumor growth, at least partially due to p19^{ARF}-dependent induction of apoptosis (Maynard et al., 2014). We now demonstrate that BMI1 loss in *Apc*$^{-/-}$*;Kras*$^{G12D/+}$*;Trp53*$^{-/-}$ (AKP) colon cancer does not reduce tumor organoid proliferation *in vitro* or colon tumor growth *in vivo.* There was a slight hint that BMI1 loss may mildly impair proliferation of *Apc*$^{-/-}$*;Kras*$^{G12D/+}$ colon tumor cells. However, a higher number of experimental replicates, particularly in the *in vivo* tumor tracking experiments with *Apc*$^{-/-}$*; Kras*$^{G12D/+}$ colon tumors, will be required to determine the strength of this phenotype. Especially

as p53 is a key downstream target of $p19^{ARF}$, any $p19^{ARF}$-dependent effects could be masked with *Trp53* deletion in the AKP setting.

Regardless, BMI1 loss in the adult, established colon tumors did not confer the pronounced, tumor suppressive phenotypes observed in the germline $Bmi1^{-/-}$ context (Maynard et al., 2014). Transcriptomic analyses of our $Bmi1^{+/+}$ and $Bmi1^{-/-}$ colon tumors indicated that BMI1 loss caused dysregulation of developmental programs and metastasis-associated processes (e.g. extracellular matrix organization and cell adhesion). This mirrors our findings in the established lung cancer setting, suggesting that BMI1's functions in governing tissue type specificity and metastatic spreading extends to multiple epithelial tumor types. Importantly, $p16^{INK4A}$ and $p19^{ARF}$ are not upregulated in either $Bmi1^{-/-}$ lung or colon tumors relative to $Bmi1^{+/+}$ controls, emphasizing that BMI1 seems dispensable for *Cdkn2a* repression in these contexts.

A critical outstanding question is how does BMI1 loss affect colon cancer stem cell (CSC) frequency or function. A key functional characteristic of CSCs is the ability to propagate tumors upon transplant into recipient animals. In the lung cancer setting, we demonstrated that the frequency of tumor-propagating cells was comparable between $Bmi1^{+/+}$ and $Bmi1^{-/-}$ cells, and lung tumors formed from serially transplanted $Bmi1^{-/-}$ cells were larger than those formed from $Bmi1^{+/+}$ cells. In the colon cancer context, we utilized *in vitro* tumor organoid formation assays as a proxy for stemness, but we have not yet assessed for tumor-propagating cell frequency and function *in vivo*. A useful experiment to address this would be a serial dilution assay where various concentrations of colon tumor cells are transplanted into mice to determine tumor propagating cell frequency. There are also putative markers of colon CSCs, namely LGR5, CD44, and CD133 (Dalerba et al., 2007; Kemper et al., 2012; O'Brien et al., 2007; Ricci-Vitiani et al., 2007; Vermeulen et al., 2008), and analyses for expression of these proteins in $Bmi1^{+/+}$ and $Bmi1^{-/-}$ colon tumor cells (such as through immunohistochemical staining of colon tumor tissues) could be informative. Given that the interest in targeting BMI1 in cancer is

predominantly founded on the potential to target CSCs, it is important to understand whether BMI1 loss in the colon cancer context confers changes in CSC frequency and function.

Compensation by other PCGF family members

One possible explanation as to why BMI1 loss does not drastically impair tumor growth in the established lung and colon cancer contexts is that other PRC1 subcomplexes provide compensatory activity. All PRC1 complexes consist of a RING1A/RING1B E3 ubiquitin ligase and a PCGF family member. There are six known members of the mammalian PCGF family, including BMI1 (PCGF4), and interaction of these PCGF proteins with RING1A/1B yields six biochemically distinct PRC1 subcomplexes (Aranda et al., 2015; Gao et al., 2012; Gil and O'Loghlen, 2014). Of note, BMI1 (PCGF4) and MEL18 (PCGF2) share a high degree of functional similarity, as both can associate with CBX proteins to form canonical PRC1 complexes that accumulate at H3K27me^3-rich regions of the genome. Chromatin immunoprecipitation studies in human embryonic kidney and mouse embryonic stem cell lines have demonstrated that the genomic loci occupied by these six different PRC1 complexes are largely distinctive with a limited degree of overlap, suggesting the lack of functional redundancy between the various PRC1 subcomplexes (Gao et al., 2012; Scelfo et al., 2019).

It has been observed that the various PRC1 subcomplexes can provide compensatory activity in certain contexts. In mouse embryonic stem cell lines, PCGF1 and MEL18 (PCGF2) co-occupied a set of target genes, and knockout studies revealed that PCGF1 and MEL18 (PCGF2) can largely compensate for each other at those loci. In cancer, BMI1 (PCGF4) and MEL18 (PCGF2) have been demonstrated to have opposing effects on tumor development, with studies indicating a tumor suppressive role for MEL18 (Guo et al., 2007; Zhang et al., 2010). Despite this, a recent study utilizing a colitis-associated mouse model of intestinal cancer indicated that single knockout of BMI1 or MEL18 had minimal effects on tumor growth, but double knockout of BMI1 and MEL18 led to severe reductions in intestinal tumor numbers and

burden (Liu et al., 2017). Thus, BMI1 and MEL18 may have overlapping roles in intestinal tumorigenesis. In our studies of BMI1 loss in lung and colon cancer, we did not observe elevated expression of other PCGF family members (data not shown). However, we cannot exclude the possibility that non-BMI1 PCGF family members are compensating for BMI1 loss at specific genomic loci, thus mitigating the effects of BMI1 loss. To elucidate this possibility, chromatin immunoprecipitation experiments to profile genomic occupancy of PCGF family members in the presence and absence of BMI1 would be highly informative. Especially given the high functional similarity between BMI1 and MEL18, it is of particular interest to elucidate the effects of concurrent BMI1 and MEL18 loss in our cancer model systems.

BMI1 loss in non-epithelial cancer types

This thesis focuses on lung and colon cancer, both of which are derived from epithelial tissue cells. However, it remains an open question whether genetic ablation of *Bmi1* in established tumors of other cancer types will confer similar effects. Consistent with the earlier discussion on the dual roles of epigenetic regulators as oncogenes and tumor suppressors, it would not be surprising to find that the functions of BMI1 differ vastly between distinct tumor types.

To this end, we have generated a model of rhabdomyosarcoma in which we can delete BMI1 specifically in the cancerous tissue. In brief, we have induced $Kras^{G12D/+};Trp53^{-/-}$ rhabdomyosarcomas autochthonously in the calf muscles of mice, and following confirmation of tumor growth, we induced BMI1 loss concurrent with expression of a fluorescent reporter that enables tumor cell isolation and characterization (Kirsch et al., 2007). We are currently in the process of analyzing the rhabdomyosarcoma tissue, including assessing for proliferation, apoptosis, and $p16^{INK4A}$ and $p19^{ARF}$ expression. We are also performing serial transplant experiments of the rhabdomyosarcoma cells to interrogate CSC exhaustion. As we continue to characterize the rhabdomyosarcoma samples, we hope to elucidate whether BMI1 loss confers

consistent or differing phenotypes, including gene expression pattern changes, across epithelial and non-epithelial tumor types.

Implications for the use of BMI1 inhibitors as cancer therapies

Based upon the findings of BMI1's pro-tumorigenic functions, there has been significant interest into the development of BMI1-specific chemical inhibitors. To date, the three most documented BMI1 small molecule inhibitors are PTC-209, PTC-596, and PTC-028 (Dey et al., 2018; Kreso et al., 2014). PTC-209 has been the most prevalently used inhibitor in experimental mouse model studies and was identified in a screen for small molecules that downregulated expression of a reporter under transcriptional control of human *Bmi1* 5' and 3' UTRs (Kreso et al., 2014). Treatment with PTC-209 abrogated growth of human colon cancer xenografts in mice, including reducing tumor-initiating cell frequency (Kreso et al., 2014). Further studies confirmed that treatment with PTC-209 inhibits tumor cell growth *in vitro* and *in vivo* through induction of cell cycle arrest in models of other cancer types, including breast cancer and cervical cancer (Li et al., 2020; Srinivasan et al., 2017). However, we utilized PTC-209 in our mouse cancer cell lines and demonstrated that treatment with PTC-209 is equally cytotoxic to $Bmi1^{+/+}$ and $Bmi1^{-/-}$ cells (data not shown) with similar IC50s as those published previously (Kreso et al., 2014). Although we cannot exclude the possibility that PTC-209 selectively targets only human BMI1, and not murine BMI1, our results indicate that PTC-209 can exert cytotoxicity through mechanisms independent of BMI1 status. Although this inhibitor has not entered into clinical trials due to poor pharmacokinetic properties, interest in developing BMI1 inhibitors has persisted, leading to the identification and development of the BMI1 chemical inhibitors PTC-596 and PTC-028 (Dey et al., 2018; Nishida et al., 2017). However, PTC-596 and PTC-028 have been demonstrated to induce toxicity through BMI1-independent mechanisms (Bolomsky et al., 2020; Eberle-Singh et al., 2019; Flamier et al., 2020).

As interest in the development of BMI1 inhibitors continues, our work cautions against the use of these inhibitors in certain contexts. In progressed *Kras*$^{G12D/+}$;*Trp53*$^{-/-}$ lung tumors and *Apc*$^{-/-}$;*Kras*$^{G12D/+}$;*Trp53*$^{-/-}$ colon tumors, loss of BMI1 activity did not confer tumor suppression, indicating that treatment of BMI1 inhibitors would not yield clinical benefits to patients with these tumor types. Moreover, as discussed above, our findings align with studies interrogating the roles of other epigenetic regulators in cancer, where disruption of epigenetic regulator function can exert pro-tumorigenic or anti-tumorigenic effects depending on the context. Together, our data and the work of many others highlight the critical need to carefully dissect the roles of epigenetic regulators in cancer development and elucidate how abrogation of their activities affects tumorigenesis.

REFERENCES

Abdouh, M., Hanna, R., el Hajjar, J., Flamier, A., and Bernier, G. (2016). The polycomb repressive complex 1 protein BMI1 is required for constitutive heterochromatin formation and silencing in mammalian somatic cells. Journal of Biological Chemistry *291*, 182–197.

Aibar, S., González-Blas, C.B., Moerman, T., Huynh-Thu, V.A., Imrichova, H., Hulselmans, G., Rambow, F., Marine, J.-C., Geurts, P., Aerts, J., et al. (2017). SCENIC: single-cell regulatory network inference and clustering. Nature Methods *14*.

Aranda, S., Mas, G., and di Croce, L. (2015). Regulation of gene transcription by Polycomb proteins. Science Advances *1*.

Avgustinova, A., Symeonidi, A., Castellanos, A., Urdiroz-Urricelqui, U., Solé-Boldo, L., Martín, M., Pérez-Rodríguez, I., Prats, N., Lehner, B., Supek, F., et al. (2018). Loss of G9a preserves mutation patterns but increases chromatin accessibility, genomic instability and aggressiveness in skin tumours. Nature Cell Biology *20*.

Bednar, F., Schofield, H.K., Collins, M.A., Yan, W., Zhang, Y., Shyam, N., Eberle, J.A., Almada, L.L., Olive, K.P., Bardeesy, N., et al. (2015). Bmi1 is required for the initiation of pancreatic cancer through an Ink4a-independent mechanism. Carcinogenesis *36*.

Bolomsky, A., Muller, J., Stangelberger, K., Lejeune, M., Duray, E., Breid, H., Vrancken, L., Pfeiffer, C., Hübl, W., Willheim, M., et al. (2020). The anti-mitotic agents PTC-028 and PTC596 display potent activity in pre-clinical models of multiple myeloma but challenge the role of BMI-1 as an essential tumour gene. British Journal of Haematology 1–14.

Cao, R., Tsukada, Y., and Zhang, Y. (2005). Role of Bmi-1 and Ring1A in H2A Ubiquitylation and Hox Gene Silencing. Molecular Cell *20*.

Casciello, F., Windloch, K., Gannon, F., and Lee, J.S. (2015). Functional Role of G9a Histone Methyltransferase in Cancer. Frontiers in Immunology *6*.

Chatoo, W., Abdouh, M., David, J., Champagne, M.P., Ferreira, J., Rodier, F., and Bernier, G. (2009). The polycomb group gene Bmi1 regulates antioxidant defenses in neurons by repressing p53 pro-oxidant activity. Journal of Neuroscience *29*, 529–542.

Dalerba, P., Dylla, S.J., Park, I.-K., Liu, R., Wang, X., Cho, R.W., Hoey, T., Gurney, A., Huang, E.H., Simeone, D.M., et al. (2007). Phenotypic characterization of human colorectal cancer stem cells. Proceedings of the National Academy of Sciences *104*.

Dey, A., Xiong, X., Crim, A., Dwivedi, S.K.D., Mustafi, S.B., Mukherjee, P., Cao, L., Sydorenko, N., Baiazitov, R., Moon, Y.-C., et al. (2018). Evaluating the Mechanism and Therapeutic Potential of PTC-028, a Novel Inhibitor of BMI-1 Function in Ovarian Cancer. Molecular Cancer Therapeutics *17*.

Dovey, J.S., Zacharek, S.J., Kim, C.F., and Lees, J.A. (2008). Bmi1 is critical for lung tumorigenesis and bronchioalveolar stem cell expansion. Proceedings of the National Academy of Sciences *105*.

Eberle-Singh, J.A., Sagalovskiy, I., Maurer, H.C., Sastra, S.A., Palermo, C.F., Decker, A.R., Kim, M.J., Sheedy, J., Mollin, A., Cao, L., et al. (2019). Effective delivery of a microtubule polymerization inhibitor synergizes with standard regimens in models of pancreatic ductal adenocarcinoma. Clinical Cancer Research *25*, 5548–5560.

Facchino, S., Abdouh, M., Chatoo, W., and Bernier, G. (2010). BMI1 confers radioresistance to normal and cancerous neural stem cells through recruitment of the DNA damage response machinery. Journal of Neuroscience *30*, 10096–10111.

Ferretti, R., Bhutkar, A., McNamara, M.C., and Lees, J.A. (2016). BMI1 induces an invasive signature in melanoma that promotes metastasis and chemoresistance. Genes & Development *30*.

Flamier, A., Abdouh, M., Hamam, R., Barabino, A., Patel, N., Gao, A., Hanna, R., and Bernier, G. (2020). Off-target effect of the BMI1 inhibitor PTC596 drives epithelial-mesenchymal transition in glioblastoma multiforme. Npj Precision Oncology *4*.

Gao, Z., Zhang, J., Bonasio, R., Strino, F., Sawai, A., Parisi, F., Kluger, Y., and Reinberg, D. (2012). PCGF Homologs, CBX Proteins, and RYBP Define Functionally Distinct PRC1 Family Complexes. Molecular Cell *45*.

Gil, J., and O'Loghlen, A. (2014). PRC1 complex diversity: where is it taking us? Trends in Cell Biology *24*.

Guo, W.-J., Zeng, M.-S., Yadav, A., Song, L.-B., Guo, B.-H., Band, V., and Dimri, G.P. (2007). Mel-18 Acts as a Tumor Suppressor by Repressing Bmi-1 Expression and Down-regulating Akt Activity in Breast Cancer Cells. Cancer Research *67*.

el Hajjar, J., Chatoo, W., Hanna, R., Nkanza, P., Tétreault, N., Tse, Y.C., Wong, T.P., Abdouh, M., and Bernier, G. (2019). Heterochromatic genome instability and neurodegeneration sharing similarities with Alzheimer's disease in old Bmi1+/− mice. Scientific Reports *9*.

Iwama, A., Oguro, H., Negishi, M., Kato, Y., Morita, Y., Tsukui, H., Ema, H., Kamijo, T., Katoh-Fukui, Y., Koseki, H., et al. (2004). Enhanced Self-Renewal of Hematopoietic Stem Cells Mediated by the Polycomb Gene Product Bmi-1. Immunity *21*.

Jacobs, J.J.L., Scheijen, B., Voncken, J.W., Kieboom, K., Berns, A., and van Lohuizen, M. (1999). Bmi-1 collaborates with c-Myc in tumorigenesis by inhibiting c-Myc- induced apoptosis via INK4a/ARF. Genes and Development *13*, 2678–2690.

Kemper, K., Prasetyanti, P.R., de Lau, W., Rodermond, H., Clevers, H., and Medema, J.P. (2012). Monoclonal Antibodies Against Lgr5 Identify Human Colorectal Cancer Stem Cells. Stem Cells *30*.

Kirsch, D.G., Dinulescu, D.M., Miller, J.B., Grimm, J., Santiago, P.M., Young, N.P., Nielsen, G.P., Quade, B.J., Chaber, C.J., Schultz, C.P., et al. (2007). A spatially and temporally restricted mouse model of soft tissue sarcoma. Nature Medicine *13*.

Kleer, C.G., Cao, Q., Varambally, S., Shen, R., Ota, I., Tomlins, S.A., Ghosh, D., Sewalt, R.G.A.B., Otte, A.P., Hayes, D.F., et al. (2003). EZH2 is a marker of aggressive breast

cancer and promotes neoplastic transformation of breast epithelial cells. Proceedings of the National Academy of Sciences *100*.

Kreso, A., van Galen, P., Pedley, N.M., Lima-Fernandes, E., Frelin, C., Davis, T., Cao, L., Baiazitov, R., Du, W., Sydorenko, N., et al. (2014). Self-renewal as a therapeutic target in human colorectal cancer. Nature Medicine *20*, 29–36.

LaFave, L.M., Kartha, V.K., Ma, S., Meli, K., del Priore, I., Lareau, C., Naranjo, S., Westcott, P.M.K., Duarte, F.M., Sankar, V., et al. (2020). Epigenomic State Transitions Characterize Tumor Progression in Mouse Lung Adenocarcinoma. Cancer Cell *38*, 212–228.e13.

Lau, A.N., Curtis, S.J., Fillmore, C.M., Rowbotham, S.P., Mohseni, M., Wagner, D.E., Beede, A.M., Montoro, D.T., Sinkevicius, K.W., Walton, Z.E., et al. (2014). Tumor-propagating cells and Yap/Taz activity contribute to lung tumor progression and metastasis. EMBO Journal *33*, 468–481.

Laugesen, A., Højfeldt, J.W., and Helin, K. (2016). Role of the Polycomb Repressive Complex 2 (PRC2) in Transcriptional Regulation and Cancer. Cold Spring Harbor Perspectives in Medicine *6*.

Lessard, J., and Sauvageau, G. (2003). Bmi-1 determines the proliferative capacity of normal and leukaemic stem cells. Nature *423*.

Li, J., Vangundy, Z., and Poi, M. (2020). PTC209, a Specific Inhibitor of BMI1, Promotes Cell Cycle Arrest and Apoptosis in Cervical Cancer Cell Lines. Anticancer Research *40*.

Liu, J., Cao, L., Chen, J., Song, S., Lee, I.H., Quijano, C., Liu, H., Keyvanfar, K., Chen, H., Cao, L.Y., et al. (2009). Bmi1 regulates mitochondrial function and the DNA damage response pathway. Nature *459*, 387–392.

Liu, X., Wei, W., Li, X., Shen, P., Ju, D., Wang, Z., Zhang, R., Yang, F., Chen, C., Cao, K., et al. (2017). BMI1 and MEL18 Promote Colitis-Associated Cancer in Mice via REG3B and STAT3. Gastroenterology *153*, 1607–1620.

van der Lugt, N.M.T., Alkema, M., Berns, A., and Deschamps, J. (1996). The Polycomb-group homolog Bmi-1 is a regulator of murine Hox gene expression. Mechanisms of Development *58*.

Ma, Q., Wu, K., Li, H., Li, H., Zhu, Y., Hu, G., Hu, L., and Kong, X. (2019). ONECUT2 overexpression promotes RAS-driven lung adenocarcinoma progression. Scientific Reports *9*.

Maynard, M.A., Ferretti, R., Hilgendorf, K.I., Perret, C., Whyte, P., and Lees, J.A. (2014). Bmi1 is required for tumorigenesis in a mouse model of intestinal cancer. Oncogene *33*.

Molofsky, A. v., Pardal, R., Iwashita, T., Park, I.-K., Clarke, M.F., and Morrison, S.J. (2003). Bmi-1 dependence distinguishes neural stem cell self-renewal from progenitor proliferation. Nature *425*.

Nishida, Y., Maeda, A., Kim, M.J., Cao, L., Kubota, Y., Ishizawa, J., AlRawi, A., Kato, Y., Iwama, A., Fujisawa, M., et al. (2017). The novel BMI-1 inhibitor PTC596 downregulates MCL-1 and induces p53-independent mitochondrial apoptosis in acute myeloid leukemia progenitor cells. Blood Cancer Journal *7*, e527–e527.

Nowell, P.C. (1976). The Clonal Evolution of Tumor Cell Populations. Science *194*.

O'Brien, C.A., Pollett, A., Gallinger, S., and Dick, J.E. (2007). A human colon cancer cell capable of initiating tumour growth in immunodeficient mice. Nature *445*.

Oguro, H., Iwama, A., Morita, Y., Kamijo, T., van Lohuizen, M., and Nakauchi, H. (2006). Differential impact of Ink4a and Arf on hematopoietic stem cells and their bone marrow microenvironment in Bmi1-deficient mice. Journal of Experimental Medicine *203*.

Oguro, H., Yuan, J., Ichikawa, H., Ikawa, T., Yamazaki, S., Kawamoto, H., Nakauchi, H., and Iwama, A. (2010). Poised Lineage Specification in Multipotential Hematopoietic Stem and Progenitor Cells by the Polycomb Protein Bmi1. Cell Stem Cell *6*.

Park, I., Qian, D., Kiel, M., Becker, M.W., Pihalja, M., Weissman, I.L., Morrison, S.J., and Clarke, M.F. (2003). Bmi-1 is required for maintenance of adult self-renewing haematopoietic stem cells. Nature *423*.

Ricci-Vitiani, L., Lombardi, D.G., Pilozzi, E., Biffoni, M., Todaro, M., Peschle, C., and de Maria, R. (2007). Identification and expansion of human colon-cancer-initiating cells. Nature *445*.

Rowbotham, S.P., Li, F., Dost, A.F.M., Louie, S.M., Marsh, B.P., Pessina, P., Anbarasu, C.R., Brainson, C.F., Tuminello, S.J., Lieberman, A., et al. (2018). H3K9 methyltransferases and demethylases control lung tumor-propagating cells and lung cancer progression. Nature Communications *9*.

Scelfo, A., Fernández-Pérez, D., Tamburri, S., Zanotti, M., Lavarone, E., Soldi, M., Bonaldi, T., Ferrari, K.J., and Pasini, D. (2019). Functional Landscape of PCGF Proteins Reveals Both RING1A/B-Dependent-and RING1A/B-Independent-Specific Activities. Molecular Cell *74*.

Snyder, E.L., Watanabe, H., Magendantz, M., Hoersch, S., Chen, T.A., Wang, D.G., Crowley, D., Whittaker, C.A., Meyerson, M., Kimura, S., et al. (2013). Nkx2-1 Represses a Latent Gastric Differentiation Program in Lung Adenocarcinoma. Molecular Cell *50*, 185–199.

Song, L.-B., Li, J., Liao, W.-T., Feng, Y., Yu, C.-P., Hu, L.-J., Kong, Q.-L., Xu, L.-H., Zhang, X., Liu, W.-L., et al. (2009). The polycomb group protein Bmi-1 represses the tumor suppressor PTEN and induces epithelial-mesenchymal transition in human nasopharyngeal epithelial cells. Journal of Clinical Investigation *119*.

Srinivasan, M., Bharali, D.J., Sudha, T., Khedr, M., Guest, I., Sell, S., Glinsky, G. v., and Mousa, S.A. (2017). Downregulation of Bmi1 in breast cancer stem cells suppresses tumor growth and proliferation. Oncotarget *8*.

Vermeulen, L., Todaro, M., de Sousa Mello, F., Sprick, M.R., Kemper, K., Perez Alea, M., Richel, D.J., Stassi, G., and Medema, J.P. (2008). Single-cell cloning of colon cancer

stem cells reveals a multi-lineage differentiation capacity. Proceedings of the National Academy of Sciences *105*.

Wassef, M., Rodilla, V., Teissandier, A., Zeitouni, B., Gruel, N., Sadacca, B., Irondelle, M., Charruel, M., Ducos, B., Michaud, A., et al. (2015). Impaired PRC2 activity promotes transcriptional instability and favors breast tumorigenesis. Genes & Development *29*.

Winslow, M.M., Dayton, T.L., Verhaak, R.G.W., Kim-Kiselak, C., Snyder, E.L., Feldser, D.M., Hubbard, D.D., Dupage, M.J., Whittaker, C.A., Hoersch, S., et al. (2011). Suppression of lung adenocarcinoma progression by Nkx2-1. Nature *473*, 101–104.

Yang, M.-H., Hsu, D.S.-S., Wang, H.-W., Wang, H.-J., Lan, H.-Y., Yang, W.-H., Huang, C.-H., Kao, S.-Y., Tzeng, C.-H., Tai, S.-K., et al. (2010). Bmi1 is essential in Twist1-induced epithelial–mesenchymal transition. Nature Cell Biology *12*.

Zhang, X.-W., Sheng, Y.-P., Li, Q., Qin, W., Lu, Y.-W., Cheng, Y.-F., Liu, B.-Y., Zhang, F.-C., Li, J., Dimri, G.P., et al. (2010). BMI1 and Mel-18 oppositely regulate carcinogenesis and progression of gastric cancer. Molecular Cancer *9*.

Zheng, Y., de la Cruz, C.C., Sayles, L.C., Alleyne-Chin, C., Vaka, D., Knaak, T.D., Bigos, M., Xu, Y., Hoang, C.D., Shrager, J.B., et al. (2013). A Rare Population of CD24+ITGB4+Notchhi Cells Drives Tumor Propagation in NSCLC and Requires Notch3 for Self-Renewal. Cancer Cell.